THE EFFECT OF SHOT PEENING ON FATIGUE AND FRETTING-FATIGUE OF ALUMINIUM ALLOYS.

G.H.Fair B.Sc. (Honours)

Thesis submitted to the University of Nottingham

for the degree of Doctor of Philosophy.

July 1988

CONTENTS

ABSTRACT

Plain-fatigue and fretting-fatigue tests have been carried out on the two peak-aged, high-strength aluminium alloys, 7010 and 8090, in the unpeened and shot peened conditions.

Shot peening produced a highly deformed surface containing many deep dimples and folds from which fatigue cracks rapidly initiated. Although initiation was early, propagation through the peened surface layers was retarded by the residual compressive stresses introduced by the peening treatment; this retardation being greatest at a depth corresponding to that of the peak residual compressive stress.

Shot peening improved the plain-fatigue properties of the 7010 alloy at high applied stresses and this improvement decreased as the applied stress was reduced. A reversed trend was observed in the 8090 alloy with shot peening being beneficial to the fatigue properties at low applied stresses and detrimental at high applied stresses.

The poor resistance of the 7010 alloy to fretting-fatigue was eliminated by shot peening and this was again attributed to the residual compressive stress induced by the peening treatment. Since the 8090 alloy in the unpeened condition is relatively insensitive to the effects of fretting, shot peening resulted in only a minor improvement in the fretting-fatigue behaviour of this alloy.

INTRODUCTION

Shot peening is the bombardment of a surface by a stream of hard shot. This treatment produces a heavily deformed surface and often results in an improvement in resistance to problems such as fatigue and fretting-fatigue. As a result of improved fatigue performances, components can be manufactured at significantly reduced weights and consequently shot peening is of particular interest in the aerospace industry.

In this work, the effects of different intensities of shot peening on the plain and fretting-fatigue performance of two recently developed high-strength aluminium alloys, of interest in the aerospace industry, are investigated.

CHAPTER ONE

SHOT - PEENING

1.1 Introduction

It is generally found that the deformation of a metal surface is beneficial to the fatigue properties due mainly to the development of residual compressive stresses in the surface layers being worked. This has the effect of nullifying any tensile stresses around stress raisers in the surface (i.e. fatigue crack initiation sites), resulting in an increased fatigue life.

There are many ways of mechanically introducing a residual compressive stress into a surface (mechanical prestressing), for example, by strain strengthening, cold rolling, hammer peening and shot peening.

a) Strain Strengthening.

In this process the component is strained in such a way that plastic flow occurs at the area where cracking is most likely during fatigue. Upon releasing, the elastic stresses in the component tend to force it back to its original shape but this is prevented by the deformed material which is thus compressed, giving the desired effect.

This process is limited to fairly simple, non-precision, non-brittle parts such as leaf springs in automobiles.

b) Cold Rolling.

In this process, a hard steel roller is passed over the surface of the component to be treated. Excessive cold working is not desirable in most cases as it is only the surface layers which need to be treated, hence only a light roller pressure is applied. This process is limited to relatively simple shapes such as axles and shafts. It is clear that some shapes would be extremely difficult if not impossible to be rolled.

c) Hammer Peening.

In this process, the surface compressive stress is induced by a series of blows by hammers of various shapes and sizes depending on the shape of the component. This is a cheap and time saving treatment since the tool can be taken to the component to be worked.

d) Shot Peening.

In this process a stream of hard steel shot (or other hard material) is fired at the component to induce a surface residual compressive stress. This is similar to hammer peening but it has the advantage of being easier to control since the shot energy and direction can be maintained at a much more constant level. This results in a reduction in mistakes caused by human error and a considerable improvement in the uniformity of the residual compressive stresses.

The benefits of peening are particularly desirable in the aircraft and automobile industries where improvements in fatigue performance allow components to be manufactured at reduced weights. This results in increased performance and improved cost effectiveness.

Peening is also used to alleviate many fatigue associated problems such as fretting-fatigue, corrosion-fatigue and fatigue at weldaments, the improvements again occurring due to the residual compressive stress induced by the peening operation.

Other uses of shot peening include peen forming, a process in which sheet metal is formed to particular shapes by peening one side to produce a curvature. Peen forming is often used in the shaping of parts such as aircraft wing sections.

Review of Literature

1.2 Shot Peening - Brief History

It has been well known for centuries that the deformation of metals can result in a large increase in strength and hardness. Bush (1) reported the dating of mechanical prestressing back to at least 2700 BC when hammered gold helmets were used, and later, during the crusades of 1100 to 1400 AD, when knights cold worked their armour to the final shape and hardness. More recently (in 1789) he reported the use of mechanical prestressing to improve the strength of gun barrels by the hammering of their outer surfaces.

At the beginning of the 20th century, with the arrival of World Wars I and II, efforts were increased to try and maximise the properties of steels and to improve their reliability.

In 1927, Herbert (2) investigated the hardness induced by severe abrasion in locomotive tyres and rails, and also in hardened steel gears and cams for motor cars. Using a recently developed test involving a pendulum hardness tester to obtain the maximum induced hardness in these materials, he discovered that articles of very hard steel could be "superhardened" by working. From this investigation, he suggested an inquiry into the possibility of the superhardening of hard steels before putting them into service as a means of resisting wear (3). As a result of this, in 1928, he invented the Cloudburst process. In this process, a stream of hard steel balls of approximately 3mm diameter was allowed to fall from a specified height on to the hard steel surface being treated and, under suitable conditions, the rapid succession of blows caused the steel surface to become work-hardened by producing a thin, superhardened layer.

In 1929, the Buick Motor Division of General Motors Corporation attempted to remove spots of scale from springs by blasting them with grit. It was found that the fatigue properties of the springs were markedly improved by this process. This provided the impetus for the development of shot peening.

As reported by Zimmerli (4), one of the first controlled shot peening operations (called shot blasting at the time) was carried out by the Associated Spring Corporation in 1929, shortly after the development of the Cloudburst process. This treatment was not taken seriously by other companies for several years. Since then,

much work has been carried out to understand the shot peening operation in order to find the optimum properties obtainable by its use. The main factor which affects the performance of components after peening is the intensity at which they have been peened.

1.3 Peening Intensity

The intensity of the peening operation is dependent upon several factors which determine how much energy is transferred from the shot to the workpiece. It is well known that peening results in an improvement in the fatigue properties of many alloys (see section 1.4). In order to obtain the optimum improvement, it is important to peen at the correct intensity and consequently, accurate measurement of the intensity is necessary.

1.3.1 Measurement of Peening Intensity

The measurement of peening intensity was developed by Almen (5) in 1963 and is still in use today. A steel strip 76mm long and 19mm wide with a hardness in the range 44-50Rc is attached firmly to a thick metal base leaving the exposed side of the strip to be peened. Upon removal of the strip, the compressive stresses induced produce a convex curvature on the peened side. The curvature is measured on the unpeened side in terms of arc height over a standard chord. The amount of curvature (i.e. arc height) of the strip represents the peening intensity.

In order to make accurate measurement of the wide range of peening intensities possible, strips of different thicknesses are used according to the intensity; they are:-

N strips, thickness 0.79 mm, for low intensity peening;

A strips, thickness 1.30 mm, for medium intensity peening;

C strips, thickness 2.39 mm, for high intensity peening.

To obtain the required peening intensity, successive test strips are passed through a shot stream and the variables adjusted until the desired arc height is attained.

A shot peening specification consists of the arc height reading of the test strip followed by the letter indicating the strip size N, A, or C.

Clarke and Birley (6) pointed out that this method is only applicable when peening materials of a similar hardness to that of the Almen strip. They stated that, for materials of a differing hardness, this problem could be overcome by such methods as:-

a) applying a suitable multiplication factor;

b) use of test strips manufactured from the component material;

c) visually estimating when complete coverage (see section 1.3.3) has taken place.

Simpson et al (7) found that the Almen strip could not be reliably used to predict coverage, especially if the hardness of the strip differed significantly from that of the workpiece. They concluded that the peening of workpieces much softer than the Almen test strip (e.g. aluminium alloys) achieved full coverage up to three

times faster than the strip due to the fact that the peening produced larger indents in the softer material. They also found that the tolerance allowable in the hardness of the Almen strip was excessive since an extra 30% error in the measurement of saturation could be incurred by using strips at either end of the hardness range.

1.3.2 Factors Affecting Peening Intensity

The main factors affecting peening intensity are:-

a) shot speed;

b) shot size;

c) angle of impingement;

d) exposure time.

a) Shot Speed

It is clear that the greater the shot speed, the greater is the amount of energy transferred to the workpiece. Meguid and Duxbury (8), investigating the variables associated with shot peening, found that increasing the average shot speed increases the depth of penetration into the surface of the workpiece, resulting in a larger arc height of the Almen strip. Niku Lari (9) showed that the relationship between shot velocity and Almen intensity is approximately linear above certain shot diameters and shot speeds (see fig. 1a).

b) Shot Size

As the size of the shot is increased, more energy is transferred to the workpiece and hence the arc height is increased. This was observed by Meguid and Duxbury (8) (see fig. 1b).

c) Angle of Impingement

No literature has been found on the effect of various peening angles on the intensity but it is assumed that at normal impact most energy is transferred to the workpiece and hence the arc height is at its greatest when compared with peening at lower angles. However, it is usual to peen at an angle slightly away from the normal as this avoids reflection of the shot back into the oncoming stream which causes "blinding" and excessive shot consumption.

d) Exposure Time

As the workpiece is first exposed to the shot stream, the arc height of the Almen strip increases rapidly but, as the exposure time increases, the rate at which the arc height increases drops until a constant peening intensity is reached. At this point, saturation has been reached and further peening is unnecessary and can even be harmful owing to excessive surface damage ("overpeening").

Clarke and Birley (6) defined saturation as the condition which exists in the Almen test strip when doubling the peening time causes a rise in the intensity value of not more than 10% (see fig. 2a).

1.3.3 Coverage

The required peening intensity should be, in most cases, the intensity obtained at saturation. This ensures adequate coverage which, as explained by Burakowski and Nakonieczny (10), is a measure of how completely a surface has been hit by a stream of shot particles. Without adequate coverage, they stated, the improvements in fatigue characteristics normally produced by peening will not be obtained owing to the unpeened areas ("holidays") which will only have the strength of the unpeened material. Because accurate measurement of peening can be made up to 98% coverage, this value has been arbitrarily chosen to represent 100% coverage. Components are often peened to a coverage greater than 100% to ensure there are no holidays present as a result of human error.

One visual method of ensuring complete coverage is to paint the surface of the material before peening with a "fluorescent tracer" (i.e. a dye which fluoresces in ultra-violet light). Since peening removes the tracer, any holidays will clearly show up as bright areas in the presence of the ultra-violet light thus ensuring 100% coverage.

An alternative method involves the examination of the workpiece surface using a microscope at 10X magnification. However, this method is less acceptable since it is time consuming and less reliable.

1.3.4 Overpeening

As stated by Clark and Birley (6), overpeening is peening for too long or at too high an intensity. This, they stated, can result in the introduction of cracks into the surface of the metal. As a consequence, the peening can lose its effect since the cracks may propagate through the peened layers under suitable stress conditions. They reported that overpeening (i.e. peening for an excessive length of time in this case) the alloy Al-4.5Zn-2.5Mg had little effect and suggested that a more harmful effect may be observed in the softer Al-4Zn-2Mg alloy.

1.3.5 The Optimum Peening Intensity

The effect of varying the shot peening intensity on bending-fatigue strength in air was investigated by Almen (11) who reported that the beneficial effect of peening passed through a maximum as the intensity increased (see fig. 2b).

Fuchs (12) stated that the optimum intensity is obtained when failures below the surface are just as likely as failures at the surface of the peened part.

1.4 Fatigue in Peened Materials

The effects of peening on the fatigue lives of materials have been neatly summarised by Fuchs (12) who made three key observations:-

a) Peening has more effect at long fatigue lives than at shorter fatigue lives.

b) Peening has more effect on high strength materials than on low strength materials.

c) Peening has far more effect on notched parts or on parts with crack prone surfaces than on nicely finished smooth specimens. Peening can often overcome the notch effect so that peened parts with notches can be as strong in fatigue as smooth unnotched parts.

1.4.1 Residual Stresses

With the discovery of the improved fatigue properties of shot peened springs by Zimmerli (4) in 1940, the question of the cause of this effect arose. Upon heating the peened springs he found that the beneficial effects disappeared and the springs behaved as in the unpeened condition. He attributed this to the cold work introduced by the peening operation and, in later discussions, decided that the treatment induced a shallow layer of residual compressive stresses of a relatively high order at the surface of the treated material.

Since then, much work has been carried out to understand the nature of these stresses and to find out how they affect the fatigue properties of materials.

1.4.1.1 Distribution of Residual Stresses

It has been found by many people that the residual compressive stresses induced by peening do not always peak at the surface as may be expected. For example, Hawkes (13) found that the peak residual compressive stress in an extruded aluminium alloy was

below the surface. Other reports have suggested that the peak residual compressive stress is at the surface. For example, Burck et al (14) observed this effect when peening a nickel base alloy with glass beads.

These conflicting observations have been explained by Wohlfahrt (15) who, examining the effect of shot of varying hardness and energy on materials of differing hardnesses, concluded that the development of residual stresses after peening included two different processes:-

a) A type of dynamic Hertzian pressure which results in a distribution of residual compressive stress with the maximum magnitude below the surface of the material if this effect is the predominant one. This occurs when hard materials are peened with shot of sufficient energy (see fig. 3a).

The depth (z) at which the peak residual compressive stress (i.e. the point at which the maximum shear stress is exerted by the impinging shot) occurs below the surface has been calculated as; z = 0.47a, where a is the radius of contact between the shot and the surface (16).

b) A direct plastic elongation of the surface layers; a kind of surface hammering which produces a maximum magnitude of the residual compressive stress at the surface if this effect is the predominant one. This occurs frequently in soft materials (see fig. 3b).

This was verified by Ebenau et al (17) who, investigating the effects of peening on a plain carbon steel in both the normalised and quenched conditions, found that the residual compressive stress peaked at the surface in the normalised steel and below the surface in the harder quenched steel.

Whether the residual tensile stress counteracting the surface residual compressive stress produced by the peening process is spread uniformly across the remainder of the section or whether the stress is concentrated in an area directly beneath the compressive layer has been a controversial point. Hawkes (13), investigating the effect of shot peening on an Al-Zn-Mg-Co alloy, found (using an X-ray stress measurement technique) that the balancing residual tensile stress was spread uniformly across the remainder of the specimens beneath the surface residual compressive stress. This is now the generally held view.

It has been found that the residual tensile stress can cause a drop in the yield stress of peened specimens. Wagner and Luetjering (18) found that the yield stress of a titanium alloy fell with increasing peening intensity.

As discussed in section 1.4.1.2 it is generally believed that shot peening improves the fatigue performance of alloys by hindering early crack propagation through the residually compressed surface layer. It is therefore often desirable to produce a deep compressive layer since the cracks have further to grow to escape the effects of these stresses. As described by Daly (19), several airframe manufacturers using high-strength aluminium alloys have

found that fatigue performances can be improved by using a greater shot size which gives a deeper layer of compression for a given intensity when compared to that produced by smaller shot sizes.

1.4.1.2 The Effect of Residual Stresses on Fatigue

It is important to understand how fatigue crack initiation and propagation are affected by the induced residual stresses in order to be able to optimise the peening treatment so that an extended fatigue lifetime can be produced.

Surface treatments which are designed to introduce residual compressive stresses into the surface of materials are often found to result in crack initiation and growth parallel to the surface beneath the compressive layer. Nakonieczny (20) found that the distribution of stresses in the surface layers had a fundamental effect on fatigue life and concluded that a low stress gradient perpendicular to the surface between compressive and tensile stresses is more beneficial than a high gradient. This was verified by the examination of diffusion-hardened and work-hardened materials. The work-hardened material had, he found, by far the lowest gradient, resulting in a decreased stress concentration between compressive and tensile layers. The high stress gradient found in diffusion-hardened surfaces leads to a much greater likelihood of sub-surface cracking and so, for this reason, surface working methods are often preferable.

However, sub-surface crack initiation does exist frequently in shot peened materials as observed by Was and Pelloux (21) who, testing lightly peened 7075 (T6) aluminium alloy specimens in push-pull fatigue, observed that:

a) The initiation of cracks was below the surface of the alloy at approximately 400μm at all applied stress levels.

b) Fracture between initiation site and surface was due to stage I type crack growth whereas in unpeened specimens, stage I growth was limited to the order of only one grain size at the surface before changing to stage II type crack growth.

This occurrence was explained by Vogelsang (22) who tested several aluminium alloys in fatigue and found that a vacuum environment enhanced crack growth on planes of maximum shear stress (as seen in sub-surface initiated cracks) whereas a humid environment such as air enhanced crack growth perpendicular to the principal tensile stress.

Dieter (23) stated that environment affects crack propagation rather than initiation. As a result, Was and Pelloux (21) deduced that the longer life of peened specimens at high stresses, where initiation is rapid, must be as a result of slower propagation of the crack. They also deduced that the critical stress for crack initiation is unchanged by shot peening although initiation may be below the surface.

Many investigations have been carried out to determine how shot peening affects fatigue crack initiation and propagation life and similar conclusions have been reached. For example, Deng Zeng-Jie et al (24) investigated the effect of shot peening on the initiation and propagation of fatigue cracks from notches in various types of steel tested in three-point bending. They concluded that :-

a) Under conditions of high cycle fatigue, shot peening extends the crack initiation period and has a comparatively minor effect on the crack propagation period (crack initiation being taken as a crack of 0.1mm in depth).

b) When the depth of the crack is shallow, the effect of shot peening on reducing the rate of crack propagation is apparent; the effect decreasing and fading out as the crack penetrates deeper.

Similarly, Burck et al (14), examining the effects of glass bead peening on a nickel base super alloy, concluded that the increase in fatigue life of the peened alloy was primarily due to the inhibition of early crack propagation by the large residual compressive stresses in the surface layers and not due to the suppression of crack initiation.

Further evidence of this was produced by Xa Jia Chi et al (25) who studied the effects of shot peening on the fatigue performance of steel leaf springs. By stopping the fatigue tests before failure and breaking open the specimens, they observed "thumbnail" type cracks on the fracture surface. It was clear that fatigue cracks had been initiated but their growth had been hindered by the layer of residual compressive stress.

Baxa et al (26) also observed thumbnail type cracks on the fracture surface of a peened steel specimen fatigue tested in a sodium chloride solution and they came to similar conclusions. They deduced that the residual compressive stresses resulting from peening significantly retarded crack growth rates during the early

stages of propagation, thus allowing more time for additional fatigue cracks to initiate before stress shielding by a major crack occurred.

The effects of the residual stresses on fatigue in a shot peened spring steel were explained further by Berns and Weber (27). They stated that, for a peened material with a peak residual compressive stress below the surface, a fatigue crack growing towards the peak from the surface will be arrested when the sum of the loading stress and the residual compressive stress attain a stress intensity value at the crack tip which is less than the threshold value for stable crack growth; the crack arrest being prolonged for higher peak compressive stresses and greater depths of the peak stress below the surface. Further growth of the crack, they explained, can only occur when the peak compressive stress is reduced by stress relaxation so as to increase the effective stress intensity at the crack tip to a value greater than that of the threshold intensity for crack growth.

1.4.1.3 Stability of Residual Stresses

The fatigue of shot peened materials often results in a relaxation of the residual stresses induced by the peening treatment. For example, James (28), investigating the effects of fatigue on shot peened aluminium alloys at stress amplitudes between yield stress and endurance limit found that the relaxation of the residual compressive stresses occurred rapidly within the first few cycles; this relaxation decreasing in rate with increasing cycles to some asymptotic value.

Boggs and Byrne (29), working with shot peened Ni20Co alloy found that relaxation of the surface stresses occurred mainly within the first hundred cycles of fatigue when using stresses above the yield stress of the unpeened alloy. However, they found that the residual stresses induced by peening a higher cobalt content alloy, Ni60Co, remained stable during fatigue testing. They concluded that this effect was caused by the different stacking fault energies of the two alloys; the Ni20Co having the higher stacking fault energy making dislocation movement, and hence relaxation, easy.

It should be pointed out that the conditions under which materials are fatigue tested are not always realistic. For instance, in service, most components experience variable amplitudes and loads and this can lead to significant differences in the fatigue lifetimes when compared with the same components tested under constant amplitude loading.

Schutz (30), examining high-strength aircraft alloys, found that the improvements in fatigue resulting from shot peening were greater under constant amplitude loading than variable amplitude loading. After simulating conditions of flight he found that, for an Al-Zn-Mg-Co-Ag alloy, the residual compressive stresses produced by peening had been completely eliminated and that this occurred after only 2% of the total fatigue lifetime. As a result, he concluded that the favourable compressive stresses introduced by peening could not explain the improved fatigue lifetime of this alloy and instead attached some significance to the increased hardness of the peened surface.

The causes of residual stress relaxation in shot peened materials have been summarised by Lieurade and Bignonnet (16) who stated that relaxation depends primarily on the microstructure of the peened material; the greatest amount of relaxation occurring in materials in which the microstructure is affected during loading or at elevated temperatures (for example, the critical temperature at which relaxation occurs in aluminium alloys is in the range of 100 to 120°C).

Relaxation, they reported, is also dependent on several other factors such as the level of cyclic loading, the R-ratio, the nature of the applied stress (e.g. bending or axial loading), the gradient of the residual stresses and the geometry of the specimens under test.

1.4.2 Effect of Surface Finish

Many researchers have concluded that the poor surface finish produced by shot peening is responsible for the rapid initiation of fatigue cracks. Was and Pelloux (21) found that a roughened surface created many fatigue crack initiation sites and surface microcracks. They stated that the fatigue life of shot peened parts is a compromise between a lowered surface tensile stress and a greater number of fatigue crack initiation sites.

Wagner and Luetjering (18), experimenting on a peened Ti-Al-V alloy in push-pull fatigue, found that the removal of the roughened surface caused a marked improvement in fatigue properties.

However, Leadbeater (31) found that the roughness produced by peening had little effect on an extruded Al-Cu-Mg alloy (tested in rotating-bending fatigue). By polishing off the roughened surface to the base of the dimples, he concluded that the surface roughness was not detrimental to the fatigue lifetime of the alloy provided that any defects present were contained within the zone of influence of the surface compressive stress.

It should be pointed out that the alloy used by Wagner and Luetjering (18) was of a considerably higher hardness than that used by Leadbeater (31). Damage in the softer alloy may well have extended to a depth below the base of the dimples (due to the higher degree of deformation). As a result, surface removal to the base of the dimples in the harder alloy could have removed all the damage, thus resulting in the improved fatigue life, whereas in the softer alloy, damage may still have been present.

1.4.2.1 Factors Affecting the Surface Finish

There are several factors which affect the surface roughness of peened materials and it is necessary to understand these in order to try and keep the roughening to a minimum. The main factors involved are shot speed, shot size, shot hardness, the angle of impingement, the degree of coverage and shot condition.

Investigating the effects of peening a steel (45SCD6) with cast steel shot, Niku-Lari (9) found the shot speed, diameter and hardness to be of importance.

a) Shot Speed

Increasing the Almen intensity by increasing the shot speed resulted in deeper indentations and consequently an increased surface roughness.

b) Shot Diameter

The roughness induced by small shot was found to be very high. As the shot size was increased, the roughness decreased until it attained a minimum value; beyond this value it was found to increase, the Almen intensity being the same in all cases.

c) Shot Hardness

Increasing the shot hardness resulted in an increase in surface roughness when using a constant shot size and Almen intensity.

d) Shot Angle

Balcar and Maltby (32), investigating the effects of glass bead peening at various nozzle angles on the surface finish of steel and aluminium specimens, found that decreasing the nozzle angle from 90° to 45° whilst keeping the Almen intensity constant resulted in an increased surface roughness.

e) Coverage

The effect of increasing the coverage on an Al-Zn-Mg alloy above 100% using glass beads was found by Kohler (33) to produce a much rougher surface (when compared to the alloy peened to 100% coverage) with layers of the alloy becoming separated from the matrix material.

f) Shot Condition

A broken shot with sharp edges can clearly produce deep, sharp indentations in a peened surface. As a result, the fatigue life of the part can be impaired due to stress concentrations which may be present below the compressively stressed layer. For this reason it is important in peening operations to screen out all damaged shot before it is fired at the workpiece.

The detrimental effects of broken shot on the fatigue properties of 4340 alloy steel were clearly demonstrated by Simpson and Probst (34) who found that specimens failed at a dramatically reduced number of cycles upon the introduction of broken shot into the shot stream.

Ideally, the shot media should be spherical and investigations are currently being carried out to find a medium which will not readily fracture during peening.

1.4.2.2 Secondary Peening

The effects of secondary peening were first officially reported by Bush et al (35) in 1963. They claimed that secondary peening with smaller diameter media at lower Almen intensities resulted in an improved fatigue life.

Steel shot is the medium normally used to shot peen materials. However, problems of considerable surface roughening can result (due to the high density of the steel) along with problems of contamination if the shot and workpiece are made from different metals. As an alternative, glass beads can be used, giving few

contamination problems but, because of their lower density, they cannot always be used to achieve the required peening intensity.

These problems can be overcome by first peening to the required intensity with the dense steel shot and following with a light glass bead peening. The secondary glass bead peening reduces the surface roughness and removes any remnants of steel shot which may be left in the surface.

Snowman and Schmidt (36), experimenting on the aluminium alloy 7075-T6 in sheet form, found that shot peening resulted in a significant improvement in fatigue life at the cost of a considerably roughened surface. Upon secondary peening with glass beads, they found that the roughness of the specimens was reduced by approximately 50%, this coinciding with a significant improvement in the fatigue life. They attributed this improvement to the smoother surface which reduced the number of crack initiation sites. In order to make a comparison, additional specimens were peened and secondary peened, with steel shot only, to the same intensity as that produced by the glass beads. The test results were found to show only a marginal improvement in fatigue life and surface roughness when compared to the specimens secondary peened using glass beads.

A similar effect was noticed as early as 1940 by Zimmerli (4) who found that a light sand blasting following the shot peening of steel springs produced an improvement in fatigue life when compared with springs which had been peened only.

Further peening treatments (i.e. multiple peening) have been discussed by Woelfel (37) who stated that peening at low intensities with successively smaller and smaller diameter media can result in further improvements in fatigue properties. The effect of this multiple peening is to increase the residual compressive stress at the surface of the peened material whilst maintaining the original depth of the initially peened layer, resulting in a greater fatigue resistance.

1.5 The Effect of Microstructure on Fatigue

Microstructure plays a large part in the improvement of the fatigue properties of alloys by shot peening. Wang et al (38), examining the effects of shot peening on different types of steel and different aluminium alloys, stated that shot peening is a process in which cyclic plastic straining takes place in the surface layers. They concluded that a high dislocation density and a fine subgrain size in the surface after peening are beneficial to the improvement of fatigue properties.

The ways in which the microstructure could be changed in order to affect dislocation motion were discussed by Hornbogen et al (39). They showed that the same amount of microplastic straining of a surface can lead to either one large slip step (heterogeneous deformation, favoured in large grained, low stacking fault energy materials where precipitates are sheared by dislocations) or to many small slip steps (homogeneous deformation, favoured in small grained, high stacking fault energy materials where precipitates are bypassed by dislocation looping). The initiation of a fatigue

crack is more likely at large slip steps (see fig.4). It therefore follows that if the precipitate particles are larger than a critical diameter they are bypassed by dislocations during plastic deformation, and a more homogeneous slip distribution is achieved, leading to smaller slip steps and hence a retardation of crack initiation (40).

In order to obtain a homogeneously deforming material and hence a delay in the time to fatigue crack initiation, Hornbogen et al (39) cold rolled a titanium based alloy before fatigue testing. This led to the expected increase in time to crack initiation but they found that the total fatigue life was reduced as a result of increased crack propagation rates. Graef and Verpoort (41) stated that a delay in fatigue crack initiation requires a homogeneous slip distribution whilst a reduction in fatigue crack propagation rates requires a heterogeneously deforming microstructure. Both of these features can be obtained by using shot peening to cold work the surface only.

On examination of the time to fatigue crack initiation of age hardenable alloys, Hornbogen et al (39) found that initiation occurred at about 20% of the lifetime in the peened alloy and at about 10% in the unpeened alloy. This, they explained, was because the dislocations in the slip bands reacted with the sessile dislocations in the deformation zone so that no sharp slip steps could be formed. Any cracks which did initiate could only grow slowly through the compressively stressed layer.

This was verified by Wang et al (42) who, carrying out fatigue tests on the aluminium 7075 alloy, observed a coarse distribution of slip bands at the surface of the unpeened alloy and a much finer distribution of slip bands in the peened alloy resulting in a much improved fatigue life (it should be pointed out that the roughened surface of the peened specimens had ben removed by electropolishing). They concluded that the microstructural strengthening produced by peening plays an important part in the improved fatigue properties of shot peened alloys.

1.6 Shot Peening Systems

Since the invention in 1926 by Herbert (3) of his Cloudburst process, two main types of shot peening system have been developed; the pneumatic system and the centrifugal system.

1.6.1 The Pneumatic System

In the pneumatic system, the shot is "blown" by compressed air onto the workpiece. The nozzle may be positioned precisely so that the shot stream can be directed onto a given area with the necessary accuracy (e.g. in areas of stress concentration such as fillets and grooves). However, as stated by Milo (43); "... peening is not enough; controlled peening is essential...", and with the pneumatic system there can be large variations in peening intensity due to changes in air pressure. This may be caused by friction effects and plugging which give rise to the wearing away of the nozzle. These problems result in uneven coverage and

excessive noise. A further problem encountered is that of excess moisture in the air stream causing problems with the shot mix or with the parts being peened.

1.6.2 The Centrifugal System

In this system, the shot is fed to the centre of a wheel rotating at high speed where it is flung out along blades radiating from the centre to strike the workpiece.

Compared with the pneumatic system, this system is much more energy efficient, having a much improved velocity control, coverage control and a much greater shot volume flow rate. In fact, centrifugal systems can be up to fifteen times more efficient than pneumatic systems.

1.6.3 Shot Peening Media

The choice of shot peening media depends upon several factors such as the hardness of the workpiece, the intensity of peening required, the nature of the residual stress distribution required, the chemical nature of the surface to be peened and various economic factors.

The main types of peening media used are:-

a) Chilled iron shot; hardness 700 - 1000 hV. This is not ideal as a peening medium since the rapid fracture of shot is undesirable in a peening operation.

b) Steel shot; hardness 300 - 500 hV. This is the most common medium used.

c) Cut wire shot; i.e. drawn wire cut into the form of identical pellets and rounded. This is a useful medium as each pellet is known to be of exactly the same dimensions as the next.

d) Glass beads; useful in cases where contamination of the workpiece by other materials may occur. They are of low density and hence can only be used for light peening operations such as secondary peening.

e) Ceramic beads; (for example ZrO_2) have a high resistance to breakdown and are comparable to steel shot in peening operations (44).

f) Stainless steel shot; a more expensive medium which may be used in some corrosive environments.

1.7 Summary

Shot peening improves the fatigue performance of many materials by introducing a residual compressive stress into the surface layers. However, this improvement is at the cost of a roughened surface which allows early crack initiation and as a consequence, fatigue in shot peened materials is generally thought to be a propagation controlled process.

It is clear from this survey that many questions about shot peening remain unanswered due to the high number of parameters that exist; the unpredictable effects of peening being further accentuated by the lack of adequate control of the peening operation.

The realisation of the requirement for more exacting controls has brought about the incorporation of computers into the shot peening system to monitor and control accurately the peening variables. However, the methods of measurement such as the use of the Almen strip to measure the peening intensity and the measurement of the coverage are still questionable and require further investigation if the shot peening operation is to be fully understood.

CHAPTER TWO

FRETTING-FATIGUE

2.1 Introduction

When the surfaces of two metals in contact undergo a small cyclic rubbing movement, damage occurs at the area of slip, especially near the edge of the region of contact. This is known as fretting, or fretting-corrosion if the debris produced is the product of a chemical reaction of the metal with its environment. When a fretting action is combined with fatigue cycling, materials often fail at a significantly lower number of fatigue cycles than the predicted number for the same material under plain-fatigue conditions.

2.2 Fretting

The following is a review of some of the theories of fretting.

In 1927, the term "fretting-corrosion" was coined by Tomlinson (45) who associated it with the damage found on steel surfaces as a result of this process. He suggested that fretting occurred because of molecular attrition and also that the cohesive forces between surface molecules resulted in their tearing away before becoming oxidised.

In 1939, Tomlinson et al (46) observed that the effects of fretting-corrosion were only found on vibrating machine components in contact. They rejected the idea that the fretting process was

abrasive, stating that it was caused by a process where two surfaces approached so closely that the force fields of the atoms of the different surfaces interacted with eachother causing molecular attrition.

In 1953, Godfrey (47) came to the conclusion that the contact of surfaces led to adhesion and that these surfaces then broke loose leaving small particles which oxidised. He also observed that fretting occurred in less than one cycle, implying that a cyclic mechanism is not necessary for this process to occur.

In 1952, Wright (48) concluded that oxygen played a major role in the fretting process.

In 1954, Uhlig (49) explained the mechanism of fretting in terms of a chemical process and a mechanical process. He assumed that damage was caused by an array of asperities which wiped off the oxide film on the metal surface, this oxide immediately reforming, only to be wiped off by the asperities in the following half of the cycle; this being the chemical factor involved. He also assumed that the metal was removed directly by asperities digging into the surface giving rise to stress raisers; this process being the mechanical factor. However, Halliday and Hirst (50) showed that the fretting process was not dependent upon the formation of an oxide layer.

In 1956, Feng and Rightmire (51) also put forward a theory of fretting, stating that the process consisted of four stages:-

a) The "initial stage" which consisted of the break-away of surface particles.

b) The "transition period" which consisted of the oxidation of these particles.

c) The "declining stage" where these oxidised particles acted as an abrasive medium.

d) The "steady stage" where the oxide became so thick that it reached a saturated level (i.e. a steady state of wear was reached).

More recently, in 1975, Waterhouse (52) stated that metallurgical structures in a metastable state, such as age-hardened materials, were particularly susceptible to fretting. He suggested that over-ageing occurred in the region of fretting of age-hardened materials.

In 1983, Leadbeater (31), conducted a study of the debris produced on the fretted surface of the aluminium alloy 2014A. He revealed that much of the debris was spherical in shape. Such debris was first observed in tribological situations, the formation of which was associated with the plastic deformation and heavy wear of non-spherical primary wear debris in sockets or against heavy ridges (53).

2.3 Fretting-Fatigue

The large reduction in fatigue life experienced by many fretted materials is, as stated by Wharton et al (54), associated with the rapid initiation of fatigue cracks in the fretted region; growth occurring at an oblique angle to the surface. Once beyond the region over which the fretting forces act, crack growth changes to a direction normal to the applied stress.

In general it is found that a region of non-slip exists adjacent to the region of slip between two fretting surfaces. There has been some confusion as to the area of initiation of fretting-fatigue cracks in this region; some authors believing that initiation occurred at the boundary between the slip/non-slip region of the fretted surface (55). However, later research has revealed that initiation occurs in the area near to the edge of the fretting/non-fretting region of the surface (56), a region which experiences the greatest shear stress. The growth of such fatigue cracks has been found to be in a direction into and underneath the contacting surfaces.

2.4 Factors Affecting the Fretting-Fatigue Process

There are many factors which affect the rate of fretting-fatigue. The principal factors are listed below.

a) Contact Pressure

An examination by Corten (57) of the effect of varying the contact pressure on the fretting-fatigue strength of two aluminium alloys revealed that this strength was only affected significantly at

pressures above approximately 20MPa. Below this value, the fretting-fatigue strengths of the alloys were found to increase.

b) Slip Distance

Investigating the effects of slip distance between surfaces in contact, Fenner and Field (58) found that the fretting-fatigue strength decreased with increased slip up to a slip amplitude of 15μm. Above this value no further decrease was observed.

c) Hardness

The hardness of the materials in contact has also been found to affect the rate of fretting-fatigue. For example, Waterhouse (59), experimenting on steels in contact with various metals and alloys, came to the conclusion that fretting damage to the steel decreased with the decreased hardness of the metal or alloy. He stated that the metal which damaged the steel least, as well as being of low hardness, was of high thermal conductivity, high stacking fault energy (and therefore low work-hardening ability) and low recrystallisation temperature.

d) Frequency

Investigating the effects of frequency on the fretting-fatigue strength of carbon steels in reversed-bending and torsion-testing, Endo et al (60) found that the lower the cyclic frequency, the shorter the lives of the specimens in terms of the number of cycles. They also found that fretting only had an effect during the first part of the test; after this the fracture process was due to fatigue only.

f) Surface Roughness

A roughened surface is generally found to be detrimental to the plain-fatigue properties of materials due to the large number of stress concentrations. However, as suggested by Waterhouse (61), an increased surface roughness may be beneficial to the effects of fretting; the peaks of the roughened surface deflecting elastically under the fretting action and thus taking up some of the relative movement (slip) between the surfaces.

2.5 The Alleviation of Fretting-Fatigue

The suppression of fretting-fatigue in aluminium alloys has been neatly summarised by Bowers et al (62), who stated that this problem can be significantly reduced by;

a) Interposing greases or resins loaded with graphite, molybdenum disulphide or PTFE between the surfaces in contact. This has the effect of preventing surface contact and thus fretting. However, the treatment is not effective over long lifetimes since the grease or resin can be squeezed out from between the contacting faces or be broken up under high stresses. Further problems of corrosion between the resin and alloy can also render this treatment unsuitable.

b) Applying sprayed metal coatings to the surfaces in contact. This treatment has been found to reduce the effects of fretting-fatigue, cracks initiating from the fretted surface but growing along, rather than across the interface, between the coating and the underlying metal. However, although fatigue failure of metal sprayed parts occurs away from the fretted

region, the fatigue properties are not raised to the stress levels achieved by polished parts tested in plain-fatigue.

c) Shot peening the surfaces in contact. This treatment has been found to be effective in nullifying the effects of fretting due to the presence of the residual compressive stress induced by the peening; fatigue cracks initiating from the fretted region being unable to grow through the residually compressed layer.

Careful attention to design can also relieve the effects of fretting. For example, Bowers et al (62) found that stress relieving grooves positioned either side of the surfaces in contact significantly improved the fretting-fatigue strength of an aluminium alloy.

2.6 Summary

The early failure of parts experiencing fretting-fatigue occurs due to the rapid initiation of fatigue cracks at the edge of the fretted region; the cracks initiating from the fretted surface and growing into the surface at an oblique angle before propagating in a direction normal to the applied stress. The effects of fretting can often be suppressed by the use of shot peening.

CHAPTER THREE

THE EFFECT OF SHOT PEENING ON FRETTING-FATIGUE

3.1 Introduction

The use of shot peening to improve the resistance of many materials to fretting-fatigue is only a recent development which has not been greatly researched.

3.2 Shot Peening and Fretting-Fatigue

As with plain-fatigue, the beneficial effects of shot peening on the fretting-fatigue performance of an aluminium alloy were found to be due to the presence of the residual compressive stress (62); the stress preventing the propagation of cracks initiated by fretting, resulting in an improved fatigue strength of the alloy under fretting conditions.

Examining the effects of fretting-fatigue on shot peened stainless steel and mild steel specimens, Waterhouse and Saunders (63) concluded that controlled shot peening, particularly of soft but work-hardenable materials, had a significant effect on the fretting-fatigue behaviour. Waterhouse (64) stated that an increase in the number of cracks in a surface resulted in a decrease in the stress intensity at the tip of these cracks and consequently in a reduction in fatigue crack growth rates.

An investigation into the effects of shot peening on the fretting-fatigue strength of the aluminium alloy 2014A, by Noble and Waterhouse (65), led to the conclusion that the improvement in fretting-fatigue properties produced by the shot peening arose mainly from the residual compressive stress, the work-hardening of the surface layers having little effect. The residual compressive stress produced by the shot peening was found to be approximately 250MPa at the surface and this stress, they found, faded rapidly under fretting conditions.

The aluminium alloy 2014A was found by Fair et al (66) to be insensitive to fretting damage if peened before the final ageing treatment. Although the compressive stress at the surface had been reduced significantly, they concluded that the insensitivity to fretting-fatigue was due to a microstructural effect; shot peening in the solution treated condition introducing a very high concentration of dislocations into the surface of the specimen and subsequent ageing resulting in extensive precipitation of the transition phase on the dislocations. The resulting microstructure was much more resistant to any stress fading caused by fatigue and fretting action.

3.3 Summary

The reduction in susceptibility to fretting-fatigue of many alloys by shot peening has been found to be primarily as a consequence of the residual compressive stresses induced by the peening treatment.

CHAPTER FOUR

THE HIGH-STRENGTH ALUMINIUM ALLOY 7010

4.1 Introduction

The 7000 series of aluminium alloys (Al-Zn-Mg) have the greatest potential of all the aluminium alloys for age-hardening. Additions of copper also been made into this system to improve the resistance to stress corrosion cracking of the very high strength alloys. However, these alloys suffer from problems of quench rate sensitivity (limiting the maximum plate thickness which can be produced), susceptibility to stress corrosion cracking and low fracture toughness. In an attempt to overcome these problems, the high strength alloy 7010 has been developed.

This chapter describes the ternary Al-Zn-Mg system upon which the 7000 series is based, the effects of copper additions to this system and the development of the new 7010 alloy by the modification of the well known 7075 alloy.

4.2 The Al-Zn-Mg System

Zinc is highly soluble in aluminium and exerts little influence on the microstructure. However, the addition of magnesium allows the precipitation of the strengthening phase η' ($MgZn_2$) to occur.

Ageing of the solution heat treated and quenched Al-Zn-Mg system produces the principal phases; α (the solid solution), G.P. zones (a metastable transition phase precipitating early on in the ageing sequence), η' ($MgZn_2$, a metastable transition phase) and η

($MgZn_2$, an equilibrium intermetallic). A further equilibrium phase, T ($(AlZn)_{49}Mg_{32}$) has been observed (67) but since it is a coarse precipitate (resulting in little improvement in strength) produced during overageing and since the alloy studied in this research project was in the peak-aged condition, little attention will be paid to the formation of this phase.

The precipitation sequence upon quenching from the solution treatment temperature is;

$$SSSS \longrightarrow \text{GP Zones} \longrightarrow \eta'(MgZn_2) \longrightarrow \eta(MgZn_2)$$

as determined by Lorimer (68).

4.2.1 G.P. Zone Formation

The nucleation of the metastable, coherent GP zones occurs homogeneously by spinodal decomposition (where rich areas become richer in solute and the poor areas become poorer); their formation requiring the movement of atoms, aided by vacancies retained during the quenching treatment, over very small distances. The resulting very small and finely dispersed precipitates are coherent with the matrix producing an increase in the strength of the alloy by the presence of the elastic strains required to accommodate them. These GP zones consist of alternate zinc-rich and magnesium-rich layers lieing on the (001) planes (69), the precipitates being spherical in shape (67).

4.2.2 The η' Phase

The η' phase has the formula $MgZn_2$. There has been some confusion as to the mechanism of formation of this phase. However, recent research has led to the theory that the nucleation of the η' phase begins at small vacancy rich solute clusters formed during quenching in low concentration alloys (where the concentration of zinc is less than 2.5% and Mg is less than 2.0%) and at GP zones in the more highly concentrated alloys (where the GP zones are above a critical size required for the nucleation of η' (70)). Other mechanisms of precipitation include nucleation at concentration fluctuations left behind by dissolving GP zones and at impurity atom clusters (71). Later work by Park and Ardell (67) on the alloy 7075 in the T651 condition found that a small proportion of the η' particles were also heterogeneously nucleated on dislocation lines.

The η' phase was found by Auld and Causland (72) to have a hexagonal structure with lattice parameters; a = 0.489nm and c = 1.374nm, the precipitates being plate shaped and forming on the (111) planes. On examination of the commercial 7075 aluminium alloy in the peak-aged condition, Park et al (67) found the plates to have diameters ranging from 3nm to 10nm. The maximum strength of the Al-Zn-Mg system has been attributed to the formation of a fine distribution of these η' precipitates.

4.2.3 The η Phase

The equilibrium η phase has the formula $MgZn_2$. Although the formula of η is the same as that of η', the crystal structure is different, being the hexagonal C14 type (where the atoms occupy different spaces in the lattice) with lattice parameters; a = 0.521nm and c = 0.860nm (73).

Three different shapes of the precipitates have been observed (plates, rods and laths) having incoherent interphase boundaries with the aluminium matrix and therefore having less influence on the strength of the alloy than the semi-coherent η' precipitate.

4.2.4 Stress Corrosion Cracking in the Al-Zn-Mg system

A major problem experienced by the Al-Zn-Mg system is that of stress corrosion cracking. This occurs in the region of the grain boundaries where the presence of precipitate free zones and large precipitates at the boundaries result in bimetallic corrosion; crack growth also preferring these zones since the alloy is softer in this region.

4.3 The Al-Zn-Mg-Cu System

Several effects on the microstructure have been observed upon the addition of copper to the Al-Zn-Mg system. Thompson (74) proposed that copper additions promoted the nucleation of GP zones and η' precipitates. Bryant (75) reported that the solubility of zinc and magnesium in aluminium was reduced by the addition of copper; resulting in an increase in the state of supersaturation of the alloy which thus more readily decomposed during quenching and

ageing than the corresponding alloy without copper. Copper has also been found to accelerate precipitation at lower ageing temperatures (76). More recent work by Livak et al (77) has indicated that copper promotes the precipitation of the η' phase by enhancing the formation of Cu-Mg-vacancy complexes during quenching which consequently act as nucleation sites for this phase. It has been suggested that additions of copper result in the precipitation of the S' (Al_2CuMg) phase. However, this phase was not observed in the commercial 7075 alloy investigated by Wert (78).

The effects of copper additions on the mechanical properties of the Al-Zn-Mg system are varied, the addition showing only a limited increase in the strength along with an increase in the quench sensitivity. However, a significant reduction in the susceptibility to stress corrosion cracking is observed due to the increased precipitation of η' in the depleted area adjacent to the grain boundaries. This causes an increase in the strength in the region of the grain boundaries along with a reduced electrochemical difference between the boundary precipitates and the matrix.

4.4 The Modification of Alloy 7075

The excellent response to age-hardening of the Al-Zn-Mg-Cu alloys has been known for many years. For example, in 1917, an alloy was developed (Al-20Zn-2.5Cu-0.5Mg-0.5Mn) which had a tensile strength of 580MPa; however, it proved unsuitable for structural use because of its high susceptibility to stress corrosion cracking.

More recently, the alloy 7075 (Al-Zn-Mg-Cu-Mn-Cr) has been developed and used in aircraft structures because of its high strength to weight ratio. The stress corrosion problems along with the quench rate sensitivity and need for improved toughness resulted in investigations by Fitzsimmons (79) to modify this alloy.

4.4.1 Quench Rate Sensitivity

Quench rate sensitivity was found in the 7075 alloy to be caused by the recrystallisation inhibitor chromium. The chromium was therefore replaced by zirconium as a recrystallisation inhibitor and as a result, the quench sensitivity of the alloy was significantly improved. Consequently, plate up to a thickness of six inches can now be produced without loss of useful strength. Polmear (80) suggested that the improvement was caused by the fact that the chromium combines with some of the principal alloying elements to form $Al_{12}Mg_2Cr$ thus removing them from solid solution, whereas zirconium forms insoluble particles of $ZrAl_3$.

4.4.2 Toughness

The low toughness of the 7075 alloy has been attributed to the high degree of impurities (especially iron and silicon) which allow the nucleation of voids by decohesion at the interface between these second phase particles and the matrix. As a result, the toughness was improved by restricting the impurity content in order to keep the volume fraction of these intermetallic phases to a minimum. A copper content of below 2% was found to assist in the minimisation of these undissolved second phases. Improvements

in toughness are also produced on the replacement of chromium by zirconium (81); the zirconium producing smaller precipitates and thus nucleating smaller, less harmful microvoids with the onset of cracking.

4.4.3 Stress Corrosion Cracking

In Al-Zn-Mg alloys, copper is added in order to improve the stress corrosion cracking resistance but at the same time, problems in castability such as hot shortness are encountered. Investigating the effect of copper content on alloy 7010, Fitzsimmons (79) found that the level of copper did not significantly reduce the stress corrosion cracking resistance when its concentration exceeded 1.7%. As a result the copper level in this alloy was decreased to 1.7%.

Gruhl (82) found that stress corrosion cracking is also kept to a minimum if the Zn:Mg ratio is kept between 2.7 and 2.9; the ratio in alloy 7010 is close to this, with a value of 2.5.

Further reductions in the susceptibility to stress corrosion cracking can be obtained by reducing the width of the precipitate free zone. This can be carried out simply by using high solution treatment temperatures and faster quenching rates; the higher solution treatment temperature increasing the vacancy concentration and the rapid quenching rate allowing less vacancy migration to the boundaries. As a result, a higher concentration of vacancies exists nearer to the grain boundaries allowing more precipitation in this region.

4.5 Specifications

The requirements by the aircraft industry were for a plate material with a British development specification DTD 5120. For a 25mm plate, the specifications in the longitudinal directions are shown in fig. 5.

4.6 Heat Treatment of Alloy 7010

The section of interest of the Al-Zn-Mg-Cu phase diagram at 6wt% Zn is shown in fig 6. The composition of alloy 7010 is shown in fig. 11.

The ageing of 7010 is carried out isothermally at 170°C after quenching from a solution treatment temperature of 475°C. The ageing curves are shown in fig 7.

4.7 Summary

The 7075 aluminium alloy derives its strength properties from the transition precipitate η' ($MgZn_2$). The development of the high strength 7010 alloy based on this system has become of interest since the problems of the low fracture toughness associated with the 7075 alloy along with the problems of stress corrosion and quench rate sensitivity have been reduced significantly by refining this alloy, adjusting the composition and by replacing the recrystallisation inhibitor chromium with zirconium.

CHAPTER FIVE

THE ALUMINIUM-LITHIUM BASED ALLOYS

5.1 Introduction

Of all the metals found in nature, lithium is the least dense and its addition to aluminium has produced an alloy of very low density. In fact, aluminium-lithium alloys are now of great interest to the aerospace industries because the low density is accompanied by a high elastic modulus and high strength properties. However, the ductility and fracture toughness properties of these alloys are low and this factor must be taken into account when designing components that are to be made from Al-Li based alloys.

5.2 The Aluminium-Lithium System

The principal phases are α (Al-Li solid solution), δ (AlLi, an equilibrium intermetallic) and δ' (Al_3Li, a metastable, ordered transition phase). The Al-Li alloys of interest contain 2-3% Li and the precipitation of the δ' phase leads to excellent strength and modulus properties.

The aluminium rich region of the phase diagram is shown in fig. 8.

The alloys based on this system are of the age-hardenable type, the precipitation sequence upon quenching from the solution treatment temperature being:-

$$SSSS \text{ -----> } \delta'(Al_3Li) \text{ ----> } \delta(AlLi)$$

as determined by Noble and Thompson (83).

5.2.1 The δ' Phase

The metastable, coherent δ' phase is homogeneously nucleated at temperatures below that of the δ' solvus. However, there is some dispute as to the mechanism of the nucleation. One mechanism by Nozato and Nakai (84), where the α solid solution undergoes precipitation of δ' via GP1, GP2 and δ" (a short range, ordered δ') has been proposed. Another mechanism proposed by Tanner and Leary (85) involves a process analogous to spinodal decomposition but this has been found difficult to prove or disprove owing to the nature of the aluminium lattice.

5.2.1.1 The Structure of δ'

The lattice parameter of the strongly ordered δ' phase is close to that of the α matrix and, because the precipitate is coherent with the matrix, a small misfit strain exists. As a consequence of the low misfit strain, the δ' precipitates are homogeneously nucleated and spherical (this being the geometry required to produce a minimum surface area to volume ratio).

5.2.2 The δ Phase

The equilibrium δ phase is heterogeneously nucleated at temperatures below the δ solvus at both grain boundaries and in the matrix, the precipitates normally being surrounded by dislocations and a δ' precipitate free zone. The dislocations are present due to the semi-coherent nature of the α/δ interface and the precipitate free zones result from preferential dissolution of the metastable δ' phase.

Few investigations have been carried out concerning the mechanisms of the δ' ---> δ transformation. One proposed mechanism by Schlegoleva and Rybalko (86) is based on the in-situ transformation from a face centered cubic structure (δ') to a body centered cubic structure (δ). However, it is more likely that the δ phase is nucleated independently of the δ' phase (87), growth of the δ taking place by the dissolution of the surrounding metastable δ'. Williams (88) is also of this opinion due to the fact that the lattice strain generated by the coherent δ' is too low to be of possible use as a heterogeneous nucleation site for δ, and concluded that the large heterogenities such as dislocations and grain boundaries would be more suitable, especially when considering the large α/δ misfit, the large change in lithium concentration, and the new crystal structure of δ.

5.2.2.1 The Structure of δ

The δ phase is cubic with a lattice parameter of 0.637nm (89). When compared to the lattice parameter of aluminium (0.405nm) it is clear that the δ precipitate must have either incoherent or semi-coherent interfaces with the matrix.

5.3 The Effect of Lithium on the Mechanical Properties of Binary Aluminium-Lithium Alloys

5.3.1 Modulus

Aluminium-lithium alloys have a 10% higher elastic modulus than the currently used aluminium alloys. It has been thought that the high elastic modulus and strength found in binary aluminium lithium alloys is caused by the presence of the δ' precipitate. However, Harris et al (90) have shown that a high elastic modulus is observed in Al-Li alloys even when all the lithium is in solid solution. They concluded that the high modulus of these alloys results from an increase in the bond strength between atoms in solution rather than from the presence of the δ' phase.

5.3.2 Density

Increasing the lithium content results in a reduction in density in an approximately linear fashion (see fig.9a). For example, the density of pure aluminium is 2,700 kg/m^3 and the density of Al 2.5wt%Li is 2,500 kg/m^3, giving a 7.5% reduction in density. When the large increase in modulus is combined with the low density it

can be seen why such an interest has been taken in the Al-Li alloy system for aerospace applications.

5.3.3 Strength

Lithium in solid solution has little effect on the mechanical strength. Significant improvements in strength can only be produced by ageing the alloys to produce a fine dispersion of δ' precipitates.

5.3.4 Ductility and Fracture Toughness

The low ductility and fracture toughness of the binary Al-Li alloys are associated with the formation of the δ' phase. As described by Gayle (91), a dislocation cutting through a δ' precipitate results in an anti-phase domain boundary in that precipitate. This boundary is of a higher energy and hence it is favourable for another dislocation to pass through this precipitate along the same plane to eliminate the fault and hence reduce the energy. As a result of this the dislocations in Al-Li alloys travel in pairs and therefore cannot easily change slip planes. This produces precipitates of smaller cross-section on a given slip plane and hence it is easier for other dislocations to follow this path, less energy being required to cut through the smaller precipitates on this plane. The result is an intense planar slip during deformation, which produces stress concentrations where the slip planes impinge on the grain boundaries, and subsequent grain boundary failure.

5.4 Improvement of the Mechanical Properties of the Binary Aluminium-Lithium Alloys

Improvement of the poor toughness and ductility characteristics of these alloys may be carried out by reducing the amount of planar slip that takes place. Such slip dispersal can be achieved by several methods, including the reduction in grain size and the addition of further alloying elements such as magnesium, copper, copper with magnesium and zirconium.

5.4.1 Magnesium Additions

Additions of magnesium produce a further reduction in the density of the Al-Li alloys; it also has the effect of reducing lithium solid solubility in aluminium resulting in a higher volume fraction of the δ' phase and therefore improved strength. Unfortunately, the additions of magnesium produce a reduction in the elastic modulus of the Al-Li alloys. However, the reduction in modulus is almost exactly balanced by the decrease in density so that the specific modulus is unchanged.

5.4.2 Copper Additions

Additions of copper produce a slight increase in the modulus relative to the binary Al-Li alloy. However, copper also produces a noticeable increase in density of this alloy (92). Consequently the specific modulus of this alloy is not much greater than that of pure aluminium.

As found by Sankaran and Grant (92), the solid solubility of pure copper is reduced when the lithium concentration exceeds a certain level. The decreased solubility of copper, they found, resulted in second phase particles which increase fatigue crack growth rates. This led to investigations from which they concluded that the copper level must be kept below 1.5 to 2.0wt% in aluminium-lithium alloys containing about 3wt% lithium in order to prevent this from occurring.

The presence of copper in Al-Li alloys promotes the precipitation of a ternary Al_2CuLi phase as well as the $\delta'(Al_3Li)$ phase (83). The Al_2CuLi precipitates as thin plates on the (111) planes and helps to disperse the slip which occurs on these planes and so produce a small increase in ductility. However, plate precipitates on the (111) planes are not very efficient at dispersing slip. As a result, combined additions of copper and magnesium have been made to the Al-Li system to promote the precipitation of another phase, $S'(Al_2CuMg)$, which is more efficient at reducing intense planar slip.

5.4.3 Copper and Magnesium

Additions of copper and magnesium to the aluminium-lithium alloys result in an overall increase in modulus and density. The effect of these additions on the specific modulus relative to the binary Al-Li alloys is therefore small. The strengthening phases are a mixture of $\delta'(Al_3Li)$ and $S'(Al_2CuMg)$, the latter growing as laths elongated in the <100> Al directions with an open-packed orthorhombic structure. These S' precipitates reduce the intense

planar slip and so improve the ductility and toughness of the alloy (93).

The S' phase is heterogeneously precipitated on dislocations but, because of the small number of dislocations present in the as-quenched alloy, the proportion of this S' phase is low. In order to increase the proportion of S' phase present and therefore improve the mechanical properties of these alloys, a pre-ageing stretch is introduced which has the effect of increasing the number of dislocations, resulting in a considerable increase in the proportion of S' precipitation on ageing.

On comparing the aluminium-lithium alloys containing 2.0wt%Mg-1.5wt%Cu and 0.5wt%Mg-1.2wt%Cu, Gregson et al (94) found that the more dilute alloy had sufficient solute present to achieve adequate strength through δ' and S' precipitation whilst still showing the required reduction in density and increase in modulus. They suggested that this alloy was the more favourable of the two as it was more likely to show superior toughness and ductility compared with the higher solute content alloys.

5.4.4 Zirconium

The intense planar slip observed in aluminium-lithium alloys can also be reduced by making alloying additions which reduce grain size and inhibit recrystallisation. This has the effect of reducing the amount of slip which may occur on a given plane, reducing the stress concentration which can occur at the grain boundaries and hence increasing the strength, ductility and fracture toughness of the alloy.

In order to reduce grain size and inhibit recrystallisation, small amounts of zirconium are normally added. Harris et al (90) showed that increasing the zirconium content of an Al-Li-Mg alloy from zero to 0.2wt% resulted in a linear increase in the tensile strength, proof stress and fracture toughness. The elongation, they found, rose to a maximum of between 10% and 15% at 0.05wt%Zr (see fig. 9b).

The grains in these alloys in which recrystallisation has been prevented are in the as-rolled condition, that is, elongated in the rolling direction. Within these grains it was found that a stable sub-structure existed, the size of which varied with zirconium content (the approximate sub-grain size, they found, was 2-4μm). It is this sub-structure which is largely responsible for the improved tensile and fracture toughness properties. In fact, the fracture toughness of this alloy increased from below 10MPa$\sqrt{m}$ to a level close to that of the 2000 series of aluminium alloys on addition of 0.2wt%Zr. Furthermore, it was found that the fracture surface of this alloy showed some evidence of plastic tearing along with the more usual intergranular fracture.

5.5 Commercial Aluminium-Lithium Based Alloys

Commercially available aluminium-lithium based alloys are now available in sheet, plate and extruded form, the percentage composition being Al-2.5%Li-1.2%Cu-0.7%Mg-0.12%Zr by weight. This is one of the alloys being studied in the present work. The alloy is solution treated at a temperature of 520°C, water quenched and then aged at temperatures between 175°C and 195°C. Typical properties produced by ageing at several temperatures are given in

fig. 10. The alloy is designated 8090, having a modulus of 81GN/m^2, a density of 2,550kg/m^3 and therefore a specific modulus of 3.2MNm/kg.

5.6 Summary

The problems associated with the aluminium-lithium system have been reduced to an acceptable level by the additions of copper and magnesium along with zirconium. The resulting 8090 alloy still experiences a high degree of slip. However, the low fracture toughness normally observed in aluminium-lithium alloys has been increased sufficiently to a value close to that of other high-strength aluminium alloys, to make this a very promising alloy for future use.

CHAPTER SIX

EXPERIMENTAL PROCEDURE

Introduction

This chapter covers the experimental procedures used throughout this research project ranging from material composition and treatment to testing and post-testing analysis.

6.1 Materials and treatments

The purpose of the research was to examine the effects of different levels of shot peening on the fatigue properties of two fully heat treated, high-strength aluminium alloys.

6.1.1 Materials

The two high-strength aluminium alloys used in this work were 7010 (Al-Zn-Mg-Cu-Zr) and 8090 (Al-Li-Cu-Mg-Zr); the analysed composition of each is given in fig. 11. Each alloy was received from the manufacturer as rolled 25mm thick plate and 9.5mm diameter extruded rod.

6.1.2 Heat Treatments

Both alloys are of the age-hardenable type and were heat treated to give peak strength properties.

Alloy 7010 was solution heat treated for 30 minutes at 475°C, quenched in water, cold stretched (in the case of the extruded rods) 2.5% and then aged for 6 hours at 170°C. Cold stretching is necessary in the 7010 alloy to restraighten the rods since quenching after solution treatment often results in a slight distortion due to the rapid drop in temperature.

Alloy 8090 was solution heat treated for 30 minutes at 530°C, quenched in water, cold-stretched to an elongation of 2.5% and then aged for 16 hours at 190°C. Since the precipitation of one of the strengthening phases, S' (Al_2CuMg), occurs on dislocations (see section 5.4.3), the cold stretching operation is not only required to restraighten distorted rods, it also introduces additional dislocations on which the S' phase can precipitate during subsequent ageing. For this reason both the rolled plate and the extruded rods were stretched by 2.5% between the solution treatment and ageing.

In order to prevent any natural ageing at room temperature, all specimens of both 7010 and 8090 alloys were kept refrigerated between solution treatment and ageing.

6.1.3 Surface Treatments

Three different surface treatments were used for both alloys in this work; the treatments being unpeened, peened to a light intensity and peened to a heavy intensity. In both cases of peening, steel shot of 1.40mm diameter with a Vickers hardness in the range 450-550 were used. The three treatments are listed below;

a) Unpeened: A number of specimens were required for testing in the unpeened condition for use as control samples.

b) Shot peened (12-16A): Specimen gauge lengths/notches were peened to a light intensity of 12-16A on the Almen scale.

c) Shot peened (8-10C): Specimen gauge lengths/notches were peened to the heavier intensity of 8-10C on the Almen scale.

Details of the peening treatments and heat treatments of both alloys are summarised in fig. 12.

6.2 Fatigue Testing (Reversed-Bending)

This research project required the testing of the two materials (with the various surface treatments) under conditions of plain-fatigue and fretting-fatigue. Reversed-bending specimens incorporating a large U-shaped notch were constructed to monitor crack growth during plain-fatigue. Rotating-bending specimens were prepared to examine the effects of fretting on the fatigue performance of the alloys (see section 6.3). This section covers the experimental procedure for testing in reversed-bending fatigue.

6.2.1 Specimen Dimensions

The dimensions of the reversed-bending specimens used in this work can be seen in fig. 13a. The specimens were initially cut from rolled 25mm thick plate, their dimensions being 120mm (length,l) x 25mm (height,h) x 20mm (width,w); the length of the specimen being

in the longitudinal rolling direction and the height being the thickness of the plate. A notch of 3mm radius was then machined across the full width of the specimen, a large radius clearly being necessary to allow adequate peening of the notch. A notch depth (D) of 6.25mm was chosen giving a D/h value of 0.25 and a theoretical stress concentration factor based on the net section of the specimens of 2.03. 6mm diameter screw holes were tapped to a depth of 5mm at the centre of each end of the specimens to allow the attachment of the current leads from the electrical p.d. power unit (see section 6.2.4.1). The length of the specimens was chosen as 120mm in order to accommodate these holes without disturbing the stresses set up in the specimen by the four-point bending system (see section 6.2.3).

6.2.2 Test Calculations

The method of calculation of the bending stresses at the base of the notch is shown in appendix 1.

6.2.3 Testing Equipment

Specimens were tested using a four-point bending apparatus as seen in plate 1a. This is shown schematically in fig. 13b where it can be seen that the outer rollers (on the notched surface) were set at a distance of 100mm apart whilst the inner rollers were set at a distance of 20mm apart.

6.2.4 Crack Monitoring Systems

Two methods of fatigue crack detection were employed during reversed-bending fatigue testing; an electrical-potential drop technique and a plastic replication technique. The potential drop technique is suitable for long crack detection and the latter more suitable for the monitoring of short cracks.

6.2.4.1 The P.D. Crack Monitoring System

In order to monitor crack growth a large electric current was passed through the specimen during fatigue testing. Probes attached by spot welding to opposite corners of the notch (see section 6.2.5) were then used to monitor the variation in potential difference across the notch as fatigue crack growth occurred. The probes were connected via amplification apparatus to a chart recorder (a JJCR600) where the electrical-potential variation across the notch was recorded as a function of time.

The electrical source for the crack monitoring equipment was a Mayes power system capable of maintaining a constant current through the specimen regardless of the potential across it. This system also incorporated the amplification unit necessary to increase the variation in potential across the notch to a quantity capable of measurement by the chart recorder.

A limitation of the electrical-potential technique of crack measurement is the lack of sensitivity to fatigue crack initiation and early growth, a limitation which becomes more pronounced as the notch radius increases (95). Since the notch radius of the reversed-bending specimens used in this project was large, this

technique was insensitive to crack initiation and early growth and, as a result, a different method of crack detection was required for the early stages of fatigue.

6.2.4.2 The Replication Technique

The replication technique is particularly useful for the monitoring of fatigue crack initiation and early growth. The method involved the use of sheets of cellulose acetate which were softened in acetone and placed over the area in which crack initiation was expected. Once applied to the specimen surface, the sheet was left to harden, after which it could be removed containing an exact imprint of the surface with all its defects. The replicas were then stored for later examination. Since fatigue crack initiation is not predictable, replicas had to be taken periodically until a crack was visible and had been detected by the p.d. technique. Fatigue cracks could then be followed back to the point of initiation by examination under an optical microscope (see section 6.4.3).

This method of crack detection was particularly useful since it recorded accurately the progress of the crack throughout its early life. However, a limitation to the method was the fact that the fatigue test had to be stopped each time a replica was taken.

6.2.5 Specimen Preparation

All the notches of the unpeened reversed-bending specimens were carefully mechanically ground in the longitudinal direction with fine 000 grade emery paper (using water as a lubricant) to produce

a smooth surface. The notch was then polished using cotton wool soaked in a liquid metal polish to give a "mirror finish".

After peening, the notches in all reversed-bending specimens were again ground in the longitudinal direction using fine 000 grade emery paper. Layers were removed until the base of the dimples produced by peening were reached. The ground surface was then polished using cotton wool soaked in liquid metal polish. This procedure was necessary to enable the progress of very small fatigue cracks to be monitored; small crack detection being practically impossible without grinding and polishing due to the rough nature of the peened surface. The removal of this roughness has been found to have little effect on the fatigue properties (31).

After surface preparation, high purity aluminium-magnesium alloy probe wires were spot welded to opposite corners of the notch, the wires being insulated and taped securely to the specimen as seen in plate 5. In order that the spot weld did not become loosened by accidental knocking, a small amount of quick setting epoxy resin was applied after welding to strengthen the junction.

6.2.6 Testing Procedure

Once prepared, the specimen was placed in the grips of the machine, the notch being placed centrally between the rollers to ensure a constant bending moment in that region. The power supply leads were connected to the specimen by means of bolts as seen in plate 1a and the probe wires were connected to the amplifier. The current through the specimen was then increased until an amplified

voltage of 0.2V was obtained on the chart recorder; this current being 5A for the 8090 alloy and 11A for the 7010 alloy. The difference in current required by the two alloys was due to their different electrical conductivities, this being particularly low in the case of the 8090 alloy owing to its high lithium content.

The specimens were tested at 6.7Hz using an R-ratio of 0.1. The applied stress range was changed to a different value for each new specimen in order that a suitable variation in data could be accumulated, tests being carried out at ranges between 340MPa and 507MPa.

The plastic replication technique was used until a fatigue crack had grown throughout the width of the specimen; beyond this point replication was clearly of no use since crack growth was away from the notch surface. The p.d. technique of crack measurement was used throughout the test from the beginning of fatigue cycling to specimen failure.

Upon completion of a test, the specimen was unloaded and stored away with the replicas and the p.d. chart for later examination and analysis.

6.2.7 Analysis of Results

In order to assess the information obtained from the reversed-bending fatigue tests, S-N curves and da/dN vs. ΔK curves were plotted.

The plotting of S-N curves was straightforward; however, the information to be obtained from these curves is very limited since each specimen gives only one point on a curve. Much more information on crack growth behaviour was obtained by constructing da/dN vs. ΔK curves, i.e. the change in crack depth (a) per cycle (N) vs. the range of stress intensity factor (K). This gave a complete curve from the testing of one specimen. The plotting of these curves required the determination of da/dN using the p.d. and replication data and the calculation of ΔK involving the use of several formulae.

6.2.7.1 <u>The Determination of Crack Growth Rate per Cycle (da/dN)</u>

In order to determine the crack growth rate per cycle, da/dN, the construction of a plot showing the variation in the maximum crack depth into the surface (a) as a function of the number of fatigue cycles (N) was required. This involved the use of both p.d. and replica information which in turn required the use of calibration curves to determine "a" from the p.d. measured across the notch and from the length of the crack along the surface as measured by the replication technique.

6.2.7.2 <u>Replication Data</u>

The replication technique only measures crack lengths along the surface of the notch and it was therefore necessary to convert the crack length obtained from measurement on the replica to crack depth. This required the determination of the shape (profile) of the growing fatigue crack.

6.2.7.3 Fatigue Crack Profiles

From the photographs of replicas taken at different stages of the fatigue process (plates 6 to 8) it is seen that cracking rarely occurred by initiation from a single point, even in the unpeened specimens (plates 6c and 6d).

Once a major fatigue crack had become established, any other cracks in that vicinity stopped growing due to the stress shielding effects of the major crack. It is these secondary cracks which have been used to determine the crack depth during the early stages of fatigue from the measured length on the surface.

To determine the maximum crack depth from the length along the surface, it was necessary to construct the profiles of the fatigue cracks by grinding through each crack in 0.1mm steps and measuring the depth of the crack at each step. The maximum depth of each crack was then plotted against its length and a curve constructed for each alloy in both the unpeened and peened conditions. As a result, any fatigue crack length obtained by the examination of replicas could be converted to the maximum crack depth, a.

6.2.7.4 The P.D. Data

To calculate the crack depth from the voltage across the notch it was necessary to calibrate the apparatus by breaking open specimens at various stages of their fatigue lives and recording the p.d. across the notch just before the moment of breaking. The maximum depth to which the fatigue cracks had grown was then measured using a travelling microscope and a plot of maximum crack

depth vs. p.d. across the notch was constructed. As a result, any p.d. measurements across the notch could be converted to a crack depth using this curve.

6.2.7.5 Calculation of the rate of crack growth per Stress Cycle (da/dN)

With the aid of the replication and p.d. calibration curves, a plot of the crack depth (a) vs. the number of stress cycles (N) was constructed for each specimen. The calculation of da/dN was carried out simply by determining the gradient at various points along the a vs. N curves for each specimen.

6.2.7.6 Calculation of the Stress Intensity Factor Range (ΔK)

The calculation of the stress intensity range for an edge crack in an infinite plate requires the use of the formula;

$$\Delta K = \Delta\sigma\sqrt{(\pi a)}$$

where a is the maximum crack depth and $\Delta\sigma$ the applied nominal stress range.

In order to take into account the finite size and the geometry of the reversed-bending specimens used in this project, this formula has been modified by Mutoh et al (96) by applying various correction factors (F1, F2 and F3) to give the following equation;

$$\Delta K = \Delta\sigma\sqrt{(\pi a)}.F1(a,\rho,K_t).F2(a,D,W).F3(a,c)$$

F1 is the correction factor for a short crack emanating from a notch of depth D and tip radius ρ and is given by the formula;

$$F1(a,\rho,K_t) = K_t/\sqrt{(1+4.5a/\rho)}$$

where K_t is the theoretical stress concentration factor (97).

F2 is the correction factor for a single edge crack in a bend specimen of width W and is given by the formula;

$$F2(\alpha,D,W) = 1.12-1.40\alpha+7.33\alpha^2-13.08\alpha^3+14.0\alpha^4$$

where α is the ratio; (a+D)/W ...(98)

F3 is the correction factor for a small surface crack in a bend specimen and is given by the formula;

$$F3(a,c) = (1.13-0.09\beta)/\sqrt{(1+1.464\beta^{1.65})}$$

where β is the ratio a/c ,c being half the length of the crack along the surface (99).

6.2.7.7 The Construction of da/dN vs. ΔK curves

The construction of the da/dN vs. ΔK curves was carried out by determining da/dN for various fatigue crack lengths and calculating ΔK at those crack lengths.

6.2.7.8 The Stress Distribution Near the Base of the Notch

In order to aid the explanation of shot peening and peening damage on the stress distribution near the base of the notch in the reversed-bending specimens, the stress distribution resulting from the effects of the peening damage at the base of the notch were

calculated and related to the residual compressive stress distribution. The method of calculation of the applied stress distribution is shown in appendix 2.

6.3 Rotating-Bending Fatigue Testing

Rotating-bending fatigue testing was carried out in order to assess the effects of fretting-fatigue on the unpeened and shot peened 7010 and 8090 alloys. Rotating-bending fatigue testing required the use of a different fatigue machine to that used in the reversed-bending tests along with specimens of a different geometry.

6.3.1 Specimen Dimensions

The dimensions of the rotating-bending specimens used in this work are given in figure 14a. The two alloys were supplied as 9.5mm diameter extruded rods and these were cut to 355mm lengths. On the rods were machined two parallel flats 38mm long and 6.4mm apart to form the gauge length of the specimen. A 50mm radius was machined at each end of the flats to avoid any sharp stress concentration. The positioning of the flats were such that the gauge length experienced a constant bending moment when the specimens were placed in the rotating-bending fatigue machine.

Fretting-fatigue tests were carried out on the rotating-bending specimens by clamping fretting bridges (consisting of the same alloy as the specimen being tested) onto the flats using a proving-ring (see section 6.3.2.2). The bridges are shown

schematically in fig. 14b and, as can be seen, were 19.05mm in length and 6.35mm wide with a foot at each end measuring 6.35 x 2.40mm. A dimple was machined into the back of each bridge to aid the positioning of the proving ring and to hold it in place during testing.

6.3.2 Testing Equipment

6.3.2.1 Plain-Fatigue

Specimens were tested in a four-point-loading, rotating-bending fatigue machine (see plate 1b). As shown schematically in fig. 14c, the specimens were held by four self-adjusting tapered bearings, the outer two being clamped in place in the machine, the inner two being connected by a free-hanging lightweight stirrup arrangement to the load. This produced a constant bending moment along the gauge length of the specimen. The distance between the outer bearings was 245mm and the distance between the inner bearings was 102mm.

The specimens were rotated at 25Hz by a 186.5 Watt electric motor connected to the drive shaft by a pulley system. The number of stress cycles applied to the specimen was recorded by a cycle counter connected to the end of the specimen.

6.3.2.2 Fretting-Fatigue

The machine described in the previous section was also used for the fretting-fatigue tests. In order to apply a fretting action to the specimen, a proving-ring clamped the fretting bridges to

the gauge length as shown in fig. 15a. Since the applied fatigue load caused only the specimen to deflect, a relative movement was set up between the bridges and the specimen during testing, resulting in fretting wear.

6.3.3 Test Calculations

The calculation of the bending stresses set up in the specimens under different loading conditions is given in appendix 3. The calculation of the slipping distance between the feet of the bridges and the specimen is shown in appendix 4.

6.3.4 Rotating-Bending Testing Procedure

6.3.4.1 Specimen Preparation and Test Procedure (Plain-Fatigue)

The gauge length of each unpeened rotating-bending specimen was ground in the longitudinal direction using fine 000 grade emery paper to produce a smooth surface. Since (as described in section 1.4.2) the improvement in fatigue properties due to shot peening remains the same whether the surface has been left in the as-peened condition or ground to the base of the peening dimples, peened specimens were left in the peened condition. All specimens were cleaned with inhibisol before testing.

Testing was carried out using loads ranging from 18.17kg to 40.93kg which produced bending stresses in the gauge length ranging from 126.5MPa to 285.0MPa. Tests were allowed to continue until either failure or a run-out value of 10 million cycles occurred.

6.3.4.2 Specimen Preparation and Test Procedure (Fretting-Fatigue)

Specimens were prepared as for the plain-fatigue tests. The feet of the fretting bridges were ground in the longitudinal direction with 000 grade emery paper before being degreased with inhibisol. All the bridges were in the unpeened, peak-aged condition.

The bridges were clamped either side of the gauge length using the proving-ring to give a contact pressure of 32MPa. The calibration of the proving-ring was carried out using a Mayes tensile testing machine; the variation in the diameter of the ring against the applied load is given in fig. 15b where it can be seen that a contact pressure of 32MPa corresponded to a diameter of 77.98mm.

6.4 Specimen Analysis

Since shot peening has such a major effect on the surface properties of the alloys used in this project, it was important to characterise the changes produced in the surface by the shot peening treatment. Tests were carried out to examine the changes in residual stress and hardness of the surface layers due to shot peening. Optical microscopy was used to examine the nature of deformation in the peened surface layers, the behaviour of crack growth through these peened layers and to examine the progress of fatigue cracks recorded by the replication technique. Scanning electron microscopy was also used to examine fatigue cracks and fracture surfaces of many fatigue-tested specimens.

6.4.1 X-Ray Residual Stress Analysis

The dramatic improvement in fatigue properties of shot peened alloys is attributed mainly to the high residual compressive stresses introduced by the peening operation into the surface layers; the stresses producing this improvement by retarding early fatigue crack growth. It is therefore of importance to investigate the nature and magnitude of these residual stresses. To determine the variation of residual stress with depth into the surface of the shot peened and the ground and polished unpeened alloys, an X-ray method of measurement was employed.

This technique determines the stress only at the surface of the alloy and, as a result, a method of surface layer removal was required to measure stresses below the surface.

6.4.1.1 Surface Preparation

The method of surface layer removal involved surface grinding followed by electropolishing, this being necessary to remove any residual stresses set up by the grinding operation. Layers were removed in 0.05mm steps (measurement being made by micrometer), the first 0.03mm were removed by careful grinding with 000 grade emery paper using water as a lubricant, the final 0.02mm being removed by electropolishing in a solution of acetic acid and perchloric acid at a ratio of 90:15 by volume. The electropolishing was carried out at a temperature of 11°C, a voltage of 40V and a current density of 0.001A/mm^2.

X-ray stress analysis can only be carried out effectively on flat surfaces. Since the surfaces of the peened specimens used in this project were extremely rough (see plate 4), the first reading could only be taken after removing a layer, as described above, to leave a flat surface containing only a few remnants of peening dimples.

6.4.1.2 The Determination of Residual Stress

The calculation of the residual stress in a metal surface requires the determination of the interplanar spacing of two differently orientated sets of crystallographic planes; the spacing being found by measuring the angle at which a beam of X-rays is diffracted by each set of planes.

The angle of diffraction (2θ) of a beam of X-rays impinging on a metal surface depends upon the interplanar spacing (d) and the X-ray wavelength (λ) for a first order diffraction, as shown by Braggs law;

$$n\lambda=2d.\sin\theta$$

The planar spacing can be calculated simply from the measurement of the angle (2θ) at which diffraction occurs, the X-ray wavelength being already known.

When a stress is applied to an alloy the planar spacing (d) changes and this results in a change in the diffracted X-ray angle (2θ), a measurable parameter. The stress in a surface can thus be calculated by measuring the interplanar spacing (d) in a stressed specimen and an unstressed specimen, calculating the corresponding strain and consequently the stress in the surface. The actual

measurements (requiring the use of the stressed specimen only) are made using the "two exposure technique", a method involving measurement of the planar spacing of planes at two different angles to the surface, these being;

a) Planes parallel to the surface. Since these planes are very close to the surface (X-rays only penetrating a very small distance into the surface) and since there is no stress at right angles to a free surface, the interplanar spacing is assumed to be that of the spacing in the unstressed alloy.

b) Planes orientated at an angle to the surface, these planes incorporating a component of the biaxial residual stress.

From these measurements, the stress calculations are made using the formula described in appendix 5.

In order to find the exact angle of diffraction, the specimen was rotated; the counter rotating at twice the speed of the specimen to detect the diffracted rays. Since diffraction from a particular plane occurs over a small range of angles, the counter does not detect a sudden increase in intensity as would be expected from ideal conditions, it detects a gradually increasing and decreasing intensity, the peak intensity being the required diffraction angle (2θ). As a result, each X-ray measurement of the diffraction angle involves a scan through several degrees to find the angle at which peak diffraction occurs.

The determination of the exact peak position was carried out using the three point method of fitting a parabola and is described in appendix 6.

6.4.1.3 Test Procedure

Testing was carried out on a Siemens Krystalflex 4 diffractometer, the specimens being prepared as described in section 6.4.1.1. The specimen to be tested was placed in a perspex jig so that the polished surface was level with that of the jig, the assembly then being slotted into place on the diffractometer axis. This ensured the correct orientation of the specimen in the machine allowing accurate diffraction measurements to be taken.

Details of the radiation, reflecting planes, diffractometer and material parameters are listed in fig. 16.

6.4.2 Hardness Testing

In order to examine the effects of the deformation produced by shot peening on the hardness of the surface layers, microhardness traverses of sections taken at right angles to the peened surface of the differently treated, untested specimens were carried out.

The traverses were carried out using a Vickers microscope with a pyramidal diamond microhardness indenter attached; specimens being mounted in a cold setting resin and ground to a 000 finish using emery paper and water as a lubricant before being polished to a 1µm finish on a diamond polishing wheel. In order to prevent the edges from becoming rounded during grinding (due to the differing hardnesses of the alloy and resin), the specimens were mounted against a "support" specimen of the same alloy. This was necessary since indentations taken on a rounded surface become distorted and consequently can yield incorrect hardness results.

6.4.3 Optical Microscopy

Optical microscopy was carried out using a Nikon Optiphot microscope capable of up to 1000X magnification. Photographs of specimens were taken using a Nikon UFX-II camera attachment mounted on top of the microscope.

In order to investigate the nature of fatigue crack growth into the surface, sections through fatigue cracks in many tested specimens (both peened and unpeened) were taken. Sections were taken longitudinally so as to show a side view of the crack growing into the specimen from the surface. These sections were ground to a 000 finish using emery paper and polished using cotton wool soaked in a liquid metal polish, before being etched in Kellers reagent (1%HF, 1.5%HCl, 2.5%HNO3, 95.0%H_2O). This method was also employed for the examination of fatigue cracks growing into the surface from the edges of fretting scars in the rotating-bending specimens of both 7010 and 8090 alloys.

Since (as described in section 5.4.3) the precipitation of the strengthening phase S' in the 8090 alloy system occurs on dislocations and since shot peening introduces a high dislocation density into the surface layers, specimens peened at both high and low intensities were reaged after shot peening to allow further precipitation on the dislocations introduced by the shot peening operation. Sections through the peened surfaces of these specimens were then taken and etched using Kellers reagent to reveal the nature of the surface layer. This was not possible in the 7010 alloy since the precipitation of the strengthening phase η' in this system does not occur to any extent on dislocations.

Optical microscopy was also used for the examination of the plastic replicas taken in the notch of the reversed-bending specimens during fatigue testing. The replicas were translucent and thus were observed using transmitted light. The lengths of fatigue cracks observed in the replicas were measured using a calibrated graticule in the eyepiece of the microscope.

6.4.4 Scanning Electron Microscopy

Examination of the surfaces of tested specimens was carried out on a Jeol 35C scanning electron microscope. Before examination, specimens were ultrasonically cleaned in inhibisol before being coated with a thin layer of gold using an Emscope SC500 coater.

6.5 Static Bend Testing

In order to assess the effects of shot peening on the static bending behaviour of the two alloys used in this project, static bend tests were carried out on specimens with the same dimensions as those of the reversed-bending specimens. Of particular interest was the effect of peening on the yield strength and the elongation of the material at the base of the notch.

The elongation was measured by marking several gauge lengths at equal distances either side of the base of the notch in the longitudinal direction. The increase in the different gauge lengths upon testing gave the elongation of the material in the region of the notch.

Testing was carried out in four-point bending (with the same spacing between loading points as used in the reversed-bending fatigue tests) using a Mayes servohydraulic testing machine with a ram speed of 1.0mm per minute.

6.6 Summary

To summarise the experimental procedure, a flow diagram showing the various procedures is shown in fig. 17.

CHAPTER SEVEN

EXPERIMENTAL RESULTS

Introduction

This chapter details the results obtained from the experimental work described in chapter 6.

7.1 The Microstructures and Peened Surfaces in the 7010 and 8090 Alloys

The following section describes the microstructures obtained by peak ageing the 7010 and 8090 alloys along with the nature of the surfaces produced by peening the alloys to the light and heavy intensities.

7.1.1 The Microstructure of Peak Aged 7010 and 8090 alloys

The microstructures of the rolled 7010 and 8090 plate in the peak aged condition are shown in plate 2 where a flat shaped grain structure can be seen, the platelets being parallel to the rolled surface and elongated in the rolling direction. The average dimensions of the grains were 150µm X 70µm X 20µm and 250µm X 125µm X 50µm for the 7010 and 8090 alloys respectively. Such grain structures are typical of partially recrystallised aluminium alloy plate.

The microstructures of the extruded 7010 and 8090 alloys after peak ageing are shown in plate 3. As expected, the grains in both alloys were elongated in the longitudinal direction. The average dimensions of the grains were 1000µm X 20µm and 1500µm X 40µm for the 7010 and 8090 alloys respectively.

7.1.2 Surface Treatments

Plate 4 shows the conditions of the peened surfaces of the alloys. As can be seen, the peening of these alloys to an intensity of 8-10C on the Almen scale produced a highly deformed surface layer with deep "craters" and high "peaks". Peening to the lighter intensity of 12-16A on the Almen scale resulted in a surface containing shallower craters and lower peaks.

7.2 Reversed-Bending Fatigue Testing

In this section, the results obtained by the reversed-bending fatigue testing of the 7010 and 8090 alloys are described.

7.2.1 S-N Curves

Following the reversed-bending fatigue testing of both alloys in the unpeened, lightly peened (12-16A) and heavily peened (8-10C) conditions, S-N curves were constructed and are shown in figs. 18 and 19.

Fig. 18 shows the S-N curves for the 7010 alloy. These curves show that shot peening results in an improvement in fatigue properties, especially at high stress ranges; the improvement at these stresses being more pronounced for the heavily peened alloy. At lower stress ranges, however, the improvements produced by shot peening were reduced significantly, especially in the case of the lightly peened alloy where a reduction in fatigue strength was observed. This is shown by the "fatigue limits" of the alloy in the unpeened, lightly peened and heavily peened conditions; these limits being at stresses of 324MPa, 306MPa and 330MPa respectively.

Fig. 19 shows the S-N curves for the 8090 alloy where it can be seen that shot peening resulted in an improvement in the fatigue life at lower stress ranges and a reduction in the fatigue life at higher stress ranges; the improvement being more pronounced with the heavily peened alloy. The stress ranges above which peening became detrimental to the fatigue behaviour were 470MPa in the case of the heavily peened alloy and 390MPa in the case of the lightly peened alloy.

During the testing of the 8090 alloy specimens, copious amounts of black debris were observed exuding from the fatigue cracks in the base of the notch; the rate of production of this debris increasing as the cracks grew. Plate 5 shows this debris in the base of the notch of a heavily peened specimen.

7.2.2 The P.D. Calibration Curve

The calibration curve converting the p.d. measured across the notch during testing to the maximum crack depth (a) is shown in fig. 20. "Va/Vo" is plotted against "a" where Va is the measured voltage across the notch at a crack length "a" and Vo the initial voltage (at a crack length of 0). The poor sensitivity to short crack detection by the p.d. technique is clearly displayed here, the shortest reasonable measurement being a crack of approximately 1.0mm in depth.

7.2.3 The Replication Calibration Curves

Some of the fatigue crack profiles determined from the two alloys in order to obtain the maximum crack depth from measurement of the crack length along the surface can be seen in figs. 21 and 22.

7.2.3.1 Alloy 7010

Fig. 21a shows typical fatigue crack profiles obtained from the unpeened 7010 alloy, showing the expected "thumbnail" shaped cracks; the shape being independent of the size of the crack. Fig. 21c shows fatigue cracks obtained from heavily peened specimens where it can be seen that the cracks had an irregular, elongated profile. The positions at which the cracks were shallower were often found to coincide with deep peening dimples which had not been completely polished out of the surface. Fig. 21b shows the fatigue crack profiles obtained from the lightly peened alloy. In this case, the shorter cracks (less than 1mm along the surface) were found to be elongated and slightly irregular whilst the longer cracks were of a similar shape to those found in the unpeened alloy.

7.2.3.2 Alloy 8090

Fig. 22a shows the typical fatigue crack profiles obtained from the unpeened 8090 alloy. These cracks were found to be of a considerably different nature to those found in the 7010 alloy specimens, showing highly crystallographic and irregularly shaped profiles. Fig. 22c shows the fatigue crack profiles found in the heavily peened 8090 specimens. These cracks showed a similar behaviour to those found in the heavily peened 7010 alloy, being

elongated and irregular. It should be noted that the small fatigue cracks did not have a highly crystallographic profile when compared to those found in the unpeened 8090 alloy. Fig. 22b shows the profiles of fatigue cracks found in the lightly peened 8090 alloy specimens. These cracks were found to be elongated and irregular with the small cracks again showing little crystallographic behaviour.

Photographs showing cross-sections of some of the fatigue cracks growing through the surface layers are shown in plates 9 and 10 and are described in section 7.6.

7.2.3.3 Calibration Curves

Due to the differing nature of fatigue crack growth in the two alloys and due to the effects of shot peening on the shape of early fatigue cracks it was necessary to construct a different calibration curve (converting the crack length along the surface to the maximum crack depth) for each alloy in each different condition (unpeened, lightly peened and heavily peened). The resulting curves are shown in figs. 23 and 24.

Fig. 23 shows the calibration curves for the 7010 alloy specimens. It is seen here how peening to the lighter intensity resulted in crack growth behaviour which followed that of the heavily peened alloy up to a maximum depth of 0.3mm. Above 0.3mm the crack depth rapidly increased with crack length, resulting in a crack shape tending towards the thumbnail shape of those found in the unpeened alloy.

Fig. 24 shows the calibration curves for the 8090 alloy specimens with the curves obtained for the 7010 alloy (shown as the dashed curves). Peening to the lighter intensity resulted in crack growth behaviour similar to that in the 7010 alloy specimens. However, it is clearly seen that the fatigue crack profiles in the 8090 alloy were shallower than those found in the 7010 alloy in all cases.

7.2.4 Maximum Crack Depth vs. Stress Cycles Curves

With the determination of the calibration curves, the information obtained from the electrical p.d. technique and the replication technique was then used to construct curves showing the maximum crack depth (a) vs. the number of stress cycles (N) for each fatigue tested specimen. Figs. 25 and 26 show the plots resulting from the testing of both alloys at the low and high applied stress ranges of 368MPa and 507MPa respectively.

7.2.4.1 Alloy 7010

Fig. 25 shows the plots of maximum crack depth vs. the number of stress cycles for the 7010 alloy in the unpeened, lightly peened and heavily peened conditions. It can be seen that in the unpeened specimens, once fatigue crack initiation had occurred, the propagation rate increased steadily to failure. At low applied stresses more time was spent in fatigue crack initiation than propagation and at high applied stresses, this trend was reversed and more time was spent in fatigue crack propagation than initiation.

Crack initiation in the peened alloy was found to start very early on in the fatigue life of the specimens, in fact, some crack like peening damage was found to be present even before the onset of cycling (see section 7.2.5). Although fatigue crack initiation was found to occur very early on, the initial stages of crack growth were found to be very slow, cracks appearing to stop at depths corresponding to the peak residual compressive stress (see section 7.4), in some cases for a majority of the fatigue lifetime of the alloy. This was especially true in specimens tested at low applied stresses. Once the crack depth had exceeded approximately 0.6mm, crack propagation was found to be similar to that in the unpeened alloy.

7.2.4.2 Alloy 8090

Fig. 26 shows a plot of the maximum crack depth vs. the number of stress cycles for the 8090 alloy in the unpeened, lightly peened and heavily peened conditions. Crack initiation in the unpeened alloy was found to occur very early in the fatigue life of the alloy. Although initiation was early, the rate of propagation did not increase rapidly as in the 7010 alloy and, as a result, a majority of the fatigue life was spent in crack propagation.

The effects of shot peening on the fatigue crack growth behaviour of this alloy are again clearly seen. As in the 7010 alloy cracks were found to be present before the onset of cycling; these cracks growing very slowly (at depths corresponding to the peak residual compressive stress), especially in the specimens tested at low

applied stresses. Once the crack depth had exceeded approximately 0.6mm, the propagation rate increased rapidly to produce crack growth rates similar to those in the unpeened alloy.

7.2.5 Examination of Replicas

The various stages of early fatigue crack growth monitored using the replication technique in the notch of both peened and unpeened alloys are shown in plates 6 to 8. Fatigue crack initiation occurred at many sites, even in the unpeened alloys. In many peened specimens crack-like defects were found to be present before the onset of cycling.

7.2.5.1 Alloy 7010

Plate 6a shows a small fatigue crack observed in the surface of an unpeened 7010 alloy specimen tested at a stress range of 507MPa after 15,000 cycles. The crack is again shown in plate 6b after 23,000 cycles, growing along the base of the notch in a direction normal to the applied stress. Fatigue failure occurred not by the initiation and growth of a single fatigue crack but by the linking of several smaller cracks to form the major fatigue crack.

Plates 7a and 7d show the damage introduced by the peening operation into the surface of untested 7010 alloy specimens peened to intensities of 12-16A and 8-10C respectively. The cracks in both cases were found to emanate from deep peening dimples which had not been completely polished out of the surface; the cracks in the heavily peened alloy being clearly visible before the onset of

cycling. Plates 7b and 7c follow the progress of the fatigue cracks in the lightly peened alloy after cycling at a stress range of 368MPa and plates 7e and 7f the progress of the cracks in the heavily peened alloy tested at a stress range of 507MPa.

7.2.5.2 Alloy 8090

Plate 6c shows small fatigue cracks found in the surface of an unpeened 8090 alloy specimen tested at a stress range of 507MPa after 13,000 cycles. The highly crystallographic nature of these cracks is clearly visible when compared to those found in the unpeened 7010 alloy. The progress of these cracks is followed in plate 6d with the major fatigue crack again being produced by the link-up of several smaller fatigue cracks.

Plates 8a and 8d show the cracks introduced by the peening operation into the surface of the untested 8090 alloy specimens peened to intensities of 12-16A and 8-10C respectively. As with the peened 7010 alloy, cracks were observed in the vicinity of the remnants of deep peening dimples before the onset of cycling. Upon fatigue cycling, the behaviour of the alloy was found to be similar to that of the peened 7010 alloy with the cracks stopping briefly before rapidly growing to link-up and form a major fatigue crack. It should be noted that these cracks did not display the crystallographic nature observed in the unpeened alloy but were more characteristic of those observed in the peened 7010 alloy.

7.2.6 Crack Growth Rate

The relationship between the fatigue crack growth rate (da/dN) and the stress intensity range (ΔK) in the unpeened, lightly peened and heavily peened 7010 and 8090 alloys are shown in figs. 27 to 38. The results are shown for specimens tested at low and high applied stress ranges (368MPa and 507MPa respectively).

Peening in all cases produced a crack growth rate which, close to initiation, increased rapidly. However, with a further increase in ΔK (i.e. with increasing crack depth "a") the growth rate decreased dramatically to a minimum value at values of ΔK corresponding to a crack depth of 0.20mm in the case of both lightly peened alloys (with the exception of the 8090 alloy specimen fatigue tested at the high applied stress) and 0.25mm in the case of the heavily peened alloys. Beyond this crack depth, the growth rate accelerated rapidly to attain the same rate as that observed in the unpeened alloy.

7.2.6.1 Alloy 7010

Fatigue testing alloy 7010 in the unpeened condition produced a crack growth rate in the Paris regime giving a slope (m) of 2.5. Beyond this region the cracks propagated rapidly in both unpeened and peened specimens, failing at a ΔK value of 23MPa$\sqrt{m}$.

It is interesting to note that in the very early stages of fatigue in the unpeened alloy (i.e. below a ΔK value of 4.0 MPa$\sqrt{m}$), crack growth was more rapid than may be expected at such low ΔK values (fig. 30); the growth rate tending towards a constant value of da/dN with decreasing ΔK. This value was 10^{-6} mm/cycle in the

specimen tested at the high applied stress. No data was obtained in this region for the specimen tested at the low applied stress.

7.2.6.2 Alloy 8090

Fatigue testing alloy 8090 in the unpeened condition produced a crack growth rate in the Paris regime giving a slope (m) of 2.3. However, cracks did not propagate rapidly to failure beyond this region as observed in the 7010 alloy, instead a decrease in growth rate was observed with increasing ΔK (at values of ΔK above 17MPa$\sqrt{m}$) before rapid propagation to failure at a ΔK value of 30MPa$\sqrt{m}$. This behaviour was observed in all the 8090 alloy specimens tested, in both the peened and unpeened conditions.

As observed in the unpeened 7010 alloy, very early crack growth rates in the unpeened 8090 alloy tended towards a constant value of da/dN with decreasing ΔK; the values being 7×10^{-7} mm/cycle and 5×10^{-6} mm/cycle for the low and high applied stress ranges respectively.

7.2.6.3 The Stress Distribution at the Base of the Notch

Fig. 39 shows an example of the stress distribution at the base of the notch in a heavily peened, reversed-bending 7010 alloy specimen, fatigue tested at an applied stress range of 368MPa. Curve "a" represents the residual compressive stress distribution determined from the heavily peened 7010 alloy (see section 7.4). Curve "b" shows the maximum applied stress distribution experienced at the base of the notch by an unpeened specimen fatigue tested at the applied stress of 368MPa. An addition of curves "a" and "b" gives curve "c", the maximum possible

distribution at the base of a smooth but shot peened notch fatigue tested at 368MPa. The effects of the surface folding induced by peening upon the stress distribution in the base of the peened notch are shown by curve "d", the damage in this case extending 0.007mm into the peened surface (since this was the depth of the damage from which the fatigue crack initiated to exhibit the growth shown in fig. 29). Curve "d" highlights the effects of peening damage upon the fatigue performance of shot peened alloys.

7.3 Rotating-Bending Fatigue Testing

Following the rotating-bending fatigue testing (in plain and fretting-fatigue) of the two alloys in the unpeened, lightly peened and heavily peened conditions, S-N curves have been constructed.

7.3.1 Alloy 7010

Fig. 40 shows the S-N curves produced by testing alloy 7010 in plain and fretting-fatigue. The behaviour of the alloy in plain-fatigue was found to be similar to that observed in the reversed-bending tests, with the peened specimens showing the greatest resistance to fatigue at high applied stresses, especially in the case of the heavily peened alloy. At lower applied stresses, however, all S-N curves approached a "fatigue limit" at a stress amplitude of approximately 160MPa.

The effects of fretting on the unpeened alloy are clearly seen; fretting being detrimental to the fatigue performance of this alloy, especially at the lower applied stress amplitudes. Although fatigue failure of the lightly peened alloy sometimes initiated at the edges of fretting scars, shot peening appeared to nullify the effects of fretting at all stresses, the specimens displaying the same behaviour as those tested in plain-fatigue.

7.3.2 Alloy 8090

The effects of peening on the plain and fretting-fatigue performance of the 8090 alloy are shown in fig. 41. It can be seen that shot peening to both intensities resulted in the same small improvement in the plain-fatigue performance of this alloy, this improvement being more pronounced in high cycle fatigue.

Fig. 41. also shows that fretting had little effect upon the fatigue performance of the unpeened 8090 alloy, especially at high applied stresses. As in the 7010 alloy, the effects of fretting on the fatigue performance of the 8090 alloy appear to have been nullified by the peening treatment.

7.4 X-Ray Residual Stress Analysis

The variations of residual stress with depth into the surface of the two alloys peened to intensities of 12-16A and 8-10C on the Almen scale are shown in figs. 42a and 42b.

Fig. 42a shows the residual stress profiles produced by peening the 7010 alloy to each intensity. It can be seen that peening produced a residual compressive stress profile which peaked below the surface at depths of 0.20mm and 0.25mm for the lightly and heavily peened alloys respectively. The magnitude of the residual compressive stress in the heavily peened alloy was 275MPa at the surface rising to 350MPa at the peak. The magnitude of the compressive stress in the lightly peened alloy was lower, being 230MPa at the surface and rising to 330MPa at the peak.

Fig. 42b shows the residual stress profiles produced by peening the 8090 alloy to each intensity. The stress profiles were again found to peak at a depth of 0.20mm and 0.25mm for the lightly and heavily peened alloys respectively. The magnitudes of the residual compressive stresses in both cases were found to be significantly lower than those observed in the 7010 alloy, being 180MPa at the surface and 270MPa at the peak in the case of the lightly peened alloy and 225MPa at the surface and 295MPa at the peak in the case of the heavily peened alloy.

No residual stresses were detected in the surfaces of the unpeened, lightly ground and polished specimens using the X-ray technique. This is important since, unless carried out with great care, even small amounts of surface removal using mechanical methods can introduce significant residual stresses into the surface layers of materials.

7.5 Microhardness Traverses

The results of the microhardness traverses through the peened surfaces of the two alloys are shown in fig. 43 as the Vickers microhardness of the alloy as a function of the depth into the peened surface.

Fig. 43a shows the microhardness traverses through the surface of the 7010 alloy peened to both light and heavy intensities. As can be seen, shot peening to both intensities resulted in only a small increase in the hardness of the deformed surface layers.

Fig. 43b shows the microhardness traverses through the surface of the 8090 alloy peened to both light and heavy intensities. As in the 7010 alloy, shot peening to both intensities resulted in a small increase in the hardness of the surface layers compared with that of the bulk material.

7.6 Optical Microscopy

Plates 9 to 11 show optical micrographs taken through sections of fatigue cracks at the base of the notch in the unpeened and shot peened reversed-bending specimens and through sections of fatigue cracks growing from the edges of fretting scars in the rotating-bending specimens.

7.6.1 Alloy 7010 in Reversed-Bending

Plates 9a and 9b show cross-sections taken through fatigue cracks growing into the surface of an unpeened 7010 alloy specimen. The cracks in the unpeened alloy were found to follow a fairly direct path through the thickness of the specimens. It is seen that fatigue cycling results in the formation of more than one fatigue crack.

Plates 9c and 9d show cross-sections through the initiation sites of fatigue cracks in the lightly and heavily peened 7010 alloy. In both cases it can be seen how shot peening results in the formation of many fatigue cracks, the cracks growing from the base of a peening dimple in the lightly peened alloy (Plate 9c) and from a highly deformed area in the heavily peened alloy (Plate 9d). The crack in the latter case follows a highly contorted path near the surface before finally growing normal to the longitudinal specimen direction. The crack on the right in Plate 9d shows a section through a fatigue crack that is well away from its point of initiation.

7.6.2 Alloy 8090 in Reversed-Bending

Plate 10a shows a cross-section taken through fatigue cracks growing into the notch surface of an unpeened 8090 alloy specimen. The crack path is seen to be highly dependent upon the orientation of the grains, the cracks growing along slip planes most favourably inclined to the applied fatigue stress. It can also be seen, as in the 7010 alloy, that fatigue of the unpeened alloy can result in the initiation of more than one crack.

Plate 10b and 10c show cross-sections of fatigue cracks observed in the heavily peened alloy. Plate 10b shows an area at which fatigue crack initiation occurred; the tendency of the folded material at the surface to "flake" in this alloy in the peened condition is clearly seen. Cracks can be seen growing from the deformed area at the base of a deep dimple. It can be seen from plate 10c that the crack path only becomes crystallographic below the deformed surface layer; whilst growing through the deformed surface layer the fatigue cracks remained approximately normal to the surface of the specimen. Similar fatigue crack behaviour was observed in the lightly peened alloy, however, the crack growth in this case became highly crystallographic at an earlier stage than that in the heavily peened alloy due to the shallower deformed surface layer.

7.6.3 Alloys 7010 and 8090 in Rotating-Bending

Sections taken through fatigue cracks growing from the edges of fretting scars in the unpeened 7010 and 8090 alloys can be seen in plates 11a and 11d respectively and show the typical angled growth into the surface that is characteristic of fretting-fatigue.

As shown in plate 11b, shot peening the 7010 alloy to the light intensity resulted in fatigue crack growth from the edge of the fretting scar at a much shallower angle to the peened surface when compared to the unpeened alloy; this angle changing at a depth of 150μm to a less shallow angle. Plate 11c shows a section through a fretting scar in the heavily peened alloy. In this case fretting resulted in the initiation of many small fatigue cracks.

The effects of fretting on the fatigue performance of the lightly peened 8090 alloy (plate 11e) shows that some delamination occurred along with the production of a large number of small fatigue cracks when compared to the lightly peened 7010 alloy (plate 11b). Delamination, as shown in plate 11f, also occurred at the fretting scar in the heavily peened alloy. In this case, fretting did not result in the flattening of the roughened peened surface.

7.7 The Precipitation of S' in the Deformed Surface Layers

Plate 12 shows sections through the peened surface of the re-aged 8090 alloy where the precipitation of the S' phase clearly marks out the regions of intense deformation and slip; the level of precipitation being high at the surface and decreasing with depth into the peened layer. The depth to which extensive precipitation occurred below the surface was 0.20mm in the case of the lightly peened alloy (plate 12a) and 0.25mm in the case of the heavily peened alloy (plate 12b).

Plate 12c shows precipitation at a dimple found in an area of low coverage near to the end of a heavily peened specimen where the region of deformation produced by the impact of a single shot can be clearly seen. The maximum depth to which precipitation occurred on slip lines is just visible at a distance of 0.25mm below the base of the dimple.

7.8 Scanning Electron Microscopy

With the aid of a scanning electron microscope it has been possible to examine the surfaces of many fatigue tested reversed-bending and rotating-bending specimens in detail.

7.8.1 Alloy 7010 (Reversed-Bending)

Plate 13 shows the typical appearence of the notch surface in an unpeened, fatigue tested, reversed-bending specimen viewed from an oblique angle. Fatigue cracks seen growing close to the region of gross fracture at the base of the notch show the non-crystallographic dependency of crack growth in this alloy.

Plate 14 shows the typical appearence of the notch surface in the heavily peened, fatigue tested alloy. Fatigue cracks growing from the remnants of deep peening dimples which have not been completely polished out of the surface are clearly visible; the fracture surface shown, being formed by the linking of these small fatigue cracks to form the major fatigue crack. It can also be seen that peening produces a layered surface structure leading to the occurrence of spalling in some of the dimples.

Plate 15 shows the notch surface of the lightly peened 7010 alloy where the importance of peening damage on fatigue cracking is again seen. The plate also shows how the light peening operation leads to the initiation of fewer fatigue cracks when compared to the heavily peened alloy. The fracture surface at the base of the dimple shown in plate 15b can be seen in plate 15c where it is clear that the base of the dimple has acted as a fatigue crack initiation site.

Typical fracture surfaces observed in the unpeened and heavily peened, reversed-bending specimens showing the characteristic ridged appearence can be seen in plates 16a, 16b and 16c. Plate 16a shows the initiation of a single crack in the surface of the unpeened 7010 alloy specimen. Plate 16b is an enlargement of this area where it can be seen that initiation occurred from a defect in the surface. Plate 16c shows a small thumbnail type crack growing into the peened surface.

7.8.2 Alloy 8090 (Reversed-Bending)

Plate 17a shows the typical appearence of the notch surface in an unpeened, fatigue tested 8090 alloy specimen. As observed on the replicas described in section 7.2.5, the cracks were of a highly crystallographic nature. Plate 17b shows a fatigue crack in the unpeened notch at a higher magnification where it is seen surrounded by and growing along slip bands; further showing the high dependency of fatigue crack growth on the microstructure of this alloy. Plate 17c shows a crack again growing along and surrounded by slip bands. However, in this specimen, material is seen being extruded from the bands.

The debris observed exuding from fatigue cracks in the notch of an 8090 alloy reversed-bending specimen (see plate 5) can be seen in in plate 18 in more detail. This is probably fretting debris resulting from the rubbing of the faceted fracture surfaces during fatigue.

Plate 19a shows the notch surface in a heavily peened 8090 alloy specimen. As in the peened 7010 alloy, many fatigue cracks can be seen growing from a single, heavily deformed dimple. An enlargement of the dimple showing the flaky nature of the folded material at the surface is shown in plate 19b.

Plate 20a shows a typical fracture surface observed in the unpeened 8090 alloy. The highly crystallographic nature of crack growth in this alloy can be seen, the cracks growing at an angle to the notch surface. Large amounts of oxide can be seen on the fracture surface near to the base of the notch.

The typical fracture surface observed in the heavily peened 8090 alloy can be seen in plate 20b. It is clearly seen that no faceted growth close to the notch has occurred in this case. Oxide debris is also seen in this figure, a small distance (approximately 200μm) away from the notch on the face of the fracture surface.

7.8.3 Alloy 7010 (Rotating-Bending)

Plates 21a and 21b show the area of the fracture surface at which plain-fatigue crack initiation occurred in the unpeened and heavily peened 7010 alloy rotating-bending specimens. Due to the low R-ratio used in these tests (R = -1), the fracture surfaces were often damaged during the compressive half of the cycle making detailed observation difficult. In all the rotating-bending specimens tested in plain-fatigue, fracture began at the edges of the flats on the specimen gauge length.

The edge of a fretting scar in the unpeened 7010 alloy along which a small fatigue crack has grown is shown in plate 22a. The fracture surface produced by such a crack is shown in plate 22b.

Plate 22c shows the edge of a fretting scar along which a small crack can be seen in the lightly peened 7010 alloy. The fracture surface produced by such a crack is shown in plate 22d.

No fatigue cracks were visible at the edges of the fretting scars in the heavily peened 7010 alloy (plate 23a). Fatigue cracking in the surface of the heavily peened alloy well away from the edge of a fretting scar is shown in plate 23b; the cracks being orientated in a direction normal to the longitudinal specimen direction.

Plate 24a. shows the fretting debris produced on the scar of an unpeened rotating-bending specimen. The debris in this case was irregular and thinly spread over the entire surface of the scar. Plates 24b and 24c show the debris observed on the scar of a heavily peened specimen. In this case, two types of debris were observed; spherical debris (plate 24b) and an unusual cylindrical type debris (Plate 24c), the longitudinal axis of the cylinders being normal to the slip direction.

7.8.4 Alloy 8090 (Rotating-Bending)

Plain-fatigue failure in both the unpeened and shot peened 8090 alloy rotating-bending specimens, as in the 7010 alloy, initiated at the edges of the gauge length flats (plate 25a). Extensive amounts of deformation between the crack faces due to the negative R-ratio again made detailed examination of these areas difficult.

Inspection of the fracture surface of the alloy, well away from the point of initiation showed the usual faceted appearence associated with this alloy (plate 25b). Large amounts of debris were produced between the crack faces of this alloy during testing and much of this had a spherical nature as shown in plate 25c.

Plate 26a shows the edge of a fretting scar in a fatigue tested, unpeened specimen. Crack initiation in this case took place at the edge of the fretting scar and, once initiated, followed a crystallographic plane favourably orientated to the applied fatigue stress. The fracture surface produced by such a crack was found to be faceted, even at the edge of the scar from where the crack initiated (plate 26b).

The fracture surface at the edge of a fretting scar in the lightly peened 8090 alloy can be seen in plate 26c. The fatigue cracks in this case grew into the surface from the edge of the scar at a very steep angle before changing to a much shallower angle. It is interesting to note that faceted growth only occurred some distance from the peened surface of the specimen.

Unlike the unpeened 7010 alloy, large amounts of fretting debris were observed on the scar of the unpeened 8090 alloy, much of it spherical (plate 27a). The debris on the scars of the 8090 alloy peened to both light and heavy intensities, however, was often found to be irregular. Plate 27b shows such debris on the scar of the heavily peened alloy.

7.9 Static Four-Point Bend Testing after Shot Peening

Shot peening alloy 7010 has been found to result in a change in the yield strength and elongation of the material at the base of the notch. Peening of alloy 8090 resulted in a similar change in the yield strength of the material. However, the elongation of this alloy at the base of the notch was relatively unaffected by peening.

Fig. 44 shows the resulting changes in yield strength and bend strength at the base of the notch for both alloys. It should be noted that these results, especially the bend strengths, were very much greater than the yield and tensile stresses of the two alloys shown in figs. 5 and 10. Fig. 45 shows the effects of peening on the elongation of the material at the base of the notch for the two alloys.

Shot peening resulted in very little change in the bend strengths of the two alloys; failure occurring by the onset of shear cracking near the base of the notch in the longitudinal specimen direction, parallel to the rolled surface as shown schematically in fig. 45.

7.9.1 Alloy 7010

Shot peening alloy 7010 to both light and heavy intensities resulted in a significant increase (approximately 200MPa) in the yield strength and only a slight increase (approximately 50MPa) in the bend strength.

The elongation of the material at the base of the notch (fig. 45) was high in the region 1.5mm to either side of the base (i.e. along the gauge length) in the unpeened specimen. Shot peening, however, produced a significant decrease in the amount of yielding at the base of the notch, the decrease being slightly greater in the heavily peened specimen.

7.9.2 Alloy 8090

As with the 7010 alloy, shot peening alloy 8090 to both intensities resulted in a significant increase in the yield strength (170 MPa) and a small increase in the bend strength (40MPa). Unlike the 7010 alloy, the maximum elongation of the material in the unpeened 8090 alloy occurred directly below the notch base and not either side; the elongation being very much lower (5%) and being unaffected by shot peening.

7.10 Summary

The shot peening of alloys 7010 and 8090 has been found to cause a reduction in fatigue crack growth rates due to the fact that the cracks had to grow through residually compressed surface layers. The fatigue cracks initiate from many damaged surface areas produced by peening. Shot peening has also been found to nullify the detrimental effects of fretting on the two alloys tested in fretting-fatigue. Static bend testing showed that shot peening significantly reduced plastic deformation at the base of the notch and increased the yield strength. A detailed discussion of the results described in this chapter is provided in chapter 8.

CHAPTER EIGHT

DISCUSSION

8.1 Introduction

Shot peening has been found to have a marked influence on the fatigue performance of the 7010 and 8090 alloys. In this chapter, the results obtained from the plain and fretting-fatigue tests on the unpeened and shot peened alloys are discussed, along with the results from the static bend testing. These results are related to the properties of the heavily deformed and compressed surface layers induced by the shot peening operation.

8.1.1 The Residual Compressive Stresses and Surface Deformation in the 7010 and 8090 Alloys

The reaging of the peened 8090 alloy provided a valuable insight into the way in which the surface layers in a peened material deform (see plate 12); the precipitates marking clearly the regions of intense planar slip. The impact of a single shot, as shown in plate 12c, resulted in slip in the region directly below the dimple. Careful examination of the figure shows a maximum depth of deformation, just off centre (probably due to a slightly angled impact of the shot) at a depth of 250μm below the surface. This indicates that the deformation was principally of the Hertzian type (as described in section 1.4.1.1) since the depth is approximately half the width of the dimple.

The intense planar slip defines clearly the direction in which the principal shear stresses and thus the principal compressive stresses acted in the peened alloys. The principal shear stresses acted parallel to the slip bands (i.e. at an angle of 45° to the peened surface). The principal compressive stresses acted along the planes orientated at an angle of 45° to the principal shear stress, parallel to the shot peened surface.

The depth of the peak residual compressive stresses induced by shot peening to the light and heavy intensities (see figs. 42a and 42b) corresponded with the depth of the severely deformed layers as observed in the reaged 8090 alloy. This is to be expected since the deformation of material occurs to relieve stress; the region at which this deformation stops marks the region at which the material can withstand the highest stress without deforming. The depth at which the deformation stopped was therefore the depth of the peak residual compressive stress; the material below the peak being deformed elastically to compensate for the plastic deformation in the surface layers.

8.2 Reversed-Bending Fatigue Testing of the Unpeened 7010 and 8090 Alloys

8.2.1 Introduction

Fatigue testing of the unpeened 7010 and 8090 alloys has highlighted the contrasting properties of the two materials. Fatigue cracking in the unpeened 8090 alloy was found to be highly dependent upon the crystallographic orientation of the grains

(plate 10a), with initiation taking place at intense slip bands at the surface such as those shown in plates 17b and 17c. The material extruded from the slip bands has been observed in other alloys by many authors and is associated with fatigue crack initiation since intrusions forming alongside the extrusions provide the stress concentrations from which fatigue cracks can grow (100). Fatigue cracking in the unpeened 7010 alloy, however, was found to be much less dependent on grain orientation (plates 9a and 9b), initiation taking place at defects in the surface such as scratches or inclusions (plates 16a and 16b).

8.2.2 Fatigue Crack Profiles

The rounded thumbnail type fatigue cracks observed in the unpeened 7010 alloy (fig. 21a) are typical of those seen in many alloys; the crystallographic orientation having little effect upon the growth behaviour of the cracks. The irregularly shaped fatigue crack profiles observed in the unpeened 8090 alloy (fig. 22a) reflect the dependency of the cracks on the crystallographic orientation; the cracks being shallower due to the angular growth into the surface. The formation of the major fatigue crack by the linking up of several of these thumbnail cracks along the base of the notch is not unusual and has been observed in notches of a wide radius in other alloys (101).

8.2.3 Reversed-Bending S-N Curves for the Unpeened 7010 and 8090 Alloys

The fatigue life of materials is dominated by the time required to initiate fatigue cracks at low applied stresses (where only a small proportion of the fatigue life is spent in fatigue crack propagation) and by the time required to propagate fatigue cracks at high applied stresses (where fatigue crack initiation is rapid). Such behaviour was observed during the reversed-bending fatigue testing of the unpeened 7010 and 8090 alloys as shown in the S-N curves in figs. 18 and 19. The resistance to fatigue crack initiation in the unpeened 7010 alloy was much greater than that in the unpeened 8090 alloy (figs. 25 and 26) and this resulted in the 7010 alloy having superior fatigue resistance at low applied stresses. However, the reverse was true at high applied stresses since fatigue cracks in the 8090 alloy follow a highly faceted path resulting in a slow fatigue crack growth.

8.2.4 da/dN vs. ΔK Curves

The fatigue crack behaviour observed in the unpeened 7010 and 8090 alloys is summarised in the da/dN vs. ΔK curves shown in figs. 27, 30, 33 and 36.

8.2.4.1 Early Fatigue Crack Growth

The usual da/dN vs. ΔK relationship is linear when plotted in log-log form (i.e. in the "Paris regime"), da/dN normally decreasing rapidly at low ΔK values to a threshold value (ΔK_{th}) below which crack growth does not take place. This threshold

behaviour was not observed in the present tests; da/dN tending to level off to a constant value. This increased rate of crack growth in the unpeened alloys at low ΔK values has been observed by many different authors and is often associated with the inadequacy of linear elastic fracture mechanics to deal with short cracks in the deformed zone at the base of notch (102). Other authors have assumed that this effect is due to the decrease in degree of crack closure that takes place in short cracks. This produces da/dN vs. ΔK characteristics that are very similar to those observed in the present work. However, microstructural effects have also been used to explain the short fatigue crack behaviour (103); cracks, being unaffected in the early stages by the presence of discontinuities such as grain boundaries, displaying a rapid growth rate; the rate decreasing as the growing small cracks come into contact with such discontinuities.

The crack lengths below which the growth rate deviated from the linear "Paris regime" in the present work were approximately 0.02mm in the case of the 7010 alloy and 0.10mm in the case of the 8090 alloy. Since the grain sizes in the S-T direction of the 7010 and 8090 alloys were 0.02 and 0.05mm respectively, it is possible that this microstructural effect is also important in the two alloys.

8.2.4.2 Fatigue Crack Propagation in the Paris Regime

The nature of fatigue crack propagation in the two unpeened alloys was found to be very different. Cracks in the unpeened 8090 alloy followed a highly tortuous path with a high degree of branching and direction changing (plate 10a), especially at crack depths

greater than 3.0mm, whilst cracks in the unpeened 7010 alloy followed a fairly direct path through the thickness of the reversed-bending specimens (plates 9a and 9b). The former behaviour is conducive to a prolonged crack propagation life due to the large degree of roughness induced closure that takes place (104) and this is reflected by the slopes of the da/dN vs. ΔK curves in the Paris regime; the slope of the curves representing the unpeened 7010 alloy being 2.5 and that of the curves representing the unpeened 8090 alloy having the lower value of 2.3 indicating a slower crack propagation rate.

8.2.4.3 Late Fatigue Crack Propagation

Severe crack branching in the 8090 alloy (in both the unpeened and shot peened condition) occurred at crack lengths greater than 3.0mm resulting in a drop in fatigue crack growth rates at high values of ΔK. Crack branching has the effect of reducing the stress intensity at the tip of each crack (104) and results in an overall reduced propagation rate. Since the determination of ΔK from the potential drop data relies on the assumption that only one crack is present, an artificially high value was calculated at the corresponding reduced growth rate and consequently a dip in the curve was produced.

The high value of fracture toughness in the unpeened 8090 alloy tested at the high applied stress (fig. 36) was again due to the assumption made during the monitoring of the fatigue cracks using the p.d. technique (i.e. that the cracks followed a fairly direct path through the thickness of the specimen). However, in

the specimen represented in fig. 36, the high applied stresses resulted in the growth of shear fatigue cracks along planes orientated at an angle of 45° to the longitudinal specimen direction, giving artificially high p.d. values and thus exaggerated ΔK values. Such growth was only observed in a few specimens tested in the high applied stress range.

Comparison of the curves for the unpeened 8090 alloy tested at both high and low stress ranges (fig. 33 and 36) shows a marked difference, the curve for the alloy tested at the low stress range showing a growth rate approximately ten times slower than that in the alloy tested at the high stress range at the same ΔK values. Since the fracture surfaces observed in the 8090 alloy were highly faceted and irregular and since extensive amounts of debris have been observed on these surfaces (plate 20a) and exuding from growing cracks (plate 18), it can be assumed that the 8090 alloy experienced a high degree of roughness induced closure during fatigue. Further evidence for this is the presence of spherical debris on the fracture surface (plate 25), typical of that produced between surfaces in contact during fatigue (i.e. fretting debris such as that seen on the fretting scar shown in plate 27). Further closure effects will have been experienced by the crack due to the effects of debris induced closure resulting from the high degree of debris produced. It is well known that fatigue crack closure results in a reduction of the effective ΔK value at the crack tip and therefore a reduction in the growth rate (104). This roughness and debris induced closure would have more effect on growing fatigue cracks in the specimens tested at low applied stresses where, during the minimum part of the applied

stress cycle, the crack faces are allowed to come into closer contact than those in the specimens tested at high applied stresses.

The absence of closure effects observed in the 7010 alloy explains the similarity between the da/dN vs. ΔK curves for the unpeened specimens tested at both high and low applied stresses (figs. 27 and 30).

8.3 Reversed-Bending Fatigue Testing of the Shot Peened 7010 and 8090 Alloys

Shot peening produced a marked change in the early fatigue crack behaviour in both 7010 and 8090 alloys when compared to that of the unpeened alloys. The crystallographic dependence of fatigue cracking observed in the unpeened 8090 alloy was nullified so that the growth behaviour was similar to that in the peened 7010 alloy (see plates 9c, 9d, 10b and 10c). In fact, shot peening appeared to normalise the differing microstructures to produce early fatigue crack behaviour which was very similar, regardless of the alloy.

8.3.1 Peening Damage

The damage introduced into the surfaces of both the 7010 and 8090 alloys by shot peening, especially at the high intensity, is evident from plates 14 and 19; deep dimples and folds are produced which act as fatigue crack initiation sites (plates 9c, 9d and 10b). The rapid growth of cracks down folds around the dimples

produced the spalling behaviour observed at the base of many of these dimples (plate 19b), these being preferential sites for crack growth since oxide trapped between the surfaces of the folds prevents rewelding during the peening operation. The large number of deep dimples and folds resulted in a large number of fatigue crack initiation sites especially in the heavily peened alloys where more damage was incurred.

8.3.2 Fatigue Crack Profiles

Shot peening alloys 7010 and 8090 produced a reduced fatigue crack growth rate (once the cracks had initiated from the deep folds or dimples) in a direction normal to the surface, allowing further growth in a direction parallel to the surface to occur. This resulted in the formation of the flattened and often irregular fatigue crack profiles shown in figs. 21b, 21c, 22b and 22c. The shorter crack lengths corresponding to the position of deep peening dimples (fig. 21c) indicate the presence of high residual compressive stresses in the vicinity of these dimples. Consequently, although the areas of deep peening damage acted as fatigue crack initiation sites, the cracks grew away from such areas into the surrounding material where the conditions for crack growth in a direction normal to the surface were more favourable.

8.3.3 Reversed-Bending S-N Curves for the Shot Peened 8090 and 7010 Alloys

8.3.3.1 Alloy 8090

The S-N curves in fig. 19 show the effects shot peening had on the fatigue of the 8090 alloy in reversed-bending; the retarding effects of the residual compressive stress on fatigue crack growth in this alloy only occurring in high cycle fatigue. The detrimental effects of peening in low cycle fatigue (peening becoming detrimental at applied stress ranges above 390MPa and 470MPa in the cases of the lightly and heavily peened alloys respectively) may be thought to be as a consequence of the high degree of surface damage resulting in rapid fatigue crack initiation. However, since fatigue crack initiation also occurred early on in the unpeened alloy (fig. 26) and since fatigue at high applied stresses is dominated by crack propagation, it is more likely that the reduced fatigue life was due to some other mechanism.

The effect of shot peening on the behaviour of early fatigue cracks in the 8090 alloy, as shown in plate 10, was to prevent faceted growth by the formation of a plastically deformed layer. plastic deformation has the effect of preventing localised slip in this alloy by introducing a high dislocation density into the surface and by breaking up the coarse grain structure at the surface. Plate 10c displays well the effects of the peening deformation, faceted growth only occurring at a depth below that of the peak residual compressive stress (beyond which no deformation by peening was incurred). As described earlier, the

retarding effects of faceted growth on fatigue crack propagation rates are well known and since no faceted growth was observed through the deformed surface layers, propagation through this region was not hindered by such growth. It can therefore be seen that fatigue in the peened 8090 alloy was controlled by two different mechanisms; the beneficial residual compressive stress (this being the dominating factor in high cycle fatigue) and the detrimental early, non-crystallographic crack growth behaviour (this being the dominating factor in low cycle fatigue).

Since no roughness induced closure occurred between the fracture surfaces of the peened 8090 alloy in the region of the deformed surface layers, no debris was produced (such debris, as described in section 8.2.4.3 being formed by the rubbing of roughened crack faces during cycling). As shown in plate 20b, debris is only present below the plastically deformed surface layer where faceted growth (and thus roughness and debris induced closure) began. Examination of the fracture surface of the unpeened 8090 alloy in plate 20a shows debris very close to the surface of the notch, indicating a reduction in growth rates due to roughness and debris induced closure, even at very short crack lengths.

8.3.3.2 Alloy 7010

Examination of the S-N curves in figs. 18 and 19 shows a differing fatigue behaviour between the unpeened and peened 7010 alloy specimens and a very similar behaviour between the specimens peened at the low and high intensities when compared to the behaviour of the 8090 alloy.

Since fatigue cracking in the low cycle region of the S-N curves is mainly propagation controlled, it can be assumed that fatigue in this region is dominated in the peened alloy by the residual compressive stress and not by the effects of the peening damage producing early fatigue crack initiation sites. Although fatigue crack initiation at these high applied stresses occurred early on in both the unpeened and peened specimens, early propagation in the unpeened alloy continued unhindered whilst early propagation in the peened alloy was retarded by the residual compressive stress. This retardation was greater in the heavily peened alloy due to the higher compressive stress, resulting in an increased fatigue lifetime when compared to that of the lightly peened alloy.

At lower applied stresses (i.e. in high cycle fatigue), fatigue is initiation controlled and a majority of the fatigue life of the unpeened alloy was spent in fatigue crack initiation in the low applied stress range. However, fatigue crack initiation in the peened alloy occurred very early on (fig. 25). As a result, the improvement in the fatigue life of the shot peened 7010 alloy at low stresses was reduced to a level close to that of the unpeened alloy (below in the case of the lightly peened alloy).

The direction of fatigue crack growth into the surface of both the unpeened and peened 7010 alloy (plate 9) was found to be very similar. The microstructure in this alloy therefore has little influence on the direction of fatigue crack growth (i.e. the cracks are unaffected by the high degree of deformation induced by the peening operation).

8.3.3.3 Stress Relaxation

An indication of the degree of residual stress relaxation in the shot peened notch of the two alloys can be obtained by making a comparison of the stresses at which the fatigue limits occurred with the values of the peak residual compressive stresses induced by the peening treatment. If, at the notch base, the value of the maximum applied tensile stress at the fatigue limit is close to that of the peak compressive stress, then it can be assumed that the residual compressive stresses have not relaxed to any great extent during cycling. This is not an accurate evaluation since it is based upon the assumption that the applied stress at the tip of a crack, which has grown a distance into the surface corresponding to that of the peak residual compressive stress, is equal to that at the surface. It has also been assumed that a threshold stress intensity for crack growth does not exist. In the case of the heavily peened 7010 alloy the limiting stress range was 330MPa. The maximum value of applied stress produced by this range (R = 0.1) was therefore 368MPa, a value close to that of the peak residual compressive stress in the heavily peened alloy (340MPa). A similar effect is observed in the lightly peened alloy, with the limiting stress range of 306MPa giving a maximum applied stress of 331MPa; this value corresponding to the peak residual compressive stress of 325MPa.

The "fatigue limits" in the peened 8090 alloy are not so well defined. However, an extrapolation of the curves would give approximate fatigue limits in the region of 300MPa and 270MPa for the heavily and lightly peened alloy respectively. Both of these values correspond to the peak residual compressive stresses

induced by peening at these intensities which again may indicate that relaxation does not occur to any great extent.

The examination of the "fatigue limits" verifies the observation by Franz et al (105) that the relaxation of residual stresses in notches only occurs to a small degree. Investigating the effects of shot peening in the notch of a titanium alloy, they suggested that the low degree of relaxation was due to the prevention of flow of material at the base of the notch during cycling.

8.3.4 da/dN vs. ΔK curves for the Shot Peened 7010 and 8090 Alloys

The da/dN vs. ΔK curves obtained by fatigue testing the peened 8090 and 7010 alloys in reversed-bending (figs. 27 to 38) show additional aspects of the fatigue behaviour of peened alloys. It is important to note that the calculated ΔK values for fatigue cracks in the shot peened alloys were based on the applied stress range; the effect of the residual compressive stress has not been taken into account since the alteration of the applied and residual stresses by a fatigue crack growing from damage at the base of the notch are not known and can only be determined accurately using complex finite element analysis techniques.

8.3.4.1 Fatigue Crack Initiation

As can be seen from figs. 27 to 38, very early crack growth (at a growth rate, da/dN of 10^{-7}mm/cycle) occurred at crack lengths roughly corresponding to the depth of the peening damage (approximately 0.05mm in the heavily peened alloys and 0.03mm in

the lightly peened alloys). It is evident from figs. 25 and 26 that surface folds opened up very early on in the fatigue life of the alloys and that fatigue cracking from these folds did not commence immediately.

The effect of the deep surface damage produced by peening, as represented in fig. 39, shows that such damage would result in a large increase in the applied tensile stresses at the base of the notch. If no such damage were present, crack initiation may well be retarded if not prevented by the effects of the residual compressive stress at the notch surface.

8.3.4.2 Fatigue Crack Propagation through the Residually Compressed Layer

The rapid increase in growth rates during the early stages of cracking was followed by a sharp decrease, as shown in the da/dN vs. ΔK curves for both peened alloys. This can be explained by considering the combined stress concentrating effects of the notch and peening damage (favouring crack growth) and the effects of the residual compressive stress (opposing crack growth). From fig. 39 it is clear that the dominating effect of the notch on a growing fatigue crack becomes weaker with distance into the peened surface and that the effects of the compressive stress becomes stronger. The addition of the stress distribution resulting from the peening damage (being 0.007mm deep in the case of the crack represented in fig. 29) results in a very large, but shallow tensile stress at the base of the damage. The depth at which the stress concentrating effects of the notch and peening damage are reduced significantly, allowing the residual compressive stress to

dominate, corresponds to the maximum value of da/dN observed in figure 29.

Comparison of the depths of the damage from which the cracks grew with the depths of the maxima support this explanation; fatigue cracks emanating from shallow damage being retarded at an earlier stage by the residual compressive stress than those emanating from deep peening damage.

The depths at which growing fatigue cracks were retarded to a growth rate below 10^{-7} mm/cycle clearly demonstrate the effects of the peak residual compressive stress on the fatigue behaviour of these alloys. However, it is unclear whether the fatigue cracks were brought to a standstill and only continued after some relaxation of the residual compressive stresses had occurred, or whether the cracks just progressed very slowly through the region of peak compressive stress. Examination of the fatigue limits of the two peened alloys, as described in section 8.3.3.3, indicated very little relaxation and thus it is assumed that the cracks progressed very slowly through the compressively stressed layer.

It should be noted that, as stated by Berns and Weber (27), fatigue cracks growing through a shot peened surface layer will be brought to a standstill when they approach the threshold stress intensity for crack growth; the increasing residual compressive stress reducing the effective applied tensile stress as the crack grows towards the peak residual compressive stress. The threshold value for crack growth in the 7010 alloy is 4.5 MPa$\sqrt{m}$ and in the 8090 alloy is 6.0 MPa$\sqrt{m}$. Since the ΔK calculation was based upon the applied stress range and not the effective stress range, the residual compressive stresses produced an applied threshold stress

intensity value well above that of the threshold intensity for crack growth. The model shown in fig. 39 is not accurate at such crack depths since the value of the effective stress intensity range for cracks at a depth corresponding to the peak residual compressive stress is 0.71MPa$\sqrt{m}$, a value well below that of the threshold stress intensity for the 7010 alloy.

Since fatigue crack growth rates were affected by the layer of residual compressive stresses, it can be assumed that the magnitude of these stresses will have some significance; increasing their magnitude (or decreasing the applied stress) would be expected to retard crack growth significantly over a wider range of crack lengths whilst decreasing the magnitude of the residual compressive stresses (or increasing the applied fatigue stress) would be expected to retard crack growth over a narrower range.

Although the present data is far from complete, this general behaviour was observed; the lightly peened alloys having narrow ranges of ΔK over which the growth rate fell (with the exception of fig. 37 which is described in more detail below) and the heavily peened alloys having wide ranges over which the growth rate fell. The narrowing effects of the higher applied stress can also be seen from these figures (again, with the exception of figure 37).

As shown in fig. 37, the effects of crack retardation by the residual compressive stresses in the lightly peened 8090 alloy tested at the high applied stress were quite small. The reversed-bending S-N curves shown in fig. 19 for the 8090 alloy show the effects of shot peening on the alloy at the high applied

stresses when compared to the unpeened alloy. It is clear that, at the high applied stress, the effects of the residual compressive stresses induced by light peening were overwhelmed by the effects of the applied stress, the applied stress range being almost twice the magnitude of the peak residual compressive stress.

Examination of the da/dN vs. ΔK curves for the lightly and heavily peened 8090 alloy fatigue tested at the low and high applied stresses respectively (figs. 34 and 38), shows a drop in growth rates corresponding to the peak residual compressive stresses. However, growth rates were only reduced to approximately 10^{-6} mm/cycle, indicating that the magnitudes of the residual compressive stresses were not sufficient to produce significant retardation in growth rates at these applied stresses. In fact, the only 8090 specimen which exhibited fatigue crack growth rates below 10^{-7} mm/cycle was the heavily peened alloy tested at the low applied stress (fig. 35). At this applied stress level, the beneficial effects of heavy peening are apparent, the residual compressive stresses clearly dominating and producing a large degree of crack growth retardation.

The retarding effects experienced by the fatigue cracks as they grow through the residually compressed layer of the shot peened alloys are very similar to those experienced by a growing fatigue crack subjected to an overloading stress cycle (106). In the latter case a compressive stress is produced by the high degree of reversed plastic flow of the material around the crack tip during the overloading cycle and this results in a retardation of growth rate until the crack has passed through the affected zone.

It is interesting to note that the growth of the fatigue crack following retardation by the residual compressive stress induced by peening resembles the growth of fatigue cracks from a threshold stress intensity; the growth rate increasing rapidly to attain the steady growth in the Paris regime before failure at the stress intensity corresponding to the fracture toughness of the material. In fact, if effective ΔK values could be accurately calculated for fatigue cracks growing through the residual compressive layer, curves very similar to those using the "load shedding" technique could be obtained; the difference being that the load shedding would occur internally rather than externally.

8.4 Rotating-Bending Fatigue Testing

8.4.1 Introduction

In this section the results obtained from the rotating-bending testing of the 7010 and 8090 alloys in plain and fretting-fatigue are discussed. This method of testing resulted in a higher degree of scatter than that observed in the reversed-bending tests, probably due to the distortion of the rods during the heat treatment, a very slight distortion often remaining even after the 2.5% stretch. The difference in positions of the S-N curves for the two alloys tested in reversed and rotating-bending was simply a size effect, the larger section of the reversed-bending specimens requiring more time for the stress intensity at the tip of the growing fatigue crack to attain the critical value for fracture (i.e. the fracture toughness of the alloy).

8.4.2 Plain-Fatigue of the Unpeened and Shot Peened 7010 Alloy

The behaviour of 7010 alloy in rotating-bending (fig. 40) was very similar to that of the alloy in reversed-bending (fig. 18), with shot peening improving the fatigue strength at high applied stresses; this improvement reducing as the applied stress was reduced. However, the differences observed in the reversed-bending tests between the specimens peened at the low and high intensities appear to have been reduced significantly in rotating-bending, especially at low applied stresses.

The effects of the residual compressive stresses induced by peening, as in the reversed-bending specimens, was to produce an improvement in fatigue properties at the high applied stresses. A small amount of stress relaxation may have occurred in the rotating-bending specimens (since they were not notched) resulting in a decreased separation of the curves for the specimens peened at the two intensities in the low applied stress range.

8.4.3 Fretting-Fatigue of the Unpeened 7010 Alloy

The typical angular growth of the early fatigue cracks into the surface of the fretted specimens, as shown in plate 11a, is a result of the shear stresses generated between the two surfaces in contact, the cracks growing normal to the applied stress once they had escaped the influence of the fretting stresses.

The short life of the unpeened 7010 alloy in fretting-fatigue resulted in the production of only small amounts of thinly spread and irregular (i.e. non-spherical) debris on the fretting scar (plate 24a). The production of greater amounts of debris,

including spherical debris, requires a higher number of fatigue cycles. The reduced fatigue life under fretting conditions can be explained by considering the time required for plain-fatigue crack initiation in the unpeened 7010 alloy. A large proportion of the fatigue life was spent in crack initiation, especially at low applied stresses, and since fretting results in a large decrease in the time to fatigue crack initiation, a much reduced lifetime was observed, particularly at low applied stresses where fatigue is largely initiation controlled.

8.4.4 Fretting-Fatigue of the Shot Peened 7010 Alloy

The nullifying effects of shot peening, especially at the high intensity, on the fretting-fatigue strength of the 7010 alloy (plate 11c) can be explained by considering the residual compressive stresses and the surface roughness induced by peening. The residual compressive stress will decrease the applied tensile stress at the specimen surface and the surface roughness will reduce the effects of the tangential stresses exerted at the edges of the region of contact between the specimen and the feet of the fretting bridges (61). Fatigue cracks were observed at the edge of the fretting scar in the lightly peened alloy (plate. 11b), indicating that the reduced tangential fretting forces along with the reduced surface tensile stresses were not sufficient to prevent fatigue crack initiation. However, a high number of very small cracks were observed growing from the fretting scar in the heavily peened alloy indicating that crack growth was being retarded by the residual compressive stress sufficiently to allow the initiation of more fatigue cracks. The effect of many fatigue

cracks in a surface, as stated by Waterhouse (64), is to reduce the stress concentration at the tip of all of them and, as a result, fatigue crack growth from the fretting scar was superceded by plain-fatigue crack growth elsewhere on the gauge length.

The presence of a large amount of highly spherical debris on the scars of the peened alloy (plate 24b) is an indication of the extended fatigue life resulting from this treatment.

The cylindrical debris observed on the fretting scar of the heavily peened 7010 alloy (plate 24c) may indicate a method by which spherical debris forms in the peened alloys. The cylindrical debris could be formed by the rolling up of spalled material (such as that shown in plate 19) on the peened surface, the rolled material then breaking up to form the observed spherical debris.

8.4.5 Plain-Fatigue of the Unpeened and Shot Peened 8090 Alloy

Shot peening of the 8090 alloy did not result in similar fatigue behaviour to that of the alloy in reversed-bending. The peening produced a slight improvement in fatigue properties over the entire applied stress range. A comparison of sections taken through fatigue cracks in reversed and rotating-bending specimens (plates 10a and 11d) reveals a much higher degree of direction changing in the reversed-bending specimens. As a result a reduced growth rate (i.e. an extended life) was observed in the reversed-bending tests, especially in the low cycle region (where propagation dominates the fatigue life), when compared to the alloy in rotating-bending. Consequently, the fatigue life of the

unpeened 8090 alloy tested in rotating-bending was reduced to a level below that of the peened alloy at all applied stresses.

The similarity between the S-N curves for the alloy peened at the two intensities may be due to the increase in scatter of results obtained in the rotating-bending tests when compared to the reversed-bending tests. In order to obtain more accurate results, many more tests would be required.

8.4.6 Fretting-Fatigue of the Unpeened 8090 Alloy

The insensitivity to the effects of fretting of the unpeened 8090 alloy (fig. 41) can be explained by considering the high degree of crystallographic crack growth in this alloy. Fretting only has a small influence on the time to fatigue crack initiation since plain-fatigue crack initiation is already early in this alloy. It is therefore likely that the life of this alloy in fretting-fatigue was dominated by the propagation of cracks which were not in the immediate vicinity of the stress concentration at the edge of the fretting scars. As a result, this alloy was insensitive to fretting.

A comparison of the debris on the fretting scars of the unpeened 8090 and 7010 alloys reflects the different lifetimes of these two materials in fretting fatigue; much of the copious amounts of debris on the scar of the unpeened 8090 alloy being spherical (plate 27a) whilst that on the scar of the unpeened 7010, as described earlier, was uneven and thinly spread (plate 24a).

8.4.7 Fretting-Fatigue of the Shot Peened 8090 Alloy

As with the rotating-bending 7010 alloy specimens, shot peening nullified the detrimental effects of fretting on the fatigue behaviour of the 8090 alloy. This again was probably due to a combination of the increased surface roughness and the decreased resultant tensile stresses at the surface. However, if these were the only factors involved, fretting would be expected to have a more harmful effect upon this peened alloy than on the 7010 alloy since the residual compressive stresses induced by peening were significantly lower in the 8090 alloy. Examination of the fatigue cracks growing from the fretting scars in the peened 8090 alloy (plates 11e and 11f) indicates that delaminating behaviour in this peened alloy may also be important. The surface delamination at the edge of the scar results in a reduction of the tangential stresses and therefore the initiation of many small fatigue cracks over a wide area thus alleviating some of the fretting action.

The single, lightly peened specimen that failed in fretting-fatigue illustrates the effect of the reduced tangential fretting stresses since the fracture surface (plate 26c) showed not the expected angular growth of the fatigue crack into the surface from the edge of the scar, but a growth normal to the applied tensile stresses in the surface. Crack growth in such a direction indicates that the dominating stress was the applied tensile stress and not the tangential fretting stress. The faceted crack growth occurring well below the peened surface in plate 26c again highlights the effects of the deformed surface layer on the nature of fatigue crack growth in this alloy.

8.5 Static Bend Testing

8.5.1 Introduction

Static bend testing of the 7010 and 8090 alloys emphasised the dramatic effect shot peening can have on the yield strength and ductility of the material at the base of the notches.

The high yield strengths obtained in the two unpeened alloys were as a result of the well known effects of "constraint"; an effect whereby material at the base of a stress concentration is prevented from yielding at the expected applied stress by surrounding material.

Very high maximum bending strengths were also measured. This was due to the inadequacy of the elastic laws, used to determine the stress concentration factor for the specimens, to take into account the effects of yielding at the base of the notch. As stated by Weiss (107), the true value of the theoretical stress concentration factor, K_t, does not remain constant but decreases with the onset of plastic flow; the decrease becoming greater with a further increase in the applied load or strain.

8.5.2 Alloy 7010

The elongation of material at the base of the notch in the unpeened 7010 alloy following static bend testing (fig. 45) shows the normal behaviour of materials with high plasticity; the material deforming either side of the notch base where the conditions for plastic deformation were most favourable.

Shot peening the material at the base of the notch resulted in a different elongation behaviour; the high residual compressive stresses reducing the effective applied stress at the base of the notch allowing intergranular failure in the longitudinal rolling direction to occur before the onset of significant yielding. Both peening intensities resulted in similar elongation behaviour since the magnitudes of the residual compressive stresses at the surface produced by peening at the two intensities were not significantly different.

The increase in the yield strength of 200MPa after peening to both light and heavy intensities (fig. 44) again shows the effects the residual compressive stresses have on the applied bending stress. The effective applied bending stress at the base of the notch is reduced by an amount corresponding approximately to the magnitude of the residual compressive stress at the surface, thus allowing a greater deflection of the specimen (i.e. a greater applied bending stress) before the onset of yielding.

The small difference between bend strengths in the unpeened and shot peened 7010 specimens shows that the shear mode of failure was relatively unaffected by the presence of a surface residual compressive stress.

8.5.3 Alloy 8090

Elongation of material at the base of the notch in the unpeened 8090 alloy was lower than that in the unpeened 7010 alloy. This is probably due to the poor resistance of this alloy to intergranular failure in the longitudinal rolling direction. The bending stress required to produce this mode of failure even in the peened specimen, was very much lower than that required to produce the same behaviour in the unpeened 7010 alloy.

Since the elongation of the material at the base of the notch in the unpeened 8090 alloy was already low, the bend testing of the shot peened alloy, as may be expected, resulted in very little change of elongation. The effect of shot peening in the notch on the yield strength of the 8090 alloy was very similar to that observed in the 7010 alloy and a similar explanation applies.

8.6 The Shot Peening Process

Fatigue cracks have been found to initiate at the regions of deep peening damage before being retarded by the residual compressive stresses induced by peening. A consideration of the stresses at the base of the peening damage has revealed the detrimental effects on fatigue of such damage and emphasises the importance of maintaining strict control over the shot energy and quality. However, although no data has been obtained, it is suspected that no amount of monitoring can ensure that all the shot are of the same energy since the shot are blown from nozzles (or thrown from wheels) in large quantities. This has the effect of producing a stream of shot with an undesirably wide range of energies; the few

shot with excessively high energies resulting in the detrimental deep peening damage from which fatigue cracks initiate.

Since it is clearly not feasible to fire each shot independently to ensure a constant energy, the technique could be improved by screening out the high energy shot after it leaves the nozzle (or wheel). This may be achieved by, for example, blowing the stream sideways through an orifice before it strikes the workpiece. As shown schematically in fig. 46, the high energy shot would continue on a relatively straight path and would thus be screened out whilst the shot of the desired energy would pass through the orifice to strike the workpiece. This method would also remove any undesirable broken shot which would be blown out of the stream before it passes through the orifice.

A further improvement could be made by shot peening in an inert environment. This would have the effect of preventing the formation of deep crack initiation sites by allowing complete rewelding between the folds during the peening operation.

CHAPTER NINE

CONCLUSIONS (AND FURTHER WORK)

It has been demonstrated that shot peening can bring about dramatic improvements in the fatigue performance of the 7010 and 8090 alloys. The following specific points have been established for these alloys as a result of the present research.

1) Fatigue in the unpeened 8090 alloy was dominated by the dependency of crack growth on the crystallographic orientation of the grains. Cracks initiated early from slip bands and followed a highly faceted path. Fatigue crack propagation in this alloy was also affected by a high degree of roughness and debris induced closure.

2) Fatigue crack growth in the unpeened 7010 alloy was not highly dependent upon the crystallographic orientation of the grains and, as a consequence, the cracks followed a fairly direct path through the thickness of the specimens. Much of the lifetime of this alloy was spent in fatigue crack initiation.

3) The plastic deformation of the shot peened surfaces extended to a depth corresponding to the peak residual compressive stress induced by the peening; this depth being 0.20mm and 0.25mm for the lightly and heavily peened alloys respectively.

4) Shot peening had a normalising effect on the two widely differing microstructures of the 7010 and 8090 alloys resulting in a crack growth behaviour through the deformed surface layers which was very similar.

5) Shot peening extended the fatigue lifetime of the 7010 alloy at high applied stresses. At low applied stresses, the fatigue lifetimes of the alloy in the peened and unpeened conditions were very similar.

6) Shot peening reduced the fatigue lifetime of the 8090 alloy at high applied stresses. At low applied stresses this trend was reversed and shot peening resulted in a significant improvement in the fatigue lifetime of the alloy.

7) Shot peening resulted in the production of a highly damaged surface containing many deep dimples and areas of weakened folded material.

8) Fatigue crack initiation in the shot peened alloys occurred from the regions of deep peening damage due to the stress concentrating effects of this damage.

9) In shot peened alloys, fatigue crack initiation was rapid but propagation through the compressed, peened surface layers was retarded, this retardation being greatest at depths corresponding to the peak residual compressive stress.

10) Crack growth beyond the peak residual compressive stress was very similar to that observed in threshold fatigue tests, the applied loads in this case being shed internally rather than externally.

11) Fretting resulted in a large decrease in the fatigue strength of the unpeened 7010 alloy due to the rapid initiation of fatigue cracks.

12) Plain-fatigue crack initiation occurs early in the unpeened 8090 alloy and therefore fretting had little effect upon the fatigue performance of the unpeened alloy, particularly at high applied stresses.

13) Shot peening alloys 7010 and 8090, particularly at a high Almen intensity, nullified the effects of fretting-fatigue.

14) Shot peening increased the yield strength and reduced the elongation of material situated at the base of the notch in the reversed-bending specimens. The reduction in elongation was greater in the 7010 alloy than in the 8090 alloy.

Further Work

1) Accurate computation of the "effective" stress intensity at the tip of a crack growing through the shot peened layer at the base of the notch.

2) Further examination of the peened 8090 alloy which has been overaged following the peening treatment to produce precipitation in the heavily deformed surface layers.

3) Transmission electron microscopy analysis of the peened surfaces to examine the nature of dislocations and thus to further aid the understanding of the peening process.

4) An investigation into the effects of fatigue on the relaxation of the residual stresses induced by peening at the base of the notch in the reversed-bending specimens and on the gauge length of the rotating-bending specimens.

5) An investigation into the effects of screening out the high energy shot during the peening process on the fatigue performance of shot peened alloys.

6) An investigation into the effects of shot peening in an inert environment (to allow full rewelding of folded material) on fatigue performance.

ACKNOWLEDGEMENTS

I would like to thank everyone who has supported me throughout this work. In particular, thanks to Keith Dinsdale for all his help and advice, to Graham Morris and Dr. Andy Dodd for their help with the computer, and also to Tony van Gool and Adam Gardner for their encouragement. In addition, thanks to all the technical staff in the department.

Last but certainly not least, I would like to thank my tutors, Dr. B. Noble and Dr. R.B. Waterhouse for their support and inexhaustible patience. I would also like to take this opportunity to wish Dr. Waterhouse all the best in his retirement.

REFERENCES

1. Bush, G.F., Almen, J.O., Danse, L.A., Heise, J.P., Soc. Auto-Engineers. ISTC, Div. 20 Meeting, Colo. Sprgs, Colo., May 21, 1962.

2. Herbert, E.G., Engineering, 470, Oct. 7, 1927.

3. Herbert, E.G., Engineering, 420, Sept. 30, 1927.

4. Zimmerli, F.P., Surface Treatment of Metals, Am. Soc. Metals Preprint, 51, 1940, pp261-278.

5. Almen, J.O., Black, P.H., "Residual Stresses and Fatigue in Metals" McGraw-Hill Book Company Inc. 1963, pp66-70.

6. Clarke, D., Birley, S.S., First International Conference on Shot Peening, Paris, Sept. 14-17, 1981, pp167-174.

7. Simpson, R.S., Probst, R.L., "Shot peening", Third International Conference on Shot Peening, Garmisch-Partenkirchen, Ed. H. Wohlfahrt, R. Kopp, O. Vohringer, Oct. 12-16, 1987, pp261-268.

8. Meguid, S.A., Duxbury, J.K. First International Conference on Shot Peening, Paris, Sept. 14-17, 1981, pp217-228.

9. Niku-Lari, A. First International Conference on Shot Peening, Paris, Sept. 14-17, 1981, pp1-21.

10. Burakowski, T., Nakonieczny, A. First International Conference on Shot Peening, Paris, Sept. 14-18, 1981, pp139-146.

11. Almen, J.O., S.A.E.J., 51, 1943, pp248-268.

12. Fuchs, H.O., First International Conference on Shot Peening, Paris, Sept. 14-18, 1981, pp323-332.

13. Hawkes, G.A., Br. Corros. J., 3, Sept. 1968, pp258-261.

14. Burck, L.H., Sullivan, C.P., Wells, C.H. Metallurgical Transactions, 1, June 1970, pp1595-1600.

15. Wohlfahrt, H. "Shot Peening and Residual Stresses" Ed. E. Kula and V. Weiss, Plenum Press, New York 1982, pp71-92.

16. Lieurade, H.P., Bignonnet, A., "Shot Peening", Third International Conference on Shot Peening, Garmisch-Partenkirchen, Ed. H. Wohlfahrt, R.Kopp, O. Vohringer, Oct. 12-16, 1987, pp343-360.

17. Ebenau, A., Vohringer, O., Macherauch, E., "Shot Peening", Third International Conference on Shot Peening, Garmisch-Partenkirchen, Ed. H. Wohlfahrt, R. Kopp, O. Vohringer, Oct. 12-16, 1987, pp253-260.

18. Wagner, L., Luetjering, G., First International Conference on Shot Peening, Paris, Sept. 14-18, 1981, pp453-460.

19. Daly, J., "Shot Peening", Third International Conference on Shot Peening, Garmisch-Partkenkirchen, Ed. H. Wohlfahrt, R. Kopp, O. Vohringer, Oct. 12-16, 1987, pp87-92.

20. Nakonieczny, A., First International Conference on Shot Peening, Paris, Sept. 14-18, 1981, pp45-50.

21. Was, G.S., Pelloux, R.M., Metallurgical Transactions A, 10A, May 1979, pp656-658.

22. Vogelsang, L.B., Report LR-222, Delft University of Technology, Delft, The Netherlands, August, 1976.

23. Dieter, G.E., Mechanical Metallurgy, 2nd Ed., McGraw-Hill Book Co., New York, 1976, p407.

24. Deng Zeng-Jie, Jin Da-Zeng, Zhov Hui-Jiu (H.C.Chov), First International Conference on Shot Peening, Paris, Sept. 14-17, 1981, pp389-394.

25. Xa Jia Chi, Zhang Ding-Quan, Shen Bang-Jin. First International Conference on Shot Peening, Paris, Sept 14-17, 1981, pp367-373.

26. Baxa, M.S., Chang, Y.A., Burck, L.H., Metallurgical Transactions A, 9a, August 1978, ppl141-1146.

27. Berns, H., Weber, L., "Shot Peening", Third International Conference on Shot Peening, Garmisch-Partenkirchen, Ed. H. Wohlfahrt, R. Kopp, O. Vohringer, Oct. 12-16, 1987, pp647-654.

28. James, M.R., "The Relaxation of Residual Stresses During Fatigue" ed. E.Kula and V.Weiss, Plenum Press, New York 1982, pp297-314.

29. Boggs, B.D., Byrne, J.G., Metallurgical Transactions, 4, Sept. 1973, pp2153-2157.

30. Schutz, W., First International Conference on Shot Peening, Paris, Sept. 14-17, 1981, pp423-433.

31. Leadbeater, G., Noble, B., Waterhouse, R.B., "Advances in Fracture Research", Sixth International Conference on Fracture, Ed. S.R. Valluri, D.M.R. Taplin, P. Rama Rao, J.F. Knott, New Delhi, India, 3, Dec. 4-10, 1984, pp2125-2132.

32. Balcar, G.P., Maltby. F.C., First International Conference on Shot Peening, Paris, Sept. 14-17, 1981, pp295-301.

33. Kohler, W., "Shot Peening", Third International Conference on Shot Peening, Garmisch-Partenkirchen, Ed. H. Wohlfahrt, R. Kopp, O. Vohringer, Oct. 12-16, 1987, pp269-278.

34. Simpson, R.S., Probst, R.L., "Shot Peening", Third International Conference on Shot Peening, Garmisch-Partenkirchen, Ed. H. Wohlfahrt, R. Kopp, O. Vohringer, Oct. 12-16, 1987, pp261-268.

35. Bush, J.J., Mattson, R.L., Roberts, J.G., U.S. Patent 3,073,022 "Shot Peening Treatments", Jan. 15, 1963.

36. Snowman, A., Schmidt, R.G., First International Conference on Shot Peening, Paris, Sept. 14-17, 1981, pp313-319.

37. Woelfel, M.M., "Shot Peening", Third International Conference on Shot Peening, Garmisch-Partenkirchen, Ed. H. Wohlfahrt, R. Kopp, O. Vohringer, Oct. 12-16, 1987, pp125-132.

38. Wang Renzhi, Li Xiangbin, Tan Youggui, Yan Minggao, First International Conference on Shot Peening, Paris, Sept. 14-17, 1981, pp185-192.

39. Hornbogen, E., Thurmann, M., Verpoort, C., First International Conference on Shot Peening, Paris, Sept. 14-17, 1981, pp381-387.

40. Hornbogen, E., Verpoort. C., 5th International Conference on Fracture ICF 5, Cannes, France, 1981.

41. Graef, M., Verpoort, C., 5th International Conference on the Strength of Metals and Alloys, ICSMAS, Aachen, West Germany, Vol II, 1207.

42. Wang, R., Li, X., Wu, H., "Shot Peening", Third International Conference on Shot Peening, Garmisch-Partenkirchen, Ed. H. Wohlfahrt, R. Kopp, O. Vohringer, Oct. 12-16, 1987, pp417-422.

43. Milo, J.H., Materials Protection, Sept. 1968, pp39-42.

44. Plaster, H.J., First International Conference on Shot Peening, Paris, Sept. 14-17, 1981, pp83-94.

45. Tomlinson, G.A., Proc. Royal Soc., 115A, 1927, p472.

46. Tomlinson, G.A., Thorpe,P.L., Gough, H.J., Proc. Inst. Mech. Eng., 185, 1939, p691.

47. Godfrey, D., NACA Technical Note 2039, 1950.

48. Wright, K.H.R., Proc. Inst. Mech. Eng., 1B, 1952-1953, p556.

49. Uhlig, H.H., J. Appl. Mech., 21, 1954, p401.

50. Halliday, J.S., Hirst, W., Proc. Royal Soc., 236A, 1956, p411.

51. Feng, I-Ming, Rightmire, B.G., Proc. Inst. Mech. Engrs., 170, 1956, p1056.

52. Waterhouse, R.B., AGARD Conference Proceedings No. 161, 1975, 8, pp1-8.

53. Smith, M.C., Smith, R.A., Wear, 76, 1982, pp105-128.

54. Wharton, M.H., Taylor, D.E., Waterhouse, R.B., Wear, 23, 1973, p251.

55. Waterhouse, R.B., Taylor, D.E., Wear, 17, 1971, pp139.

56. Alic, J.A., Hawley, A.L., Urey, J.M., Wear, 56, 1979, p351.

57. Corten, H.T., T. and A.M. Report No. 88, 1955.

58. Fenner, A.J., Field, J.E., Trans. N.E. Coast Institute of Engineering Shipbuilders, 76, 1956-1960, p184.

59. Waterhouse, R.B., Proc. Inst. Mech. Engrs., 179, 1964-1965, part 33, p258.

60. Endo, K., Goto, H., Nakamura, T., Bull. Jap. Soc. Mech. Engrs., 12, 1969, p1300.

61. Waterhouse, R.B., "Fretting Corrosion", Pergamon Press, Oxford, 1972.

62. Bowers, J.E., Finch, N.J., Goreham, A.R., Inst. Mech. Engrs., 182, 1967-1968, part 1, p703.

63. Waterhouse, R.B., Saunders, D.A., Wear, 53, 1979, p381.

64. Waterhouse, R.B., "Corrosion Fatigue", Corrosion, Shrier, Newnes, Butterworth, London, 2nd ed. 1, 1965, pp8:96-8:113.

65. Noble, B., Waterhouse, R.B., Final Report on Contract No. 407.409, Dept. of Metallurgy, University of Nottingham, 1979-1981.

66. Fair, G.H., Noble, B., Waterhouse, R.B., Advances in Surface Treatments, Gournay, Vol. 1, Sept. 1984.

67. Park, J.K., Ardell, A.J., Met. Trans. A, 14A, Oct. 1983, pp1957-1965.

68. Lorimer, G.W., Nicholson, R.B., "The Mechanism of Phase Transformations in Crystalline Solids", Inst. Metals, London, 1968, p36.

69. Schmalzried, H., Gerold, V., Z. Metallkd., 49, 1958, p291.

70. Loffler, H., Kovacs, I., Lendvai, J., J. Mater. Sci., 18, Aug. 1983, pp2215-2240.

71. Ryum, N., Z. Metallkd., 66, 1975, pp338-344.

72. Auld, J.H., Cousland, S.M., Scr. Met., 5, 1971, p765.

73. Gjonnes, J., Simensen, C.J., Acta Met., 18, 1970, p881.

74. Thompson, D.S., "Inorganic Materials and Physical Chemistry", ed. R.F. Schwenker Jr. and P.D. Garn, Academic Press, New York, 1969, 2, pp1147-1170.

75. Bryant, A.J., J. Inst. Metals, 94, 1966, pp94-98.

76. Smith, W.F., Grant, N.J., Met. Trans. 2A, 1971, pp1333-1340.

77. Livak, R.J., Papazian, J.M., Scr. Met. 18, 1984, pp485-488.

78. Wert, J.A., Scr. Met., 15, 1981, pp445-447.

79. Fitzsimmons, P.E., "A Review of the Properties of Aluminium 7010 Plate", August, 1981.

80. Polmear, I.J., "Light Alloys - Metallurgy of Light Metals", Edward Arnold Ltd., 1981, p86.

81. Baker, C., Martin, D.C., Aluminium Alloys in the Aircraft Industry, Proc. Symp. Turin, Oct.1-2, 1976, pp63-69.

82. Gruhl, W., International Congress on Aluminium Alloys in the Aircraft Industry, Turin, 1976.

83. Noble, B., Thompson, G.E., Metal Science Journal, 1971, 5, 1971, p114.

84. Nozato, R., Nakai, G., Trans. J.I.M., 18, 1977, pp679-689.

85. Tanner, L.E., Leary, H.J., Order-Disorder Transformations in Alloys, Springer-Verlag, Berlin, 1974, pp180-239.

86. Schlegoleva, T.V., Rybalko, O.F., Phys. Met. Metallog., 42, 1976, pp83-93.

87. Williams, D.B., "Aluminium-Lithium Alloys",Ed. T.H. Saunders Jr., E.A. Starke Jr., AIME Warrendale, PA, 1981, p89.

88. Williams, D.B., Proc. First International Aluminium-Lithium Conference, Stone Mountain, Georgia, May 19-21, 1980, pp89-100.

89. Kuriyana, K., Masaki, N., Acta. Cryst., B31, 1975, p1973.

90. Harris, S.J., Noble, B., Dinsdale, K., The Metallurgy of Light Alloys, Spring Residential Conference, 20, March 1983, pp48-56.

91. Gayle, F.W., Proc. First International Aluminium-Lithium Conference, Stone Mountain, Georgia, May 19-21, 1980, pp119-139.

92. Sankaran, K.K., Grant, N.J., Proc. First International Aluminium-Lithium Conference, Stone Mountain, Georgia, May 19-21, 1980, pp205-227.

93. Peel, C.J., Evans, B., Baker, C.A., Bennett, D.A., Gregson, P.J., Flower, H.M., Proc. First International Aluminium-Lithium Conference, Stone Mountain, Georgia, May 19-21, 1980, pp363-392.

94. Gregson, P.J., Flower, H.M., Peel, C.J., Evans, B., The Metallurgy of Light Alloys, Spring Residential Conference, 20, March 1983, pp57-61.

95. Stigerwald, E.A., Hanna, G.L., Proc. ASTM, 62, 1962, pp885-905.

96. Mutoh, Y., Fair, G.H., Noble ,B., Waterhouse, R.B., Fatigue Fract. Engng. Mater. Struct., 10, No4, 1987, pp261-272.

97. Lukas, P., Klesnil, M., Mater. Sci. Engng. 34, 1978, pp61-66.

98. ASTM Standard E647-83, "Test Methods for Constant-Load-Amplitude Fatigue Crack Growth Rates Above 10^{-8}m/cycle.

99. Newman, J.C.Jr, Raju, I.S., Eng. Fract. Mech. 15, 1981, pp185-192.

100. Lynch, S.P., Metal Science, 9, 1975, pp401-410.

101. Foth, J., Marrisen, R., Trautman, K.H., Nowack, H., "The Behaviour of Short Fatigue Cracks", Ed. K.J.Miller and E.R. de los Rios, Paston Press, Norwich, 1986, pp353-368.

102. Guiu, F., Stevens, R.N., "The Behaviour of Short Fatigue Cracks", Ed. K.J.Miller and E.R. de los Rios, Paston Press, Norwich, 1986, pp407-421.

103. Schijve, J., "Fatigue 84", 2nd International Conference on Fatigue and Fatigue Thresholds, (EMAS, Warley), pp751-772.

104. Venkateswara, K.T., Yu, W., Ritchie, R.O., "Fatigue Crack Propagation in Aluminium-Lithium Alloys", Part I, Center for Advanced Materials, Department of Materials Science and Mineral Engineering, University of California, Berkely, CA94720.

105. Franz, H.E., Olbricht, A., "Shot Peening", Third International Conference on Shot Peening, Garmisch-Partenkirchen, Ed. H. Wohlfahrt, R. Kopp, O. Vohringer, Oct. 12-16, 1987, pp439-446.

106. Parker, A.P., "The Mechanics of Fracture and Fatigue: an Introduction", A.P. Parker, London, Spon., 1981, p133.

107. Weiss, V., "Fracture", Ed. H. Liebowitz, Acad. Press, London, 13, 1971, pp227-264.

108. Cullity, B. D., "Elements of X-Ray Diffraction", Addison-Wesley Publishing Company, London, 2nd Ed., 1978, p462.

APPENDICES

APPENDIX ONE

Calculation of the Applied Bending Stresses at the Base of the Notch in the Reversed-Bending Specimens

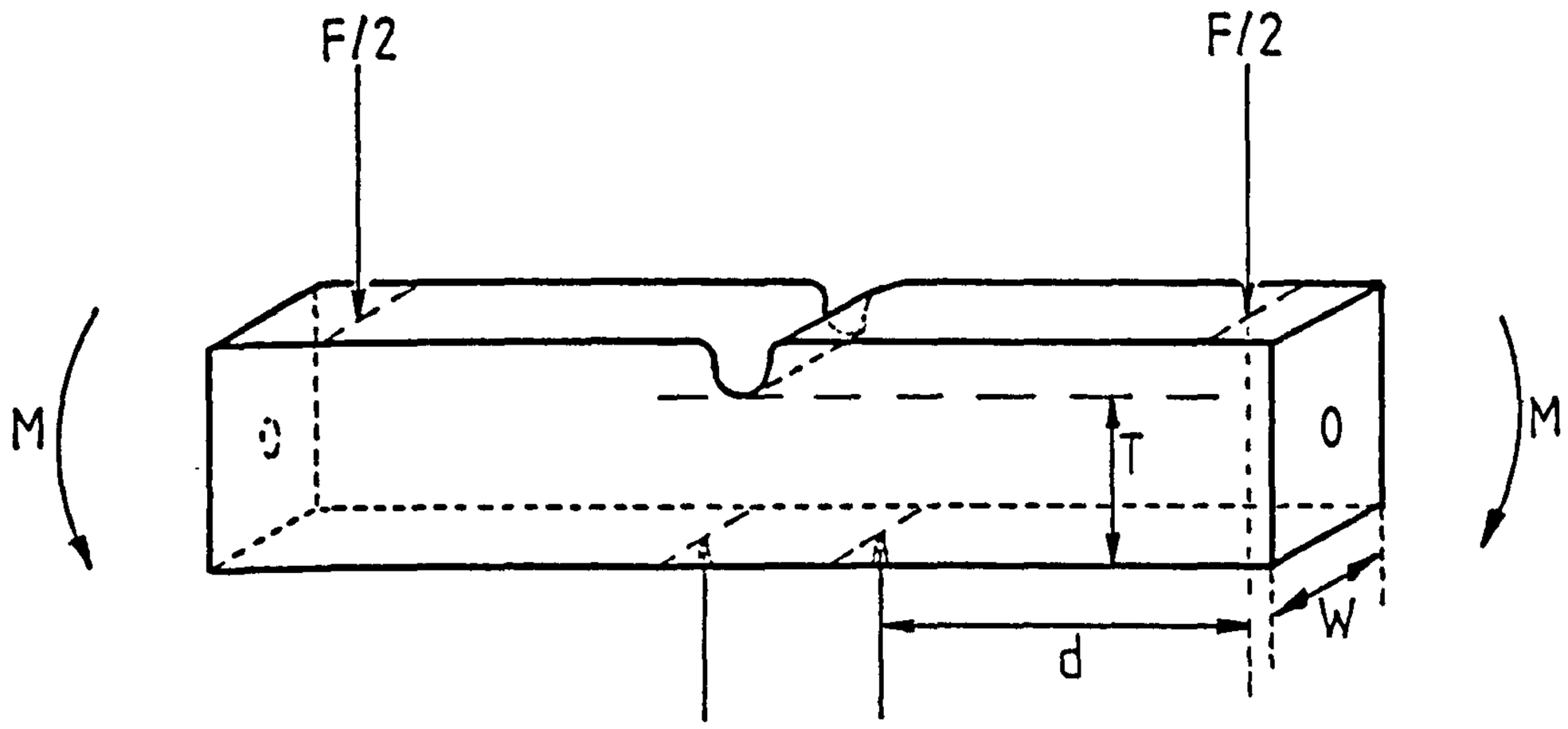

The figure above shows schematically a reversed-bending specimen in which a bending moment (M) has been applied. The calculation of the bending stresses produced at the base of the notch by applying such a moment is carried out by first determining the bending stress produced in an un-notched beam of thickness, T, before multiplying by the stress concentration factor, K_t (K_t being based upon the minimum section of the specimen).

From bending theory, the bending stress, σ, resulting from the application of a moment, M, is;

$$\sigma = MT/2I \quad \text{----------(1)}$$

where I is the second moment of area for a specimen of width, W, and is given by the formula;

$$I = WT^3/12 \quad \text{----------(2)}$$

The bending moment, $M = Fd/2$ ----------(3)

where F is the applied force and d is the distance between the outer and inner loading points.

Substituting (2) and (3) into (1) gives;

$$\sigma = 3Fd/WT^2 \quad \text{----------(4)}$$

The values of T, d and W for the reversed-bending specimens used in this work were;

$$T = 18.75 \times 10^{-3}m$$

$$d = 40.00 \times 10^{-3}m$$

$$W = 20.00 \times 10^{-3}m$$

The value of σ produced by applying a bending moment to an un-notched beam of thickness, T, can thus be calculated by inserting these values into equation (4) to give;

$$\sigma = 17{,}067F$$

Multiplying by K_t (which, as described in section 6.2.1, has a value of 2.03) gives the value of the bending stress produced at the base of the notch.

$$\underline{\sigma(\text{notch}) = 34{,}645F}$$

APPENDIX TWO

The applied stress distribution through the thickness of a reversed-bending specimen from the base of a circular notch (resulting from the application of a bending moment as shown in appendix 1) has not been found in previous literature. In order to make a reasonable estimation of this distribution, the applied stress in the y-direction near a hole in an infinite plate, as shown below, was modified.

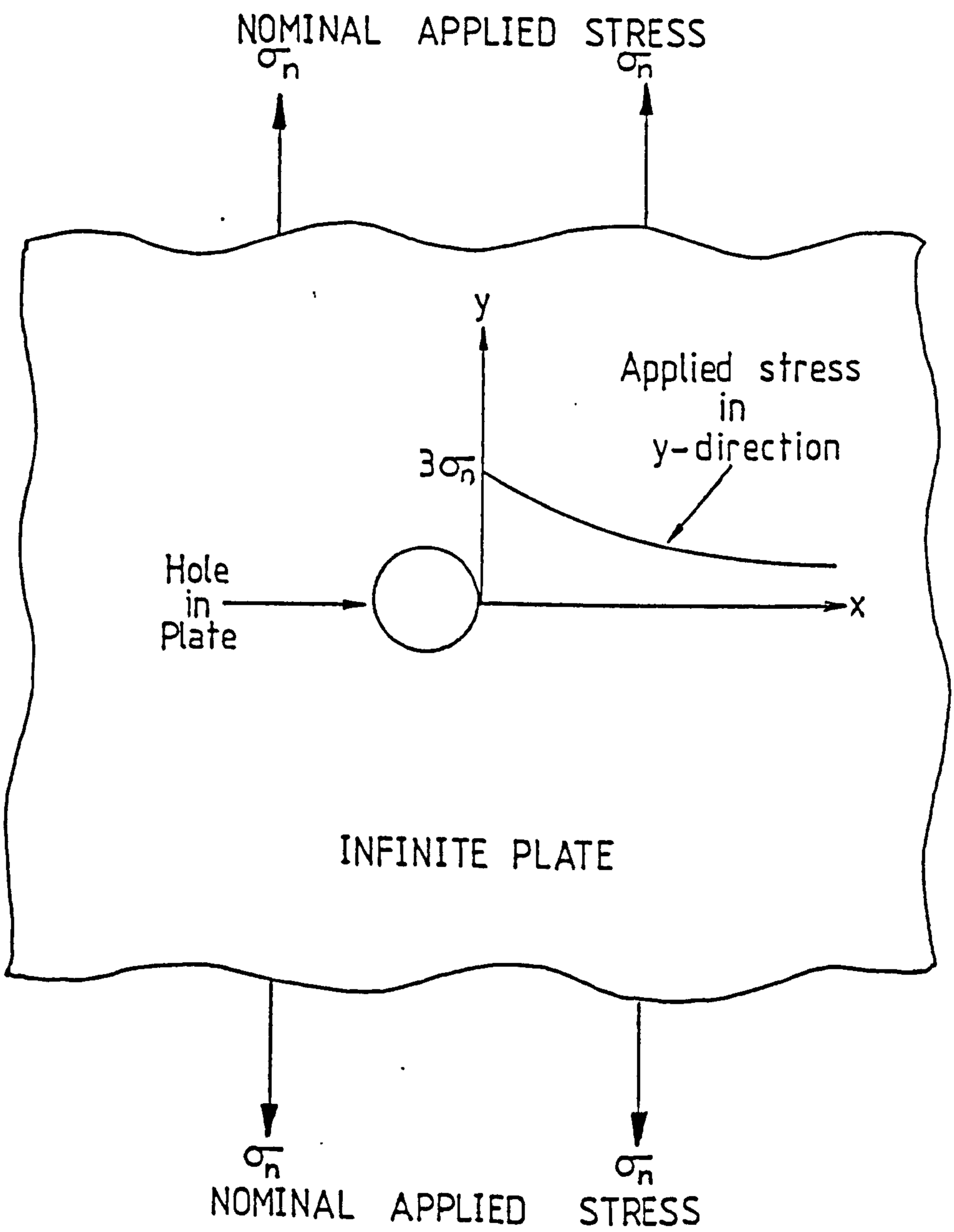

The formula for such a distribution in the y-direction is;

$$\sigma_y = \sigma_n/2\ (2 + (a/x)^2 + 3(a/x)^4) \text{ ----------(1)}$$

where; σ_y = the value of the applied stress in the y direction at a distance, x, away from the centre of the hole.

σ_n = the nominal applied stress.

and a = the radius of the hole.

From equation 1, it can be seen that the stress concentration factor (K_t) of such a hole (i.e. where x = a) is 3. The stress concentration factor, as described in section 6.2.1, for the reversed-bending specimens used in this work was 2.03 and thus equation 1 was multiplied by 2.03/3 to give;

$$\sigma_y = 0.338\sigma_n(2 + (a/x)^2 + 3(a/x)^4) \text{ ----------(2)}$$

which gives a stress concentration value of 2.03.

Although the applied stress in the case of the infinite plate was tensile whilst that in the reversed-bending specimen was in bending, the distribution near to the edge of the hole was assumed to be close to that given by equation (2) near to the base of the notch. The distribution given by the equation is shown in fig. 39b.

The addition of the residual compressive stress induced by shot peening to the applied stress distribution (as shown in fig. 39c) does not give a realistic description since the folded material, from which cracking often initiated, will result in a further increase in the stress concentration at the base of the notch.

From plates 9d and 10b, it can be seen that fatigue cracking in the peened alloys often initiated from the base of spalled regions in the heavily deformed surface. Since such damage had a roughly semi-circular profile, it is assumed that the stress distribution resulting from such damage is similar to that described by equation 1, with the radius of the hole being equal to half the length of the crack measured along the surface prior to testing (such as those shown in plates 7d, 8a and 8d) and the applied nominal stress being equal to that at the base of the notch. In order to take into account the stress gradient near the peened notch, the difference between the resultant stress at a distance, x, below the notch surface and that at the surface of the notch ($\Delta\sigma_x$) was subtracted from the stress value calculated for the effects of the surface damage at that depth as shown in the following figures.

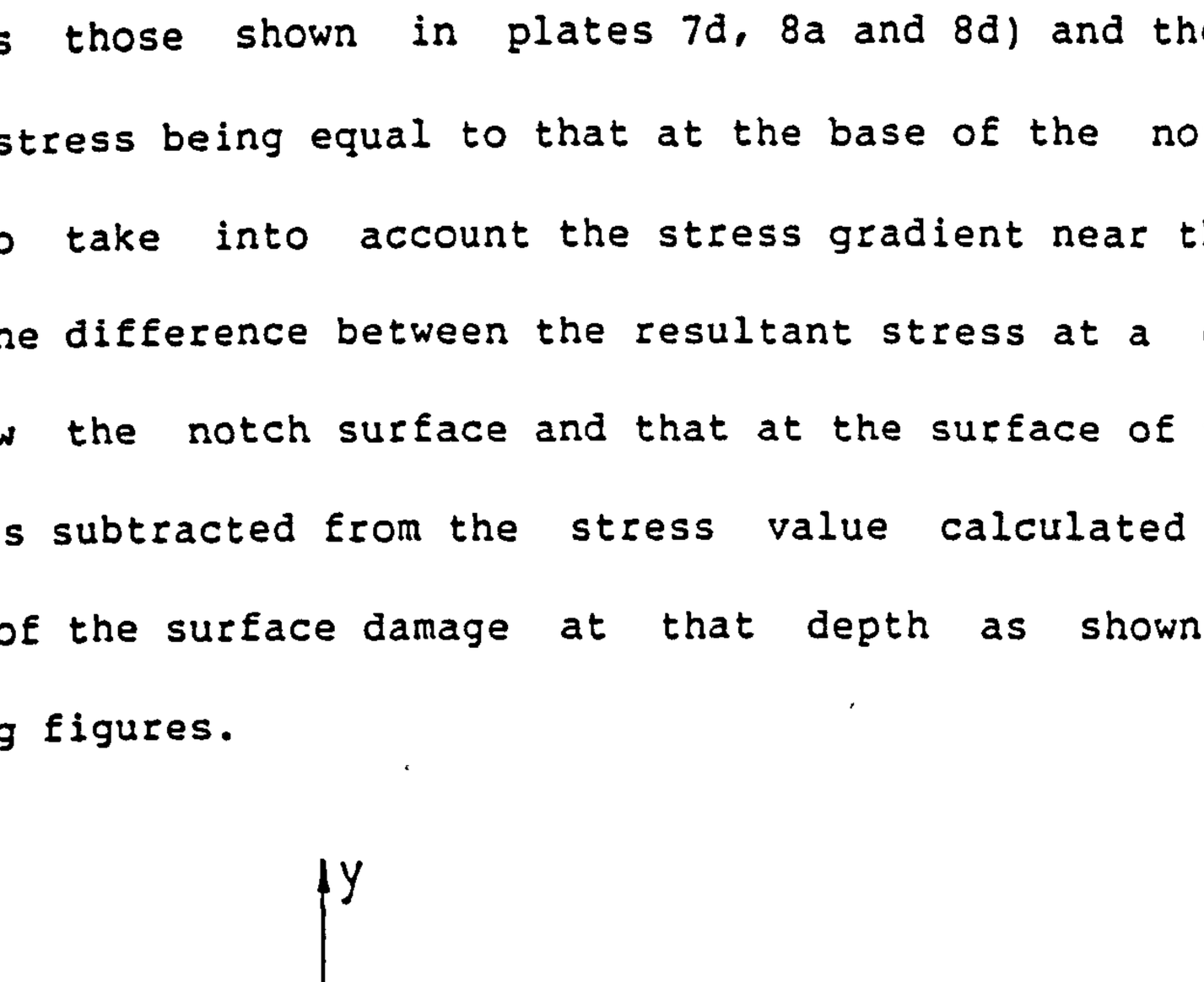

Fig. A2a) The distribution of stress in the y-direction at a distance, x, below the base of the notch in a heavily peened (and damage free) reversed-bending 7010 alloy specimen.

Fig. A2b) The modification of the residual stress distribution shown in fig. A2a, due to the effects of surface damage.

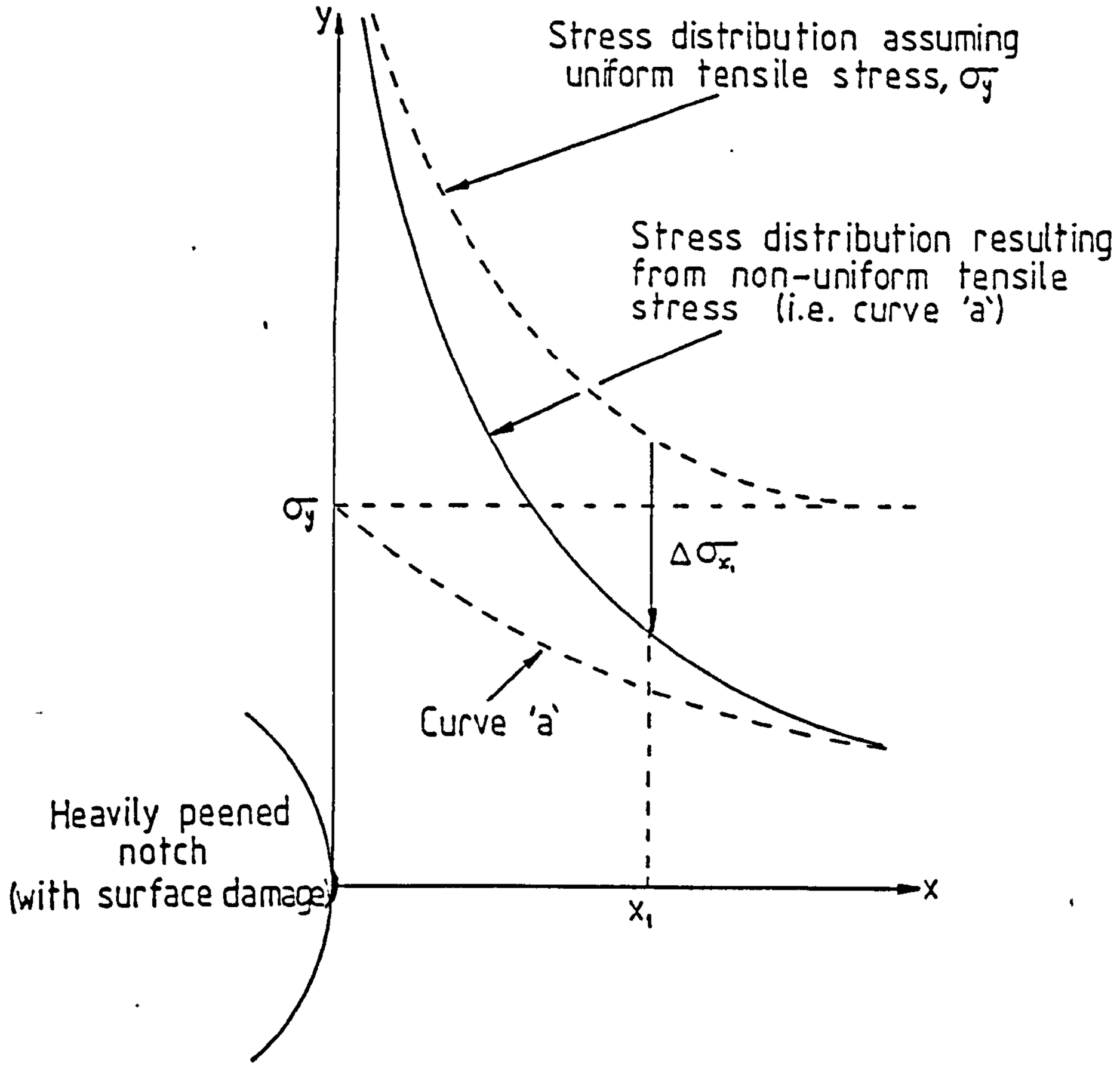

APPENDIX THREE

Calculation of the Bending Stress in the Gauge Length of the Rotating-Bending Specimens

To calculate the bending stress in the rotating-bending specimens, it was neccesary to find the second moment of area, I, for the specimen section shown below.

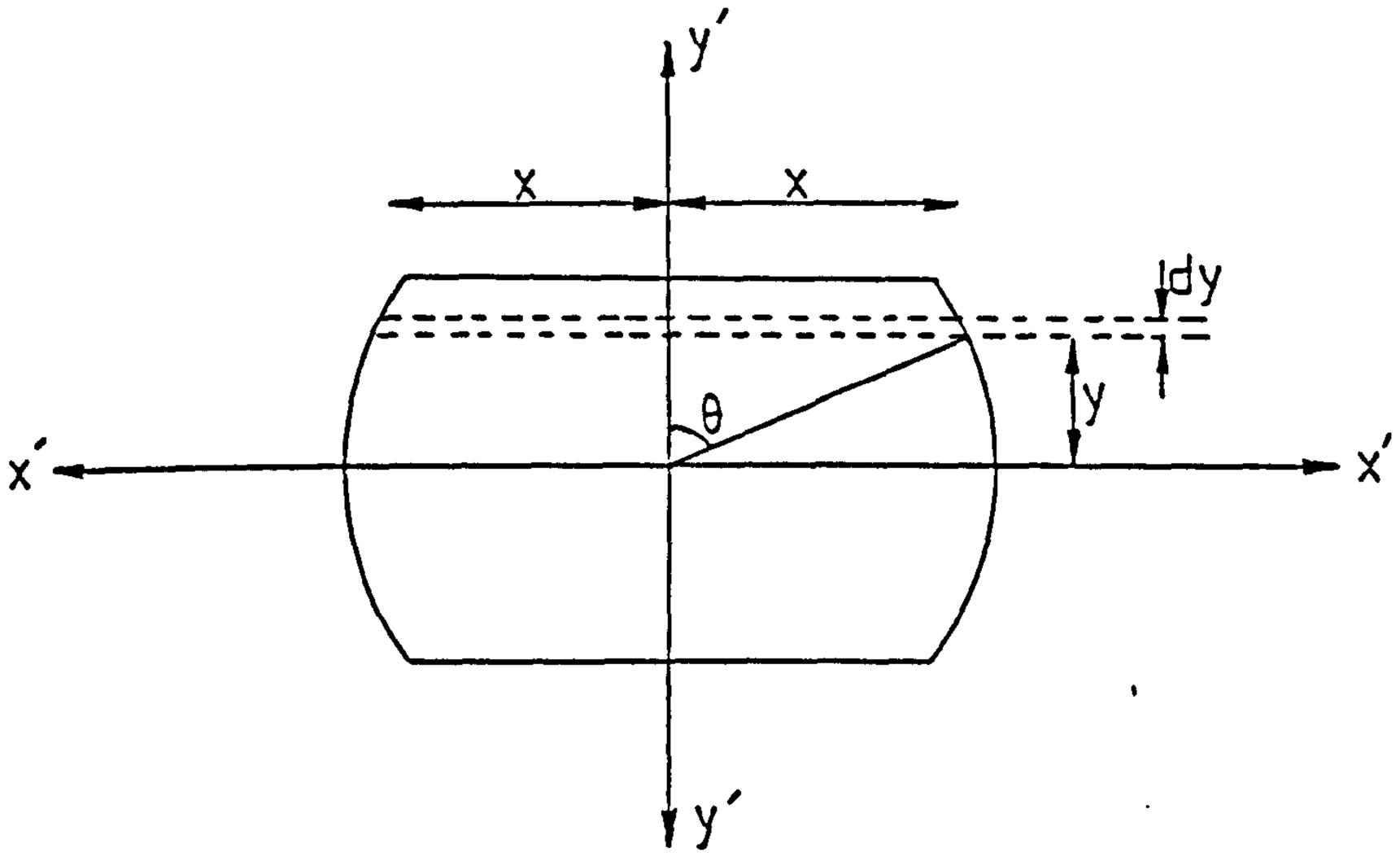

The area of the thin strip, of length 2x, shown in the figure is 2xdy.

the second moment of area, I, about the neutral axis, x'x' is;

$$Ix'x' = \int_{y=0}^{y=a} 2xy^2 dy \quad \text{----------(1)}$$

The equation of a circle, radius, r, is

$$x^2 + y^2 = r^2$$

Therefore; $x = (r^2 - y^2)^{1/2}$ ----------(2)

substituting (2) into (1) gives;

$$Ix'x' = 4\int_0^a y^2(r^2 - y^2)^{1/2}dy \quad \text{----------(3)}$$

Let; $y = r.\cos\theta$ ----------(4)

Therefore; $dy = -r.\sin\theta$ ----------(5)

Substituting (4) into (2) gives;

$$x = r(1 - \cos^2\theta)^{1/2}$$

Since,

$$1 - \cos^2\theta = \sin^2\theta$$

$$r(1 - \cos^2\theta)^{1/2} = r\sin\theta \quad \text{----------(6)}$$

Substituting (4), (5) and (6) into (3) gives;

$$Ix'x' = -4\int_{\pi/2}^{\cos^{-1}a/r} r^4\cos^2\theta\sin^2\theta d\theta \quad \text{----------(7)}$$

We know that;

$$\sin2\theta = 2\sin\theta\cos\theta$$

which substituted into (7) gives;

$$Ix'x' = r^4\int_{\cos^{-1}a/r}^{\pi/2} \sin^2 2\theta d\theta \quad \text{----------(8)}$$

Since $\cos4\theta = 1 - 2\sin^2 2\theta$,

$$\sin^2 2\theta = (1 - \cos4\theta)/2$$

Substituting into (8) gives;

$$Ix'x' = r^4/2\int_{\cos^{-1}a/r}^{\pi/2}(1 - \cos4\theta)d\theta$$

This integral can now be solved to give;

$$Ix'x' = r^4/2[\theta - (\sin 4\theta)/4]_{\cos^{-1}a/r}^{\pi/2} \quad \text{----------(9)}$$

Since $\cos\theta = a/r$ ----------(10)

$\cos^{-1}a/r = \theta$ ----------(11)

and $\sin\theta = [1 - (a/r)^2)]^{1/2}$ ----------(12)

and $\sin 4\theta = 4(\sin\theta\cos^3\theta - \sin^3\theta\cos\theta)$ ----------(13)

(10), (11) and (12) can be substituted into (13) to give;

$$\sin 4\theta = 4[1 - (a/r)^2]^{1/2}(a/r)^3 - [1 - (a/r)^2]^{3/2}a/r$$

$$= 4a/r[1 - (a/r)^2]^{1/2}[2(a/r)^2 - 1] \quad \text{----------(14)}$$

Therefore, by substituting (14) into (9) and solving we get;

$Ix'x' = r^4/2[\pi/2 - \cos^{-1}a/r + a/r(2(a/r)^2 - 1)(1 - (a/r)^2)^{1/2}]$ --(15)

For the specimens used, r = 4.75mm and a = 3.2mm

Therefore, by substituting into (15),

$$Ix'x' = 1.765 \times 10^{-10}m^4$$

The positions of the loading points on the rotating-bending specimens are shown in the figure below.

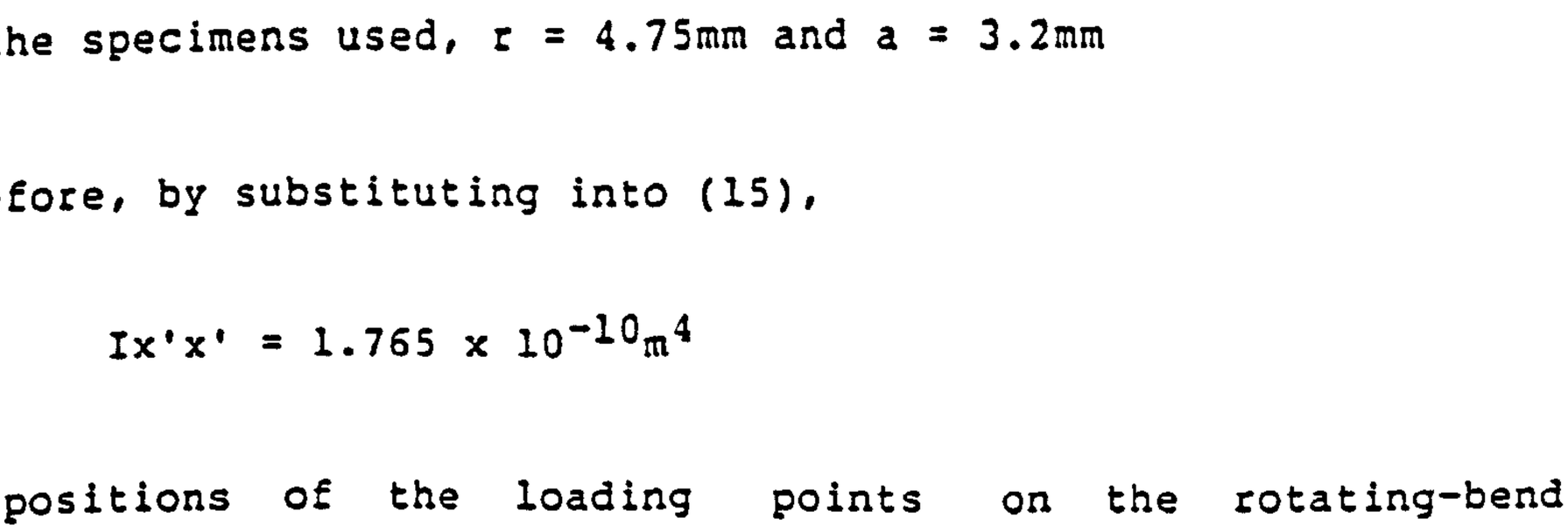

The portion at the centre of the specimen, length 'a', is under a constant bending moment, M, where;

$$M = wb/2 \quad \text{----------(16)}$$

where w is the load applied to the specimen and b is the distance between outer and inner loading points.

From theory, it can be shown that;

$$M/I = F/y \quad \text{----------(17)}$$

where; M = bending moment

I = second moment of area

F = maximum bending stress

y = distance from neutral axis to outer edge of specimen

By substituting (16) into (17) we get;

$$F = wby/2I$$

For the specimen used in this experiment;

$$b = 71.5 \times 10^{-3}m$$

$$y = 3.20 \times 10^{-3}m$$

$$I = 1.765 \times 10^{-10}m^4$$

From this data, the resulting bending stresses in the specimens can be calculated from the applied load (w).

The bending stresses set up in the rotating-bending specimen gauge length by various applied loads

APPLIED LOAD		BENDING STRESS
lbs	kg	MN/m^2
20	9.07	58.80
30	13.61	88.20
40	18.14	117.60
50	22.68	147.00
60	27.22	176.40
70	31.75	205.80
80	36.29	235.20
90	40.92	265.20
100	45.36	294.00

APPENDIX FOUR

Calculation of the Maximum Slipping Distance During Fretting-Fatigue

A schematic diagram showing a fretting bridge in contact with the gauge length of a rotating-bending specimen experiencing an applied bending moment is shown below.

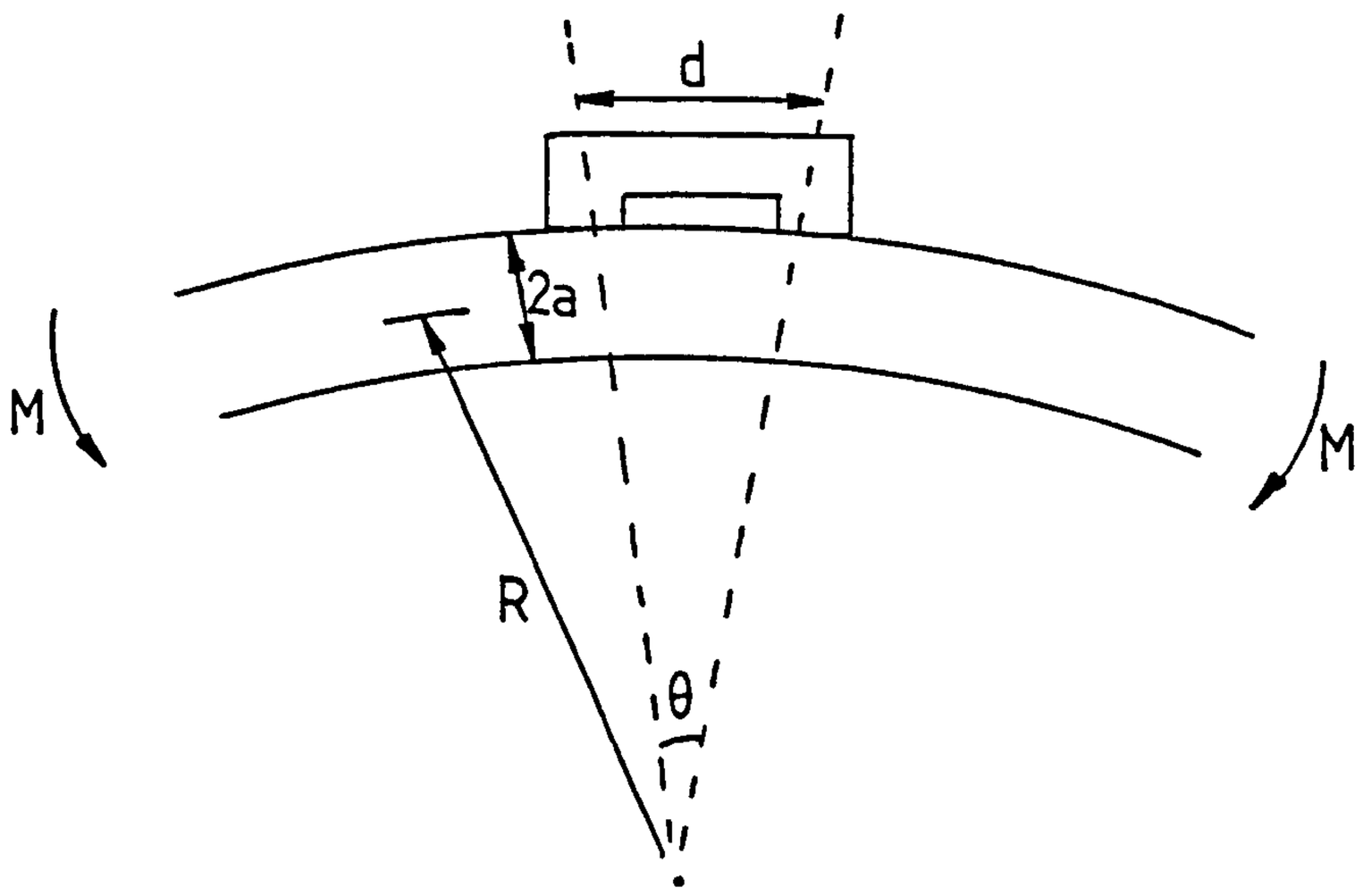

The slip distance, s, distributed over both feet of the bridge is;

$$s = a\theta$$

where 'a' is half the thickness of the specimen and 'θ' the angle between the feet of the fretting bridges as shown above.

From previous bending theory,

$$R = IE/M$$

where, I = the second moment of area

E = Youngs modulus

M = the bending moment

In this work, R, the radius of curvature in the specimen produced by the bending moment, M, was much greater than d, the length of the fretting bridges.

Therefore, $d = R\theta$

that is, $\theta = d/R = dM/IE$ ----------(1)

The formula for the bending moment in a beam is;

$$M = wb/2$$

The maximum load, w, used in the rotating-bending tests was 401N and since the distance between the inner and outer loading points;

$$b = 71.5 \times 10^{-3}m$$

the maximum bending moment,

$$M = (401 \times 71.5 \times 10^{-3})/2$$

$$= 14.33NM$$

We know that; $d = 0.0166m$

and, from data; $E = 70 \times 10^{9}N/m^{2}$

from appendix 3, $I = 1.765 \times 10^{-10}m^{4}$

Substituting these values into (1) gives;

$$\theta = (0.0166 \times 14.33)/(1.765 \times 10^{-10} \times 70 \times 10^{-9})$$

$$= 1.9 \times 10^{-2} \text{ radians}$$

The slip distance, $s = a\theta$

and; $a = 3.2mm$

Therefore, $s = (3.2 \times 10^{-3}) \times (1.9 \times 10^{-2})$

$= 6.1 \times 10^{-5}m$

The maximum possible slip,

$\underline{s = 61\mu m}$

This value would be less in practice since the effects of friction between the two surfaces during fretting have not been taken into account.

APPENDIX FIVE

Calculation of the Residual Stresses Determined Using the X-Ray Stress Measurement Technique

The stress in the surface of the specimen under test is given by the formula;

$$\sigma_x = E.\cot\theta(2\theta_n - 2\theta_i)/2(1+\nu).\sin 2Y$$

where,

σ_x = The stress in the surface in a direction x along the surface.

E = The youngs modulus of the material.

θ = The calculated angle of incidence of X-rays diffracted from a chosen unstressed plane.

$2\theta_n$ = The observed value of the diffraction angle from planes parallel to the surface.

$2\theta_i$ = The observed value of the diffraction angle from planes inclined at an angle (Y) to the surface.

ν = Poissons ratio for the material under test.

Y = The angle which the plane containing a component of the biaxial stress makes with the specimen surface.

Since E, θ, ν and Y are all constants, the formula can now be rewritten;

$$\sigma = K(2\theta_n - 2\theta_i) = K(d2\theta)$$

where,

$$K = E.\cot\theta/2(1+\nu)\sin 2\theta$$

and is referred to as the "stress constant" of the material.

The stress in a surface can thus be found by measuring the two different angles of diffraction from a specified set of planes orientated at two different angles, 0 and Y ° to the surface.

APPENDIX SIX

The Determination of Peak Position Using the Three Point Method of Fitting a Parabola

A simple method to determine the peak position of diffracted rays was devised by Koistinen and Marburger (108). This method requires the measurement of three points on the diffraction profile (with coordinates x_1y_1, x_2y_2, and x_3y_3); these points being separated by an angular interval, c, as shown below.

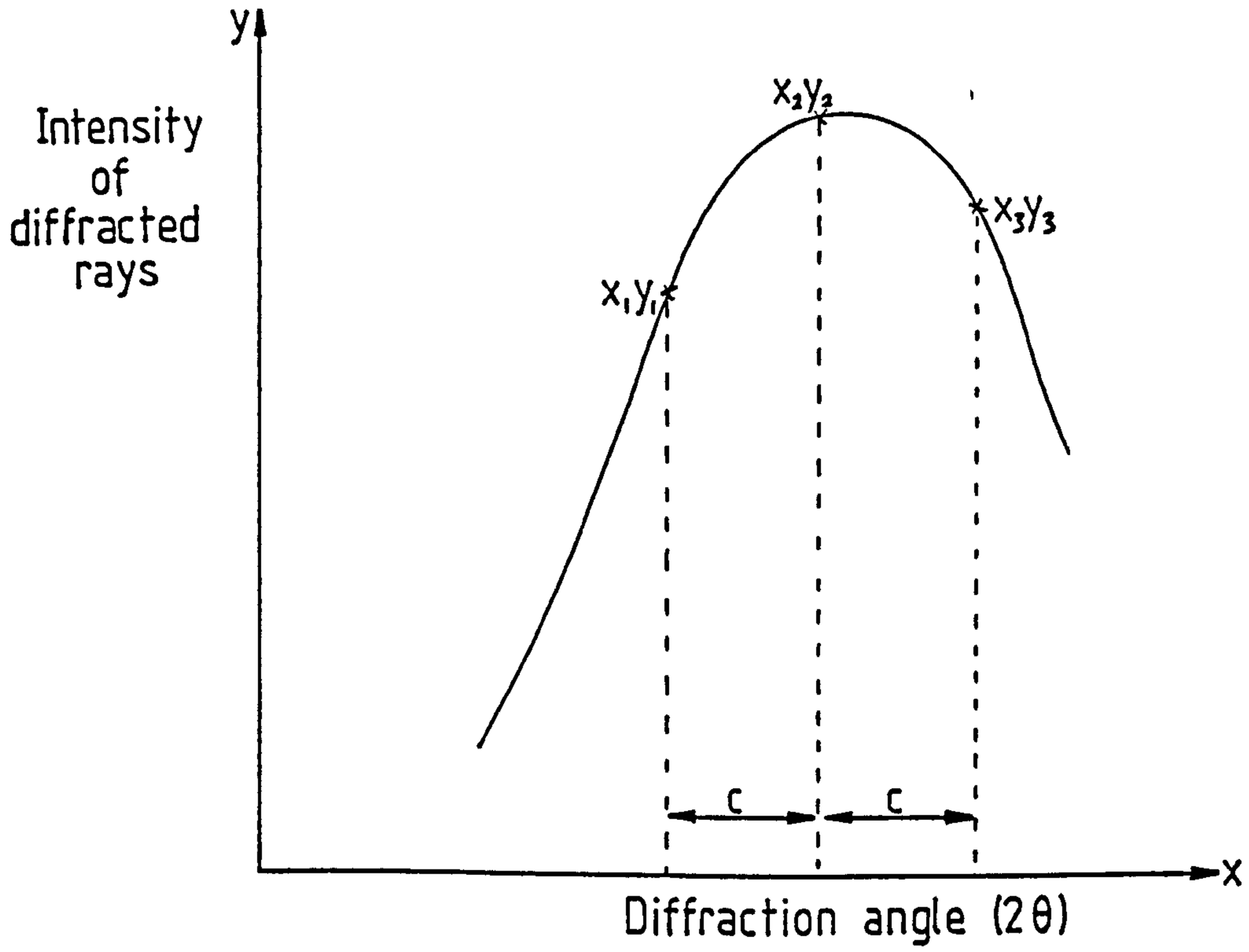

The y-axis in this case is the intensity of the diffracted rays and the x-axis the angle, 2θ, at which the diffracted rays were measured. The central of the three points, as shown in the figure, should be near to the peak position of the curve, and the outer two points should be about 85% of the peak value.

In order to locate the angular position of the peak, the following formula is used;

$$h = x_1 + c/2[(3a + b)/(a + b)]$$

where,

h = the peak position of the diffracted rays

x_1 = the angular value as shown in the figure

$a = y_2 - y_1$

$b = y_2 - y_3$

FIGURES AND PLATES

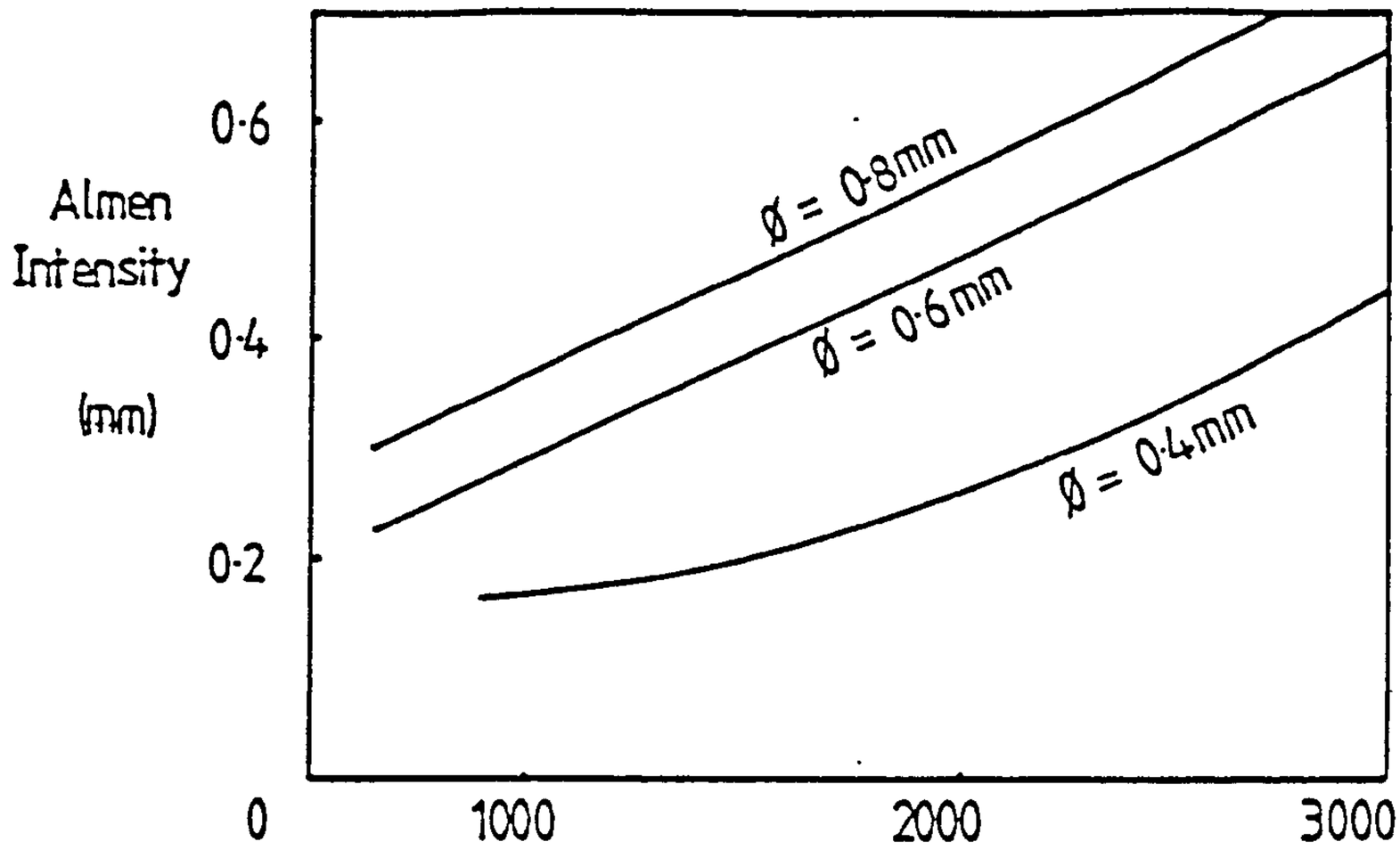

1a) Variation in the Almen intensity as a function of wheel speed for various shot diameters (9).

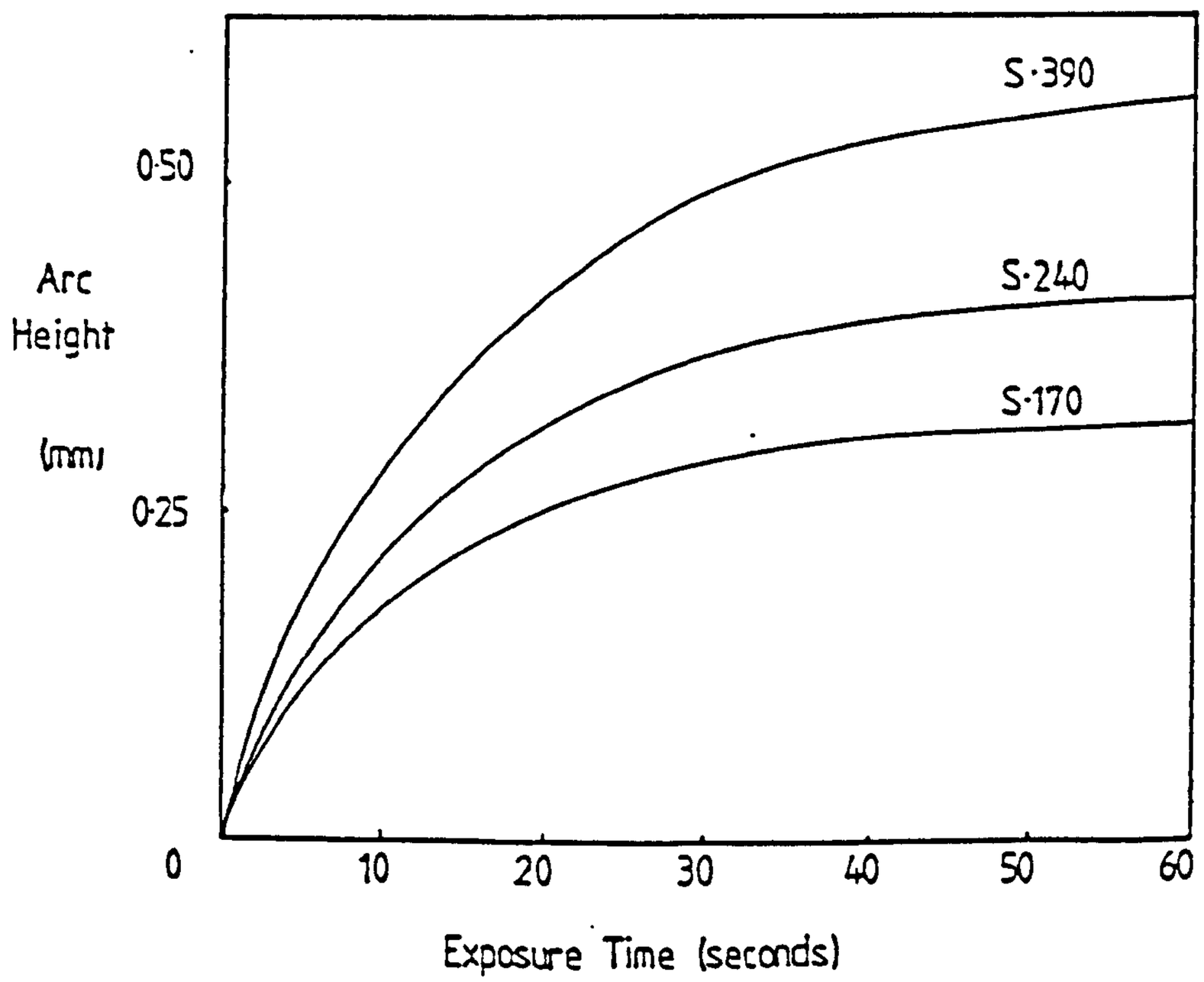

1b) Effect of exposure time on arc height for various shot diameters (8).

Fig. 1) The effects of shot speed and exposure time on the arc height of the Almen strip using shot of various diameters

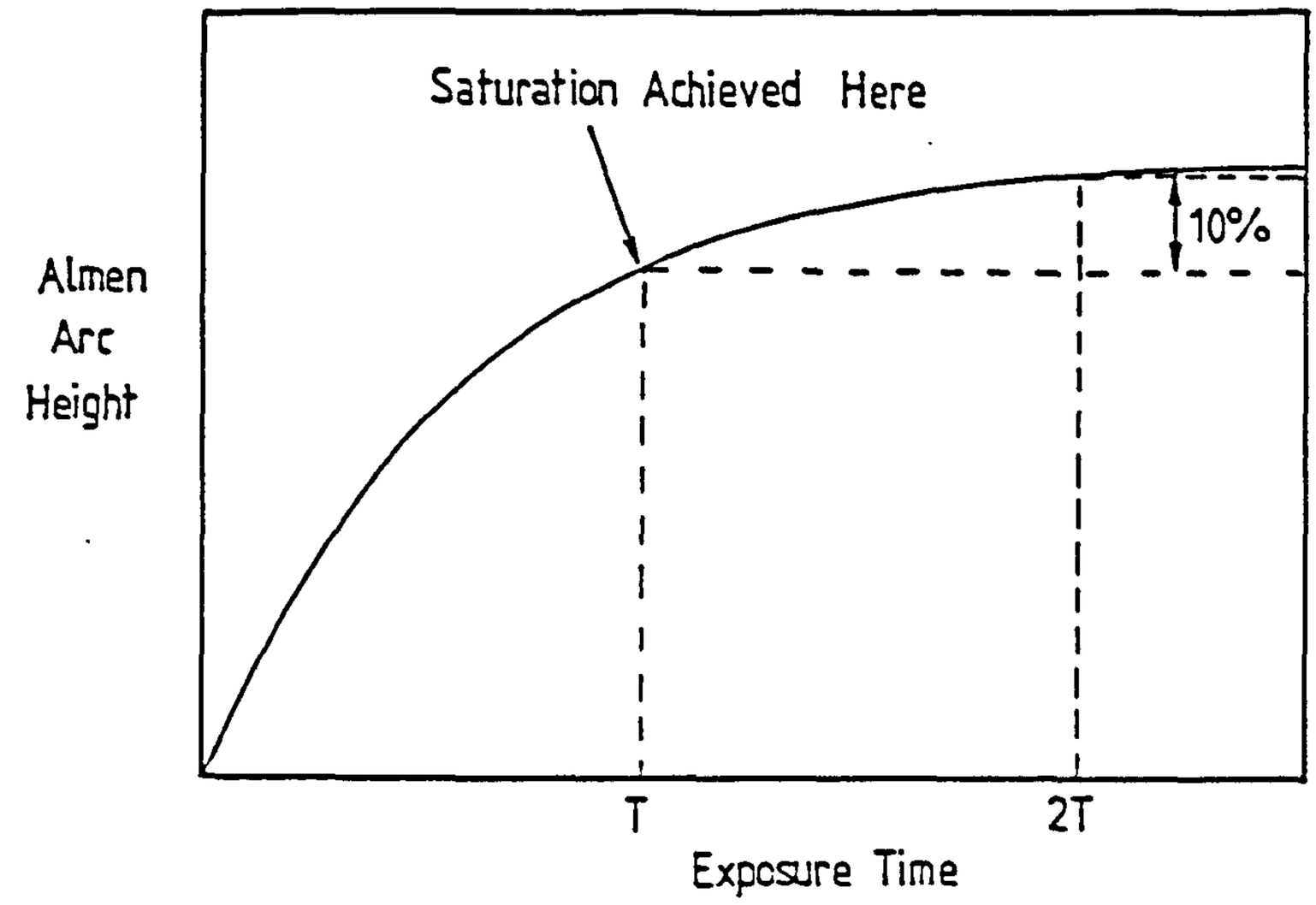

2a) Plot of Almen arc height vs. exposure time showing point at which saturation is reached (6).

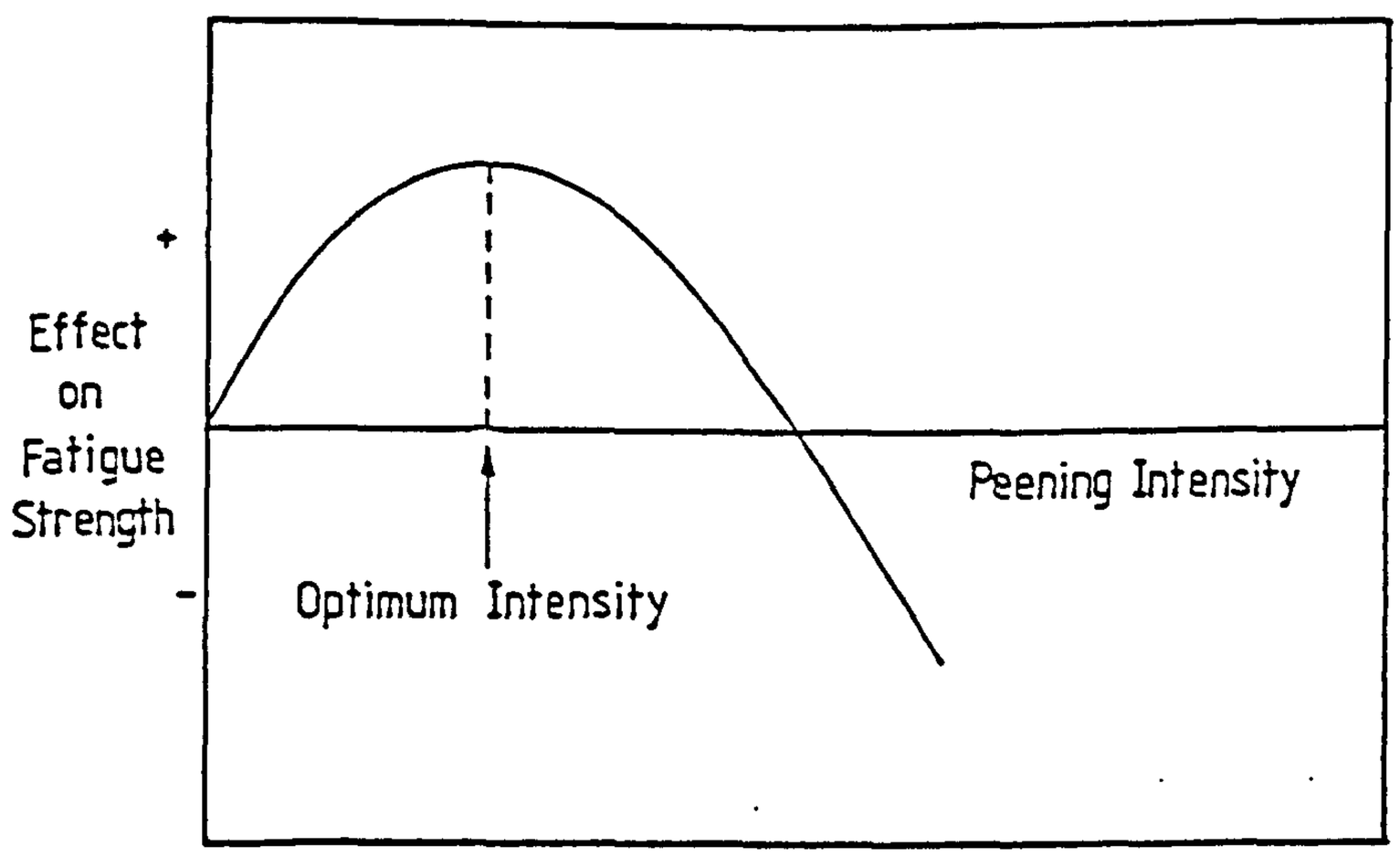

2b) Effect of peening intensity on bending fatigue life (11).

Fig. 2) The effects of various peening parameters on the arc height of the Almen strip and bending fatigue strength.

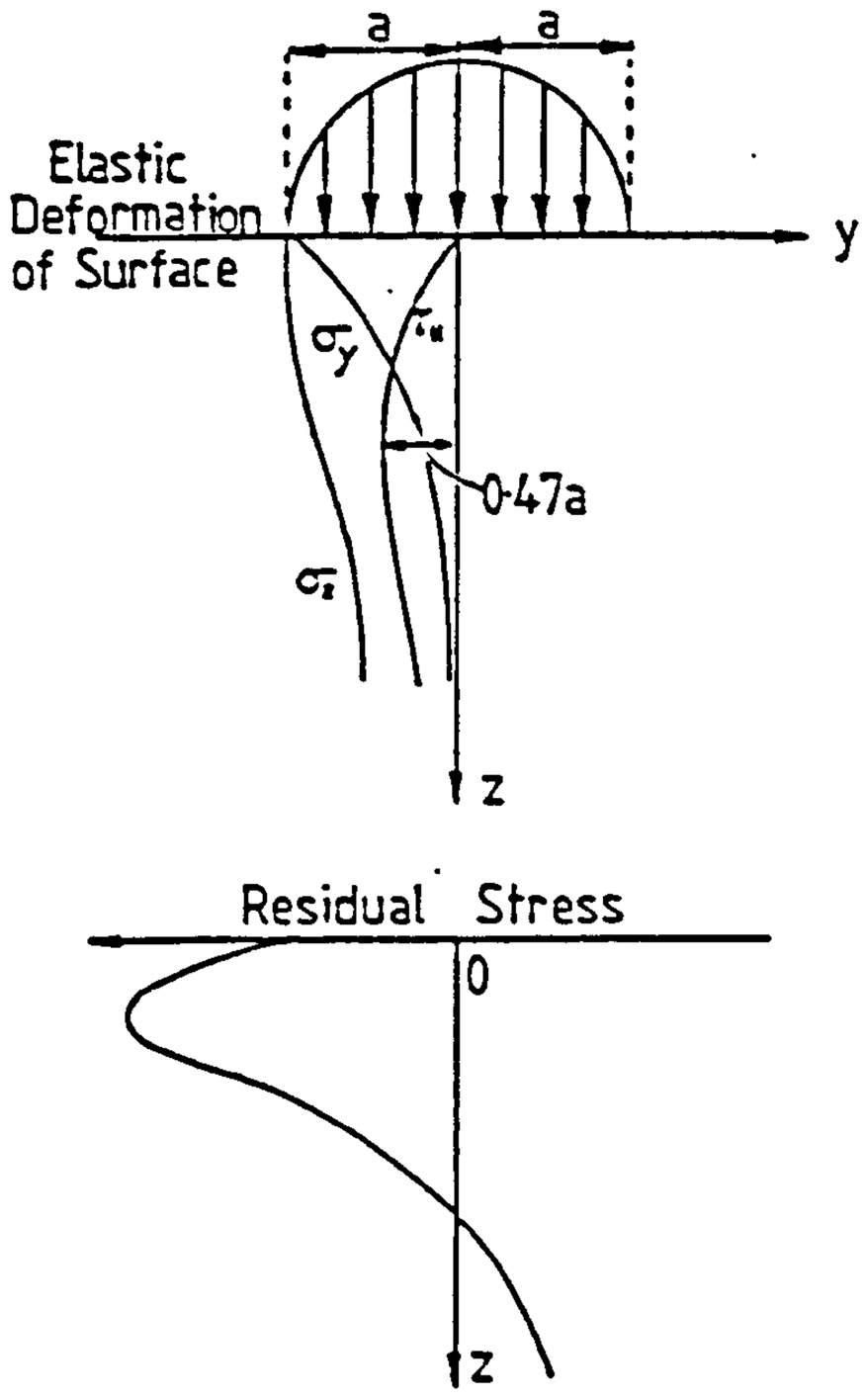

3a) Hertzian pressure as a consequence of the vertical forces connected with the impact of shot balls- effect is possible with a soft shot and a hard workpiece.

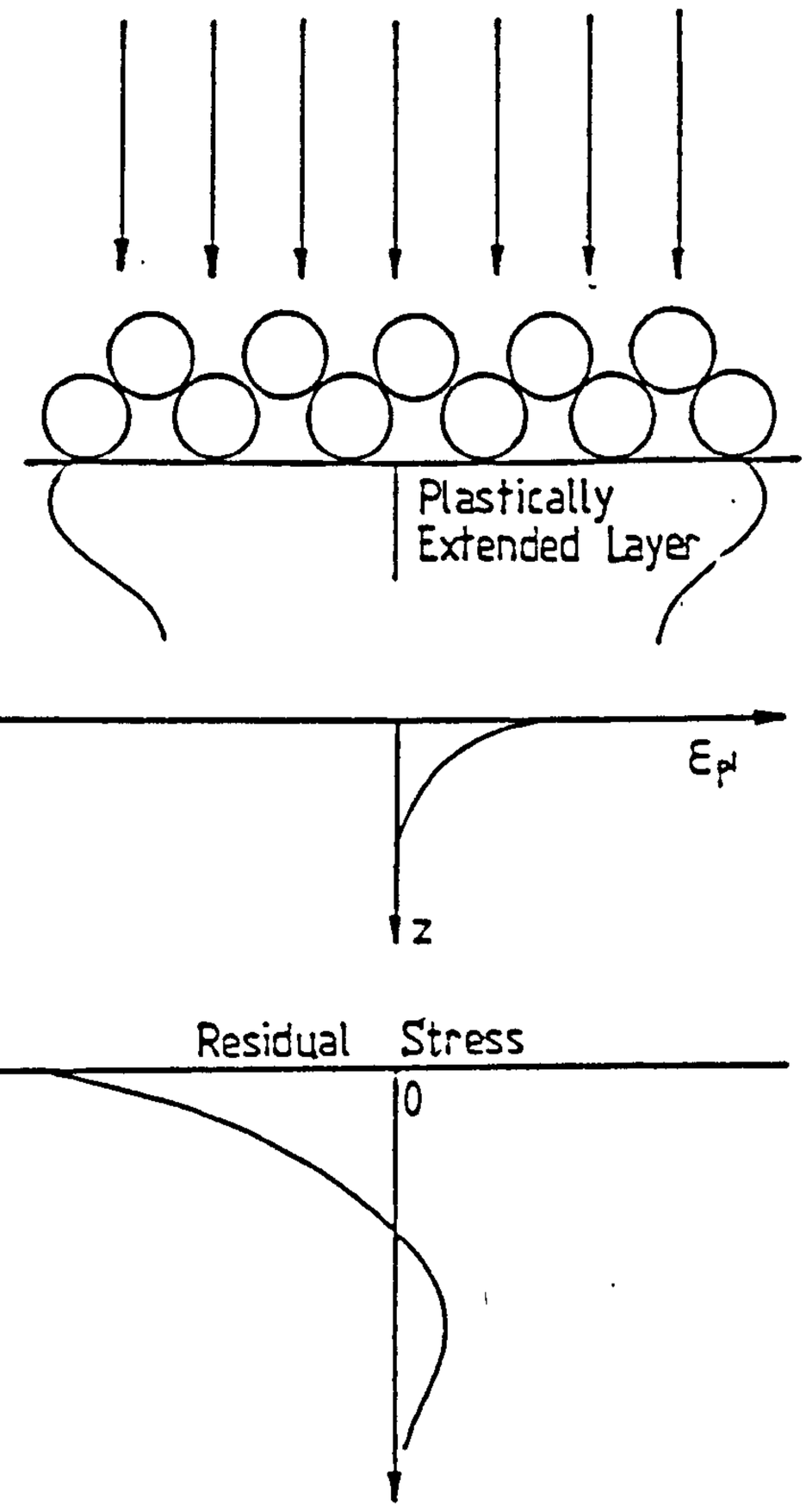

3b) Stretching of a surface layer as a consequence of "surface hammering"- effect is marked with a hard shot and a soft workpiece.

Fig. 3) Schematic illustration of the formation of residual stresses as a consequence of two different processes in shot peening: Hertzian pressure and direct stretching of the surface layers (15).

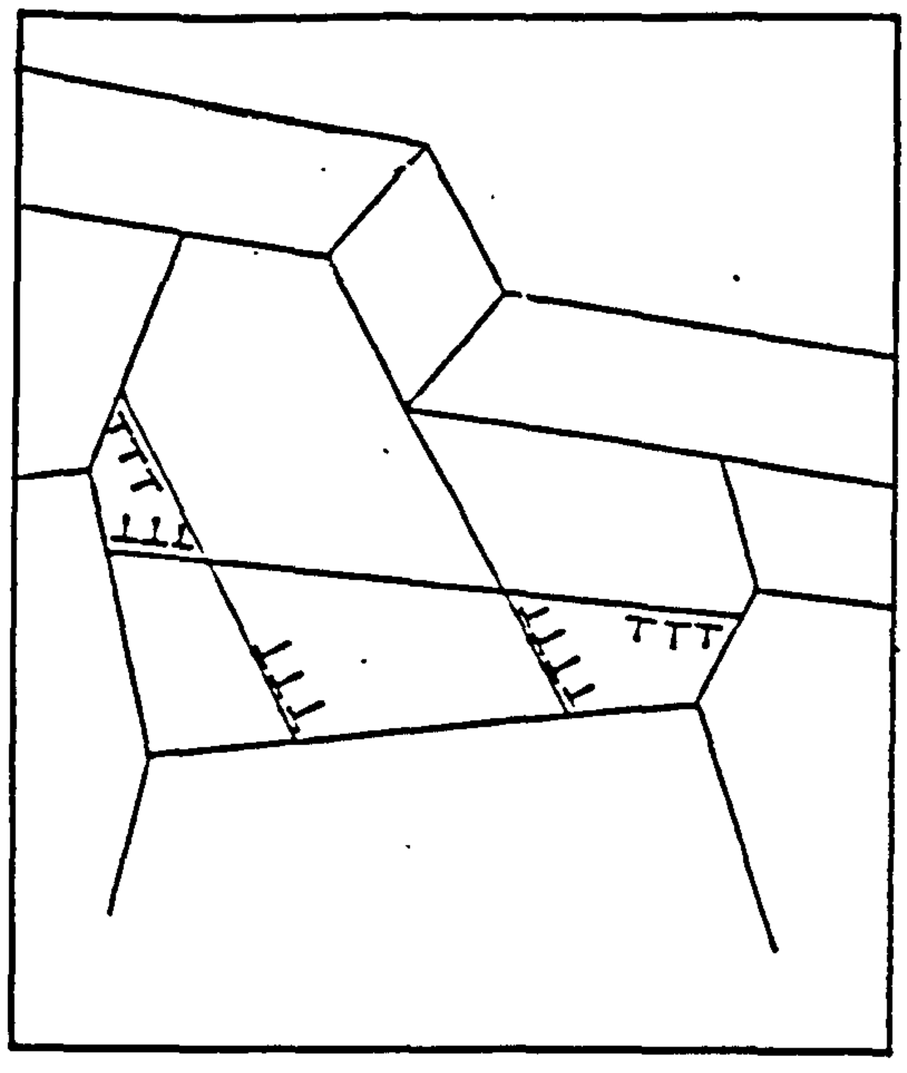

4a) Large slip steps favoured by low SFE materials with a large grain size where shearing of particles can occur.

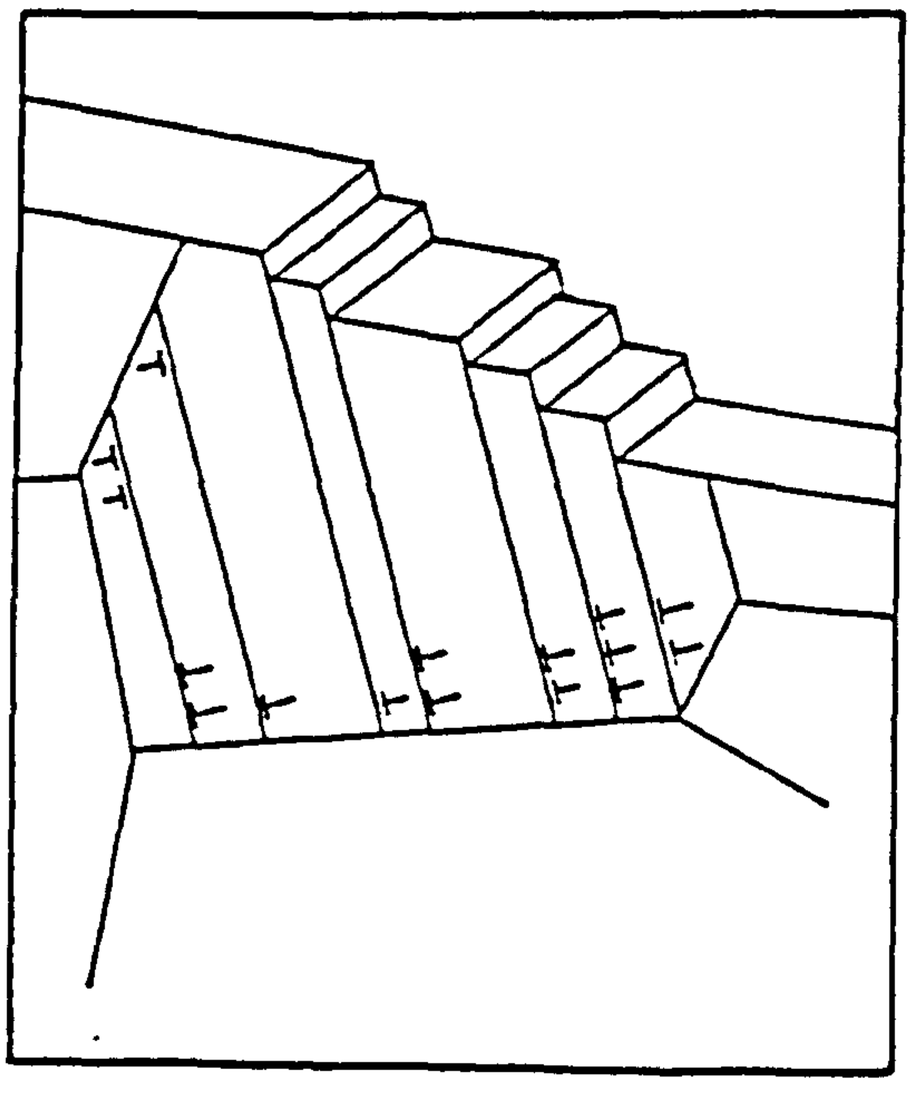

4b) Small slip steps favoured by high SFE materials with a small grain size where by-passing of particles occurs.

Fig. 4) Homogeneous and inhomogeneous distribution of plastic deformation (39).

Fig. 5) British development specifications DTD 5120 for a 25mm plate in the longitudinal direction.

	Minimum	Maximum
0.2%PS (MPa)	450	495
UTS (MPa)	530	
Elongation (%)	6	
K_{IC} (L-T) (MPa$\sqrt{m}$)	28.0	
K_{IC} (T-L) (MPa$\sqrt{m}$)	25.0	
Stress Corrosion Life at 175 MPa (days)	30	

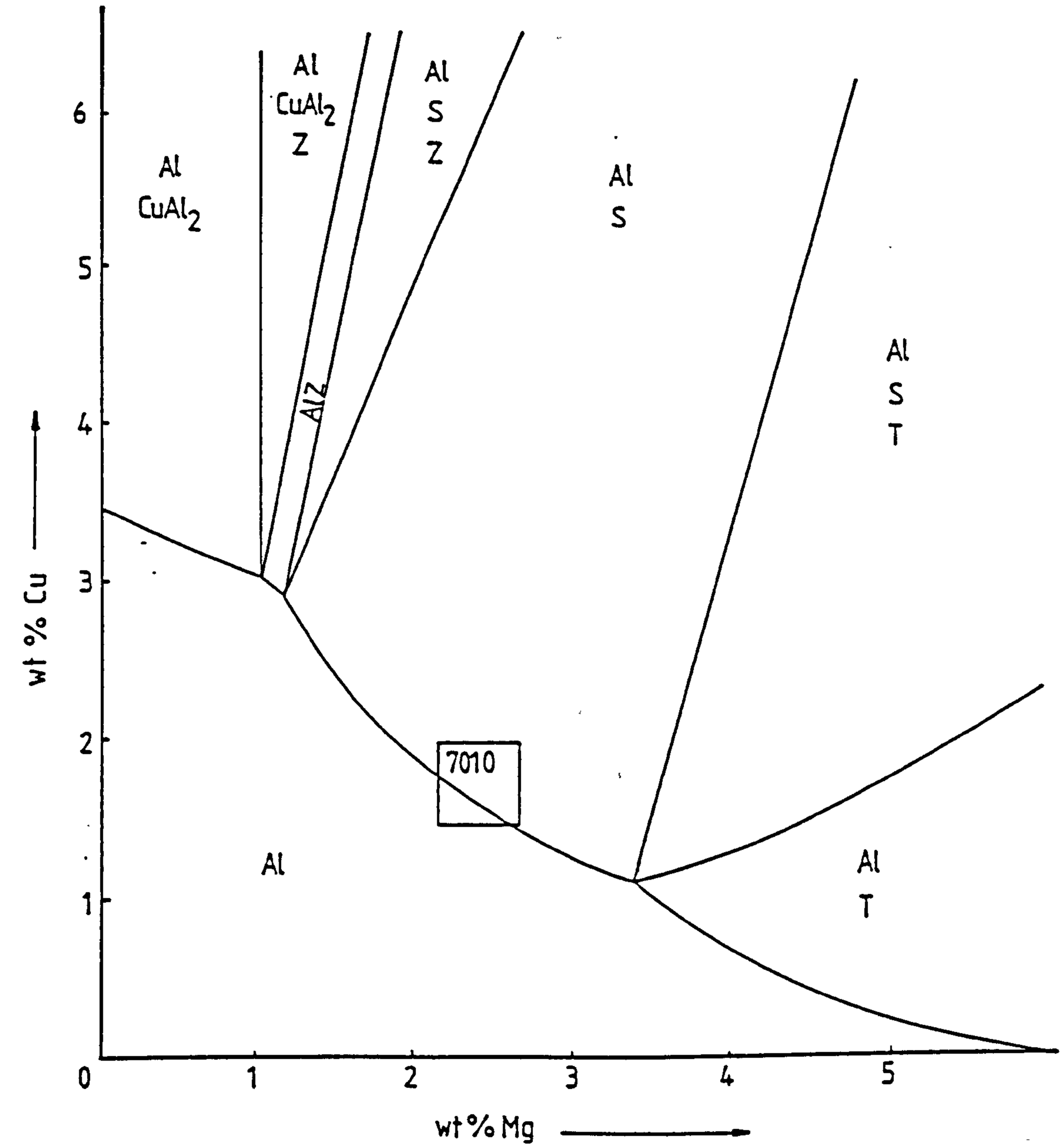

Fig. 6) Section of the Al-Zn-Mg-Cu phase diagram isothermals at 460°C and 6%Zn (79).

Fig. 7) Ageing curves for alloy 7010 (79).

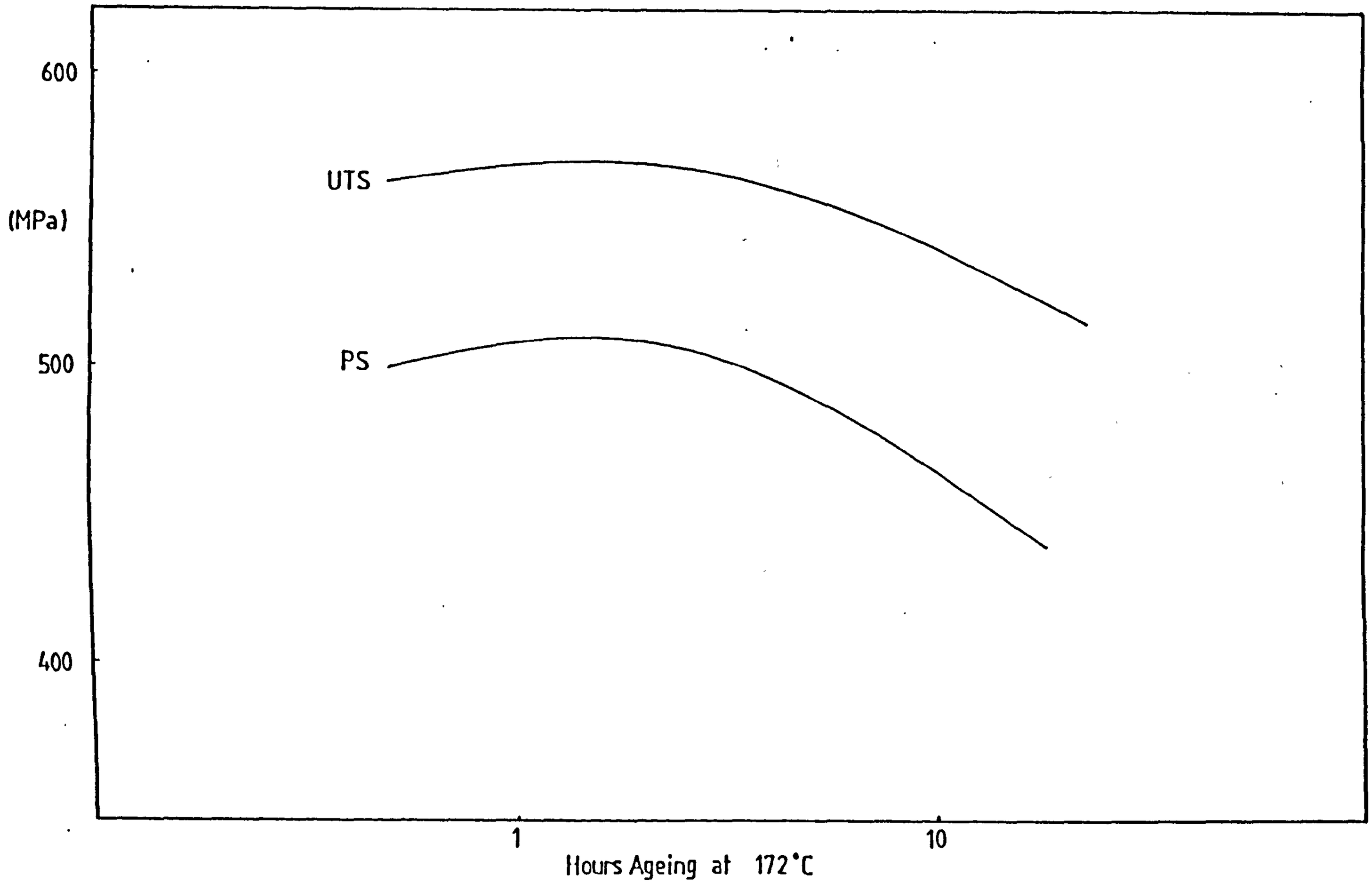

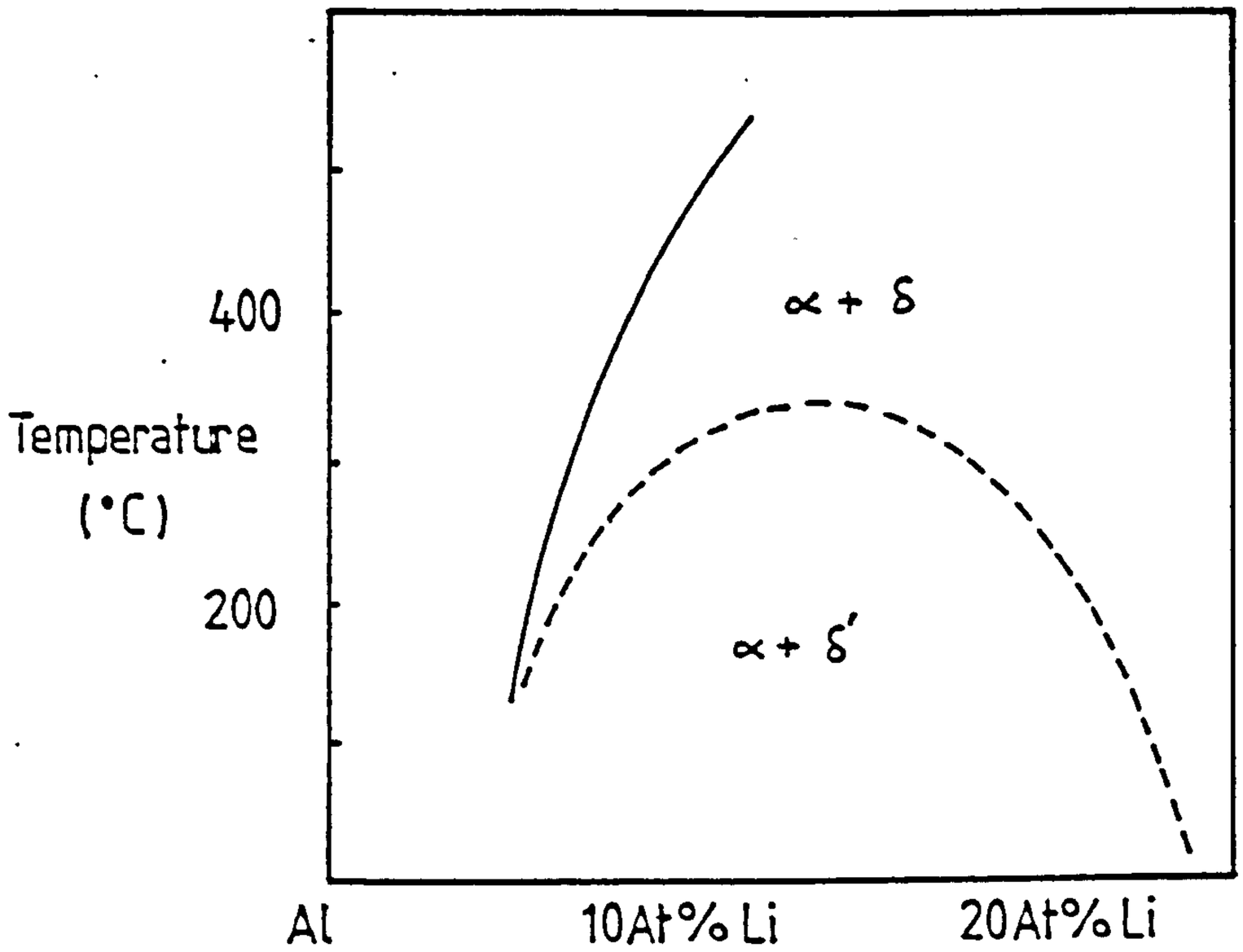

Fig. 8) The aluminium-lithium phase diagram showing the aluminium rich region.

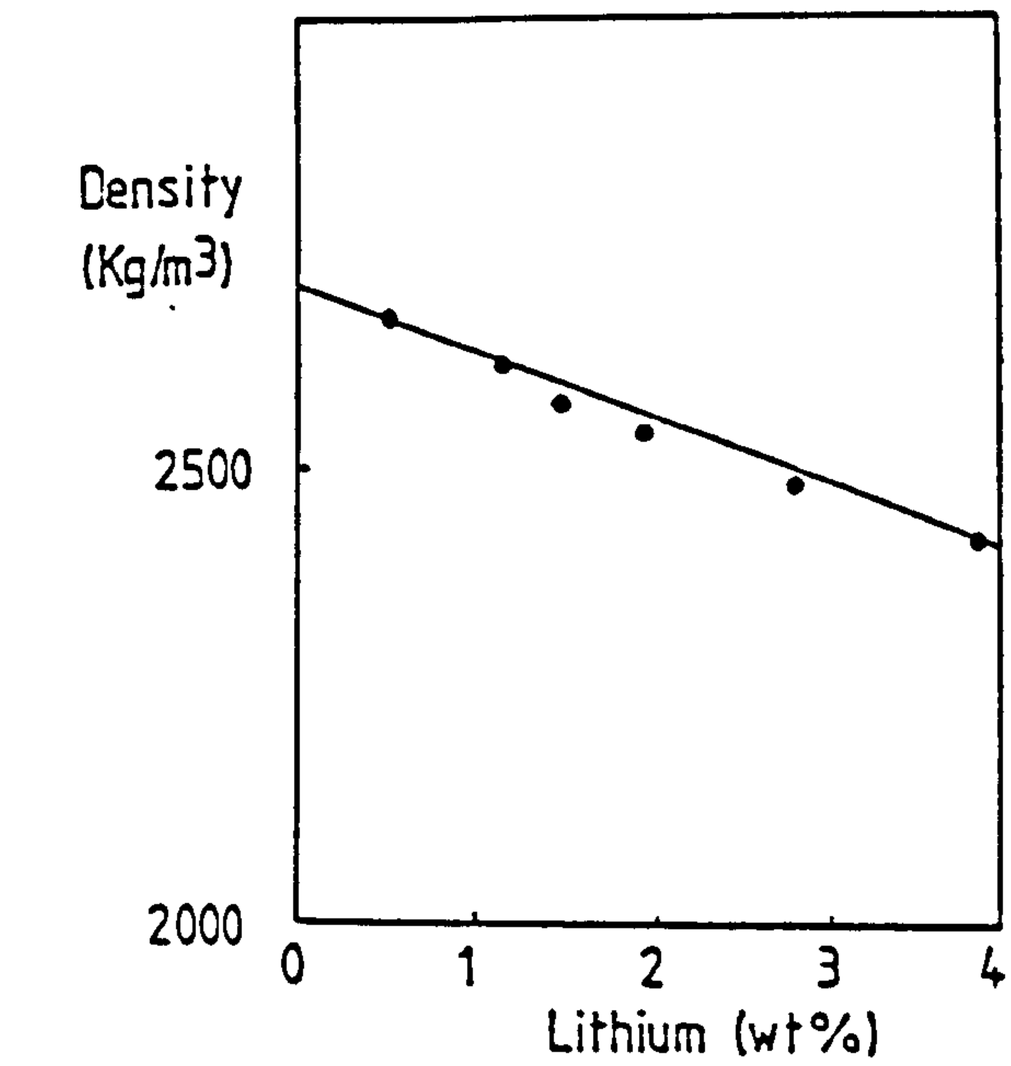

9a) Effect of increasing the lithium content on the density of binary aluminium-lithium alloys (90).

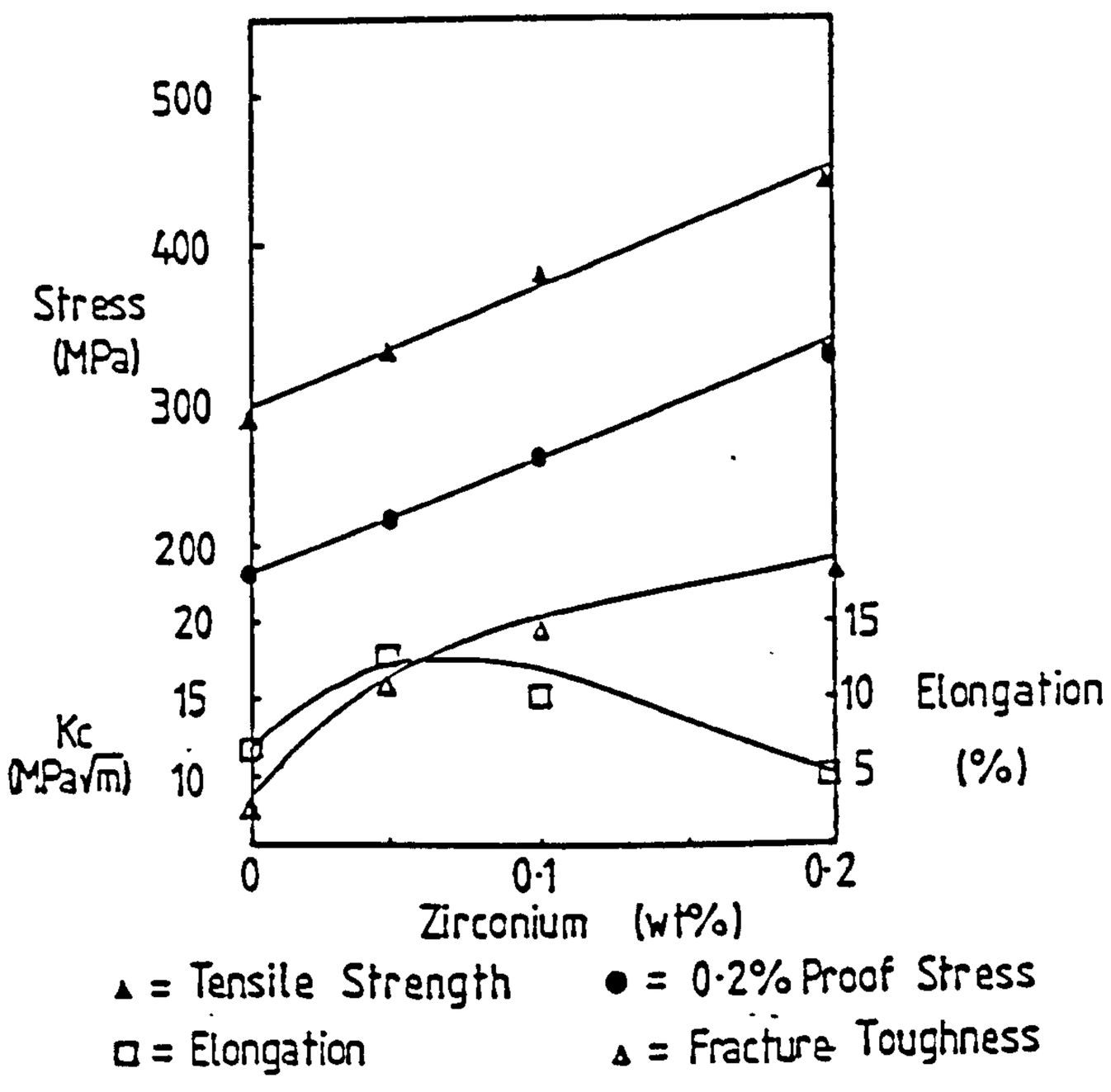

9b) Effect of increasing the zirconium content on the mechanical properties of Al-2%Li-2%Mg alloy (90).

Fig. 9) The effect of varying the lithium and zirconium contents on the mechanical properties of the Al-Li system.

Fig. 10) Mechanical properties of alloy 8090 in the longitudinal direction at various temperatures and ageing times.

Ageing Time (Hours)	Mechanical Properties	Ageing Temperature		
		170°C	190°C	210°C
8	PS MN/m^2	475	445	414
	UTS MN/m^2	493	499	477
	E GN/m^2	81	80	84
	El %	7	7	5
16	PS MN/m^2	428	459	362
	UTS MN/m^2	484	507	446
	E GN/m^2	81	80	84
	El %	7	7	7
24	PS MN/m^2	443	463	308
	UTS MN/m^2	497	512	403
	E GN/m^2	81	80	80
	El %	7	6	7

Fig. 11) The analysed compositions of the 7010 and 8090 alloys used in this work (wt%).

Alloy	Li	Cu	Mg	Zn	Zr	Fe	Si
7010	----	1.70	2.50	6.20	0.14	0.10	0.07
8090	2.56	1.22	0.68	----	0.12	0.06	0.07

Fig. 12) Details of heat treatments and peening treatments for the 7010 and 8090 alloys.

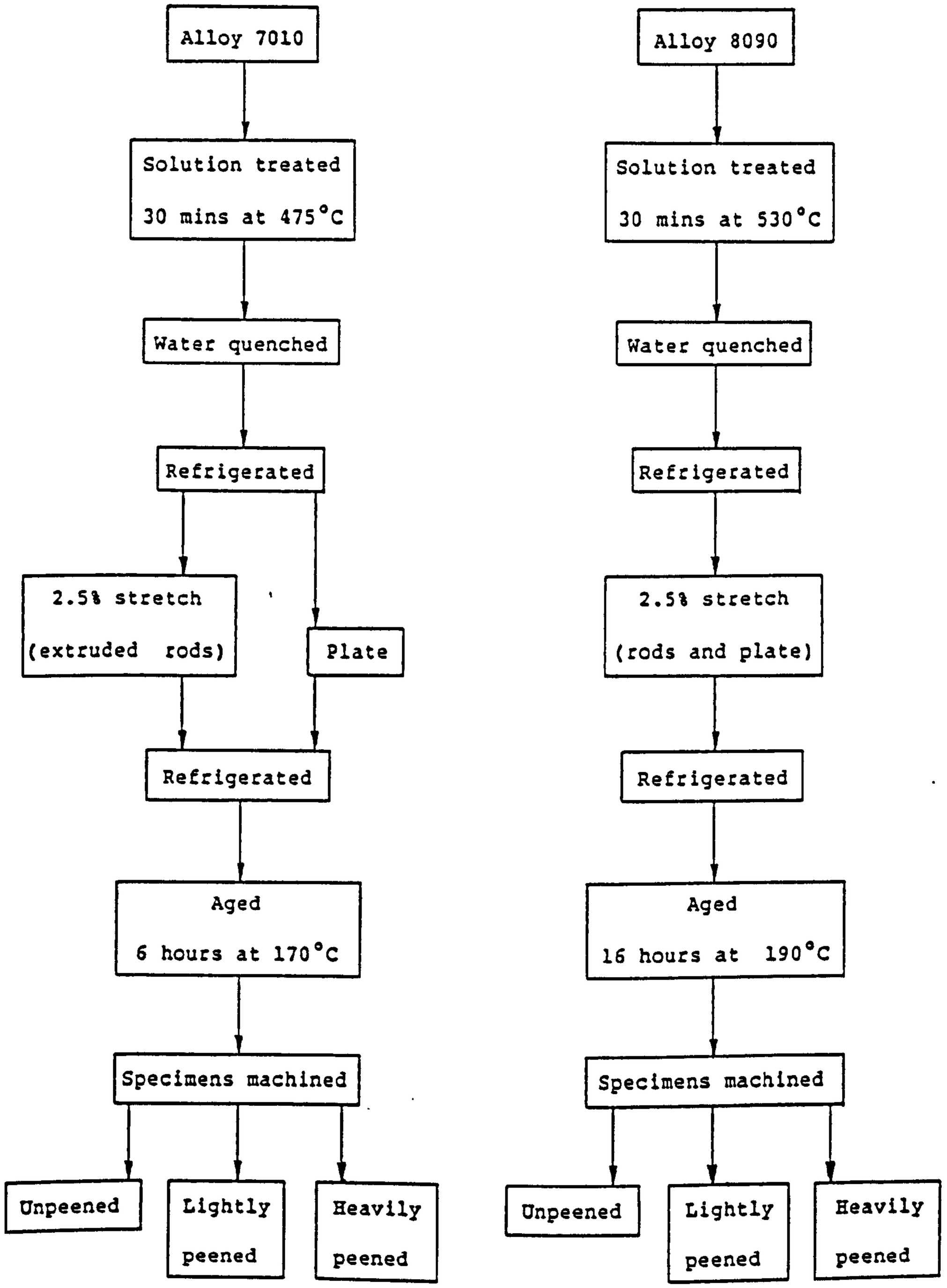

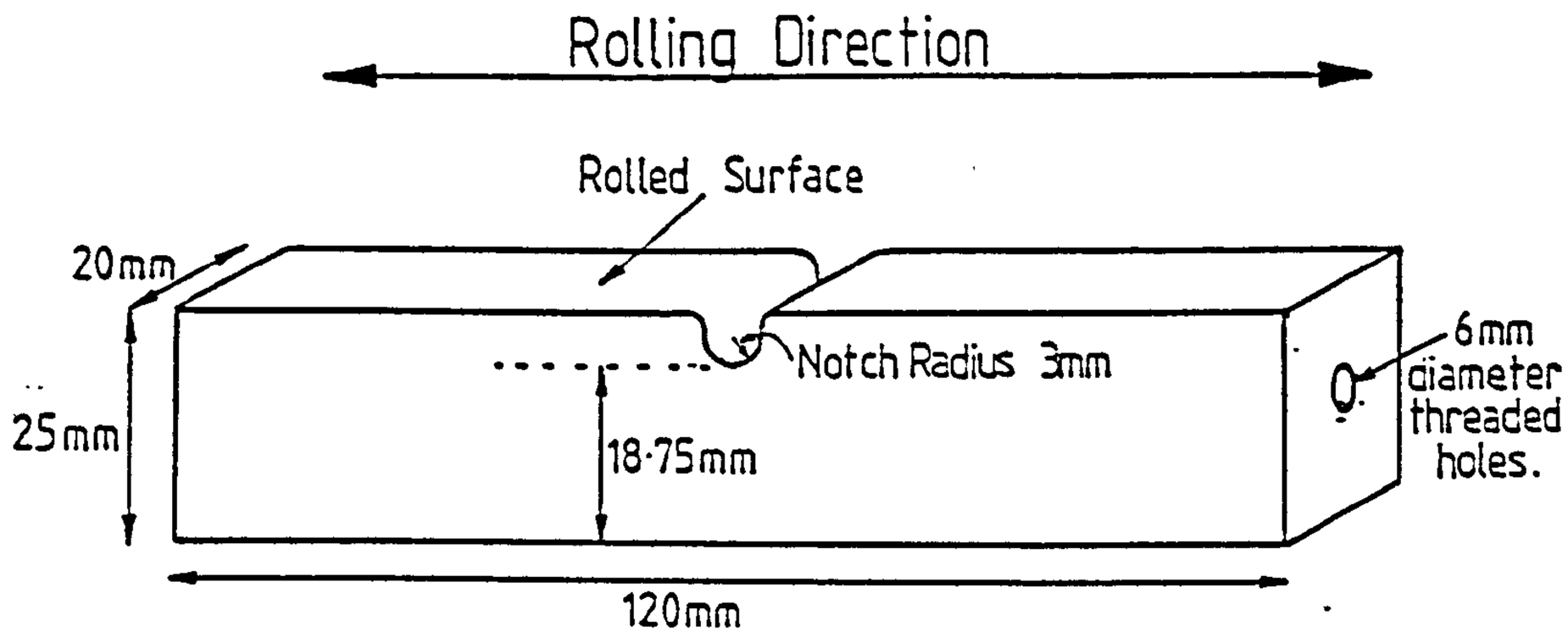

13a) Dimensions of the reversed-bending specimens.

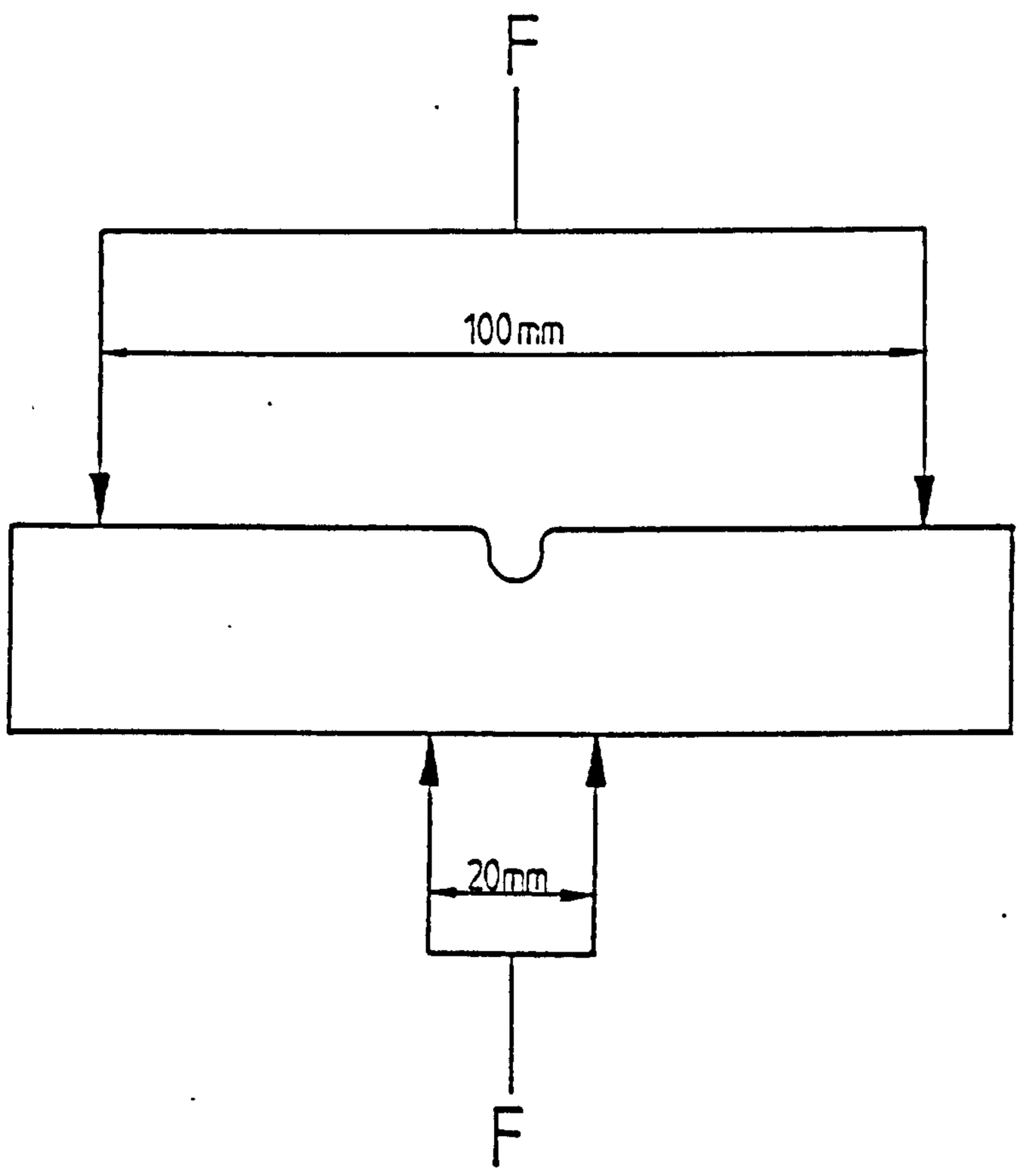

13b) Loading arrangement used in the reversed-bending tests.

Fig. 13) Specimen dimensions and loading arrangement used in the reversed-bending tests.

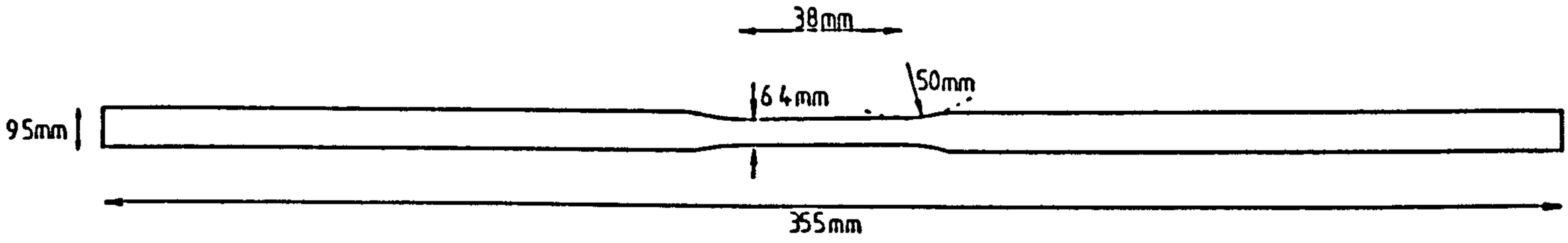

14a) Dimensions of the rotating-bending specimens.

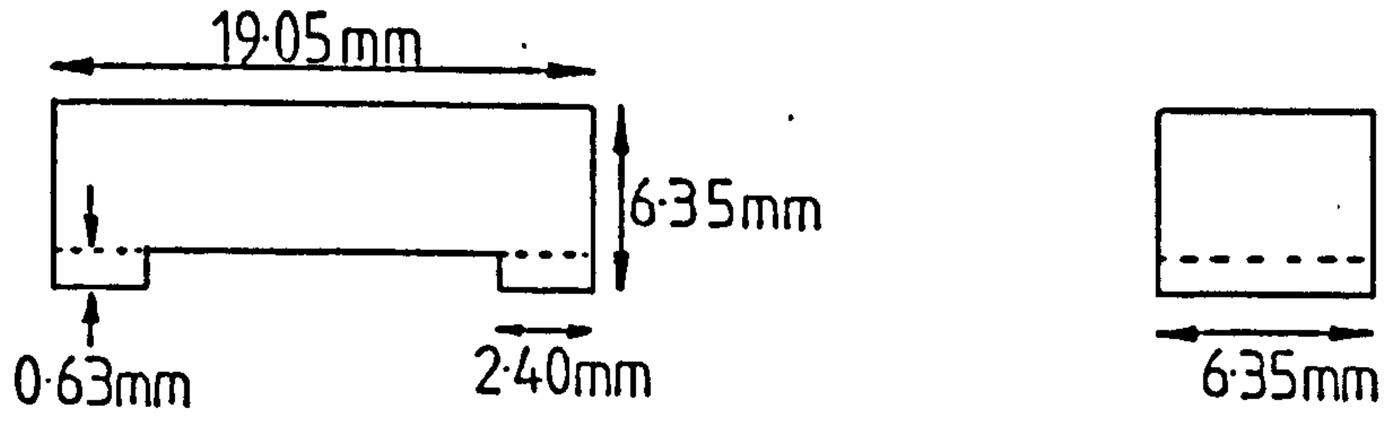

14b) Dimensions of the fretting bridges.

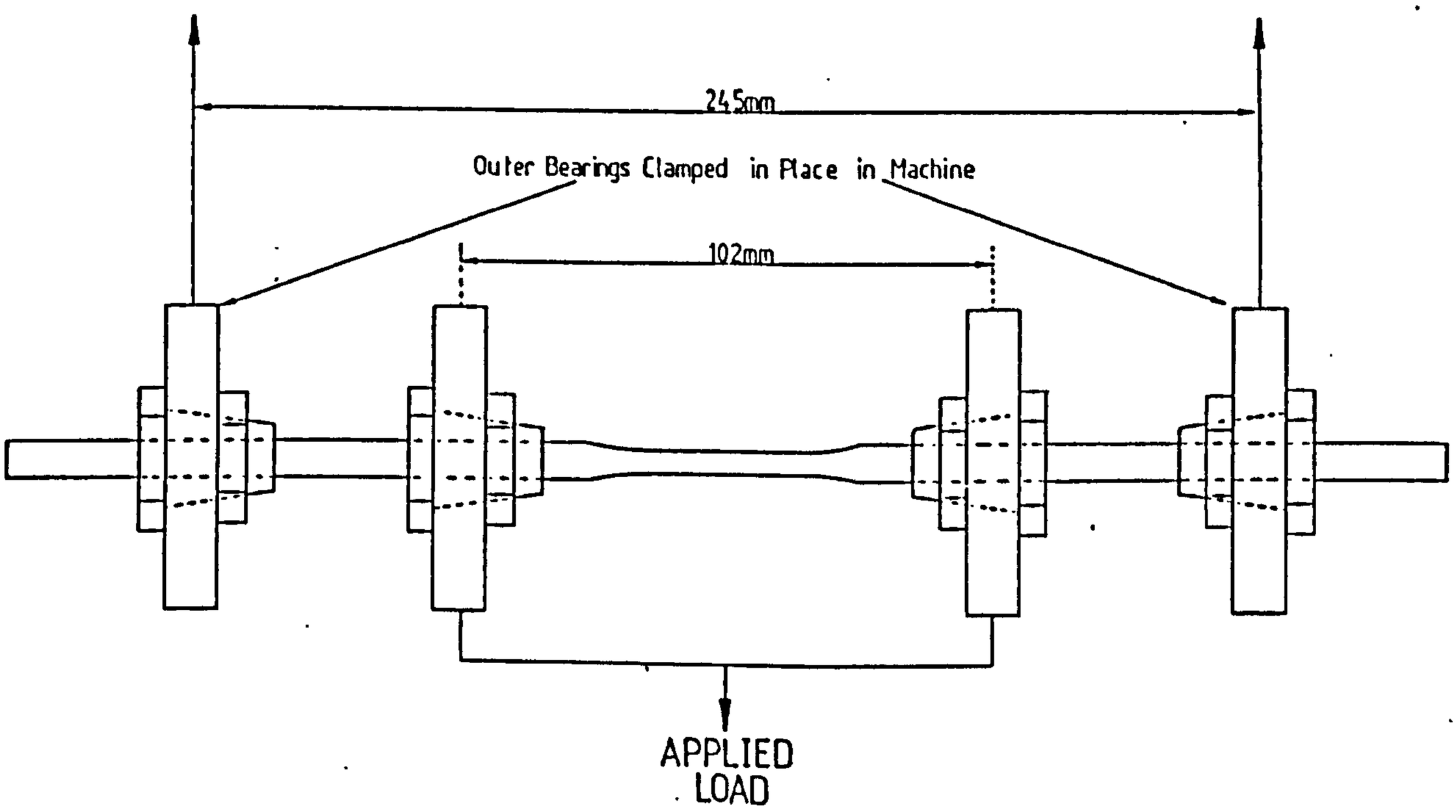

14c) Loading arrangement used in the rotating-bending tests.

Fig. 14) Specimen dimensions and loading arrangement used in the rotating-bending tests.

15a) Arrangement of proving ring and fretting bridges for a fretting-fatigue test.

15b) Relationship between the proving ring diameter and the contact pressure exerted by the feet of the fretting bridges on the specimen gauge length.

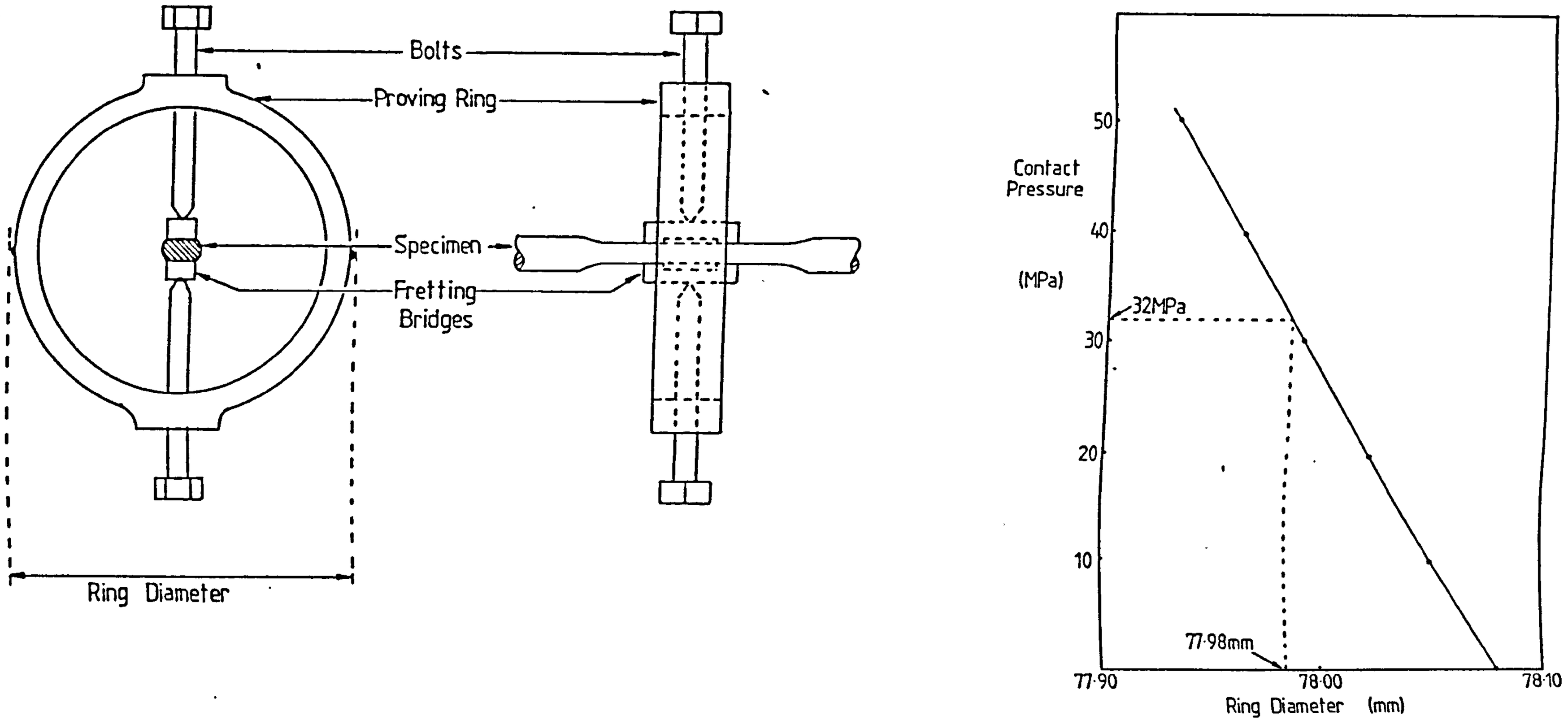

Fig. 15) Fretting arrangement and calibration of proving ring used in the rotating-bending fatigue tests.

Fig. 16) The parameters required to determine the residual stresses in a surface using the X-ray diffraction technique.

Radiation	= CuKα
Wavelength of radiation	= 1.542 Angstroms
Accelerating voltage	= 40kV
Current	= 20mA
Diffraction plane (h,k,l)	= (4 2 2)
Diffraction plane orientation (Y)	= 45°
Diffraction angle (2θ)	= 137.6°
Specimen rotation speed	= 0.05°/minute
Counter rotation speed	= 0.1°/minute
Youngs modulus (E) for 7010	= 71.7 GPa
Poissons ratio (ν) for 7010	= 0.33
Youngs modulus (E) for 8090	= 80.0 GPa
Poissons ratio (ν) for 8090	= 0.33

Fig. 17) Flow diagram summarising the experimental procedure used in this work.

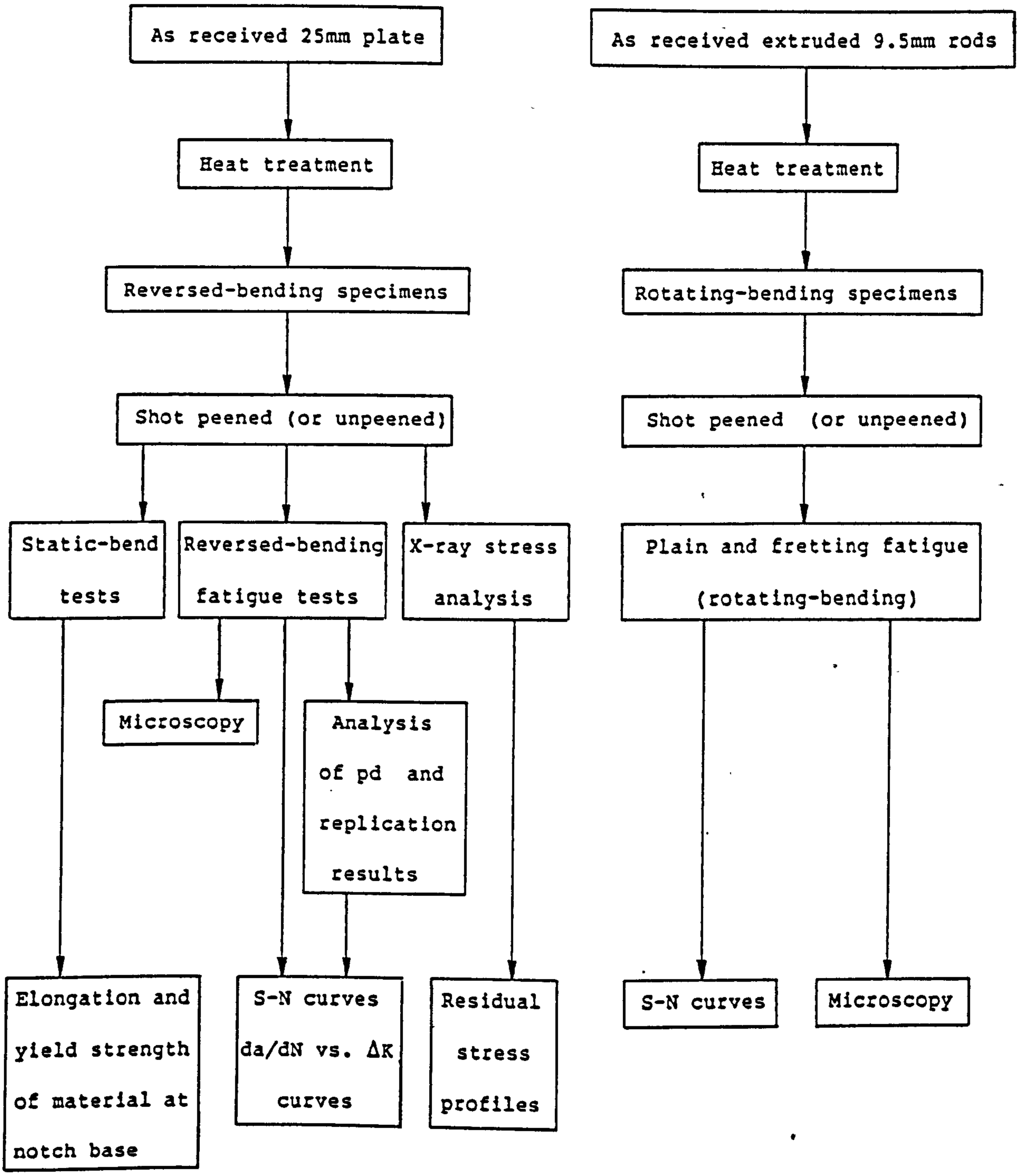

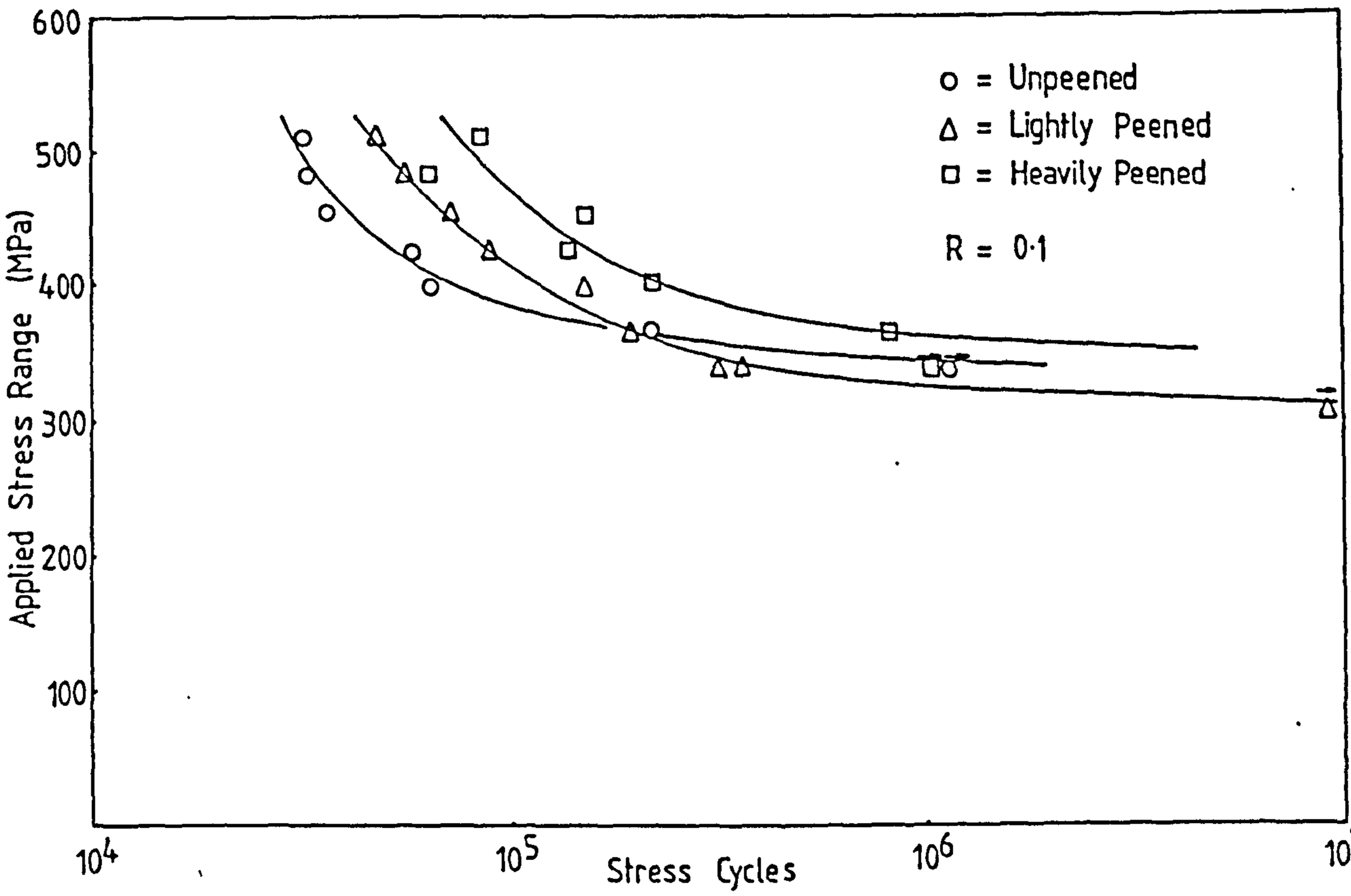

Fig. 18) S-N curves showing the reversed-bending fatigue properties of alloy 7010.

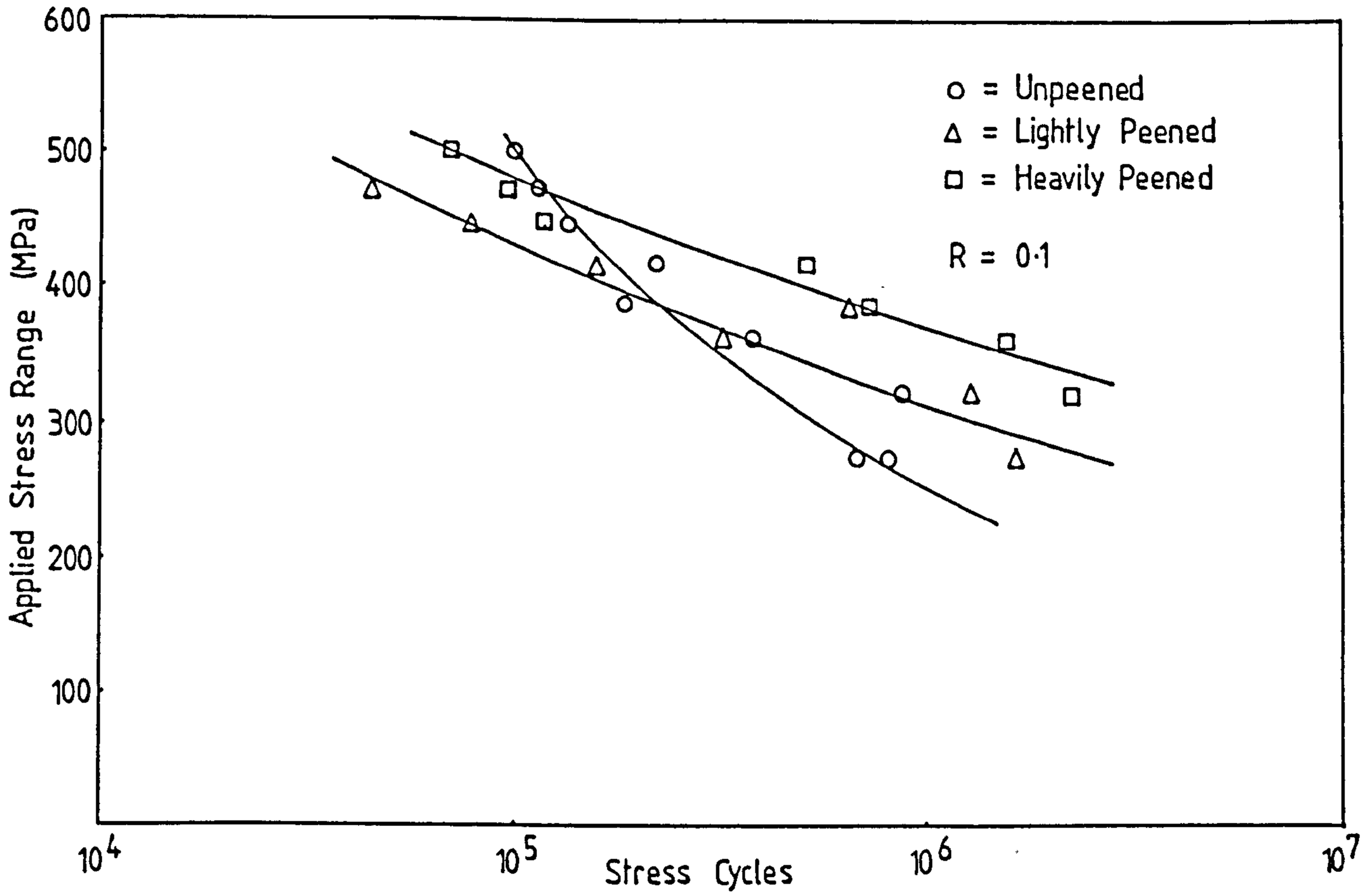

Fig. 19) S-N curves showing the reversed-bending fatigue properties of alloy 8090.

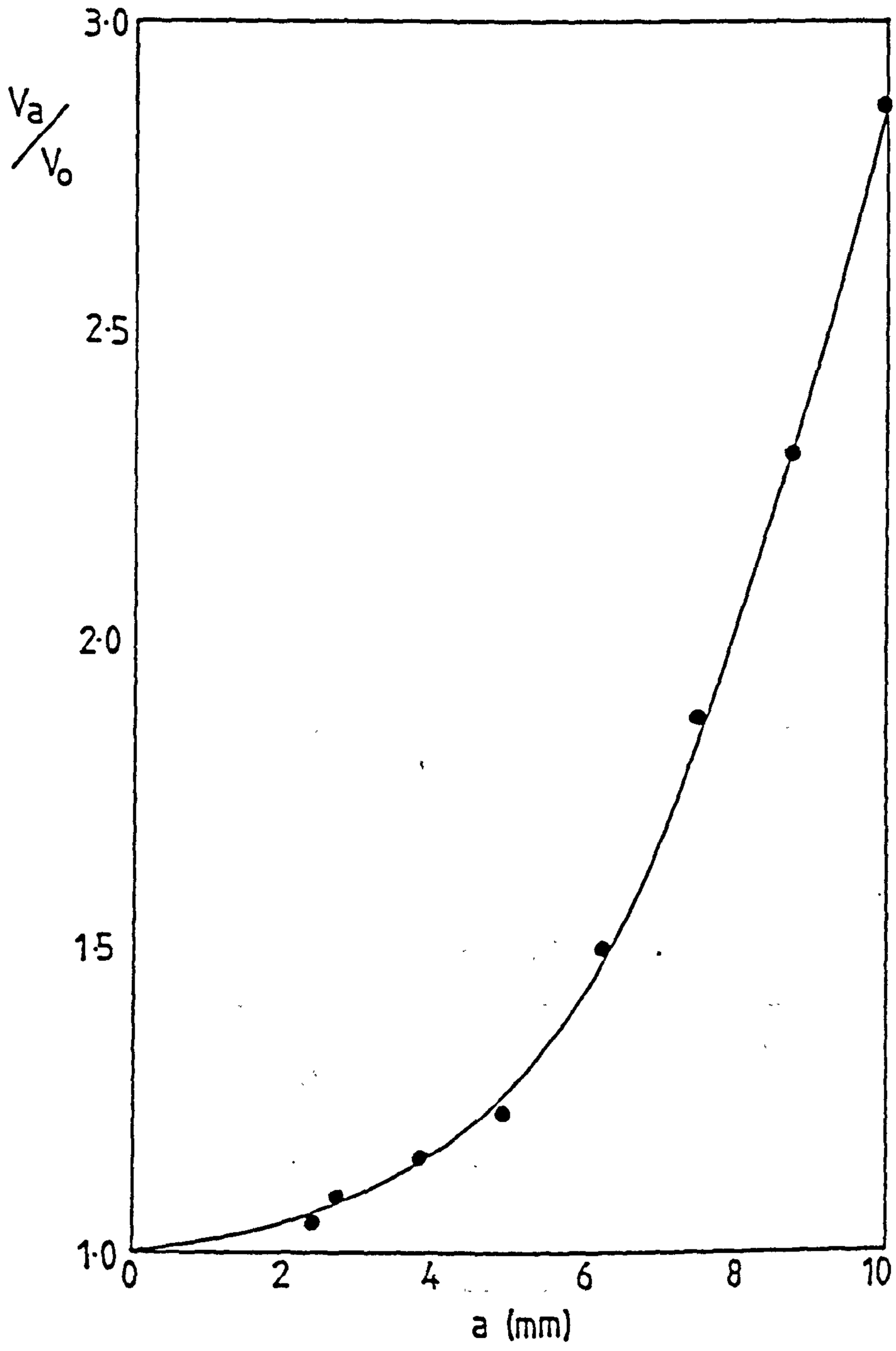

Fig. 20) Relationship between the voltage across the notch and the crack length in the reversed-bending specimens during fatigue testing.

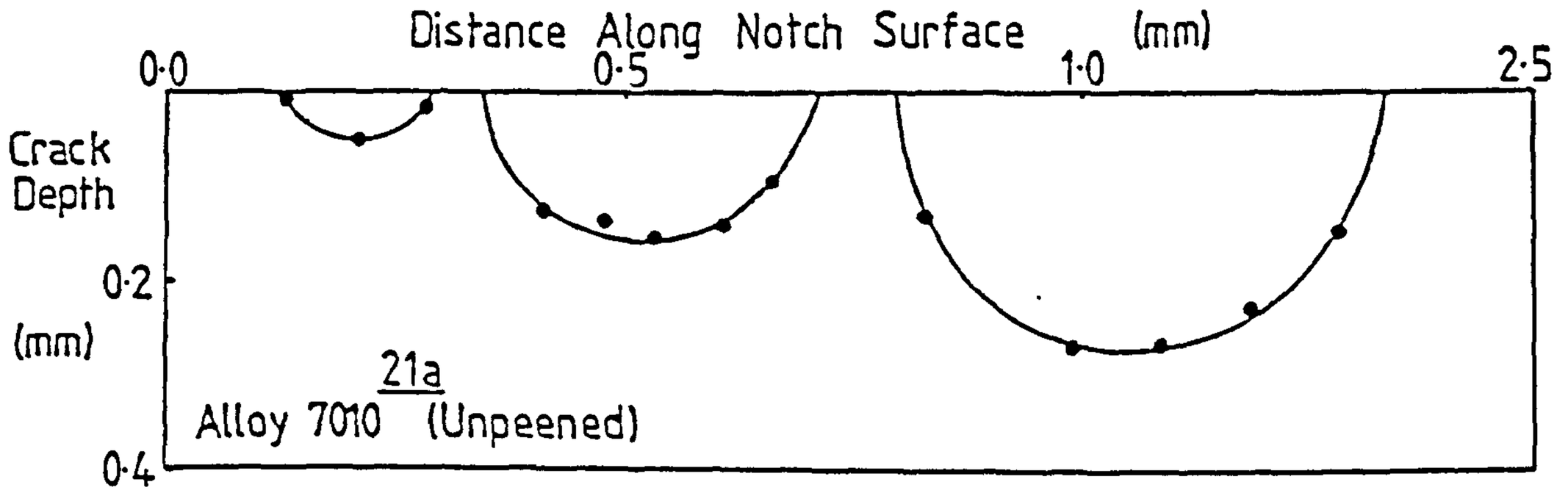

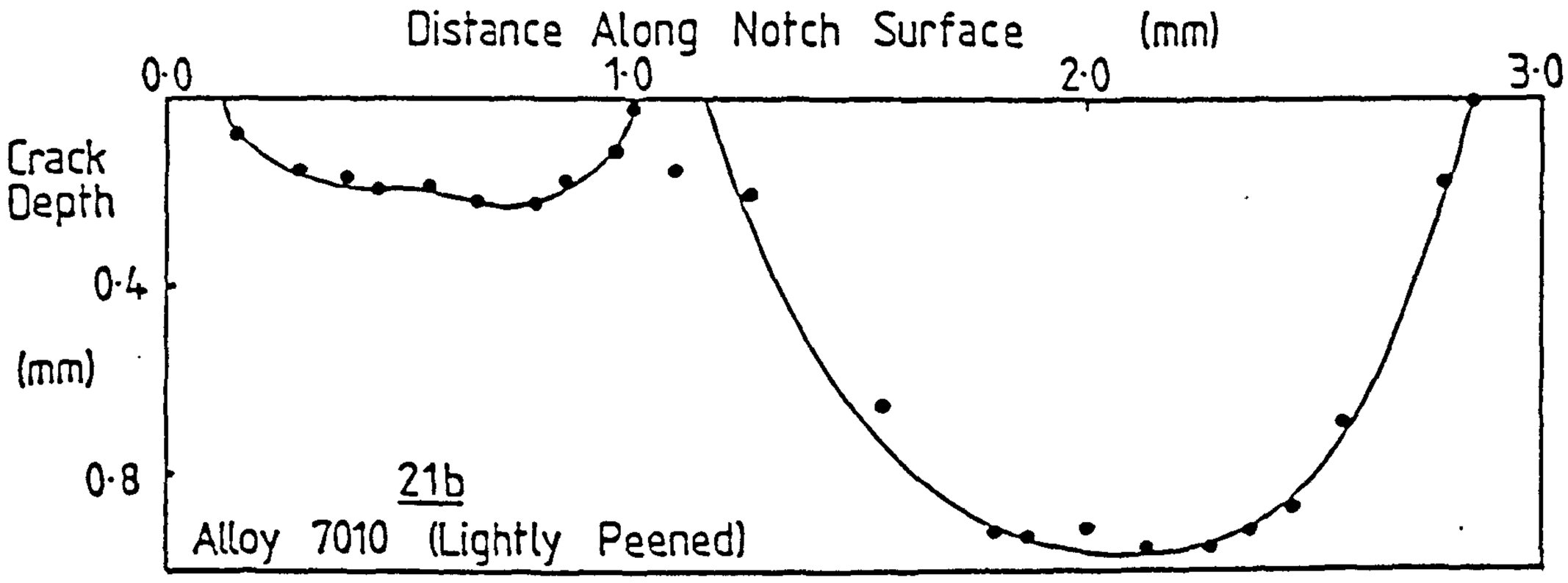

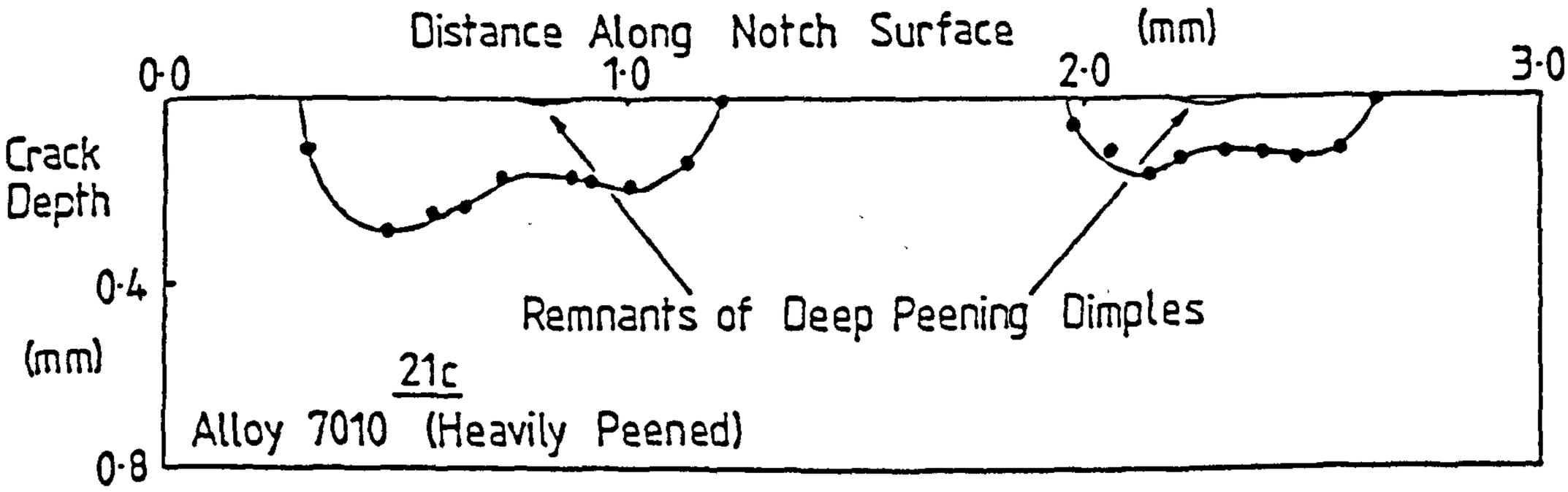

Fig. 21) Fatigue crack profiles in the unpeened, lightly peened and heavily peened reversed-bending specimens (alloy 7010).

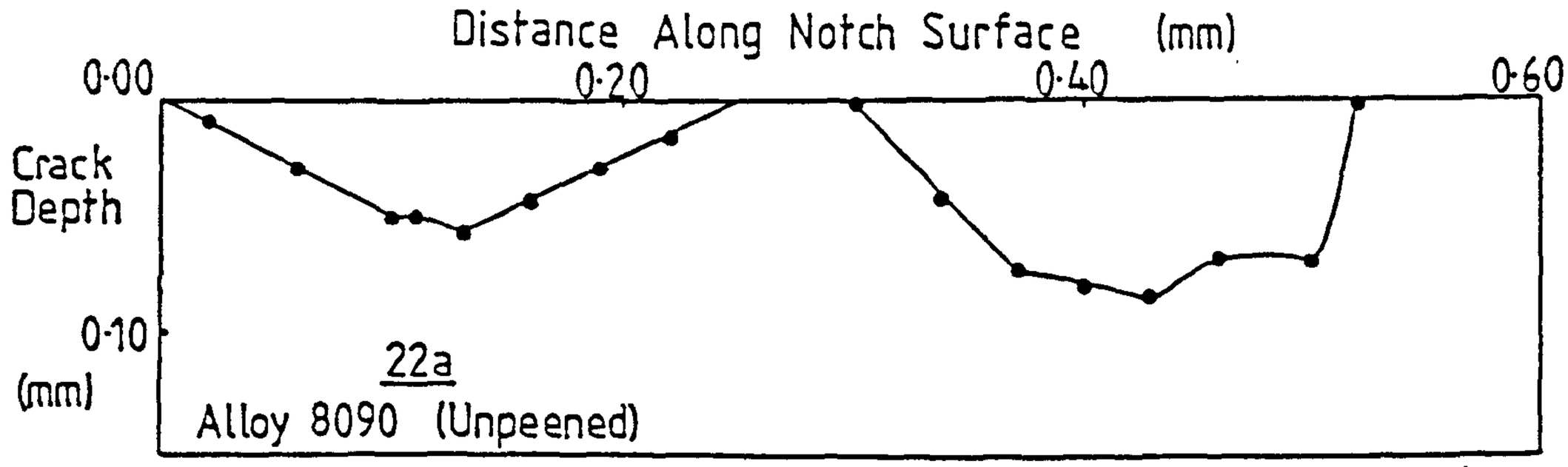

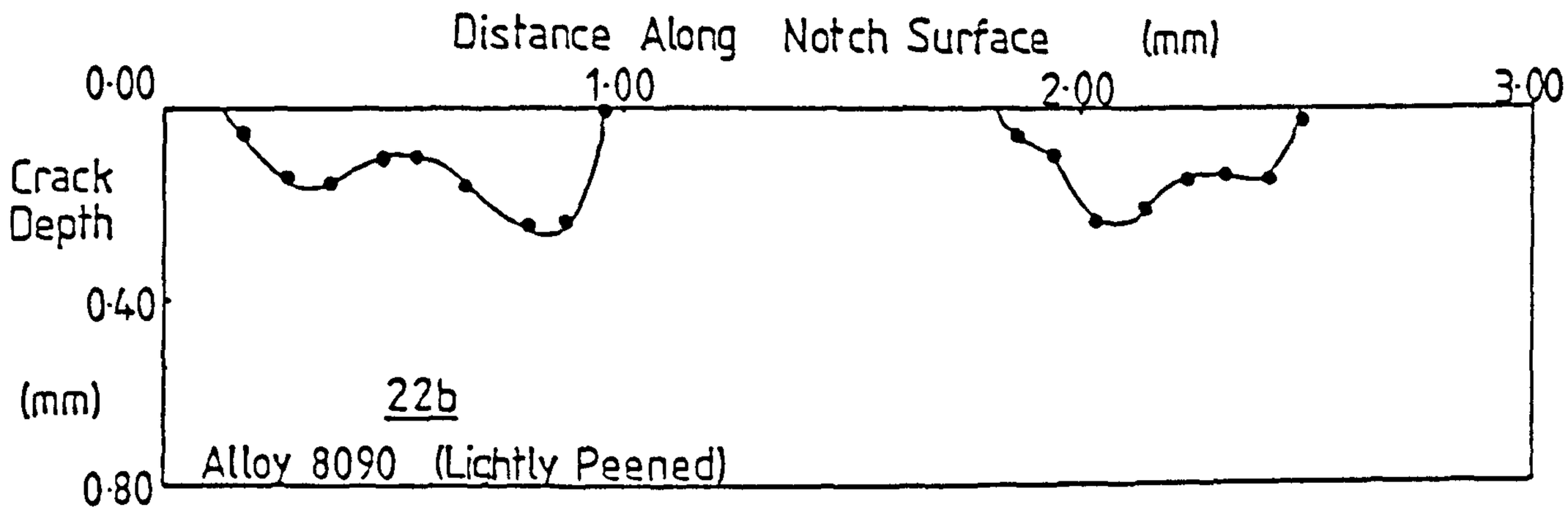

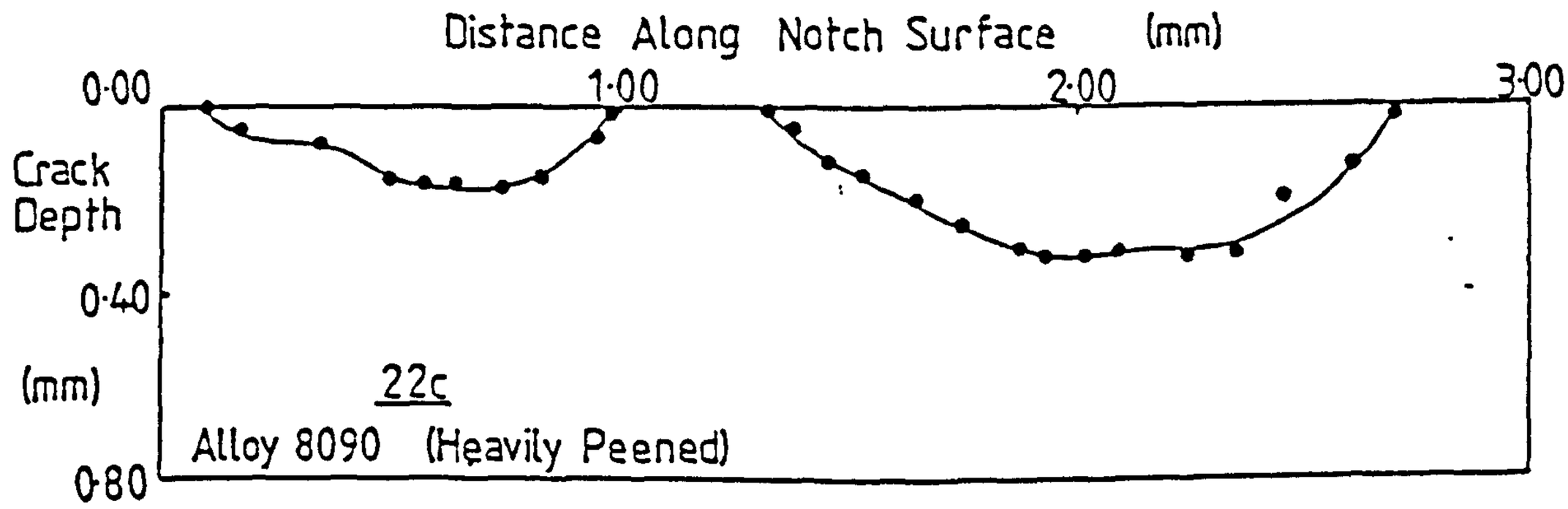

Fig. 22) Fatigue crack profiles in the unpeened, lightly peened and heavily peened reversed-bending specimens (alloy 8090).

Fig. 23) Plot of crack length vs. maximum crack depth for the unpeened, lightly peened and heavily peened reversed-bending specimens (alloy 7010).

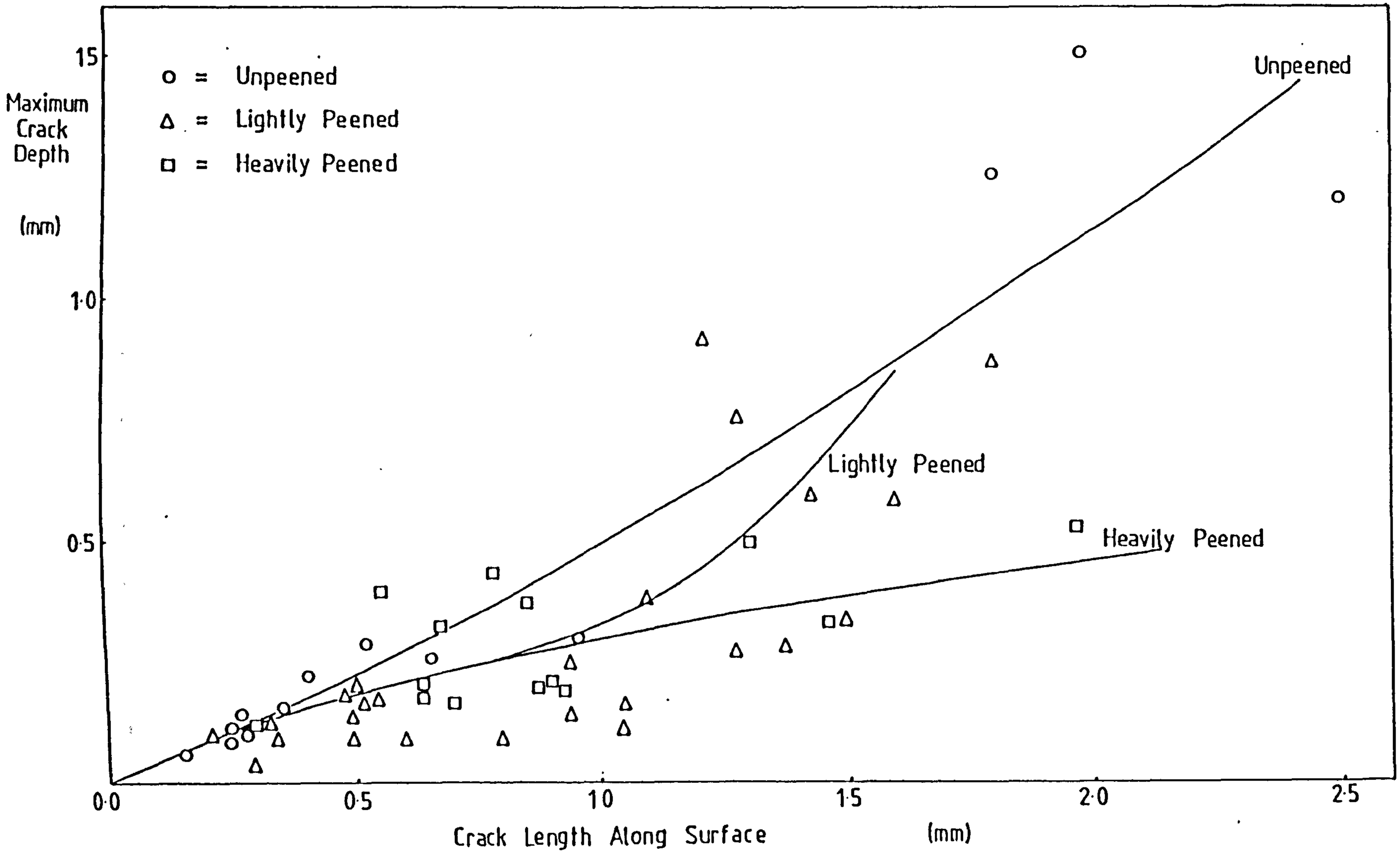

Fig. 24) Plot of crack length vs. maximum crack depth for the unpeened, lightly peened and heavily peened reversed-bending specimens (alloy 8090).

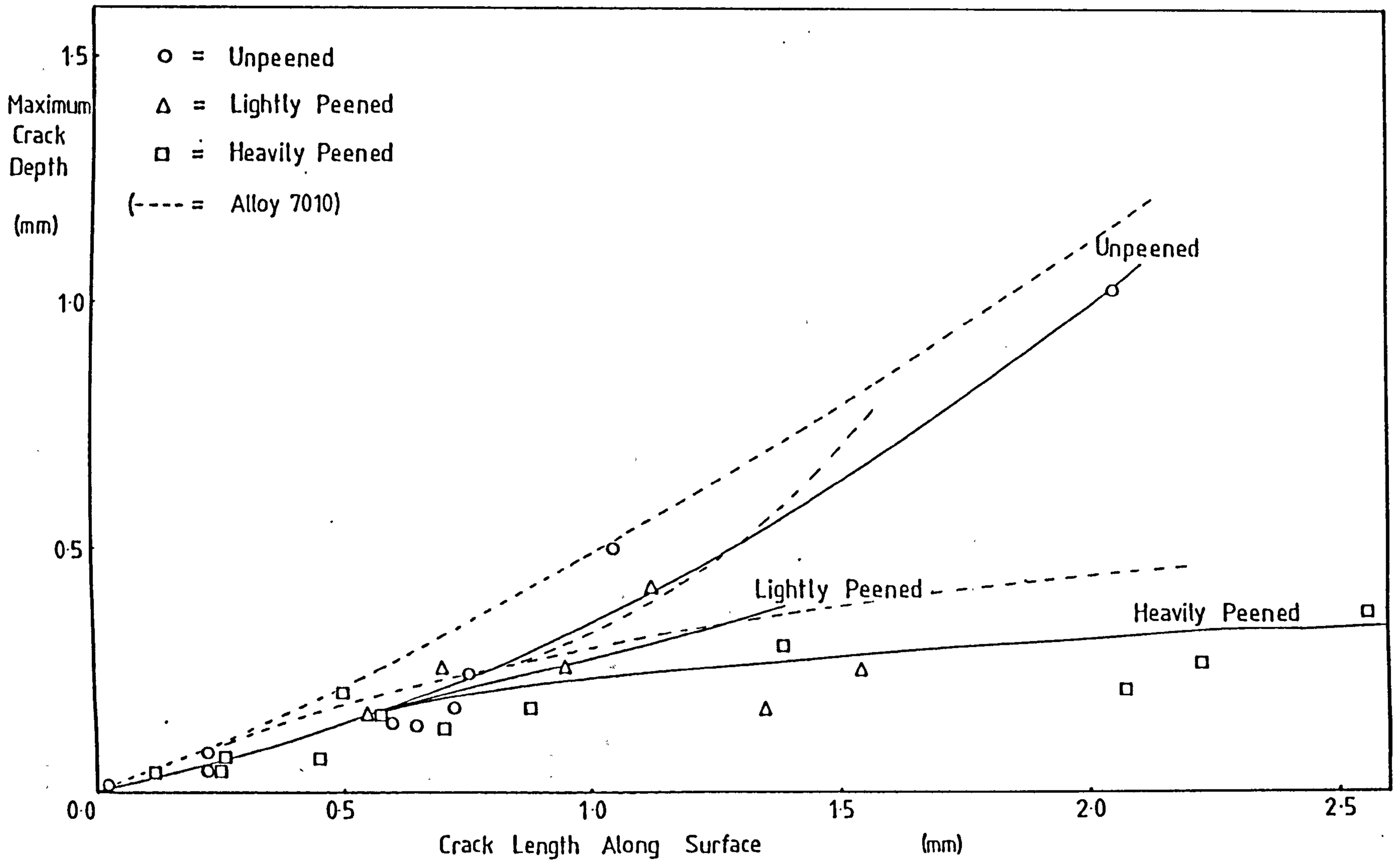

Fig. 25) Plot of crack depth vs. number of cycles for the unpeened, lightly peened and heavily peened 7010 alloy reversed-bending specimens fatigue tested at applied stresses of 368MPa and 507MPa.

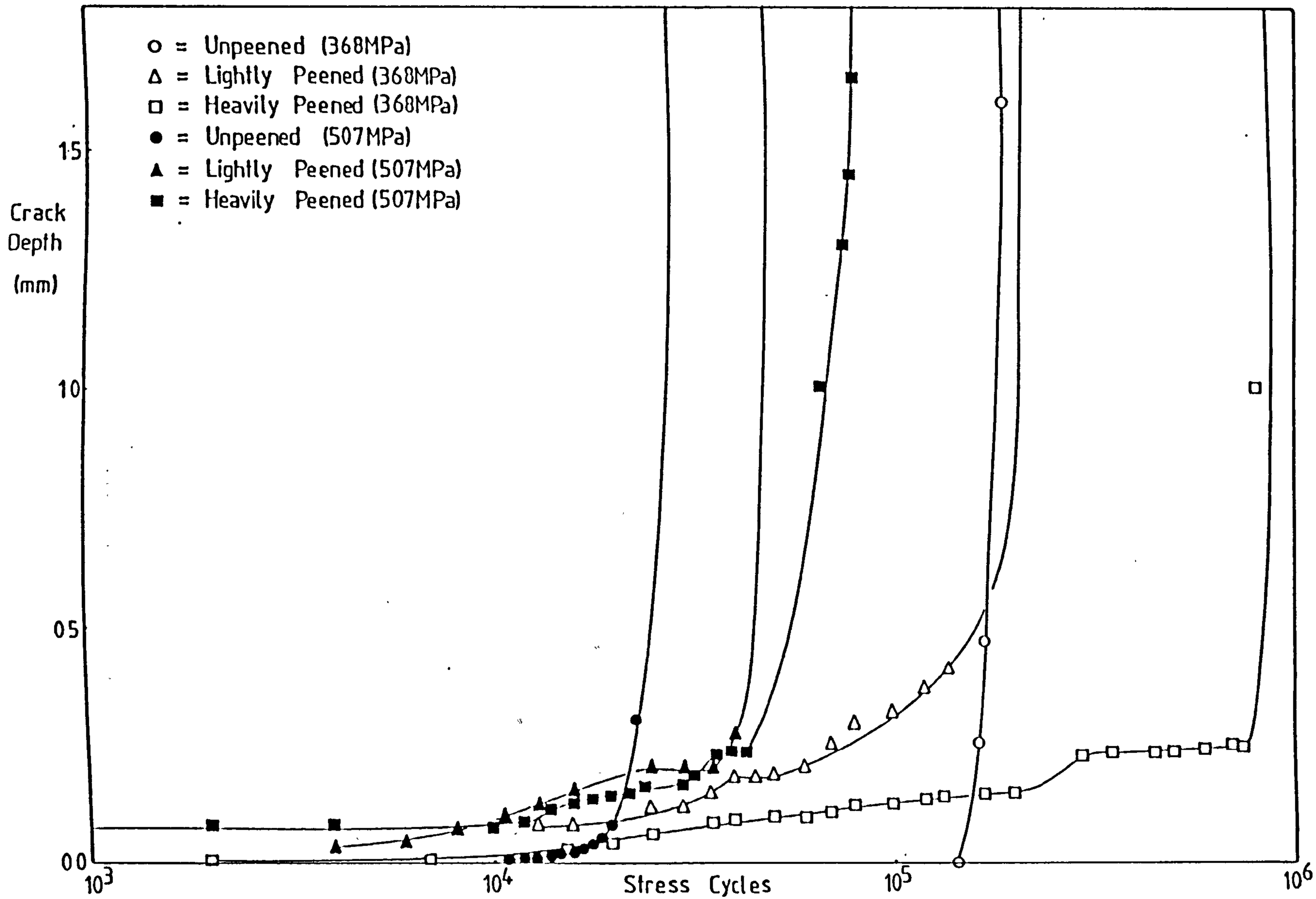

Fig. 26) Plot of crack depth vs. number of cycles for the unpeened, lightly peened and heavily peened 8090 alloy reversed-bending specimens fatigue tested at applied stresses of 368MPa and 507MPa.

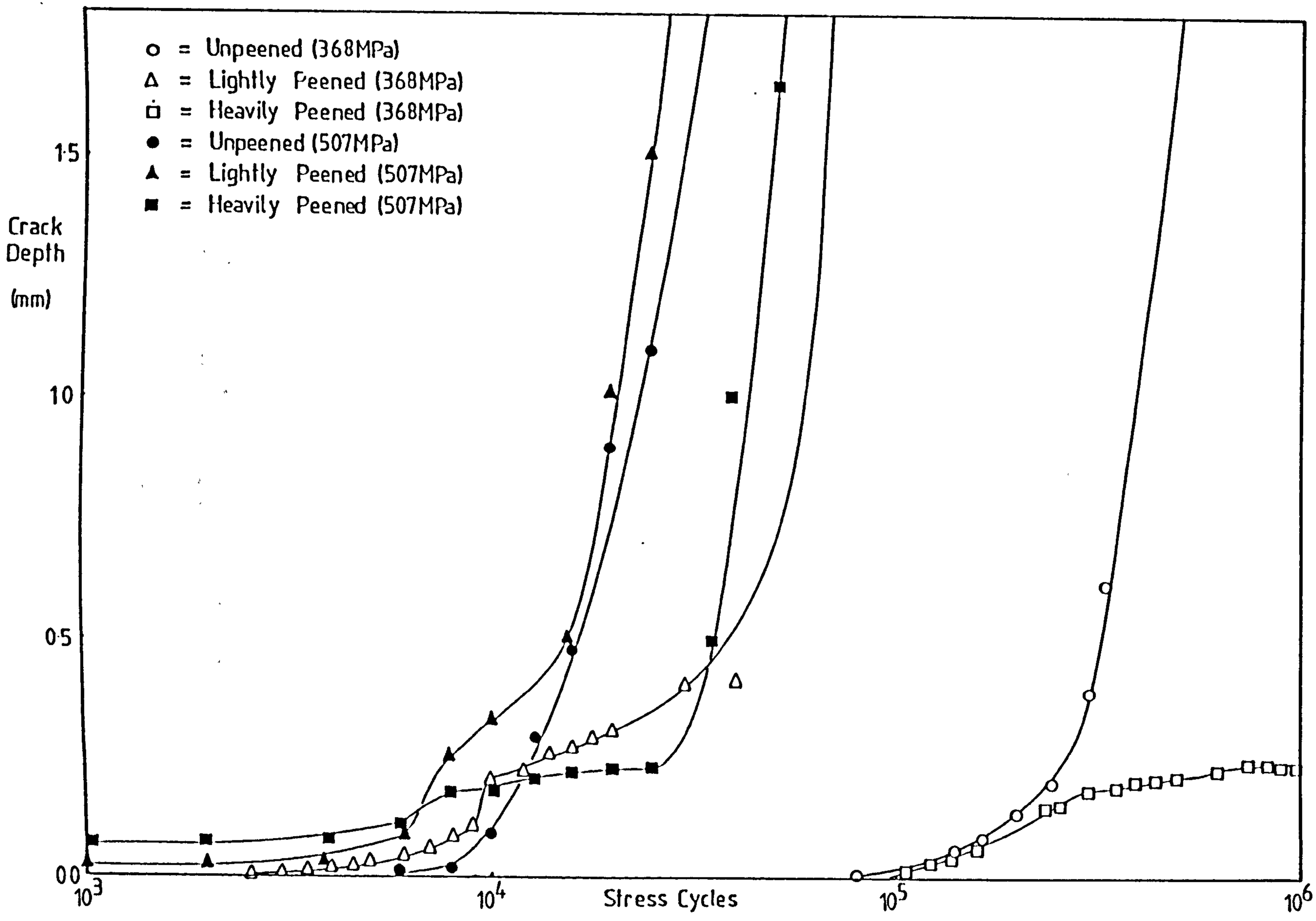

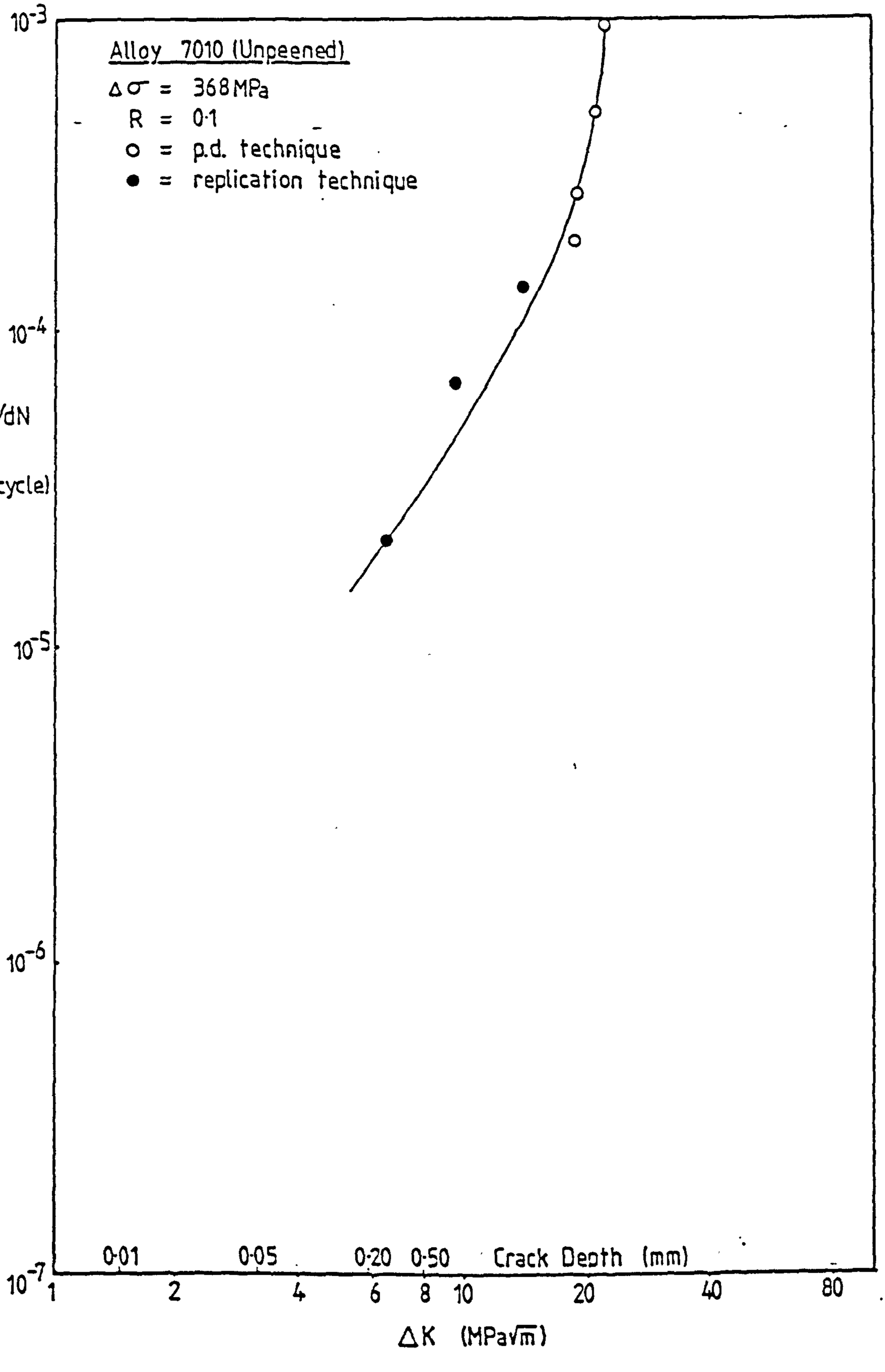

Fig. 27) Variation of fatigue crack growth rate, da/dN with stress intensity, ΔK, for the unpeened 7010 alloy tested at an applied stress range of 368MPa.

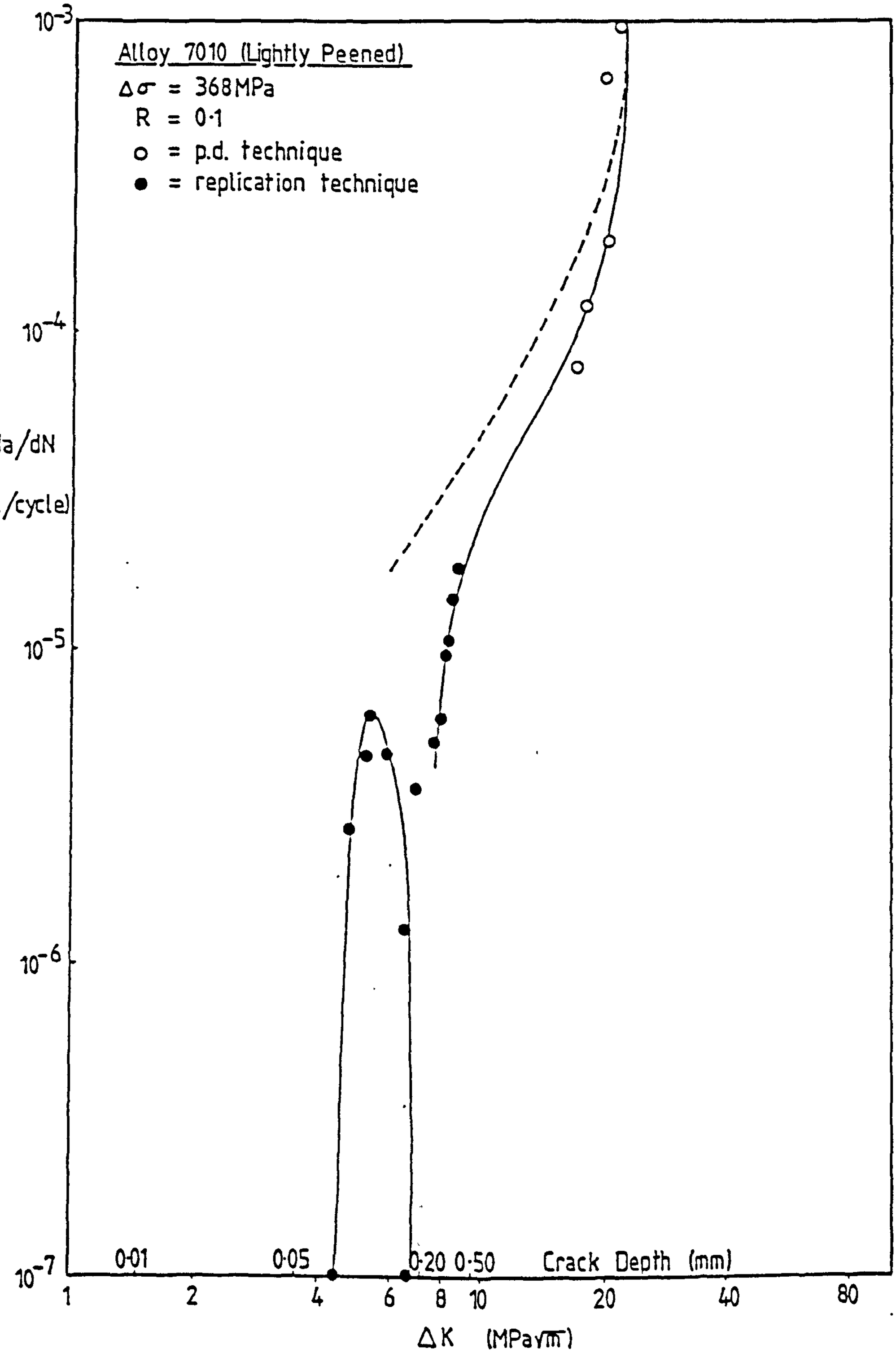

Fig. 28) Variation of fatigue crack growth rate, da/dN with stress intensity, ΔK, for the lightly peened 7010 alloy tested at an applied stress range of 368MPa.

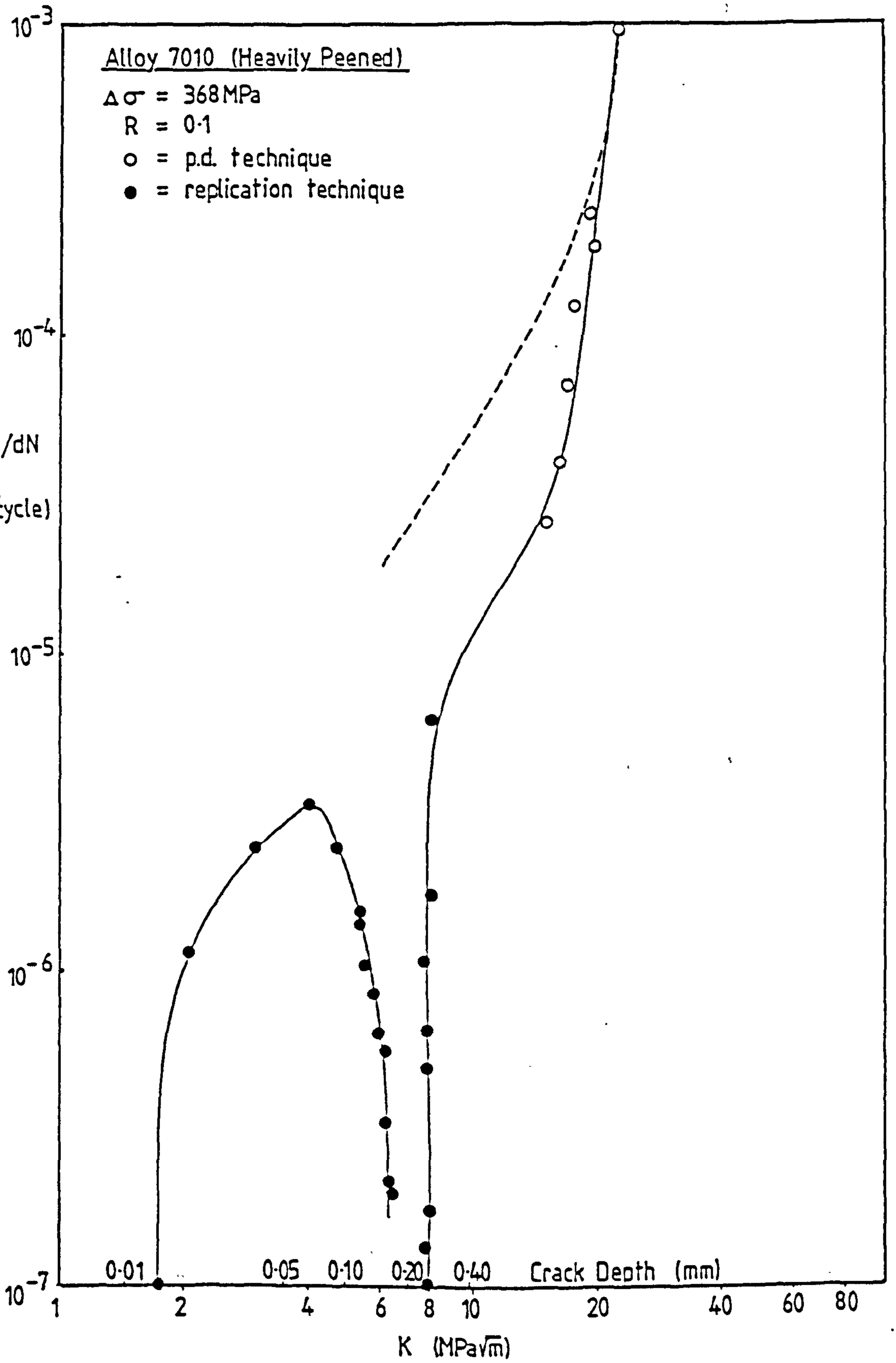

Fig. 29) Variation of fatigue crack growth rate, da/dN with stress intensity, ΔK, for the heavily peened 7010 alloy tested at an applied stress range of 368MPa.

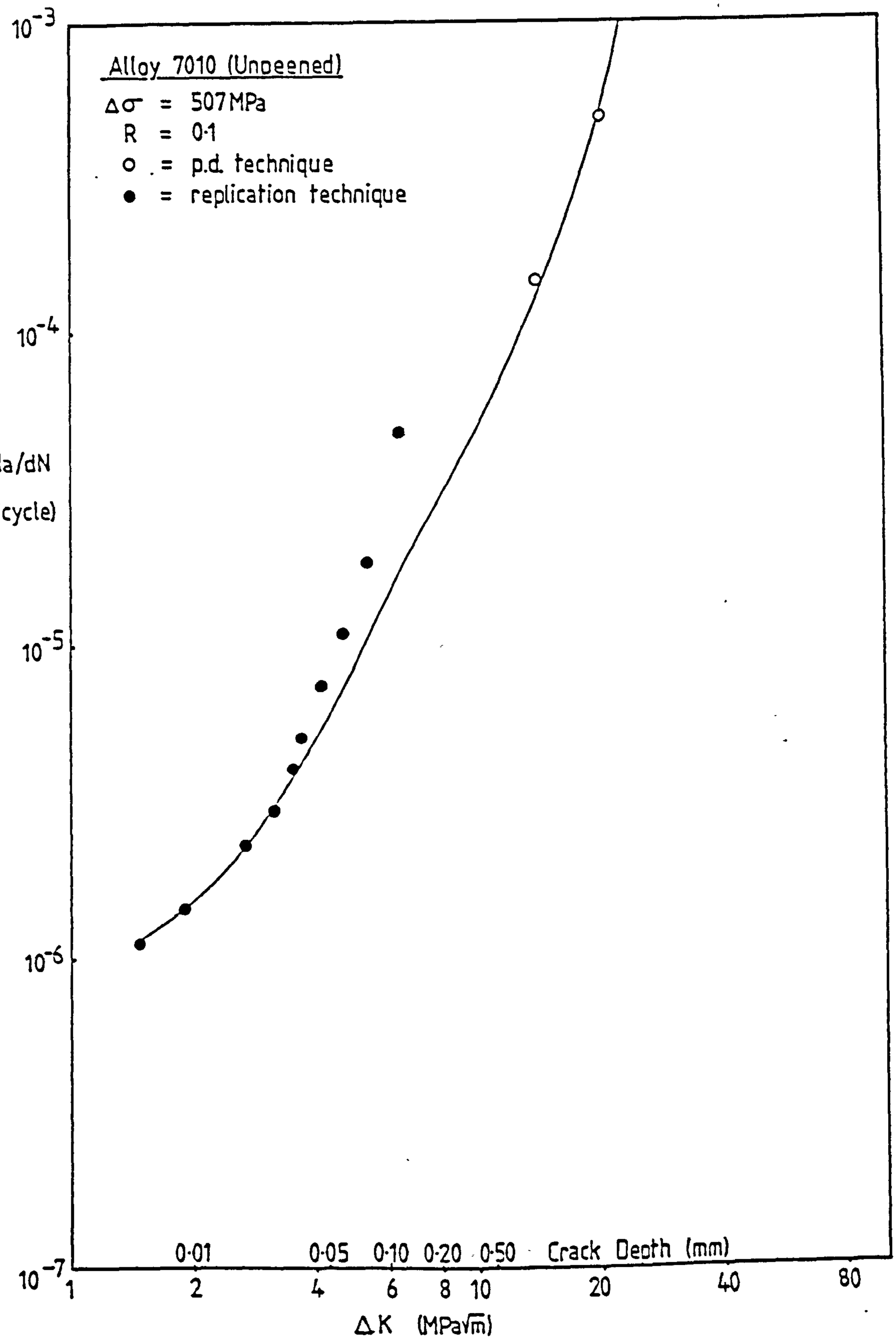

Fig. 30) Variation of fatigue crack growth rate, da/dN with stress intensity, ΔK, for the unpeened 7010 alloy tested at an applied stress range of 507MPa.

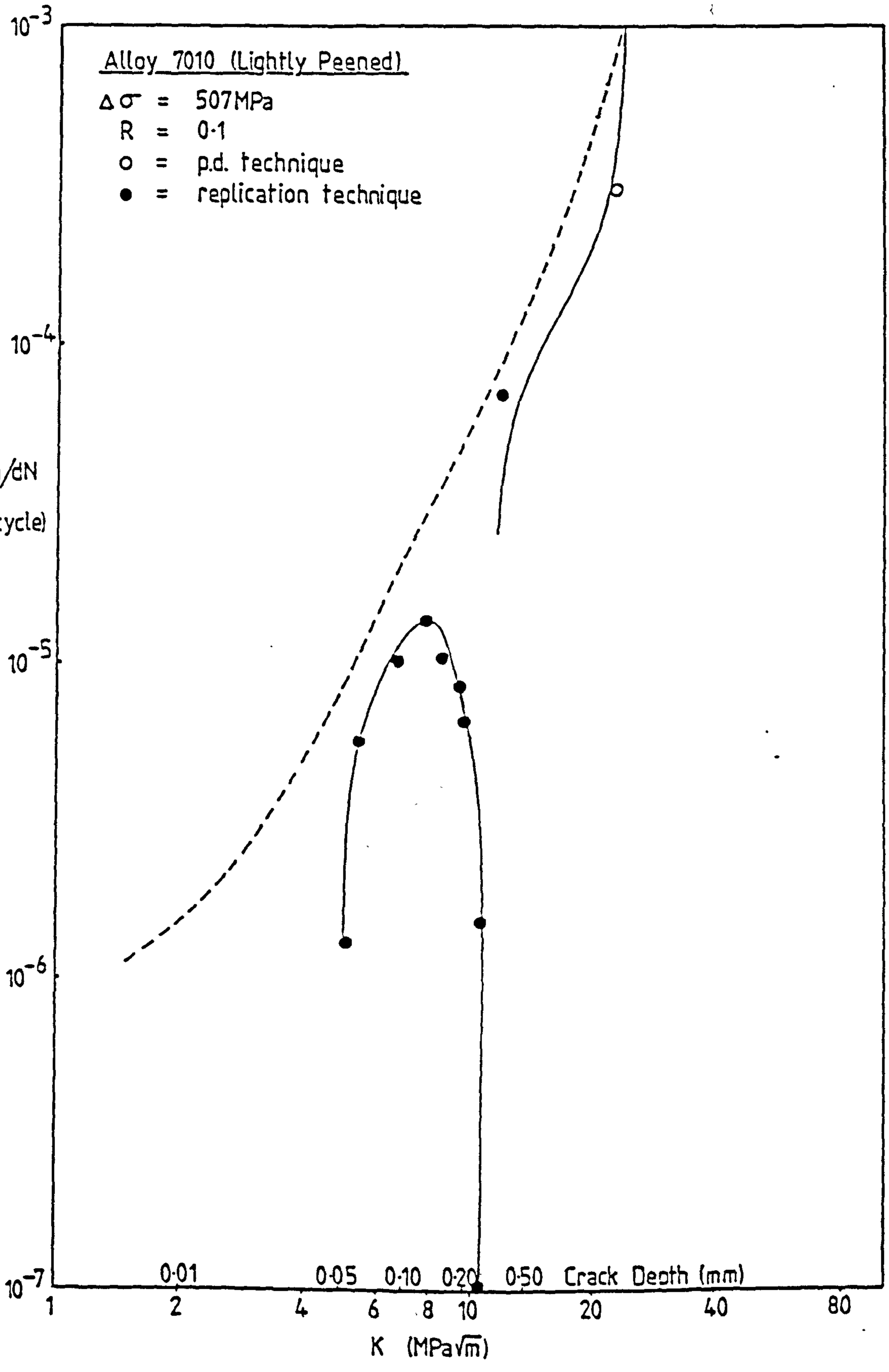

Fig. 31) Variation of fatigue crack growth rate, da/dN with stress intensity, ΔK, for the lightly peened 7010 alloy tested at an applied stress range of 507MPa.

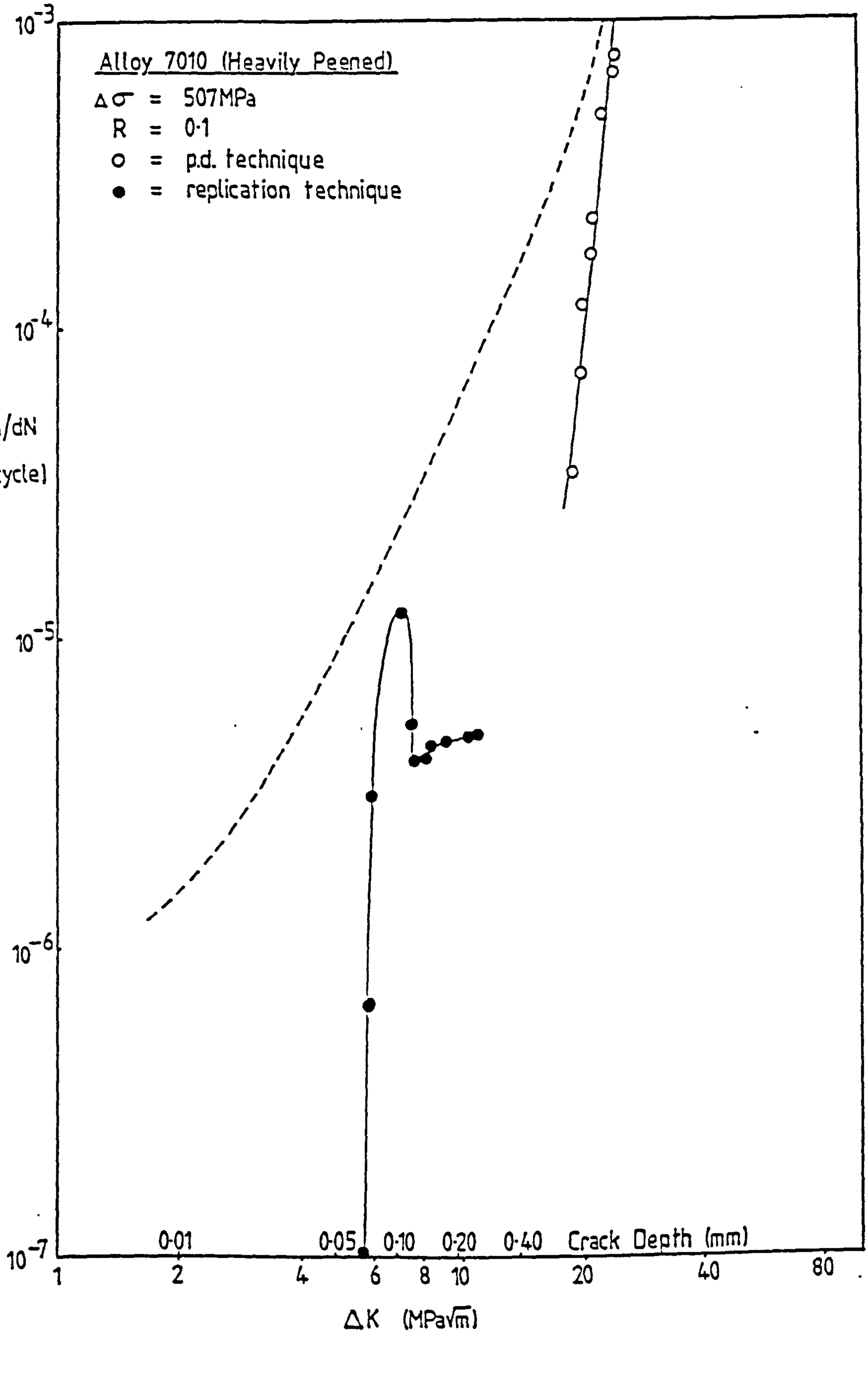

Fig. 32) Variation of fatigue crack growth rate, da/dN with stress intensity, ΔK, for the heavily peened 7010 alloy tested at an applied stress range of 507MPa.

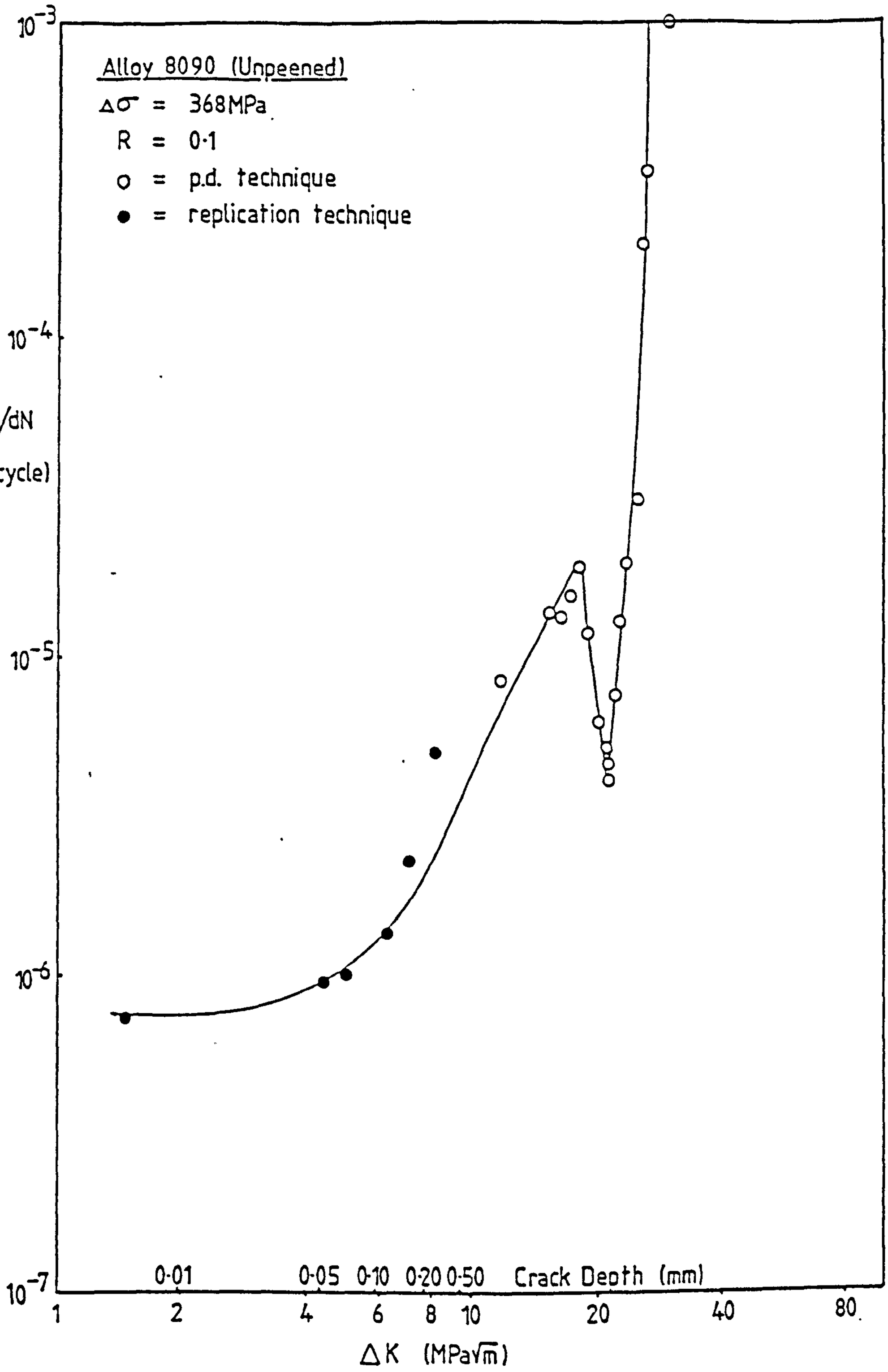

Fig. 33) Variation of fatigue crack growth rate, da/dN with stress intensity, ΔK, for the unpeened 8090 alloy tested at an applied stress range of 368MPa.

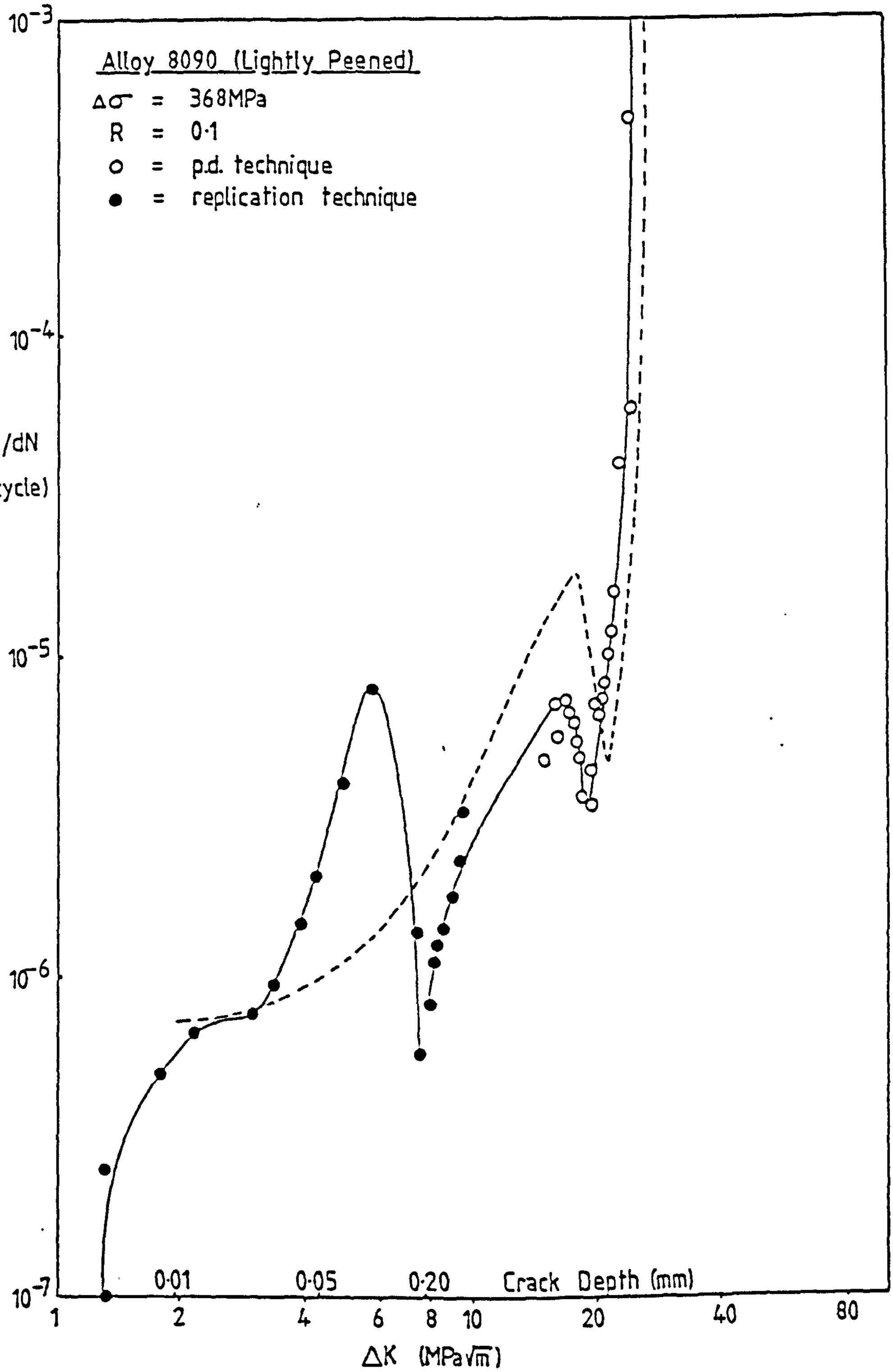

Fig. 34) Variation of fatigue crack growth rate, da/dN with stress intensity, ΔK, for the lightly peened 8090 alloy tested at an applied stress range of 368MPa.

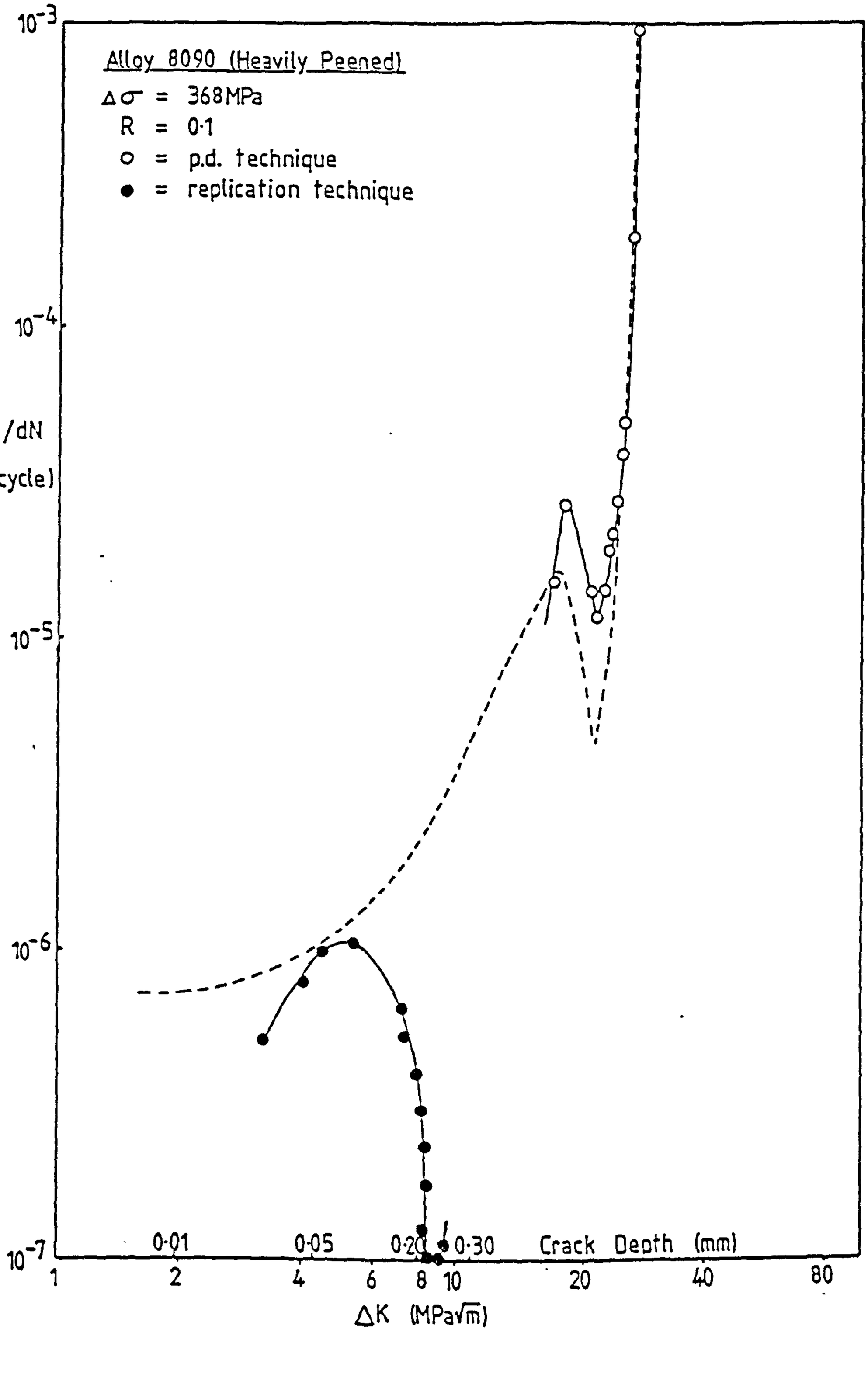

Fig. 35) Variation of fatigue crack growth rate, da/dN with stress intensity, ΔK, for the heavily peened 8090 alloy tested at an applied stress range of 368MPa.

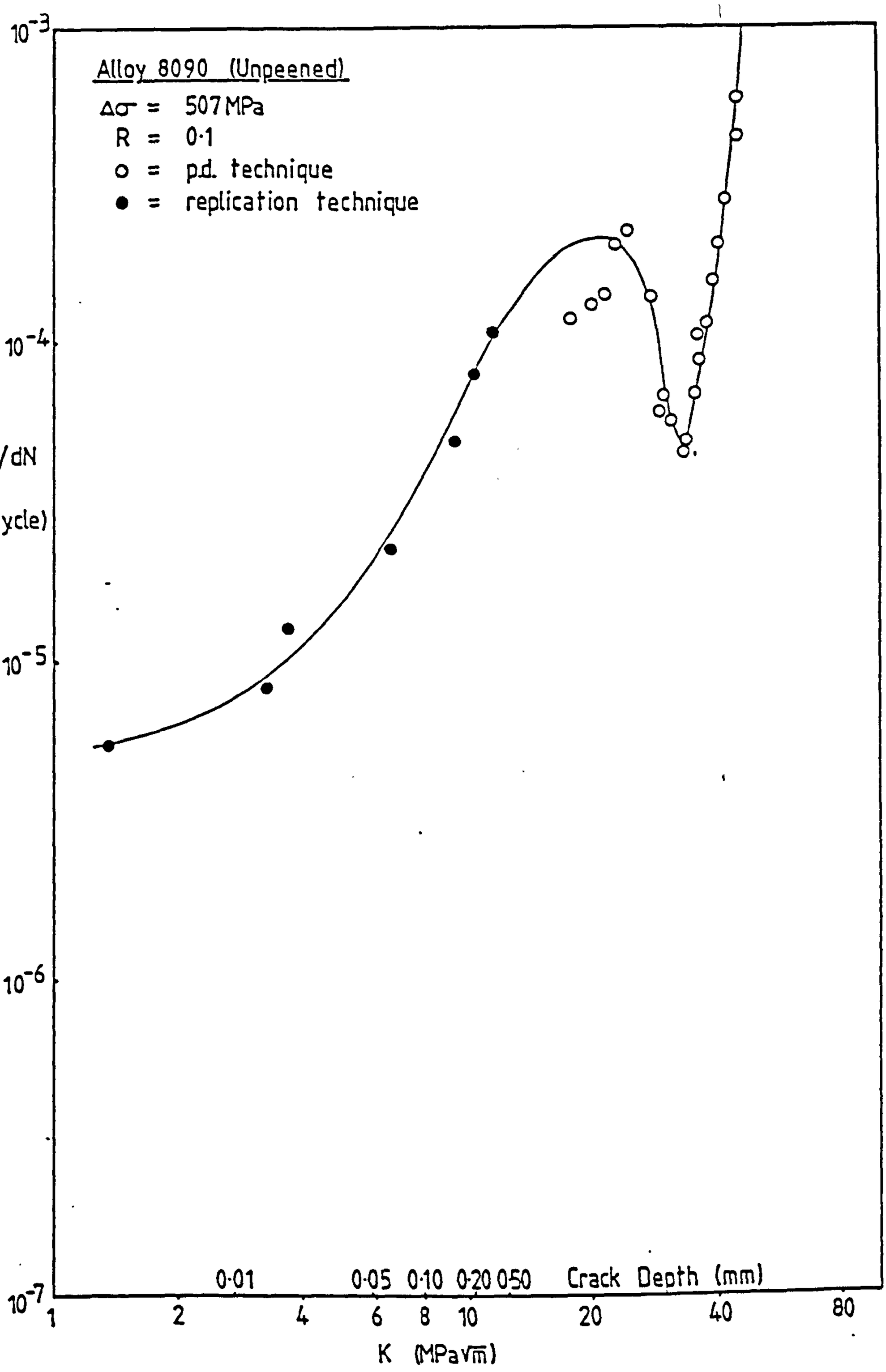

Fig. 36) Variation of fatigue crack growth rate, da/dN with stress intensity, ΔK, for the unpeened 8090 alloy tested at an applied stress range of 507MPa.

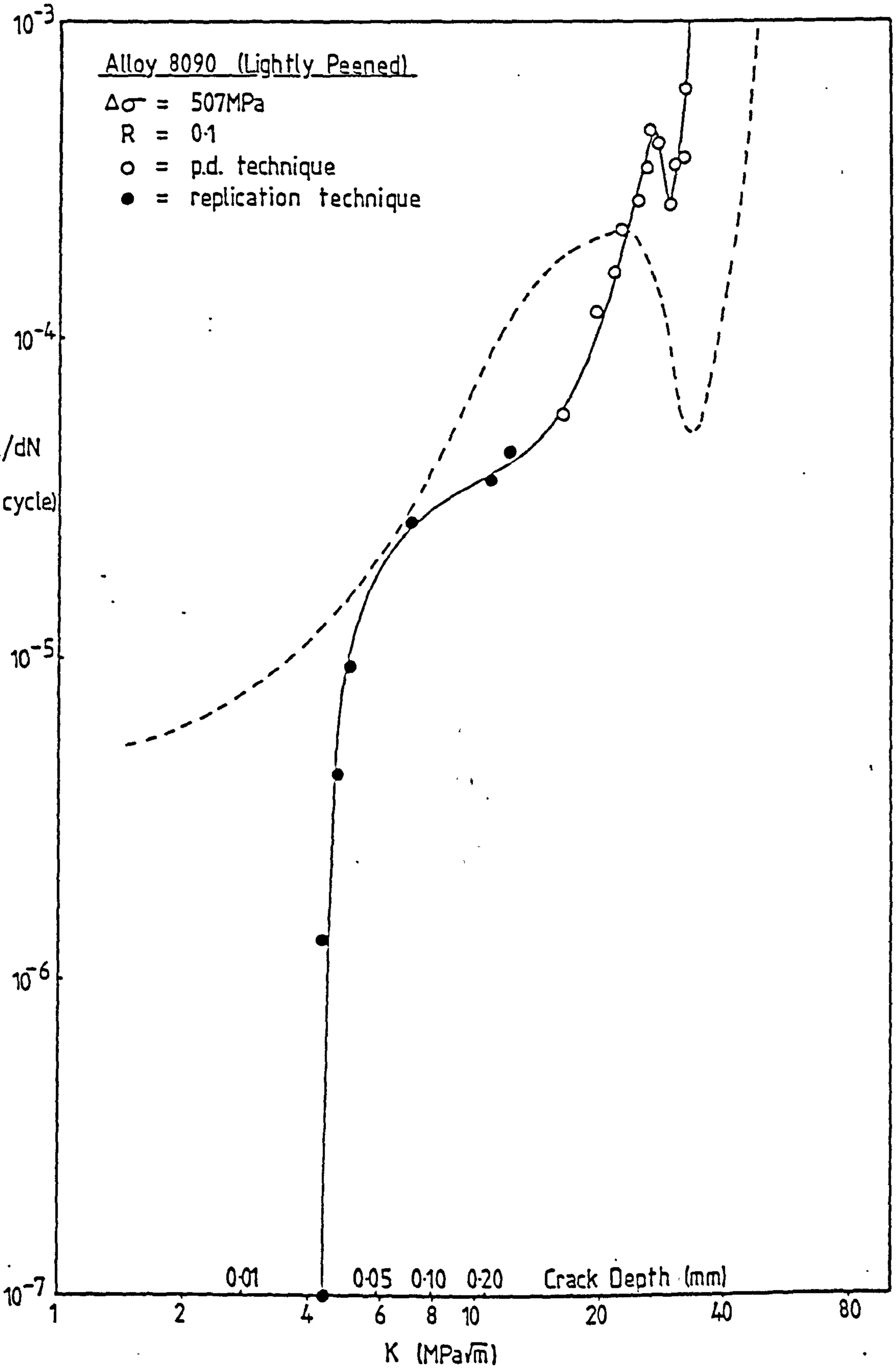

Fig. 37) Variation of fatigue crack growth rate, da/dN with stress intensity, ΔK, for the lightly peened 8090 alloy tested at an applied stress range of 507MPa.

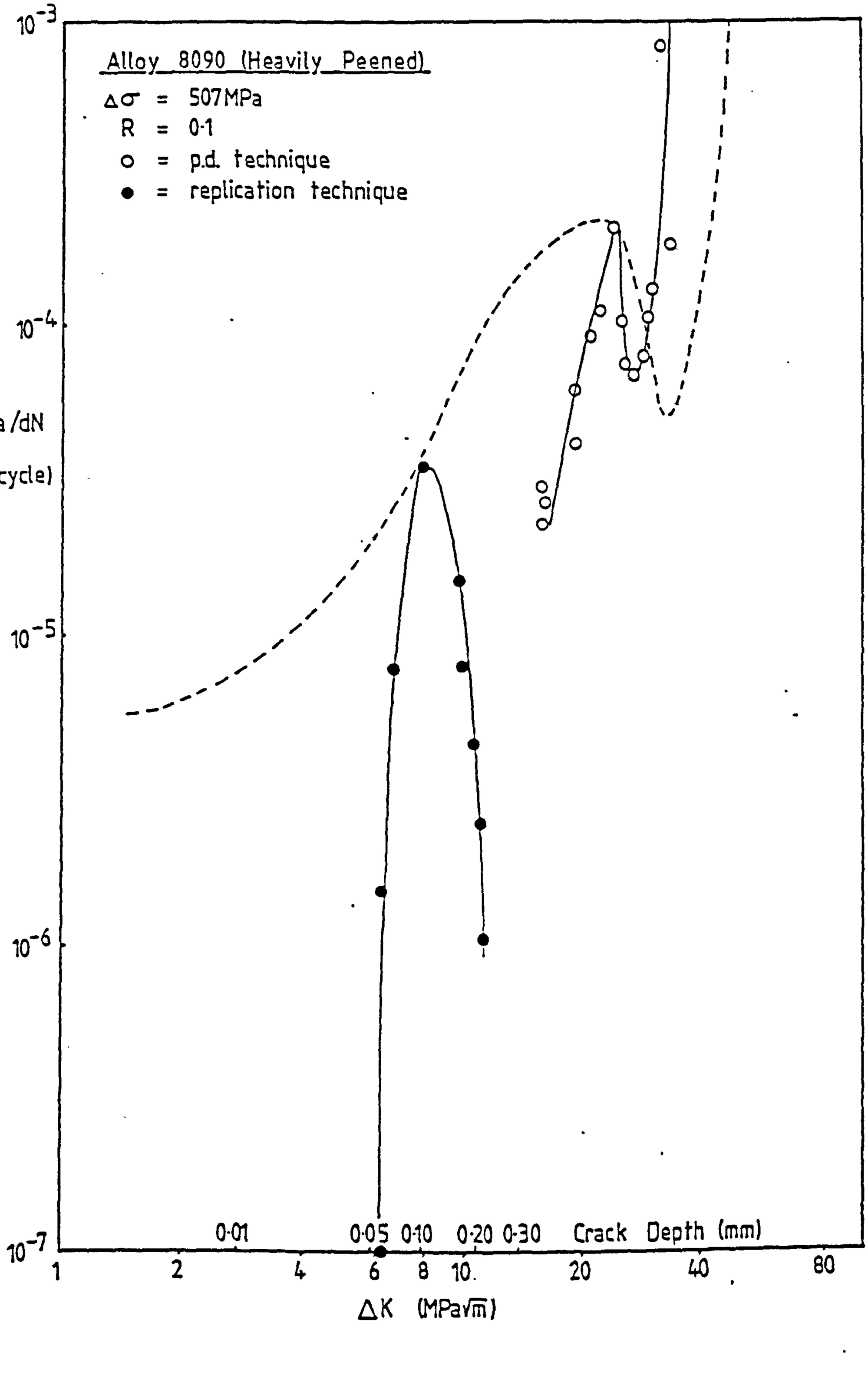

Fig. 38) Variation of fatigue crack growth rate, da/dN with stress intensity, ΔK, for the heavily peened 8090 alloy tested at an applied stress range of 507MPa.

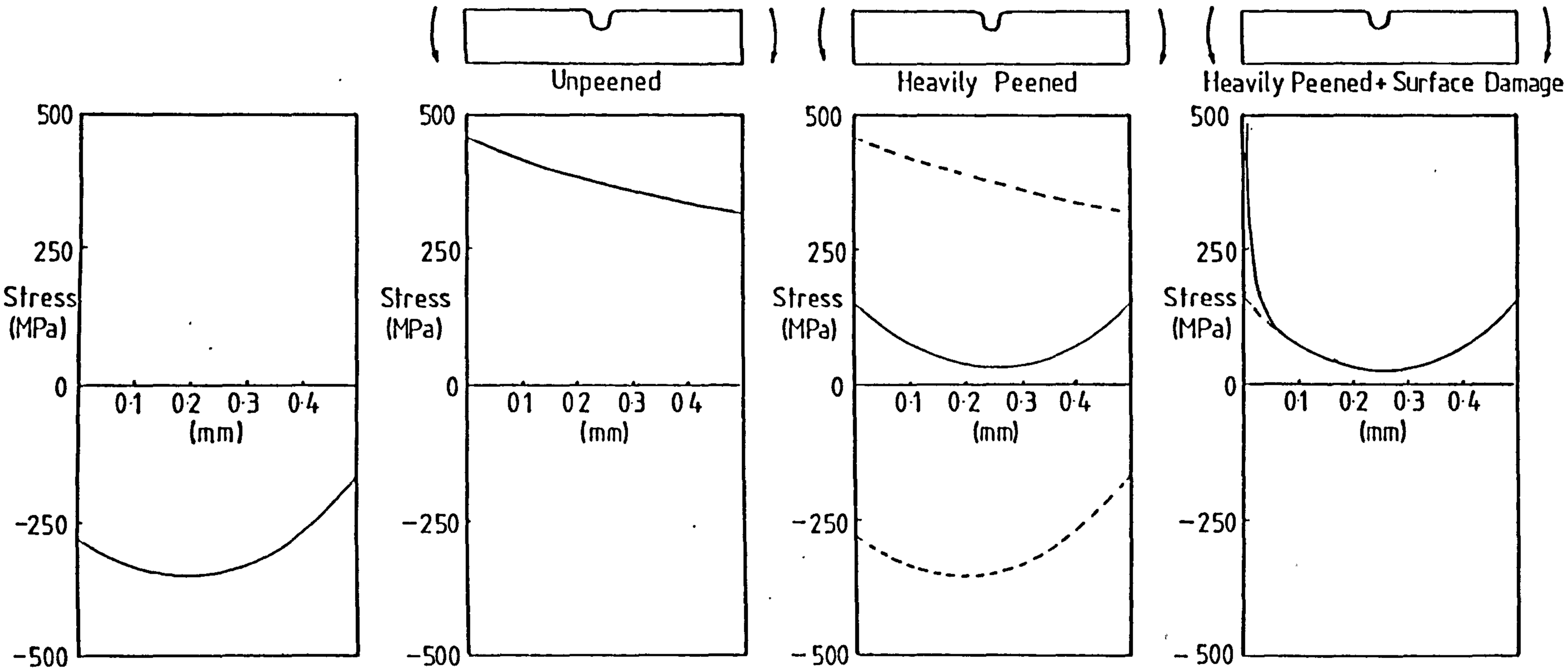

a) Residual stress distribution in the heavily peened 7010 alloy.

b) Stress distribution at base of notch in an unpeened specimen with bending moment applied.

c) Stress distribution at base of notch in a heavily peened specimen with bending moment applied

d) The effect of surface damage on the stress distribution shown in "c".

Fig. 39) The residual stress distribution at the base of the notch in a reversed-bending 7010 alloy specimen in which a bending moment has been applied.

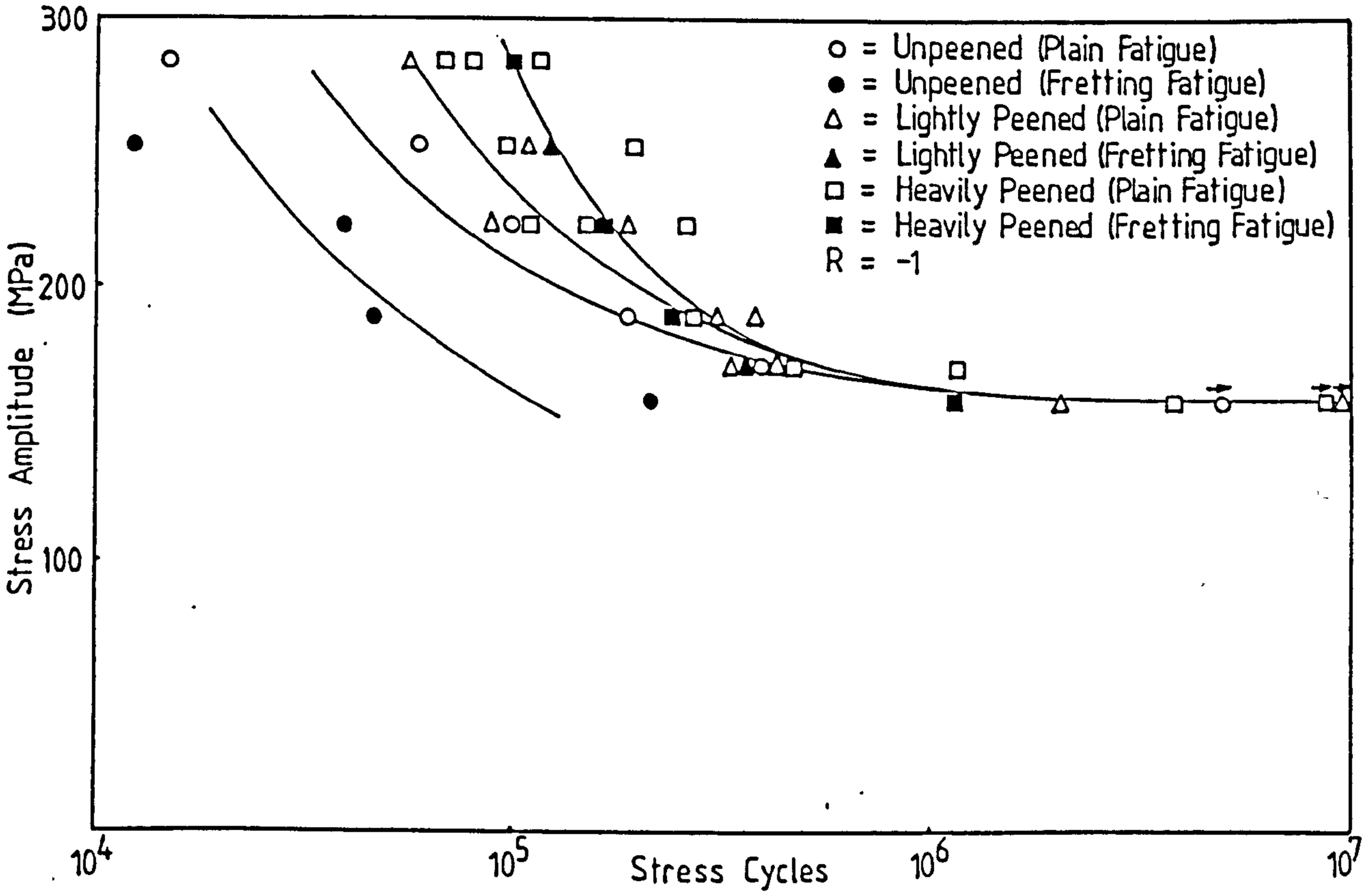

Fig. 40) S-N curves showing the plain and fretting-fatigue properties of alloy 7010 in rotating-bending.

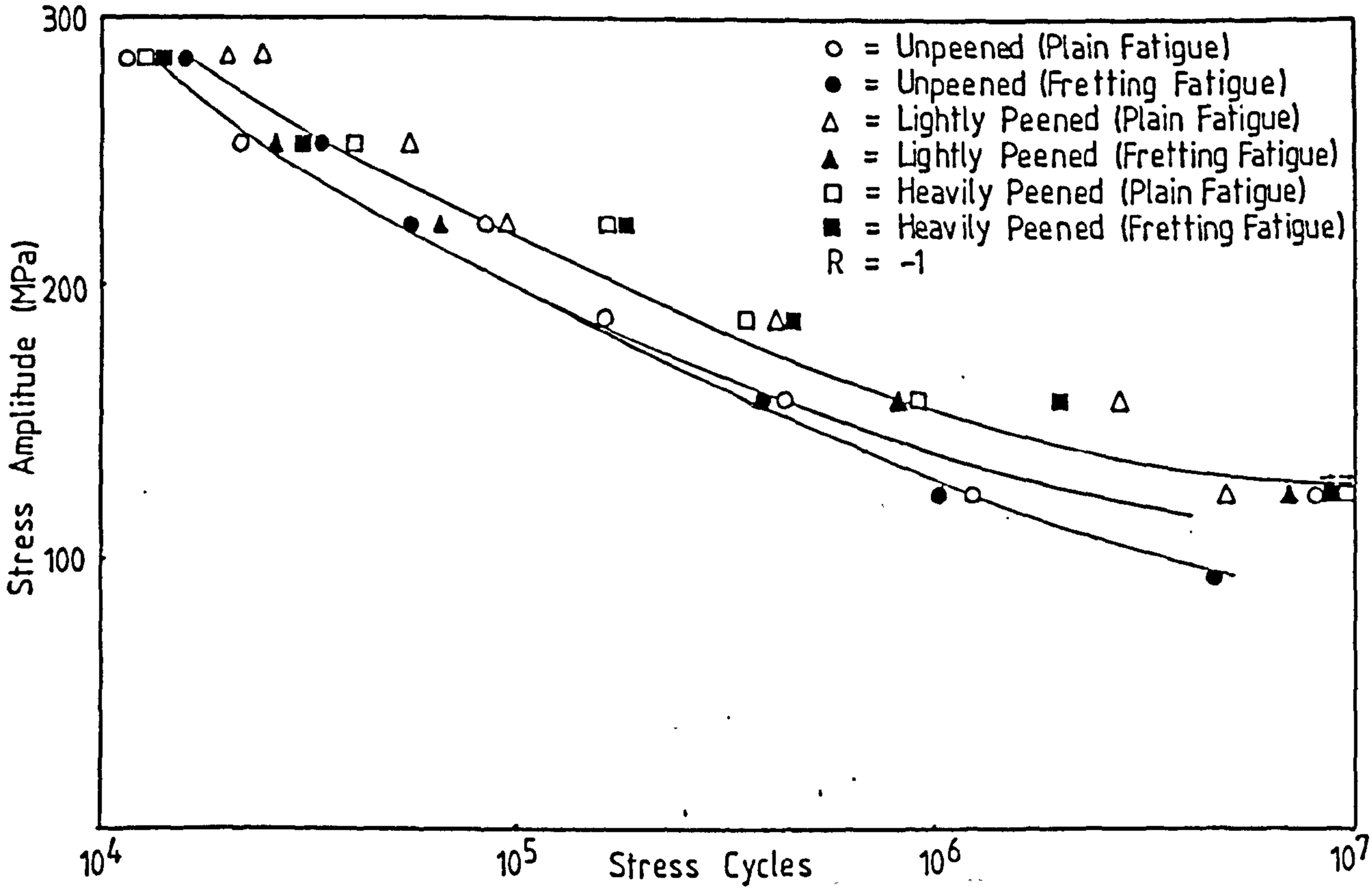

Fig. 41) S-N curves showing the plain and fretting-fatigue properties of alloy 8090 in rotating-bending.

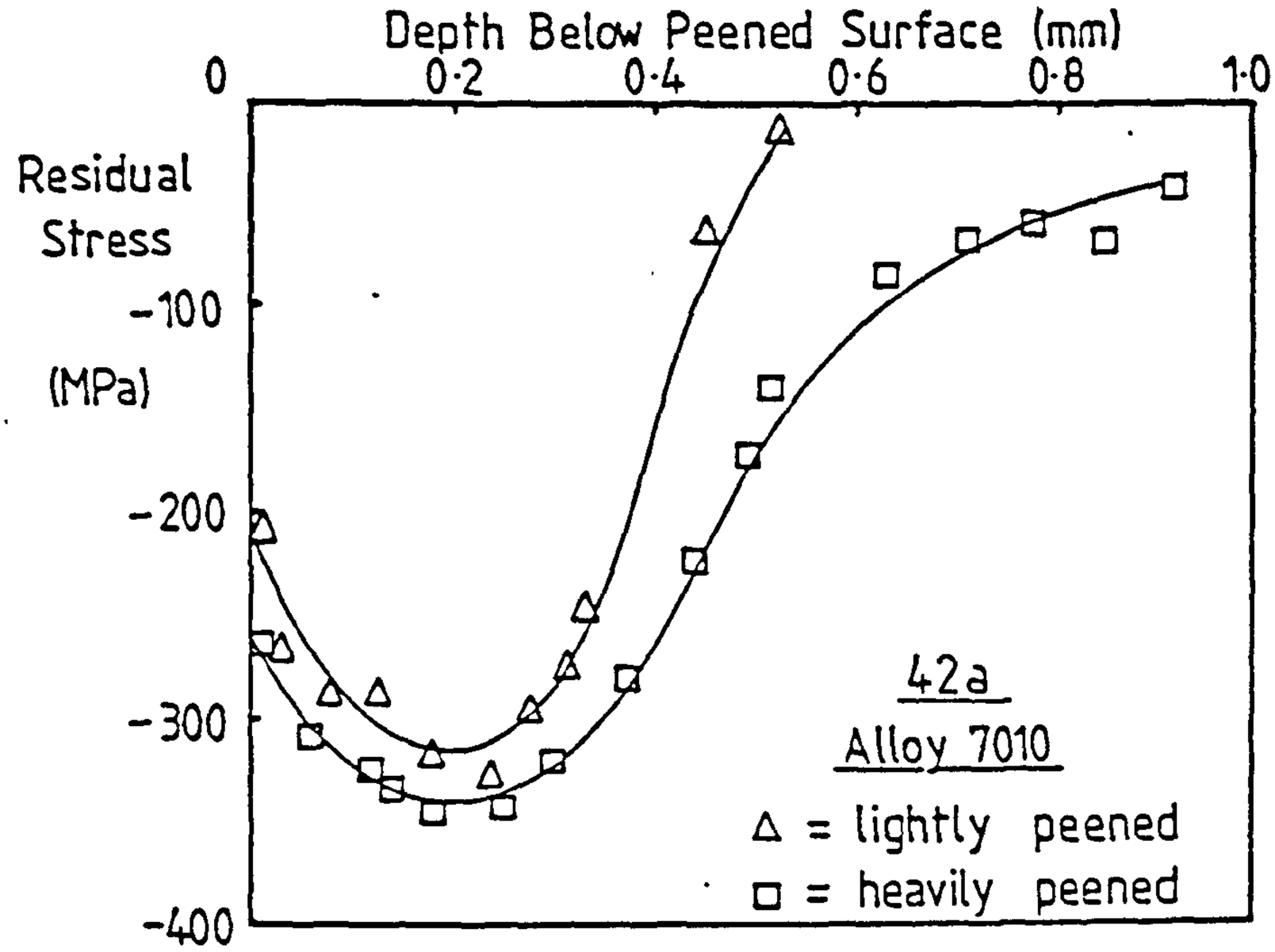

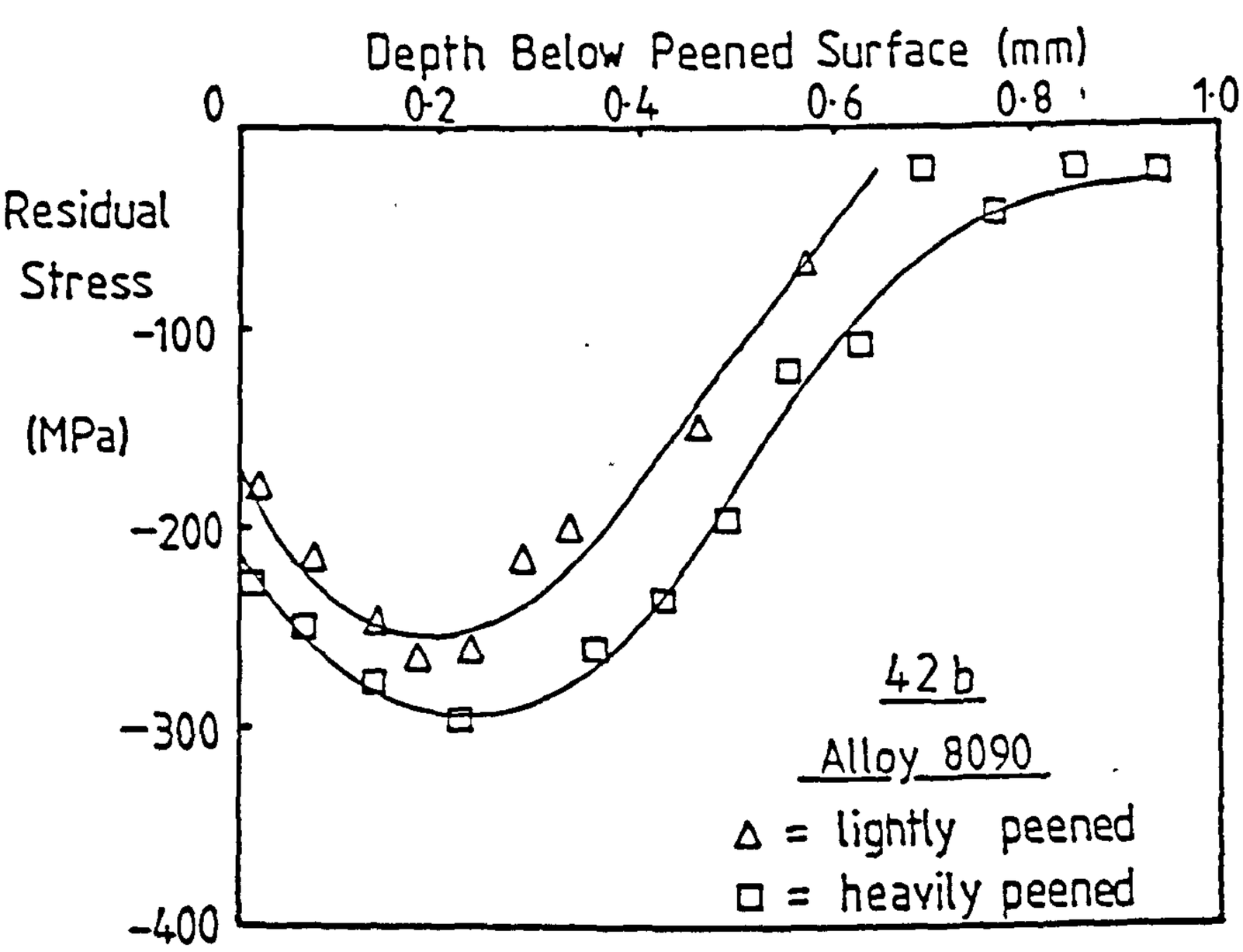

Fig. 42) Distribution of the residual stresses below the surface of the lightly and heavily peened 7010 and 8090 alloys.

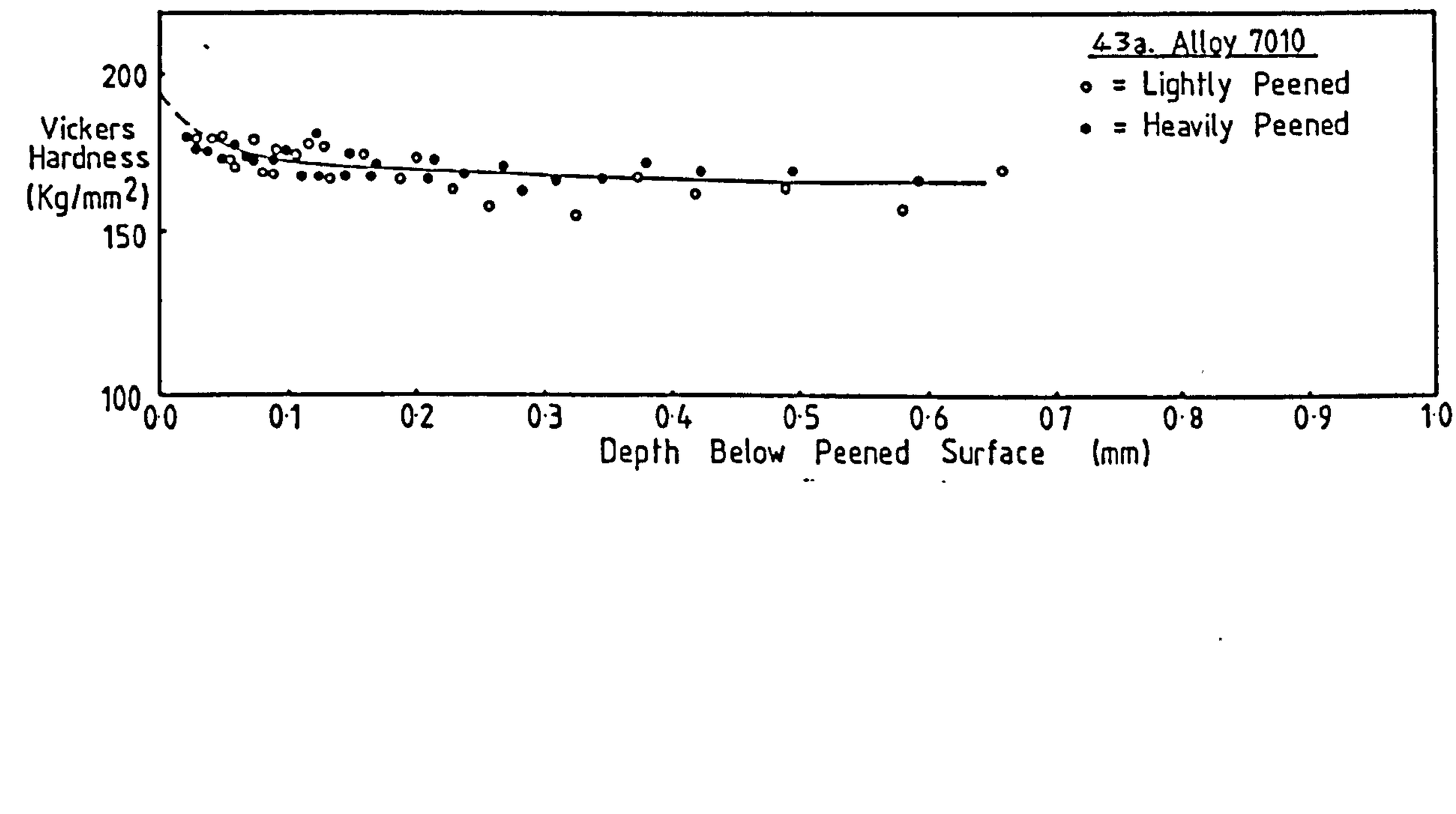

fig. 43) Plots showing the Vickers microhardness of the lightly and heavily peened 7010 and 8090 alloys as a function of the depth into the surface.

Fig. 44) The effect of shot peening on the static yield and bend strengths of the 7010 and 8090 alloys.

Alloy 7010	Yield strength (MPa)	Maximum bending strength (MPa)
Unpeened	540	1970
Lightly peened	730	2040
Heavily peened	750	2010

Alloy 8090	Yield strength (MPa)	Maximum bending strength (MPa)
Unpeened	520	1210
Lightly peened	690	1250
Heavily peened	690	1250

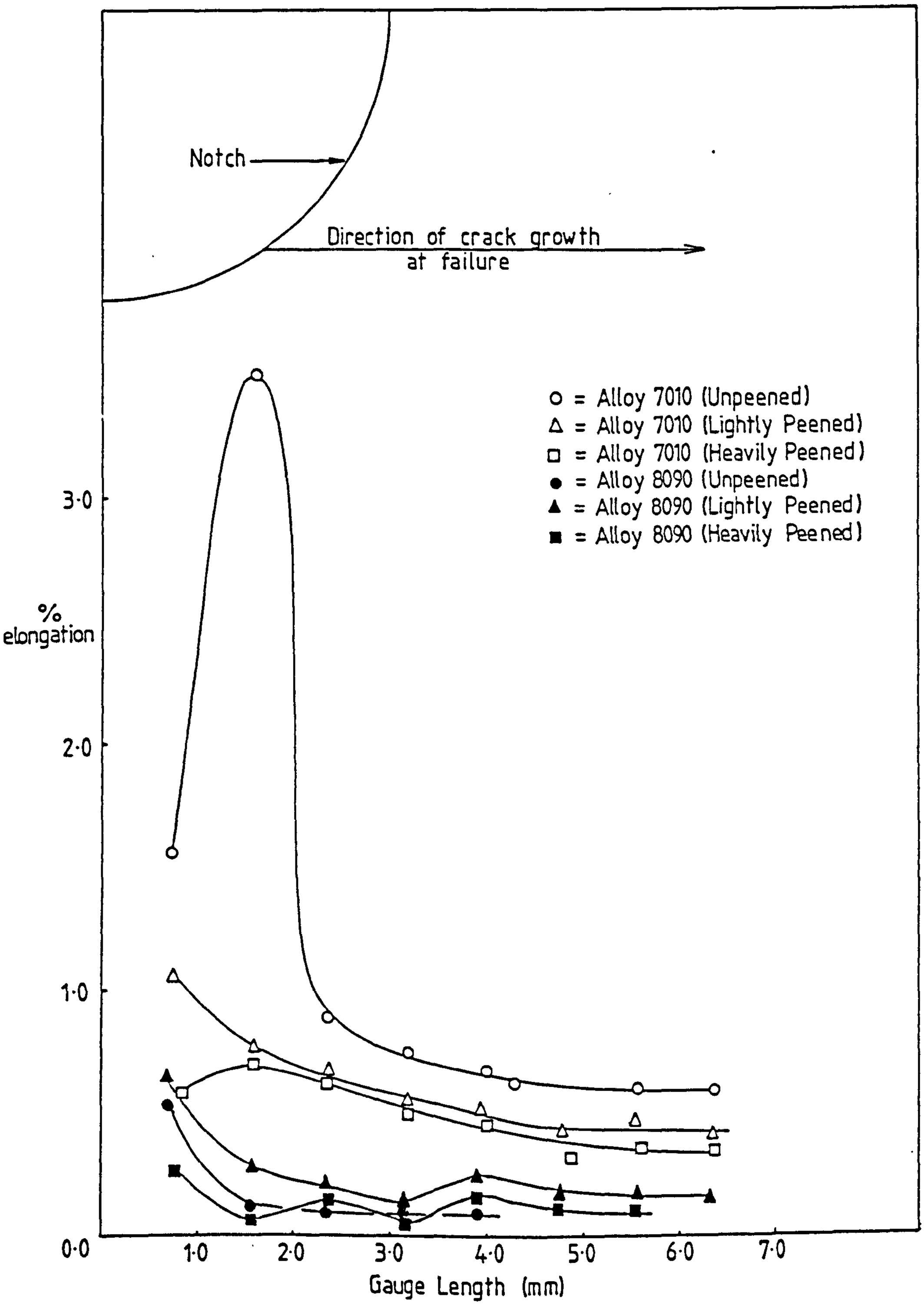

Fig. 45) The effect of light and heavy peening on the elongation of material near the base of the notch in the 7010 and 8090 alloys.

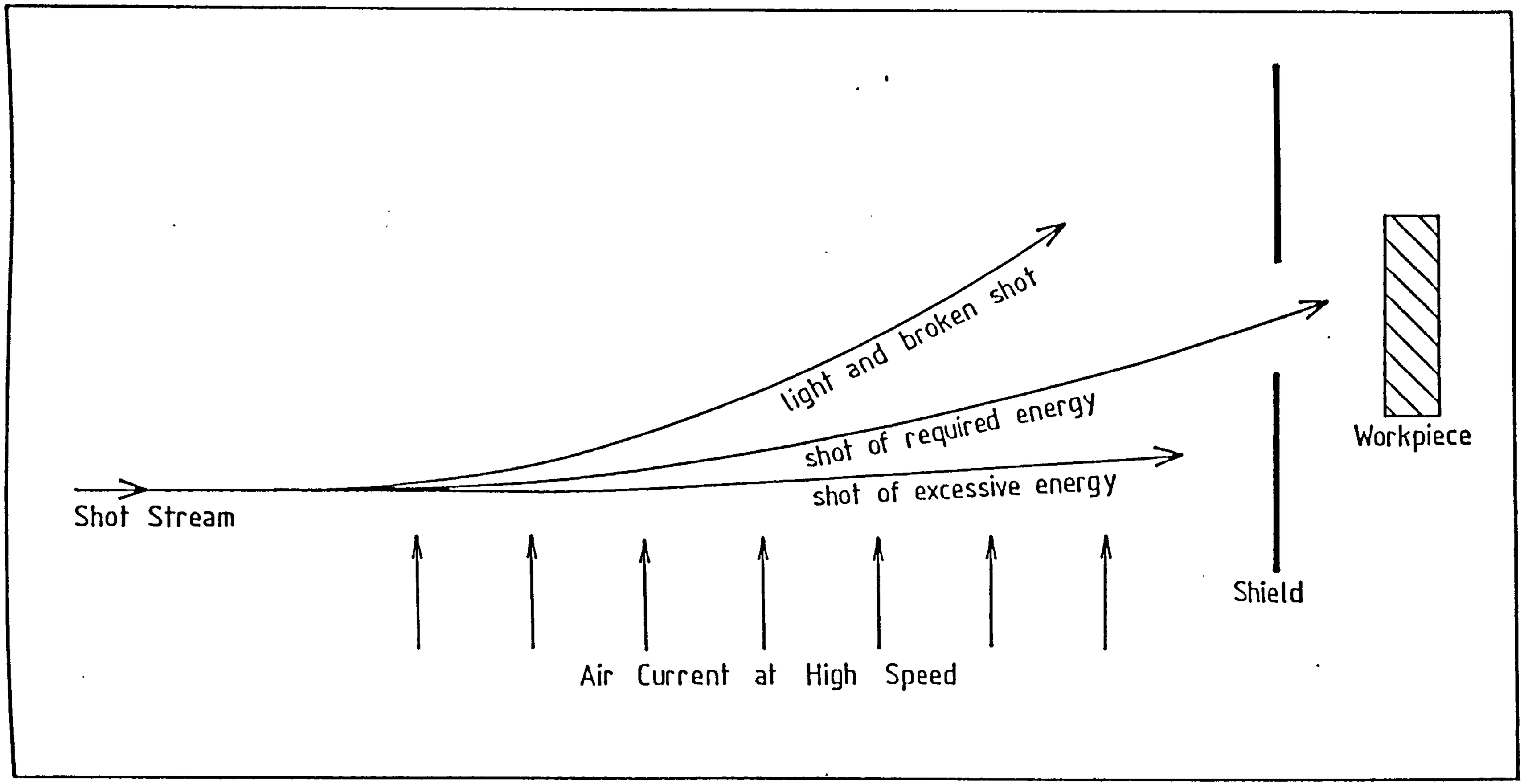

Fig. 46) Schematic diagram showing a proposed modification to the shot peening system.

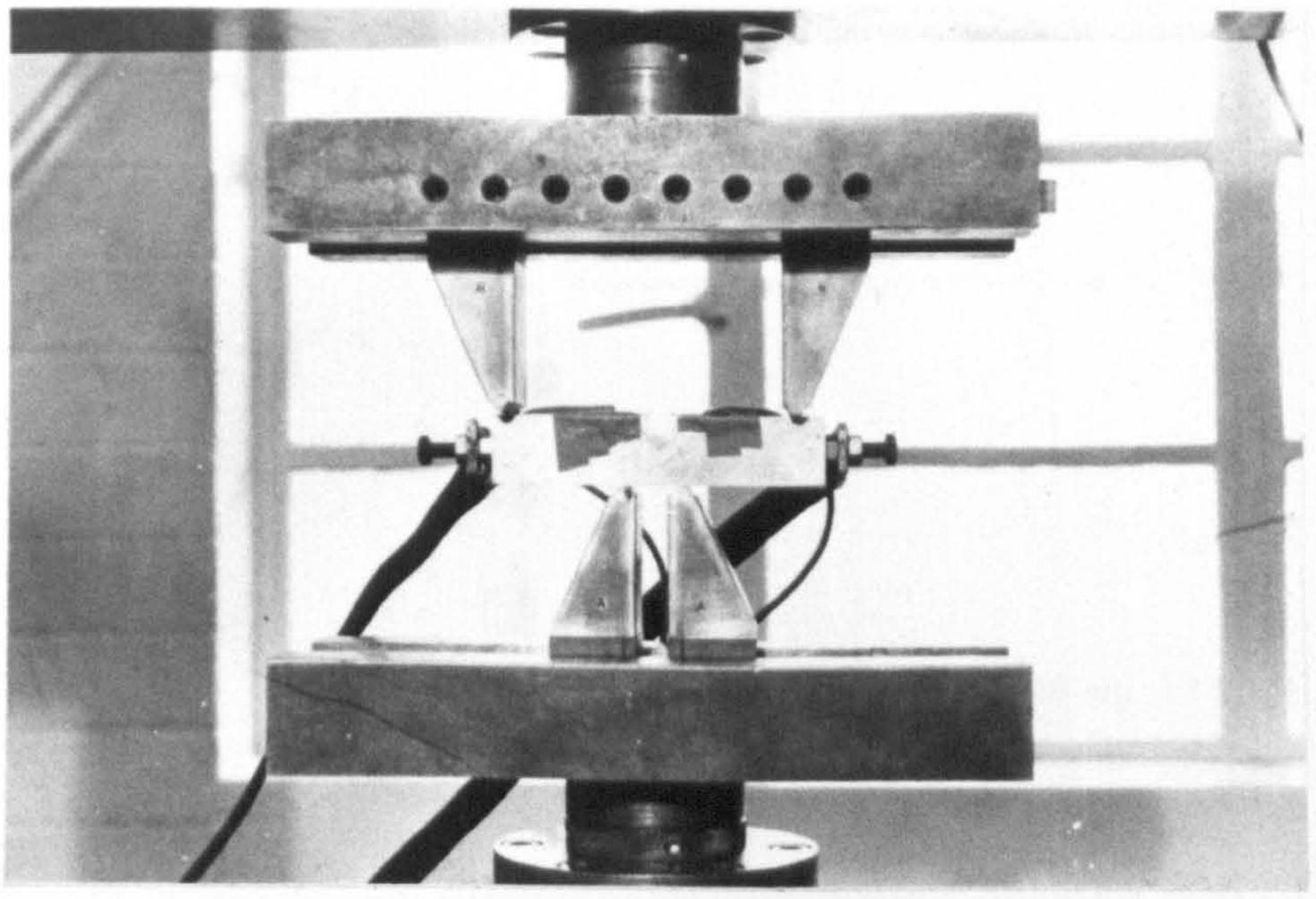

1a) The four-point loading arrangement used for reversed-bending fatigue testing.

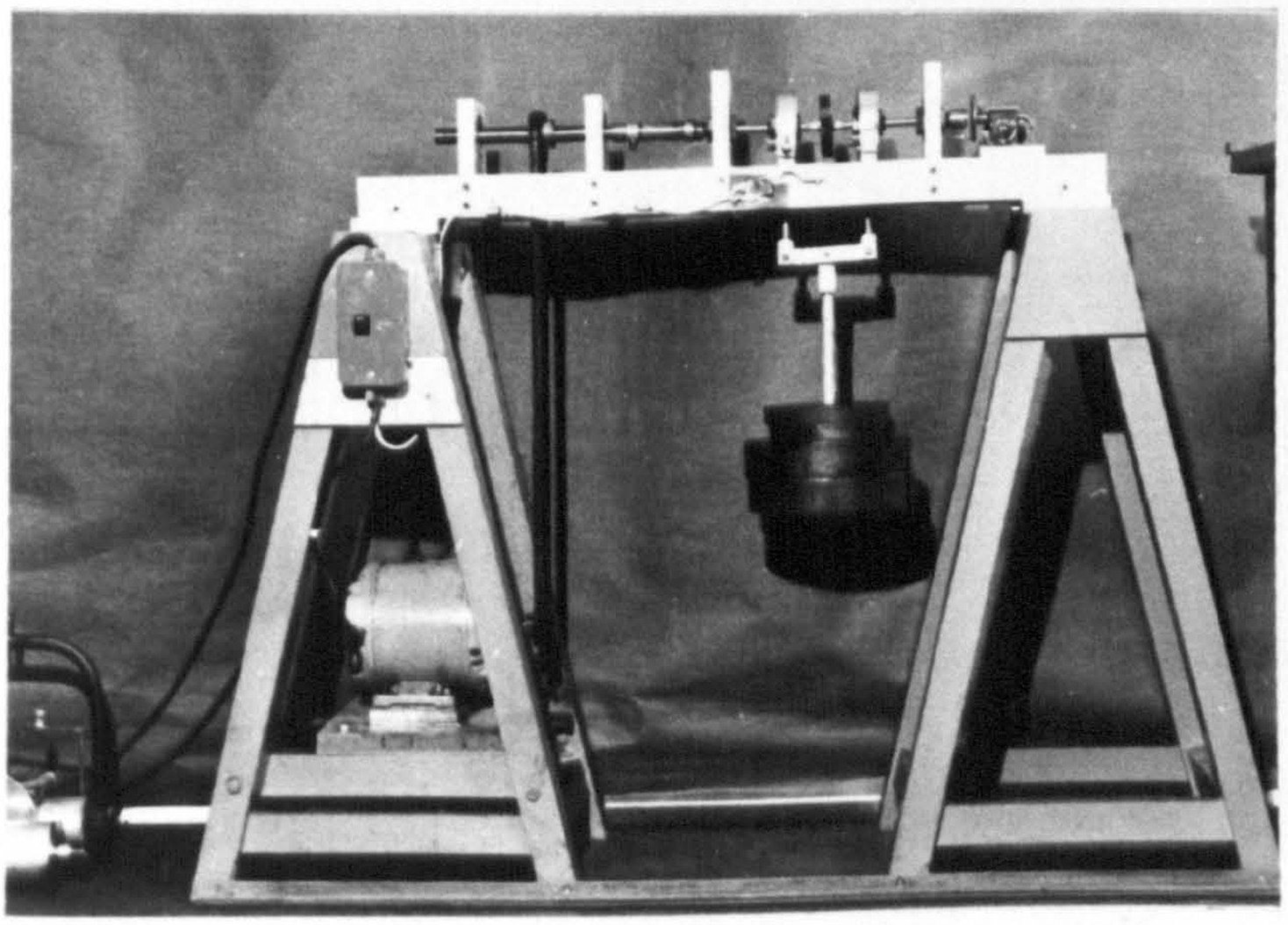

1b) The rotating-bending fatigue machine.

PLATE 1. The reversed-bending and rotating-bending fatigue apparatus.

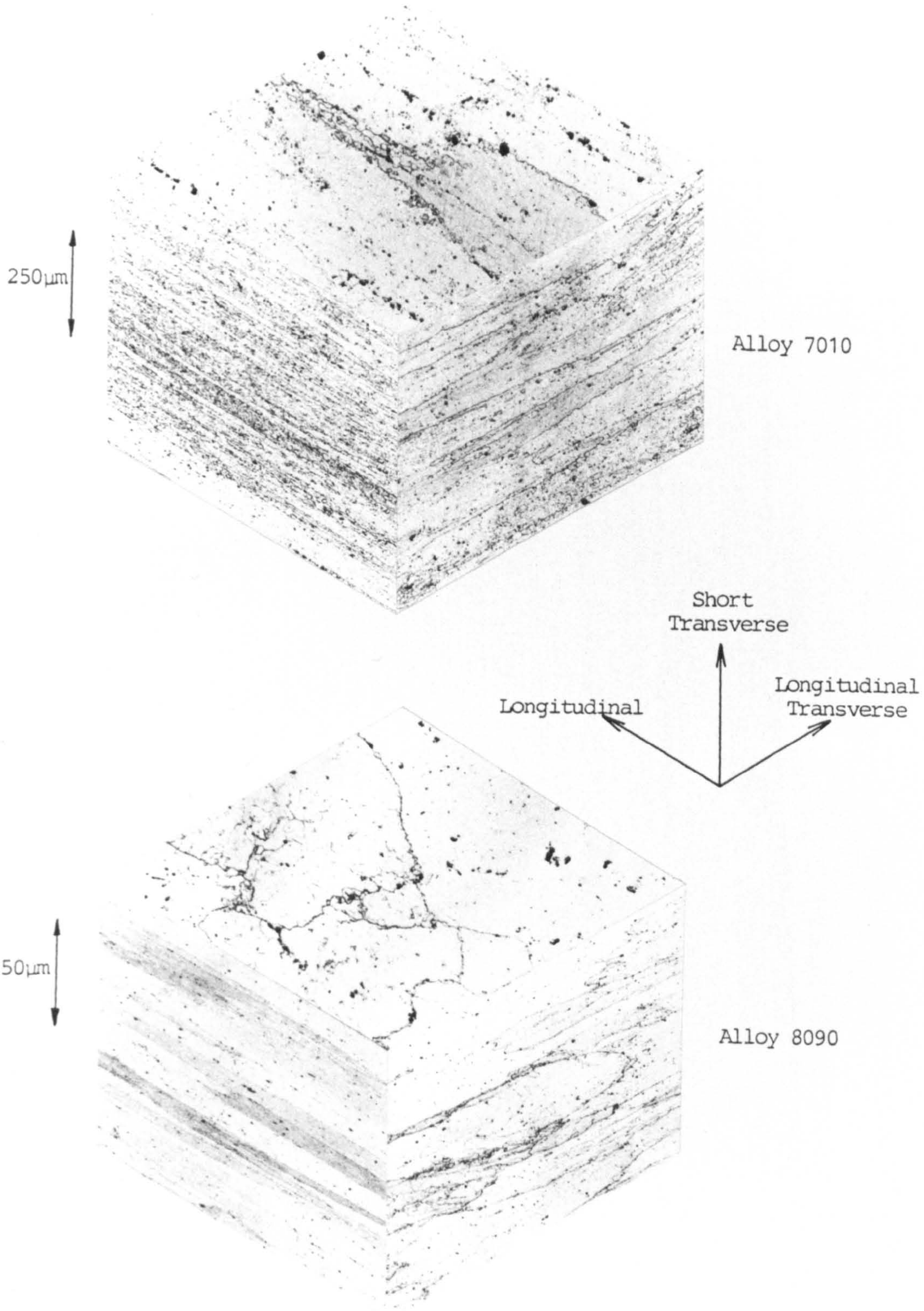

PLATE 2. Microstructural sections of alloys 7010 and 8090 plate.

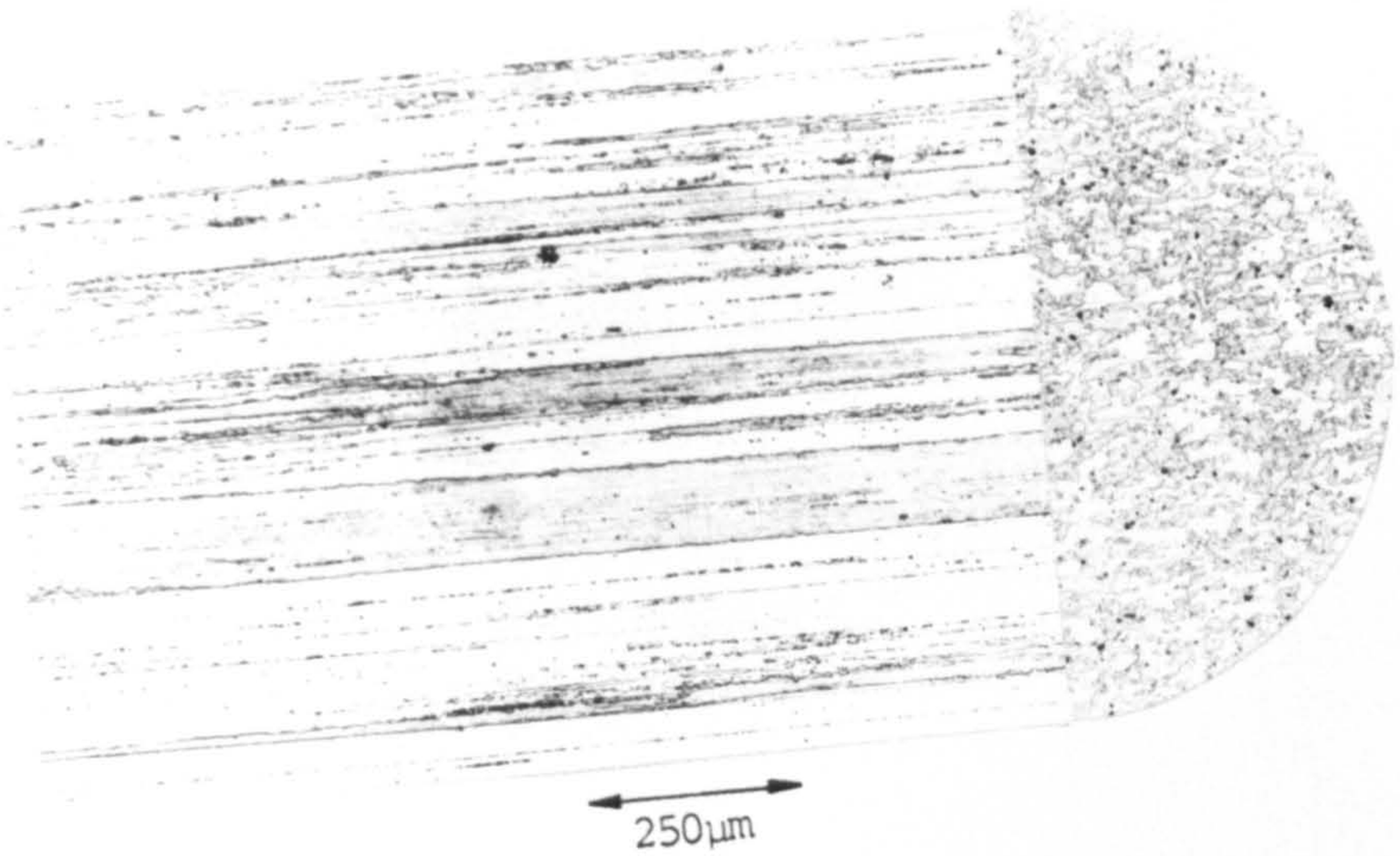

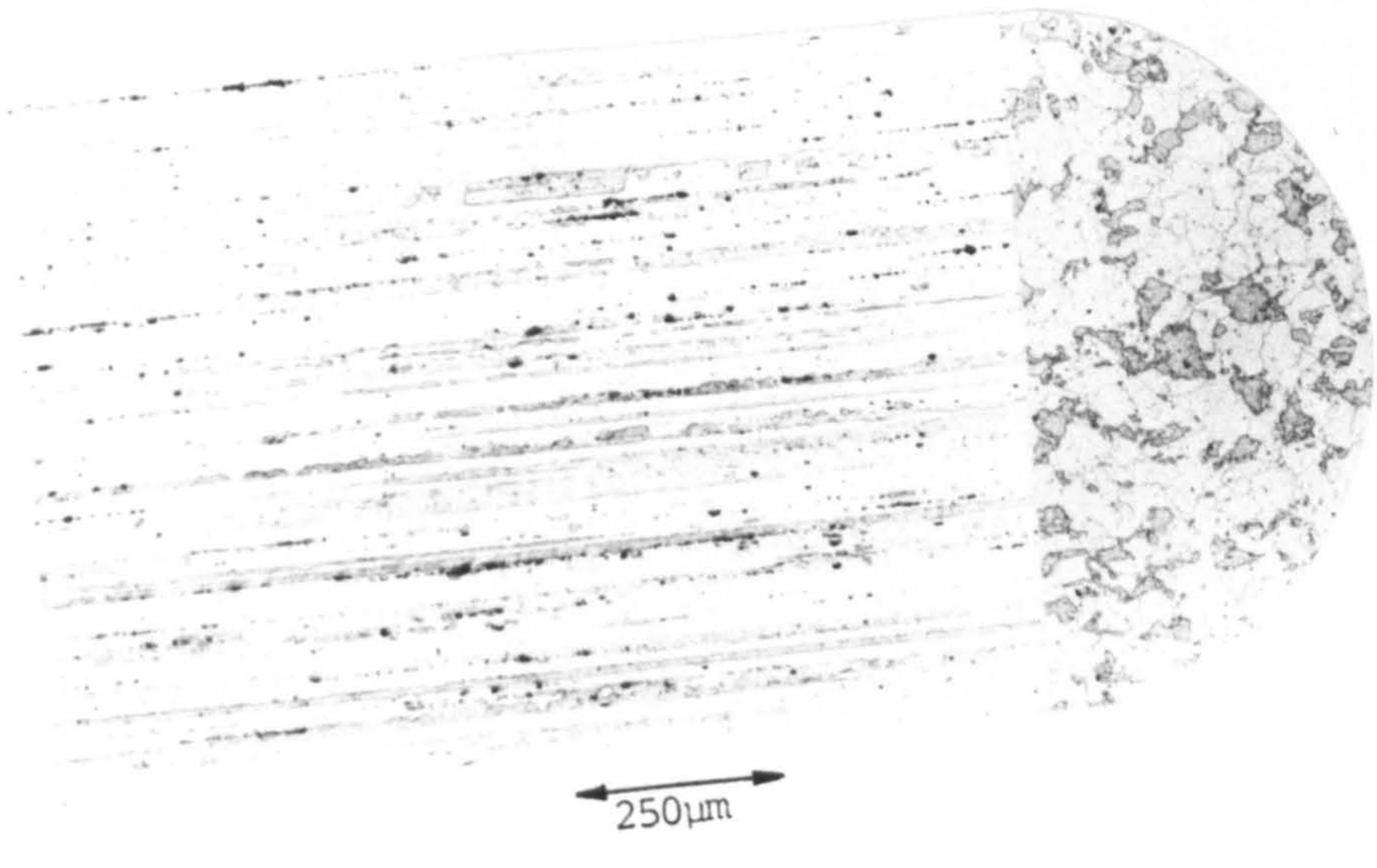

PLATE 3. Longitudinal and end sections of the extruded 7010 and 8090 alloys.

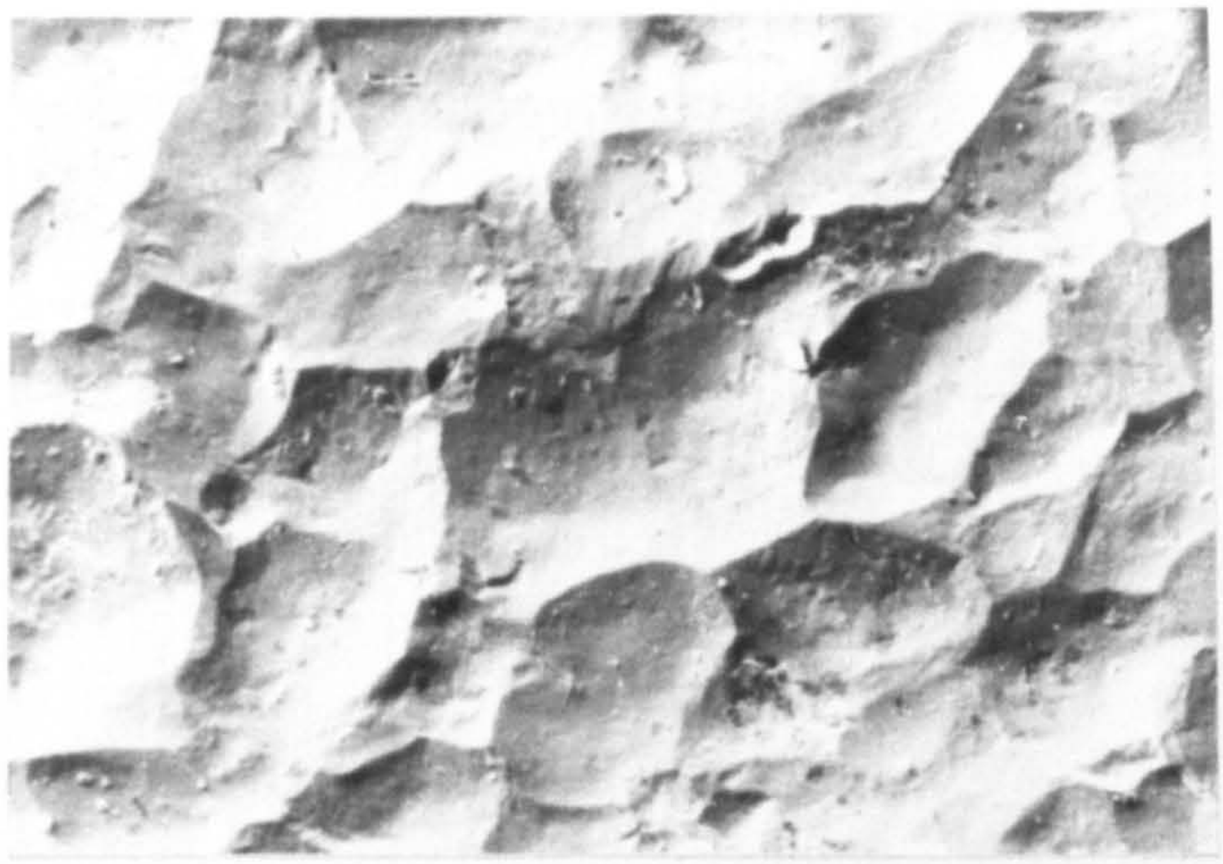

4a) Lightly peened surface (12-16A).

250µm

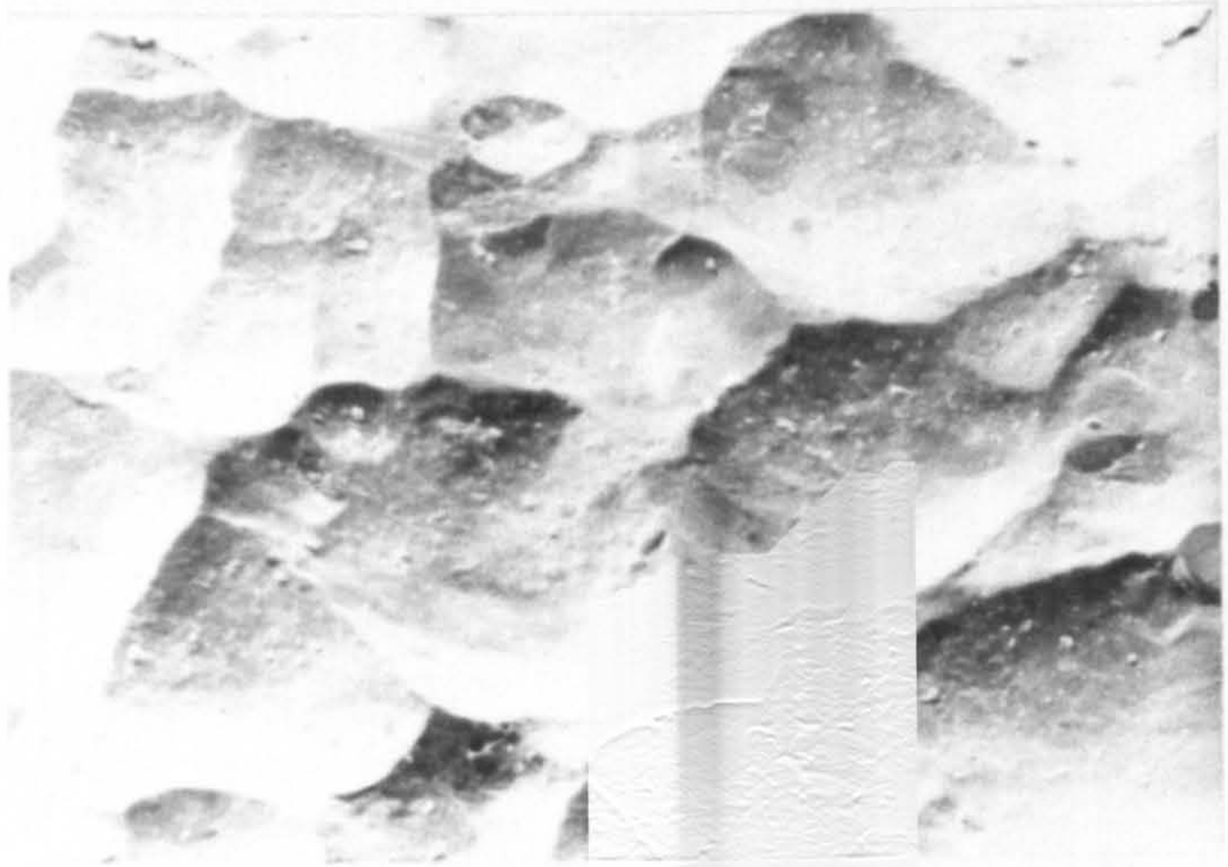

4b) Heavily peened surface (8-10C).

250µm

PLATE 4. The roughened surfaces resulting from shot-peening to light and heavy intensities.

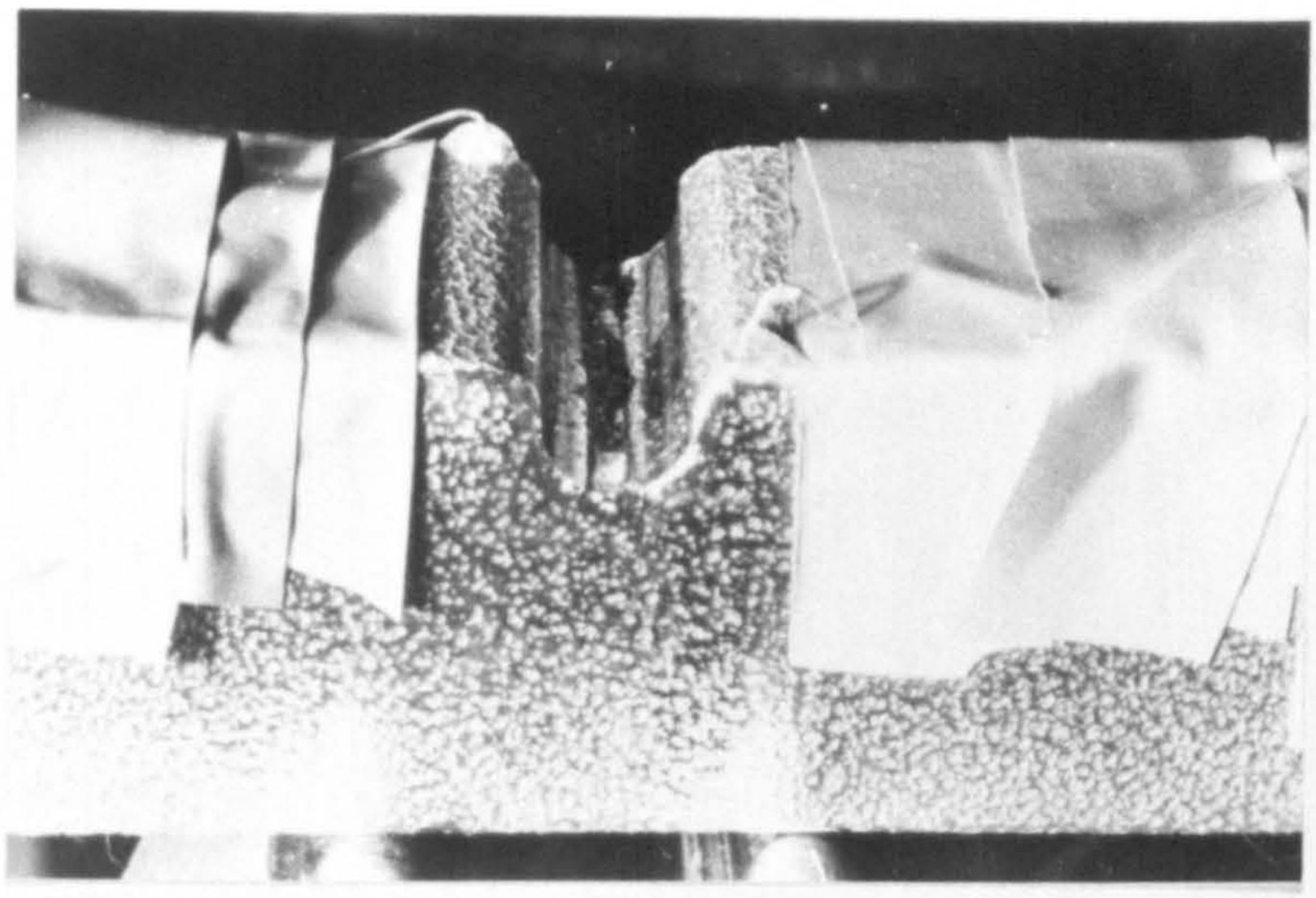

PLATE 5. Debris in the notch of a shot-peened 8090 alloy reversed-bending specimen during fatigue testing.

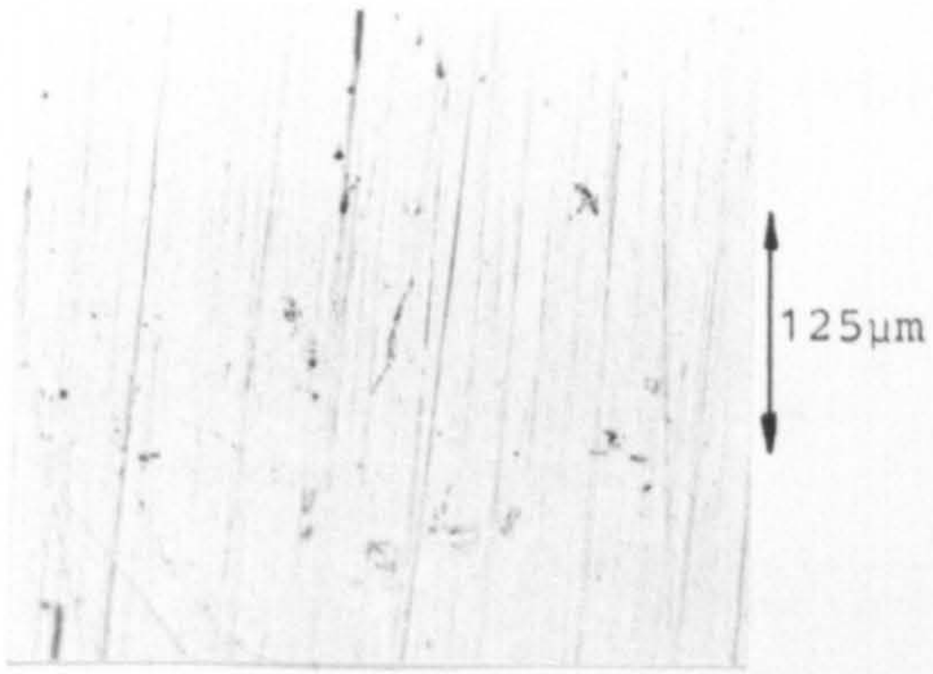

6a) Alloy 7010
(15,000 cycles)

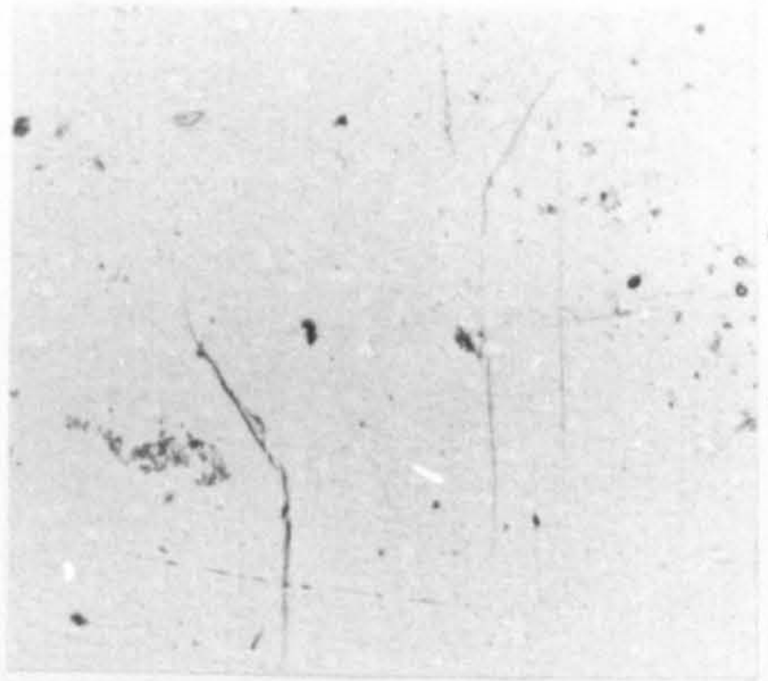

6c) Alloy 8090
(13,000 cycles)

Stress Direction

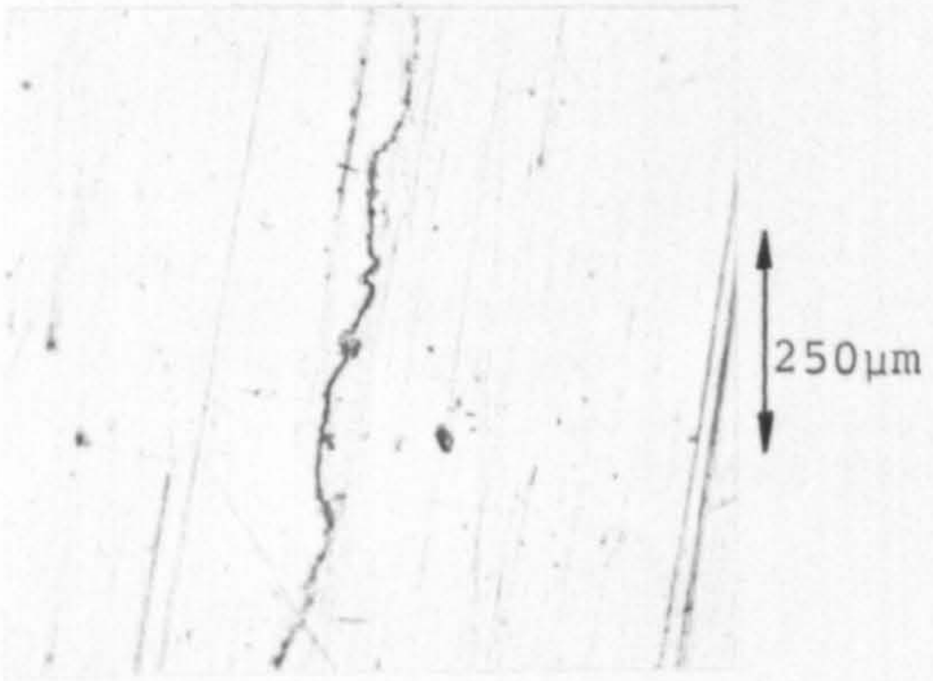

6b) Alloy 7010
(23,000 cycles)

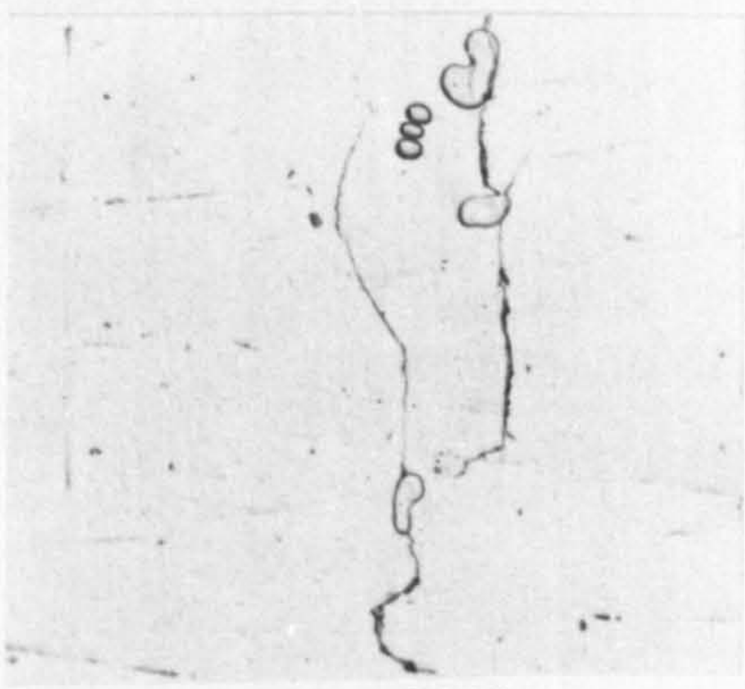

6d) Alloy 8090
(20,000 cycles)

Stress Direction

PLATE 6. Fatigue crack growth along the base of the notch in the unpeened 7010 and 8090 alloy reversed bending specimens.

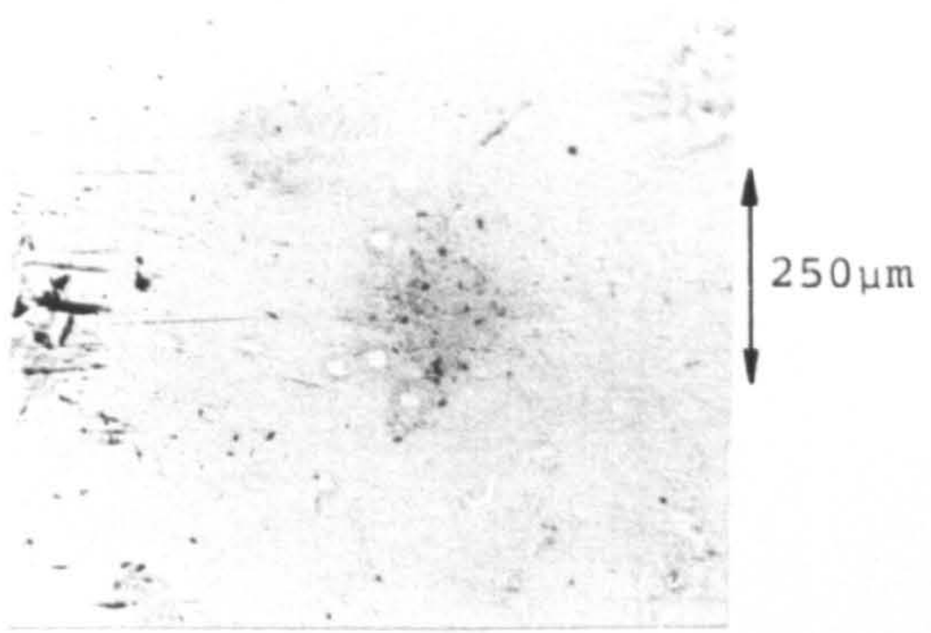

7a) Lightly peened
(0 cycles)

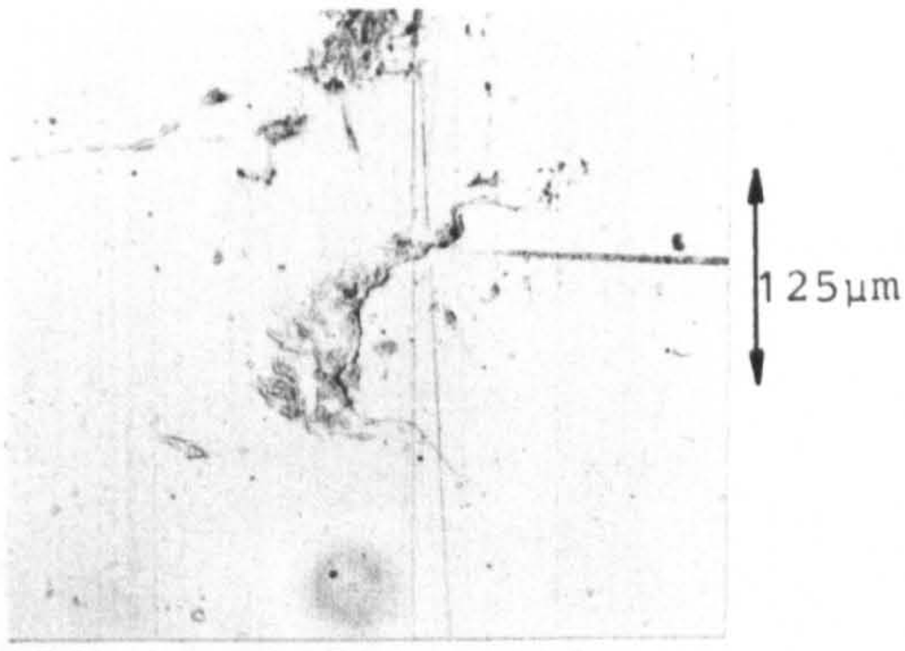

7d) Heavily peened
(0 cycles)

Stress Direction

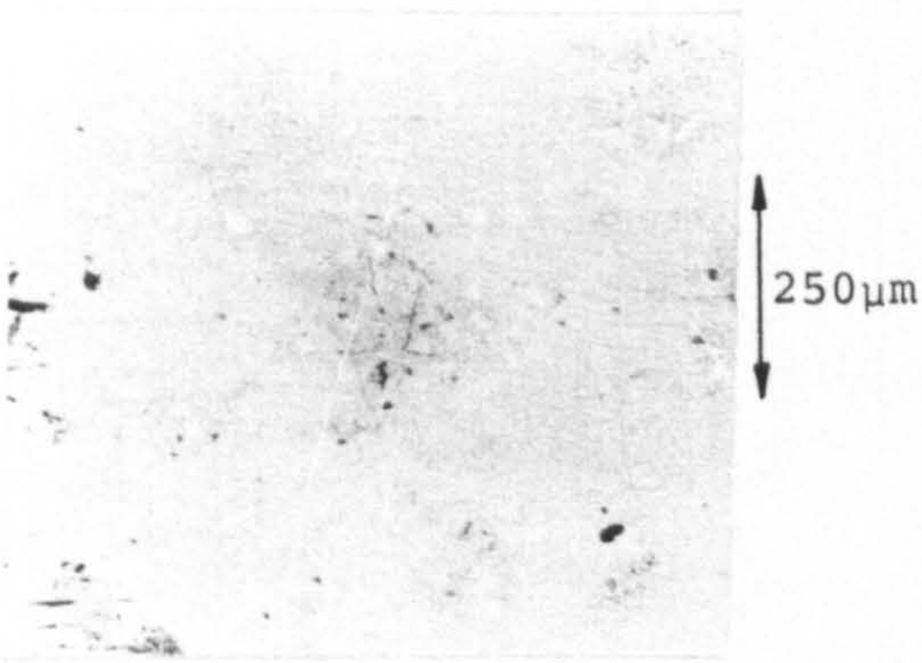

7b) Lightly peened
(20,000 cycles)

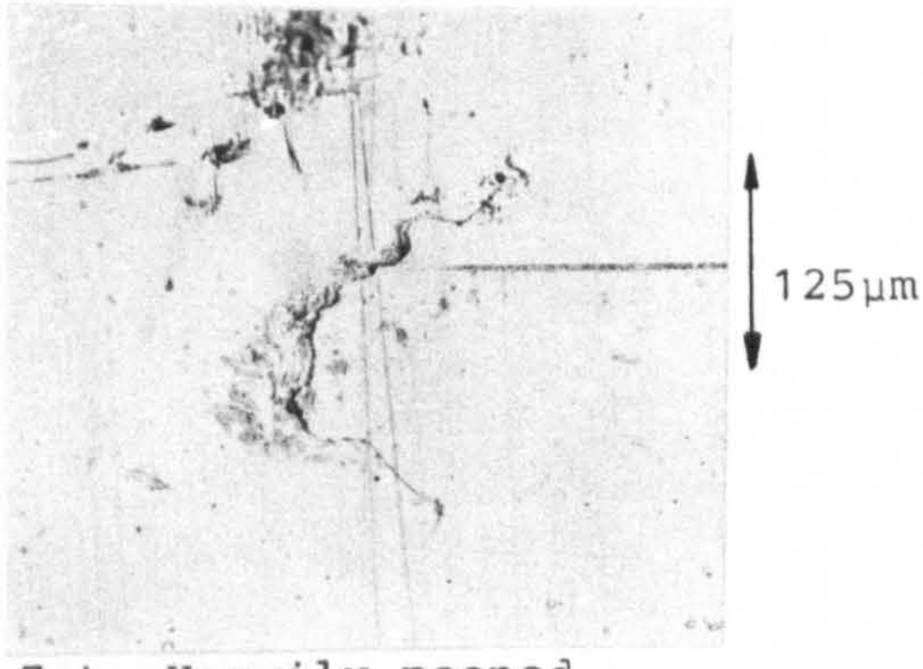

7e) Heavily peened
(2,000 cycles)

Stress Direction

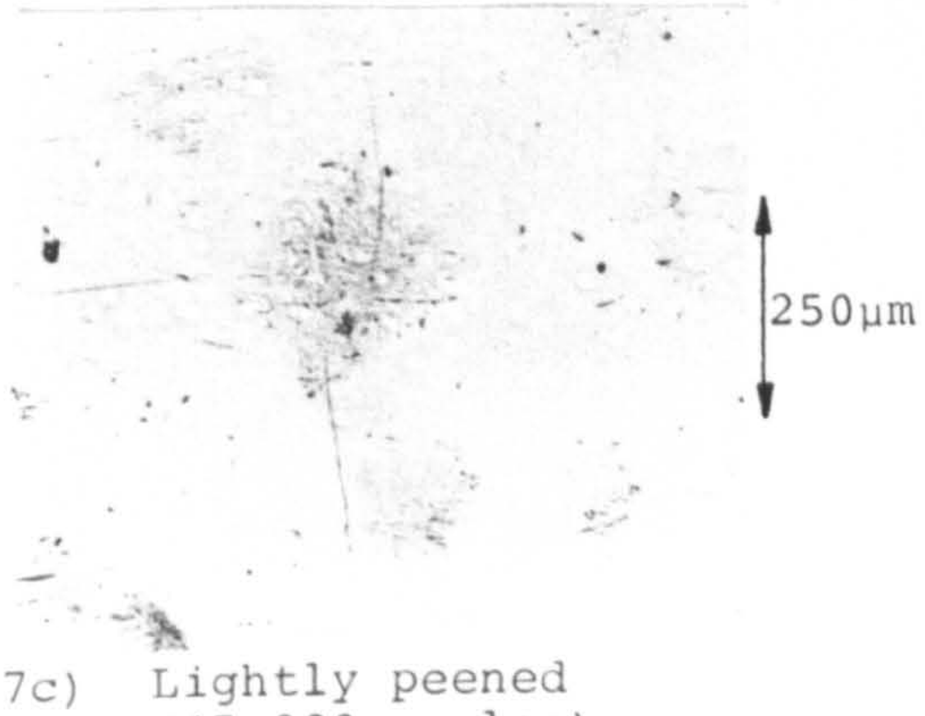

7c) Lightly peened
(45,000 cycles)

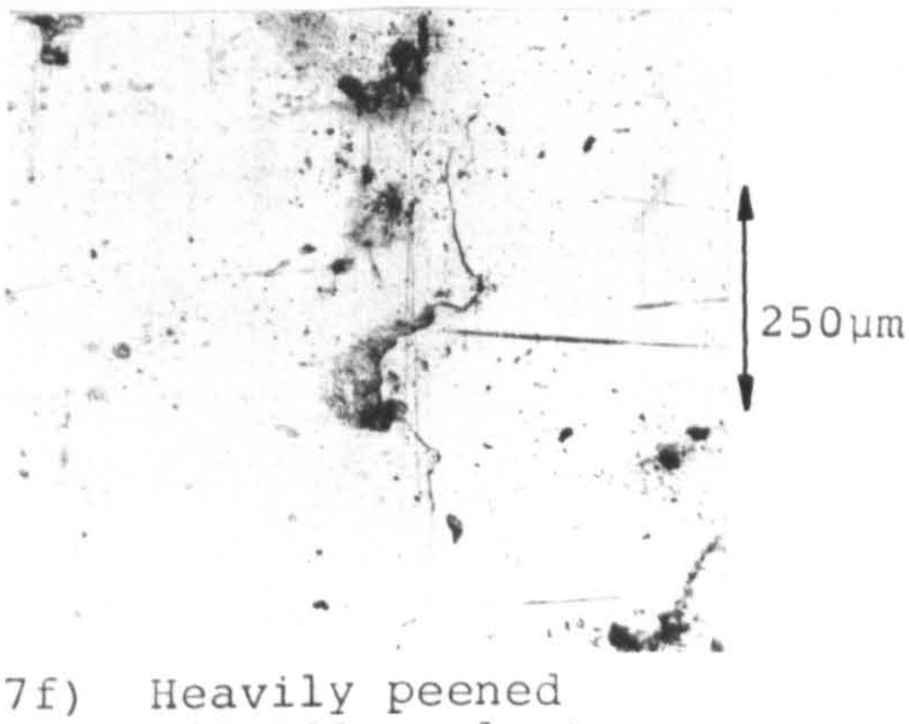

7f) Heavily peened
(16,000 cycles)

Stress Direction

PLATE 7. Fatigue cracks growing from the remnants of dimples in the lightly peened and heavily peened 7010 alloy reversed bending specimens.

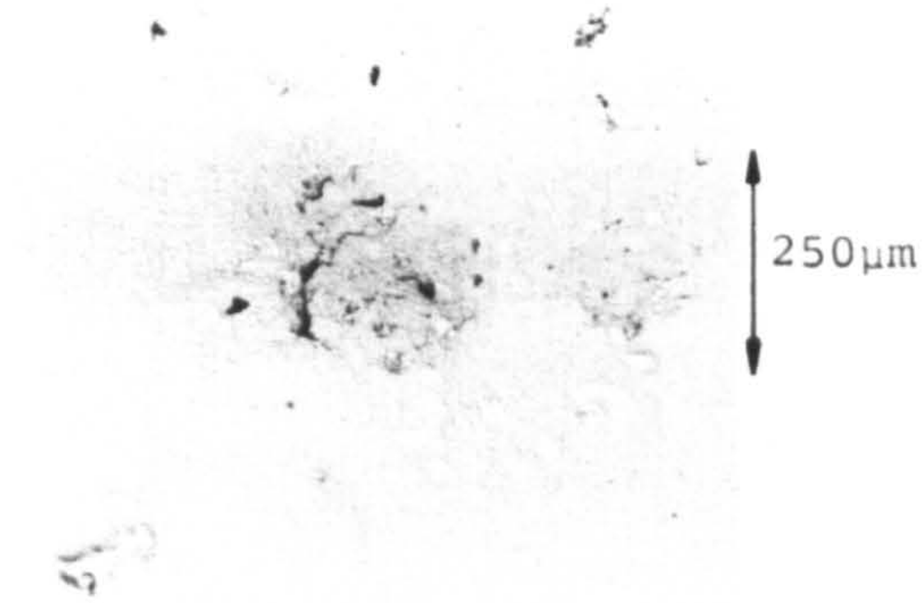

8a) Lightly peened
(0 cycles)

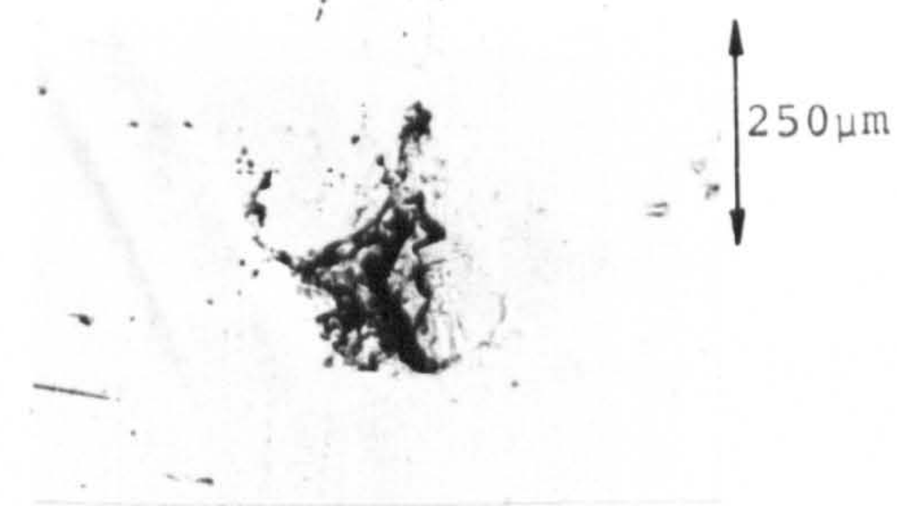

8d) Heavily peened
(0 cycles)

Stress direction

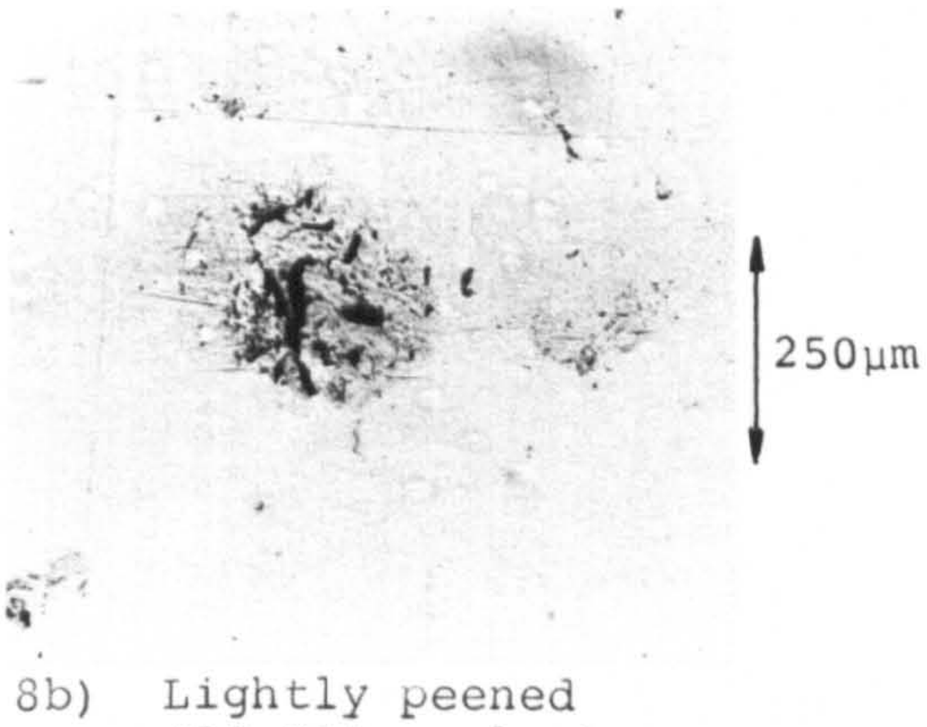

8b) Lightly peened
(20,000 cycles)

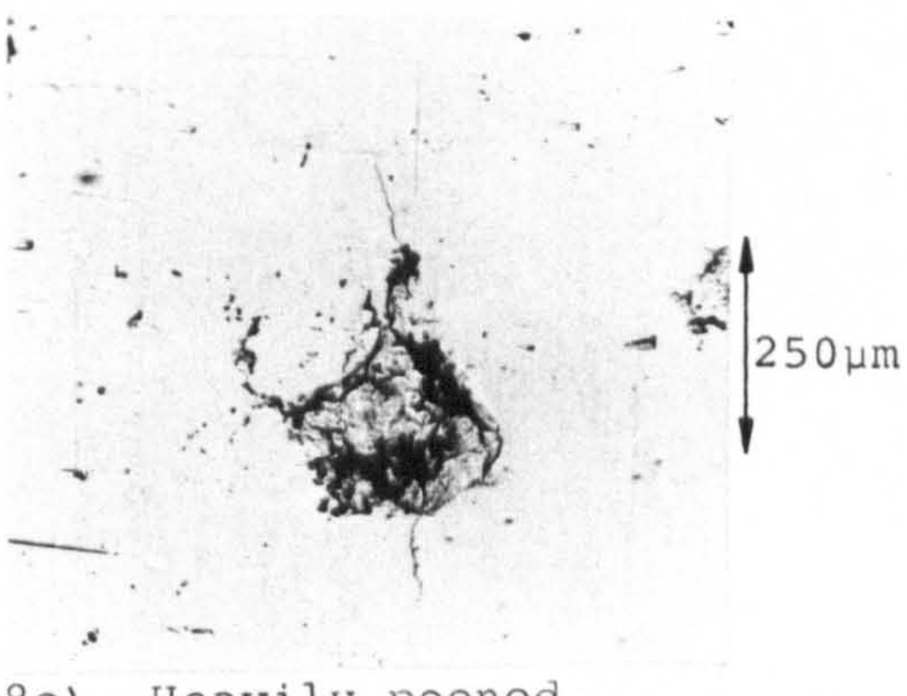

8e) Heavily peened
(6,000 cycles)

Stress Direction

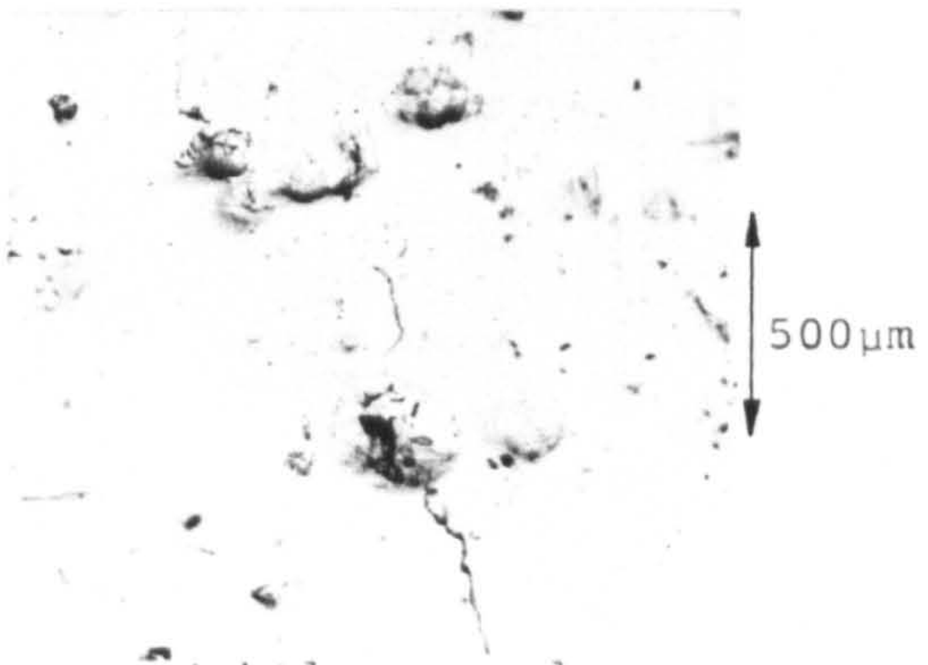

8c) Lightly peened
(25,000 cycles)

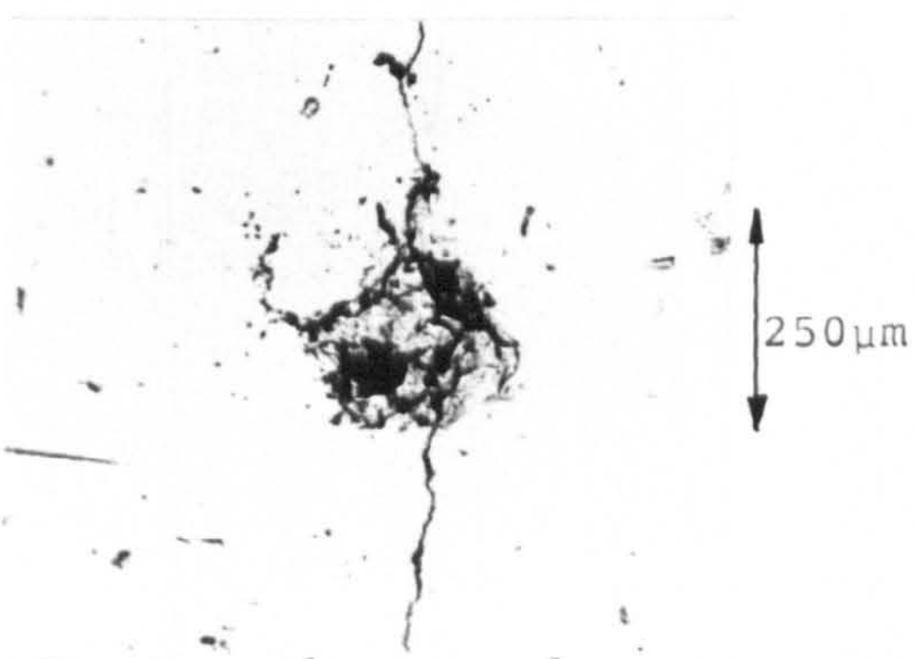

8f) Heavily peened
(13,000 cycles)

Stress Direction

PLATE 8. Fatigue cracks growing from the remnants of dimples in the lightly peened and heavily peened 8090 alloy reversed bending specimens.

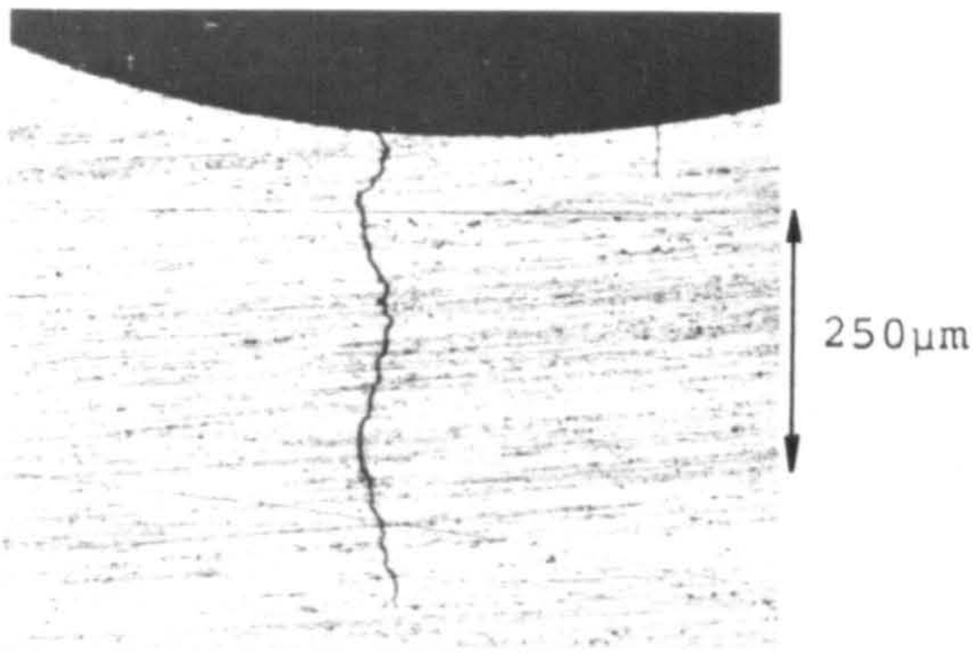

9a) Alloy 7010
(unpeened)

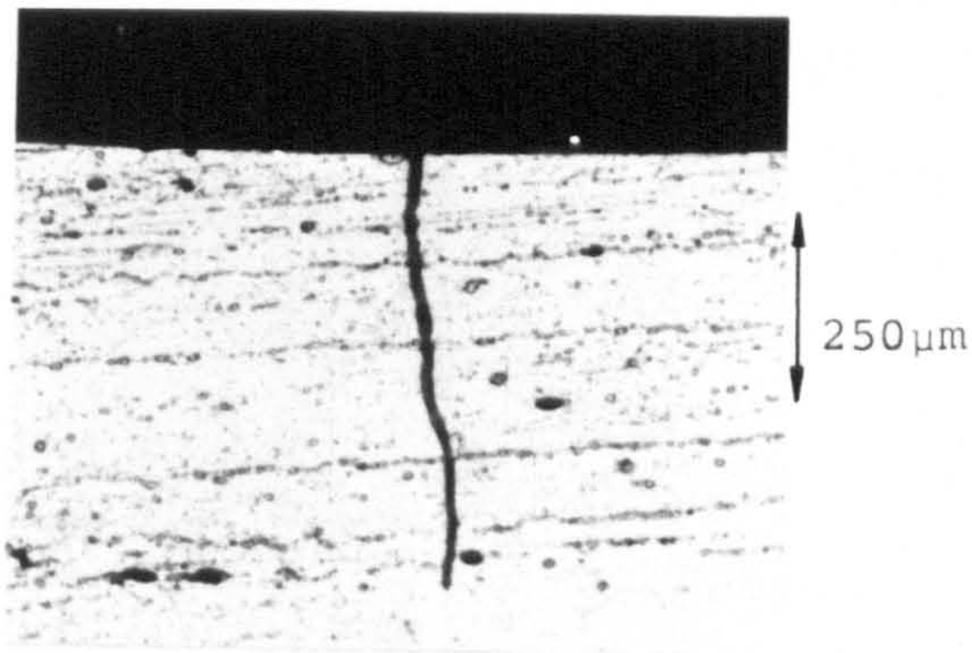

9b) Alloy 7010
(unpeened)

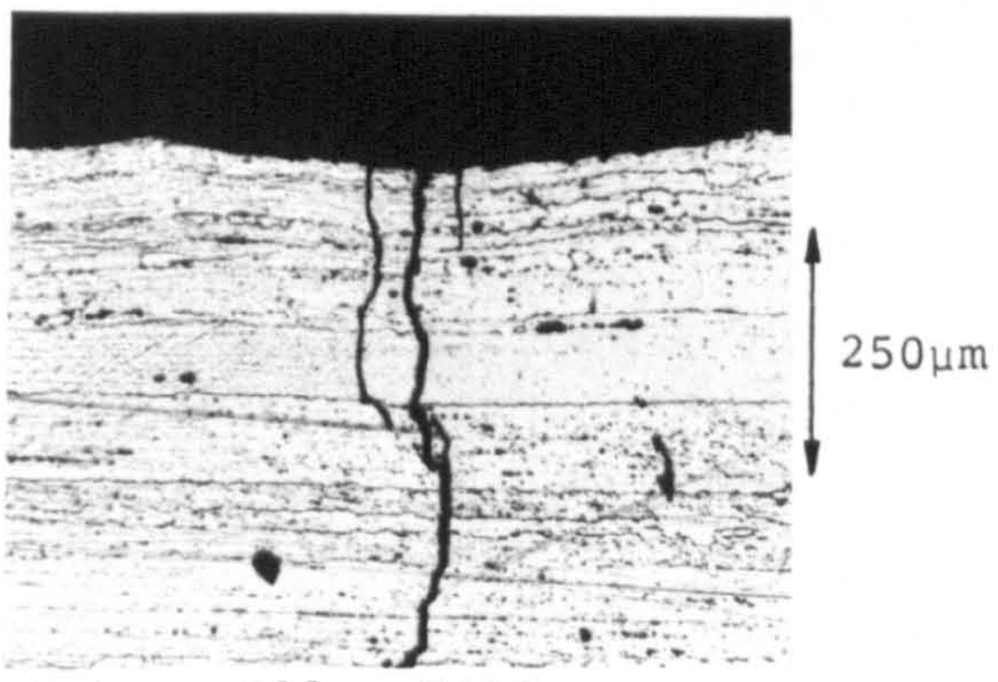

9c) Alloy 7010
(lightly peened)

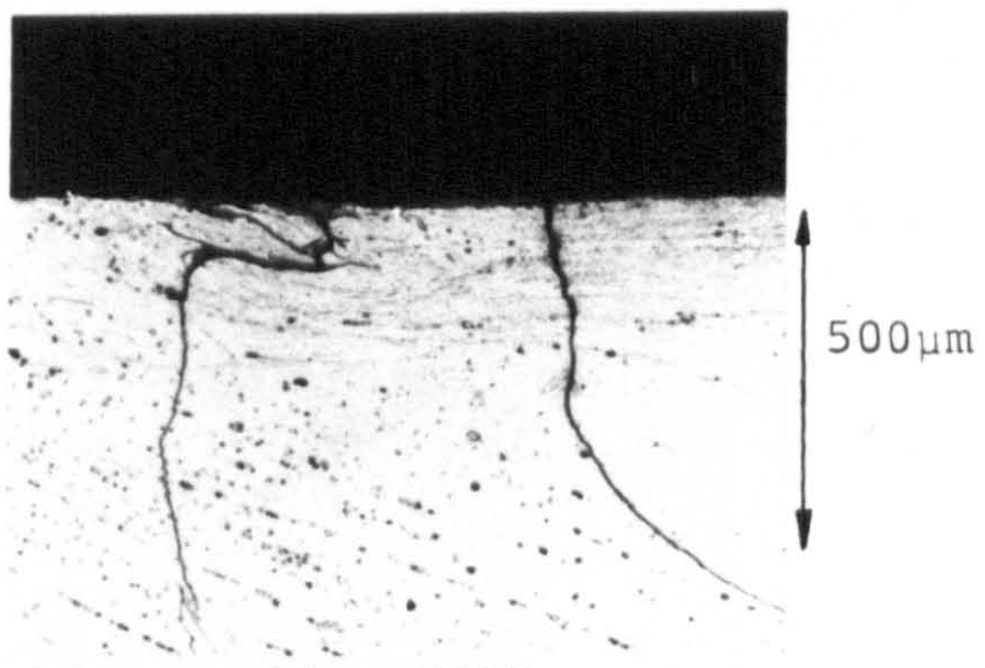

9d) Alloy 7010
(heavily peened)

PLATE 9. Cross-sections through small fatigue cracks in the notch of the unpeened, lightly peened and heavily peened 7010 alloy.

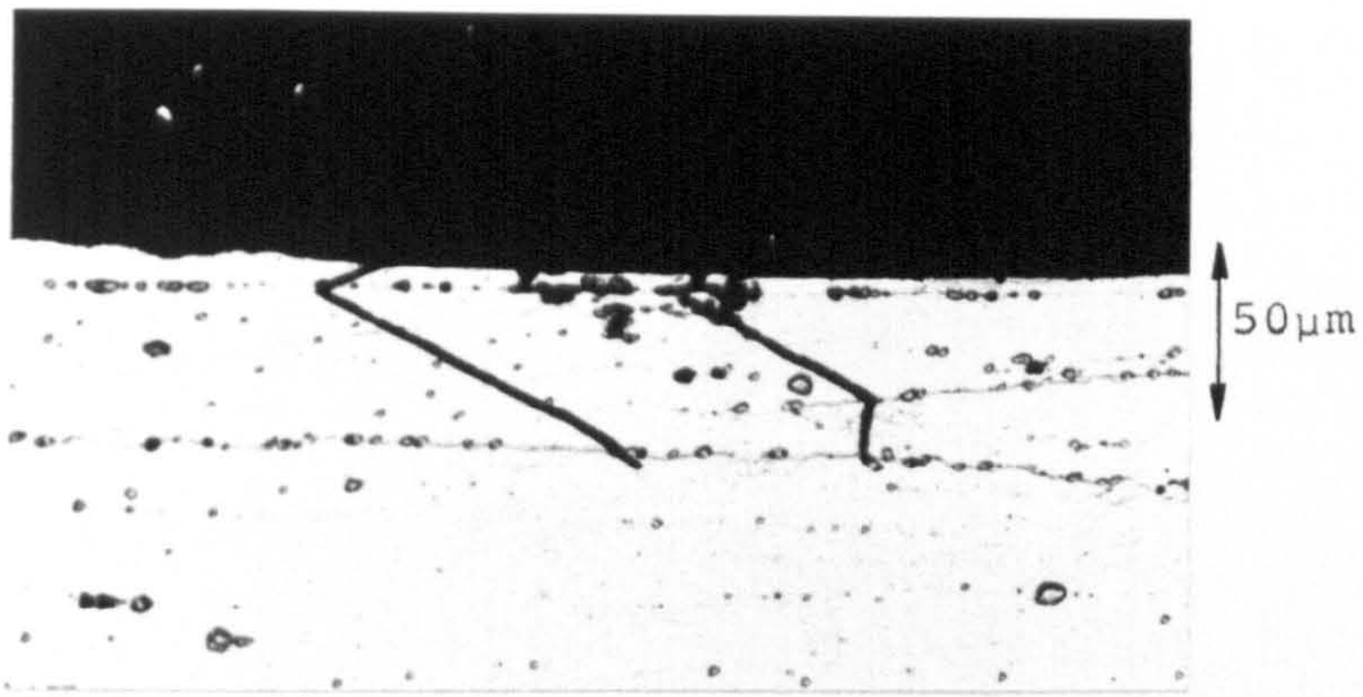

10a) Alloy 8090 (unpeened)

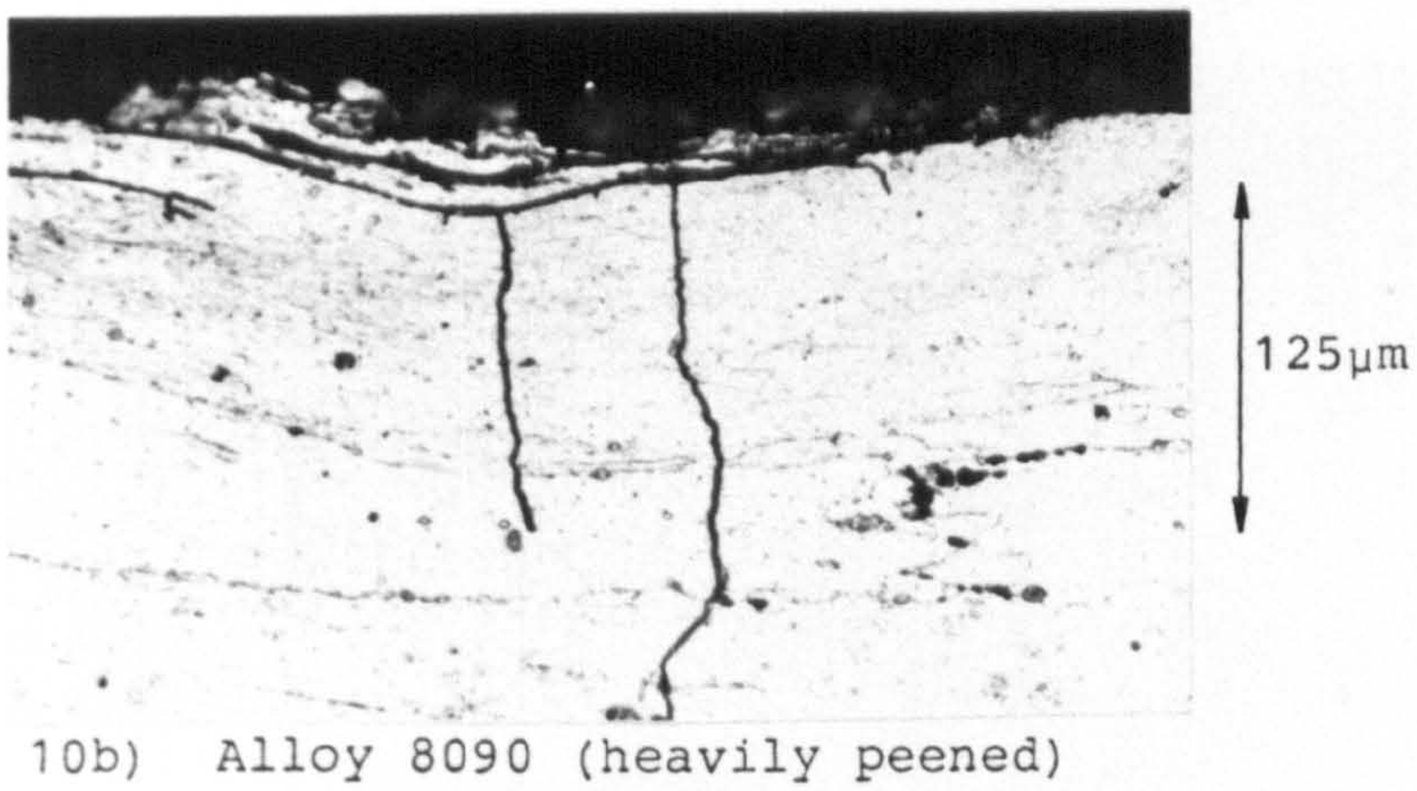

10b) Alloy 8090 (heavily peened)

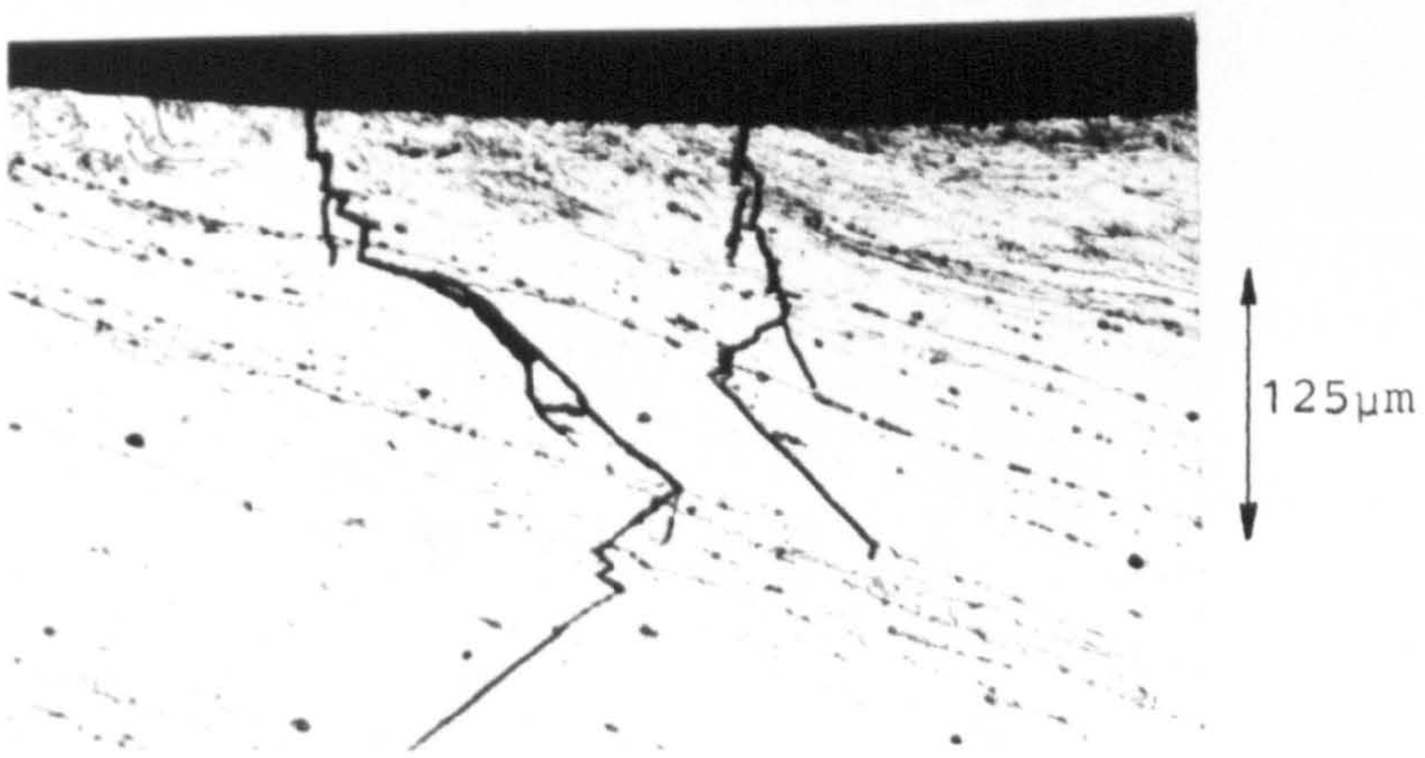

10c) Alloy 8090 (heavily peened)

PLATE 10. Cross-sections through small fatigue cracks in the notch of the unpeened and heavily peened 8090 alloy.

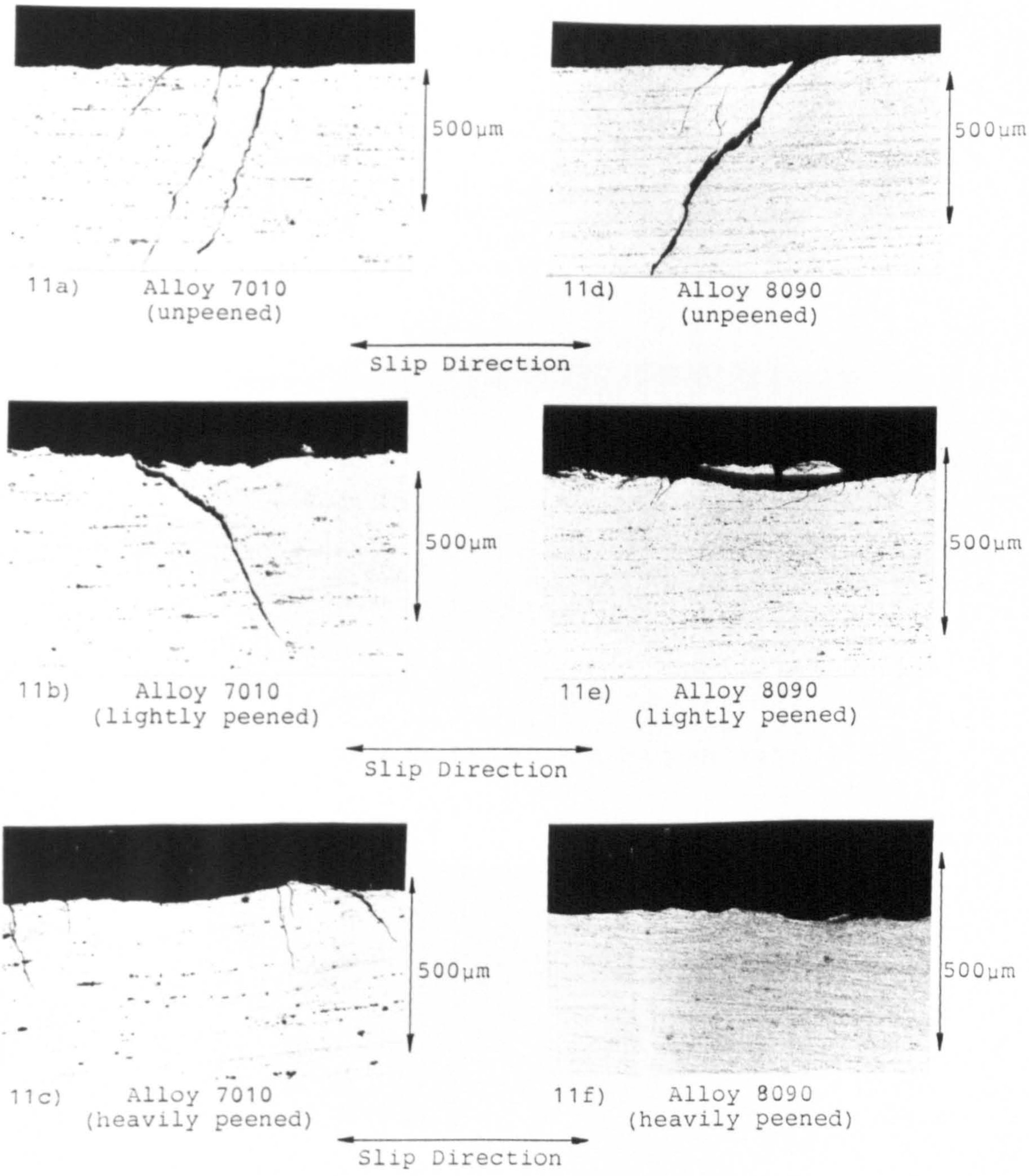

11a) Alloy 7010 (unpeened)

11b) Alloy 7010 (lightly peened)

11c) Alloy 7010 (heavily peened)

11d) Alloy 8090 (unpeened)

11e) Alloy 8090 (lightly peened)

11f) Alloy 8090 (heavily peened)

PLATE 11. Sections through fretting scars in the 7010 and 8090 alloy rotating-bending specimens.

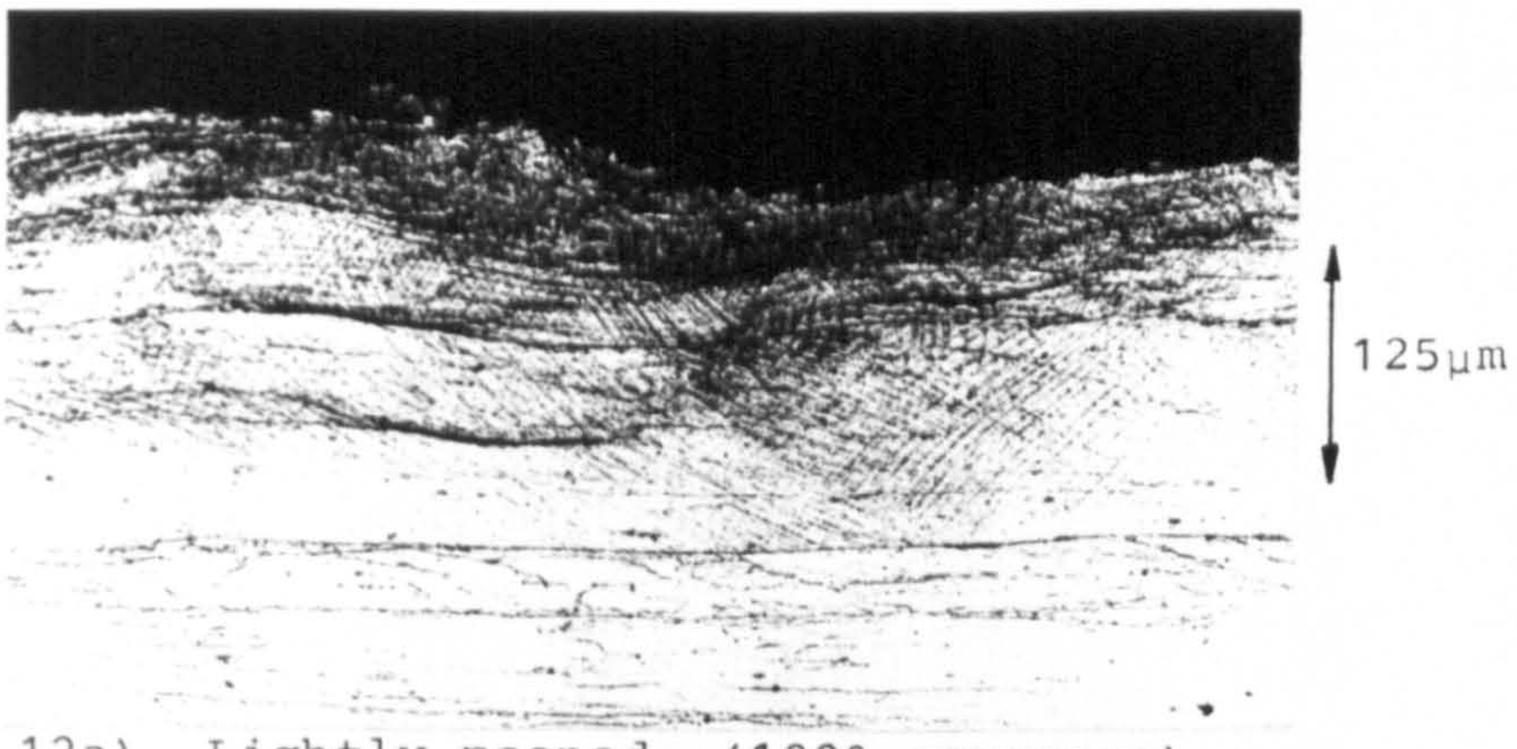

12a) Lightly peened (100% coverage)

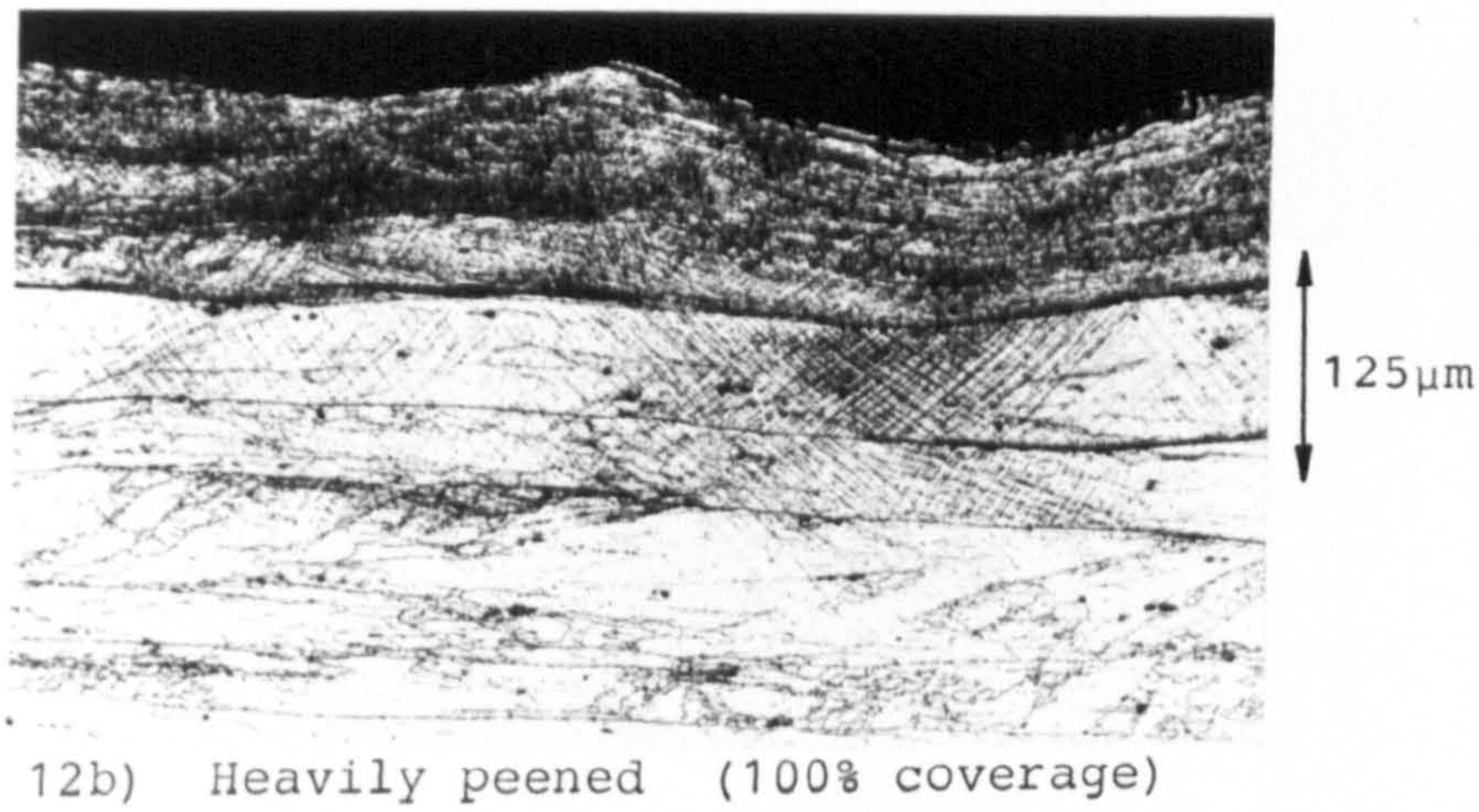

12b) Heavily peened (100% coverage)

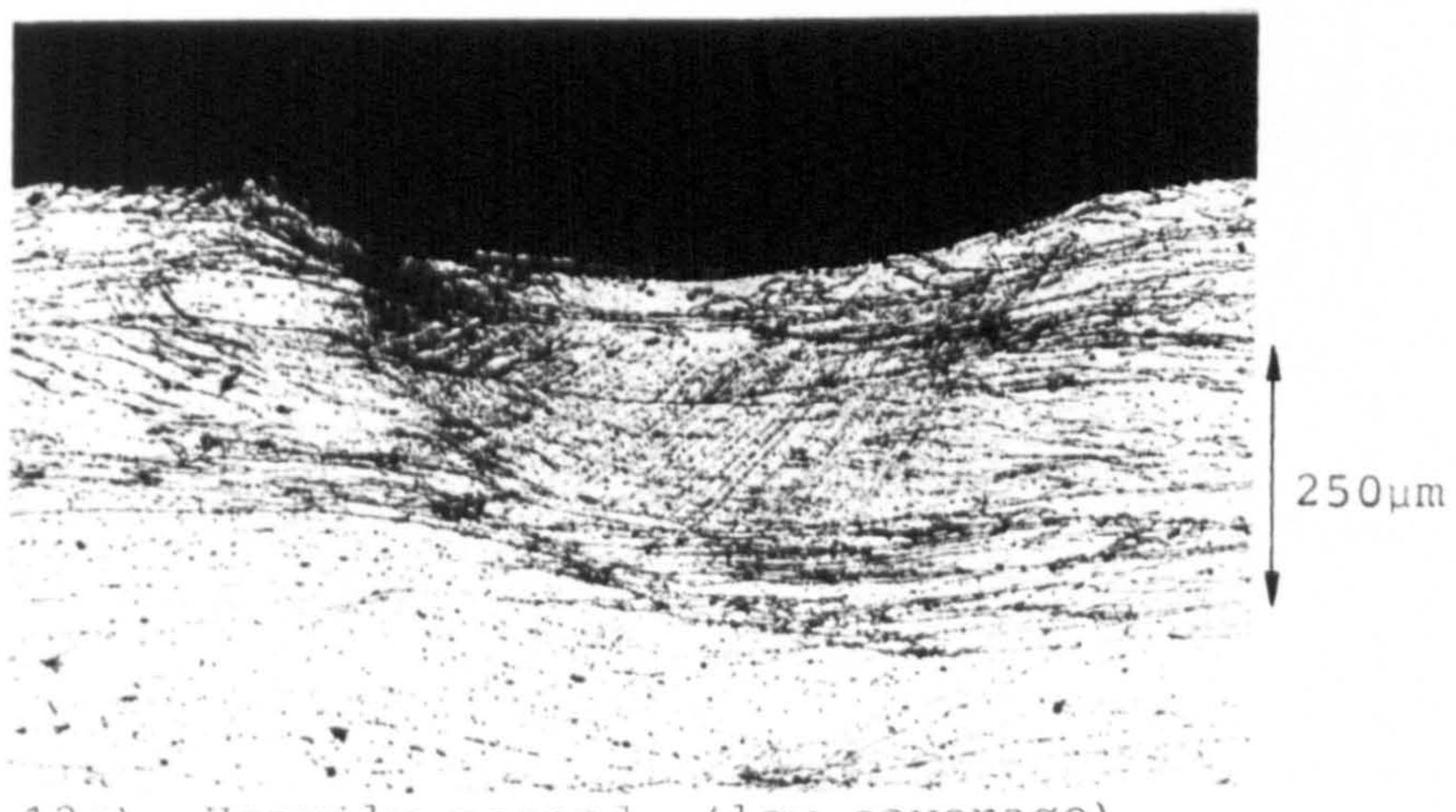

12c) Heavily peened (low coverage)

PLATE 12. Cross-sections showing the precipitation of S' on slip bands in the surface of alloy 8090 reaged after peening.

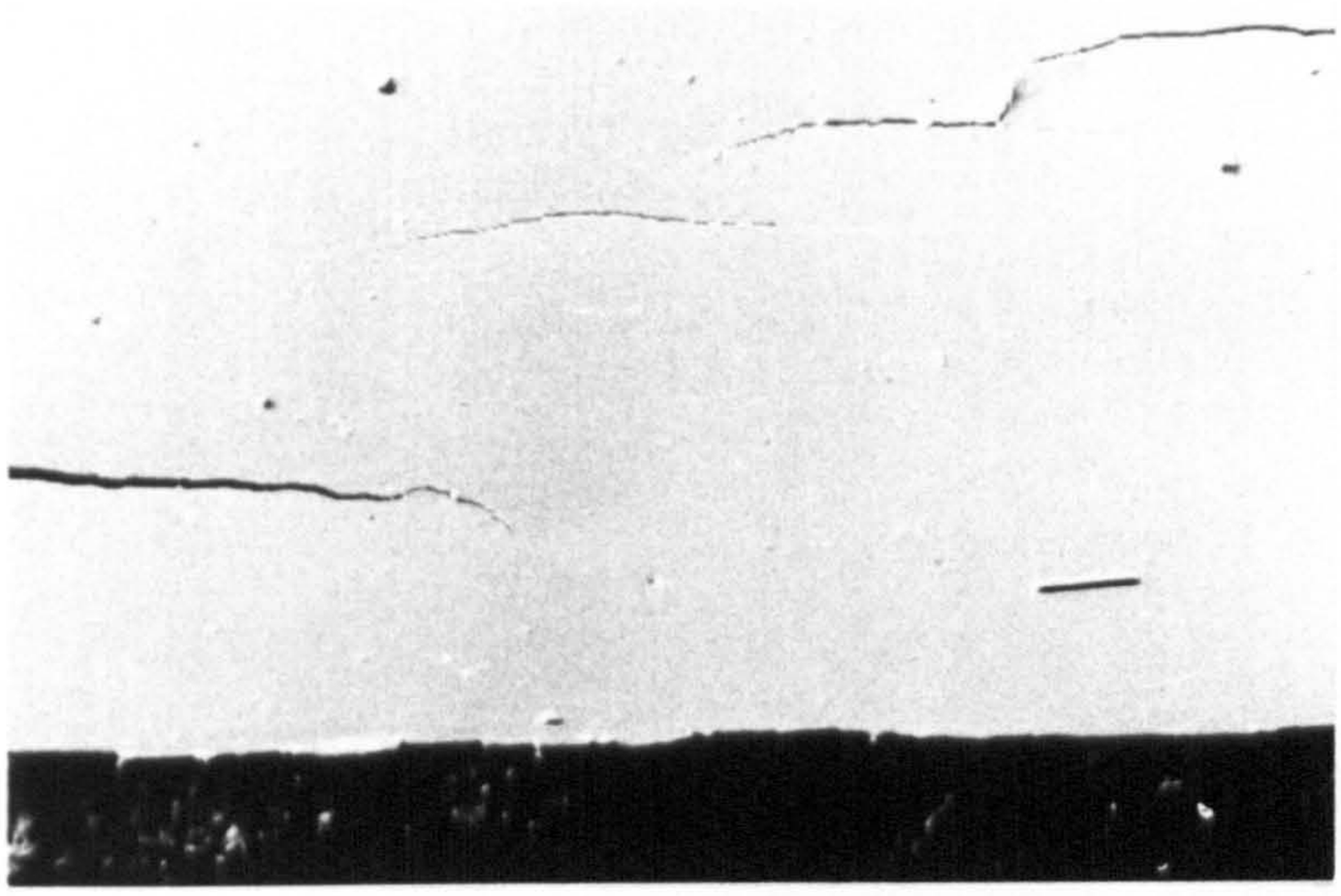

PLATE 13. Fatigue cracks at the base of the notch in a fractured, unpeened reversed bending specimen. (alloy 7010).

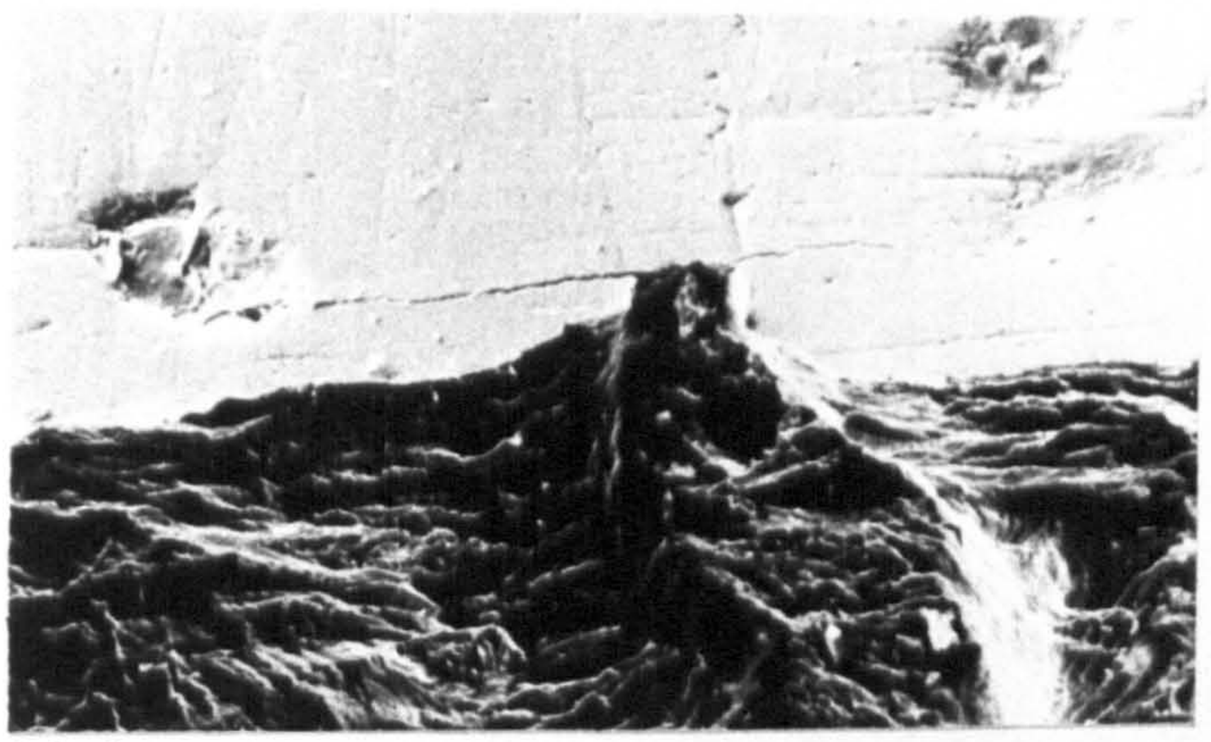

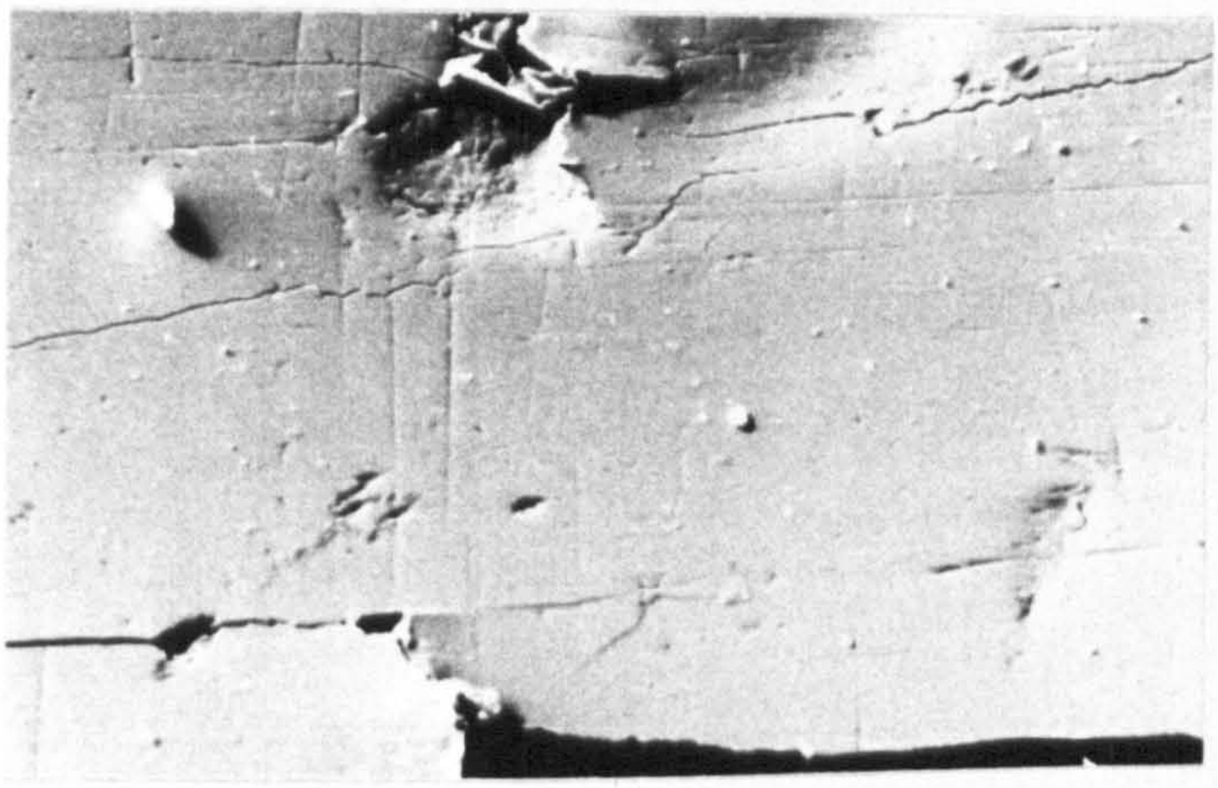

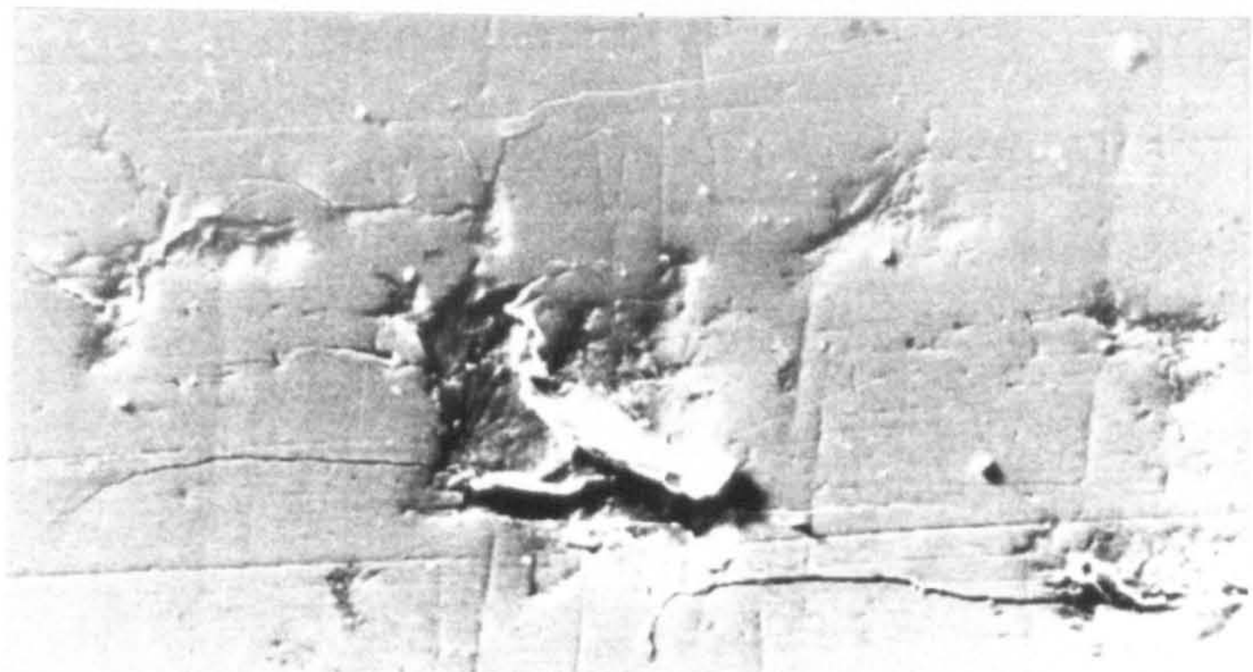

PLATE 14. Fatigue cracks growing from dimples at the base of the notch in a fractured, heavily peened reversed specimen (alloy 7010).

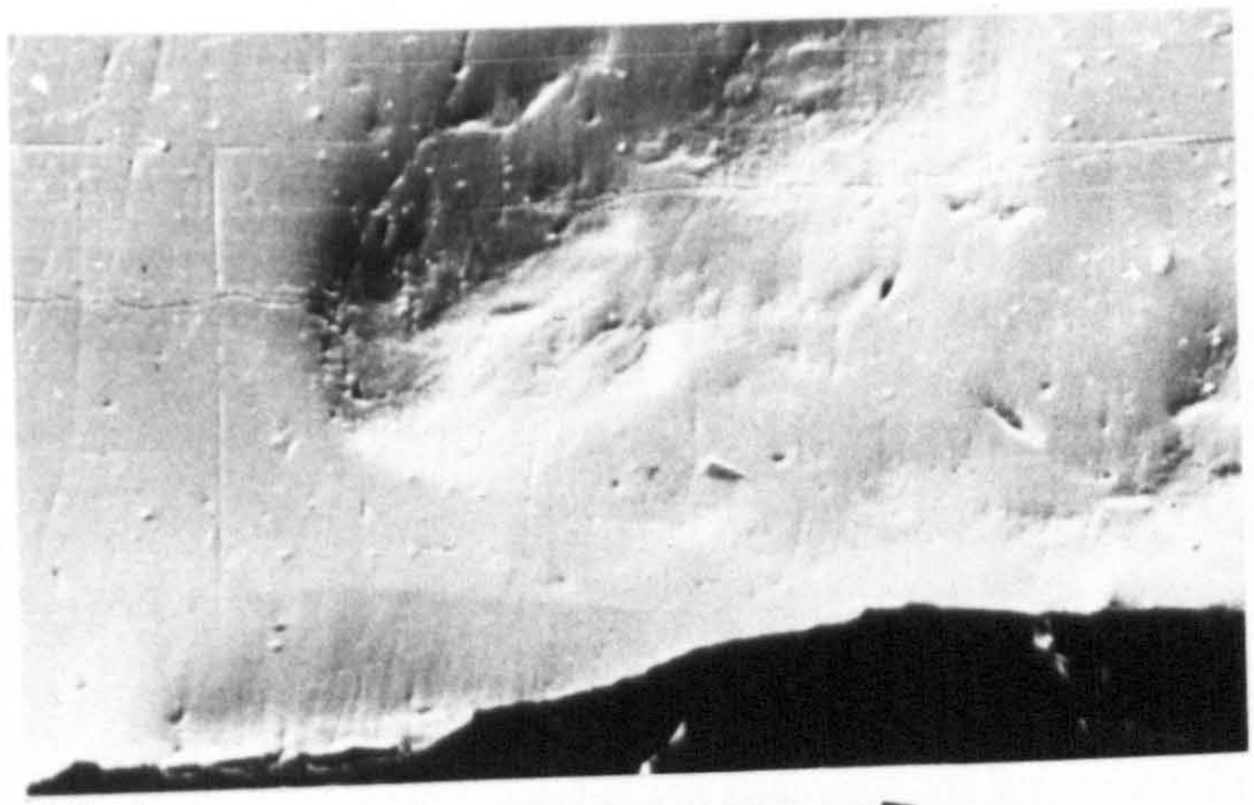

15a)

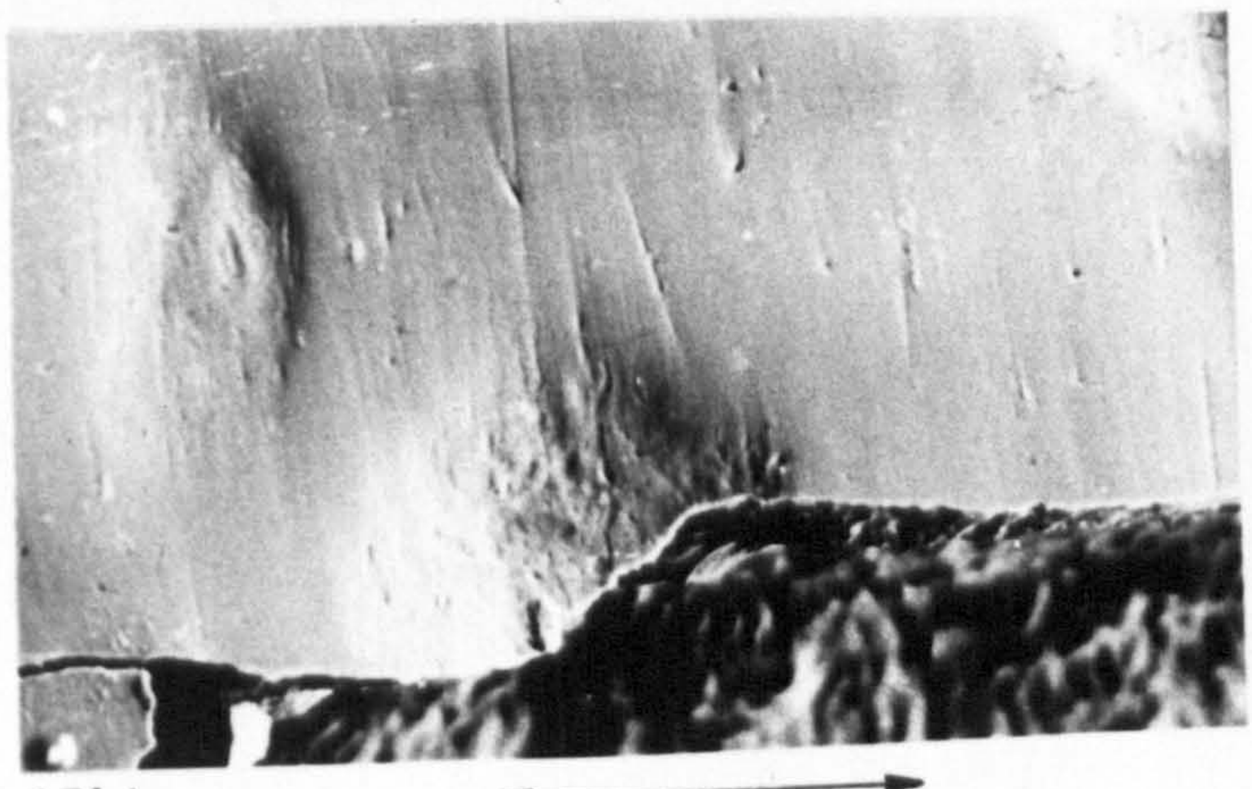

15b)

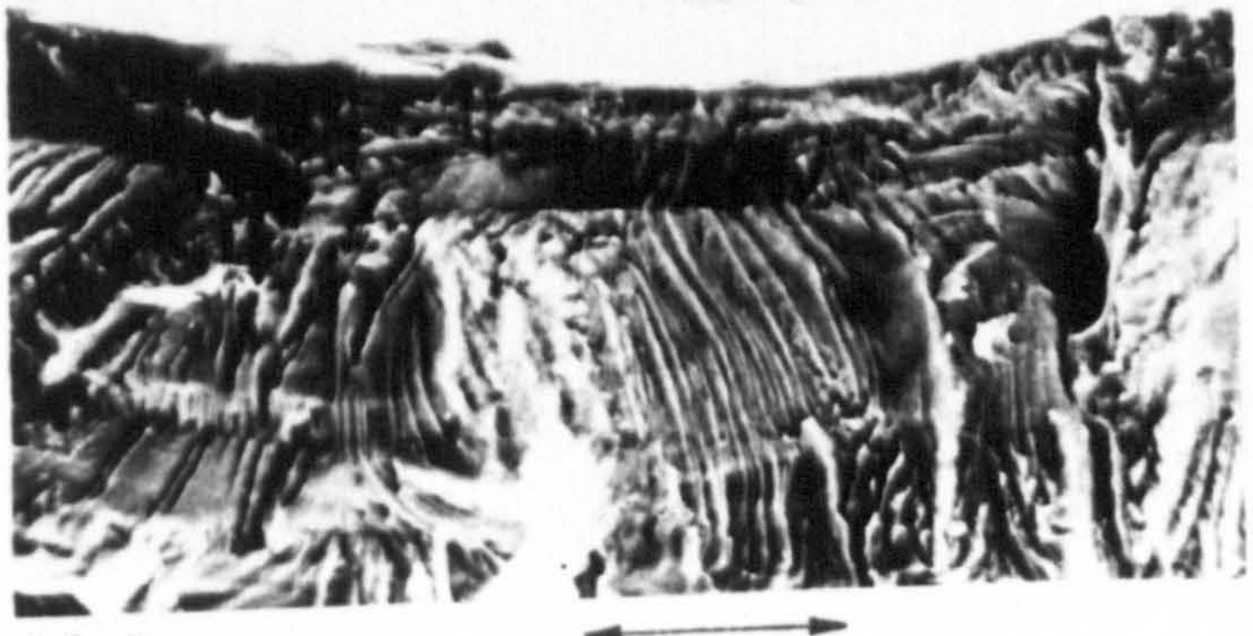

15c)

PLATE 15. Fatigue cracks growing from dimples at the base of the notch in a fractured, lightly peened reversed-bending specimen (alloy 7010).

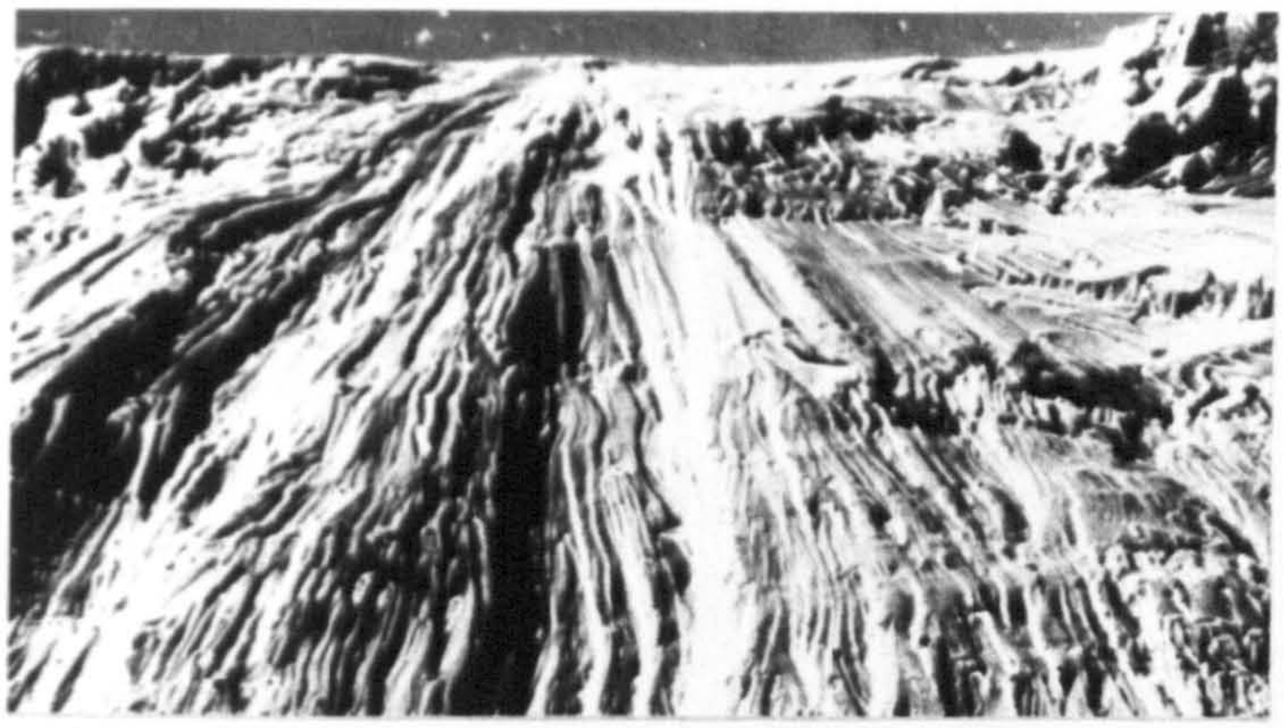

16a) Alloy 7010 (unpeened).

250μm

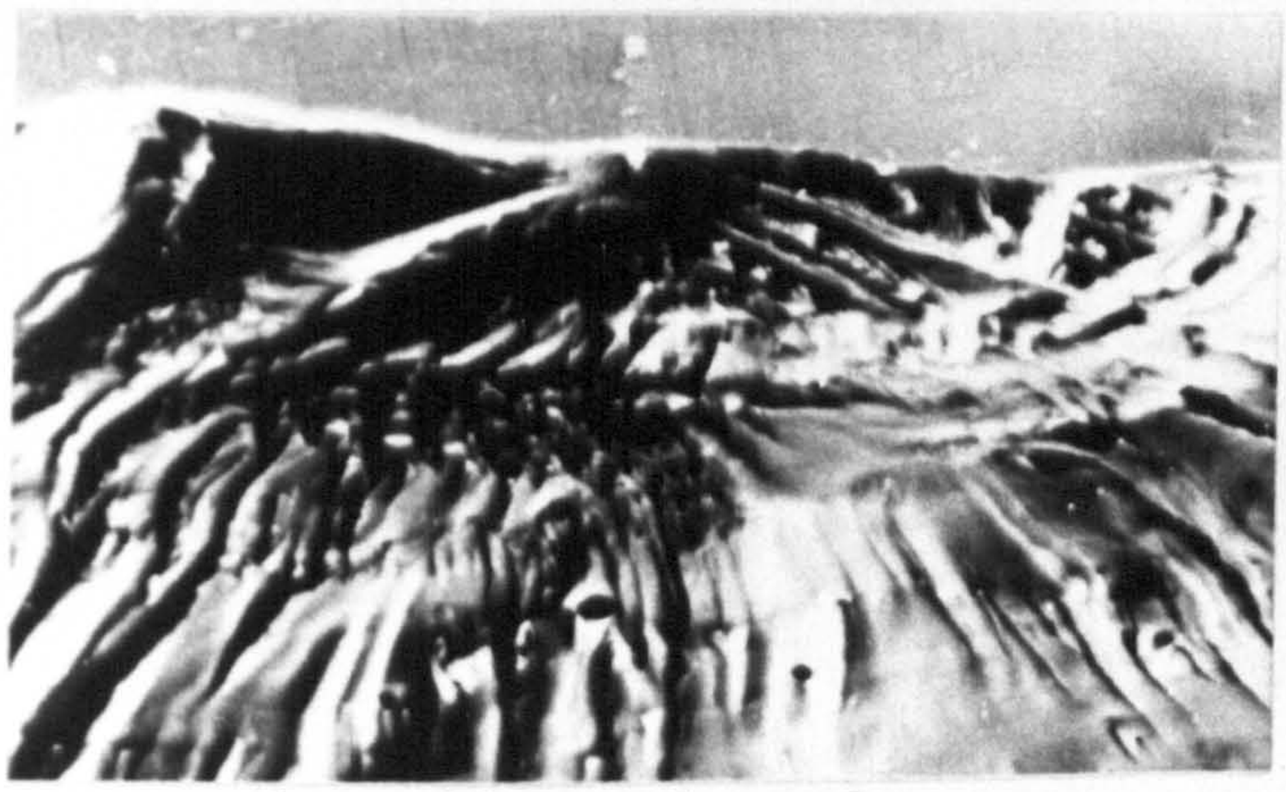

16b) Plate 16a) enlarged.

25μm

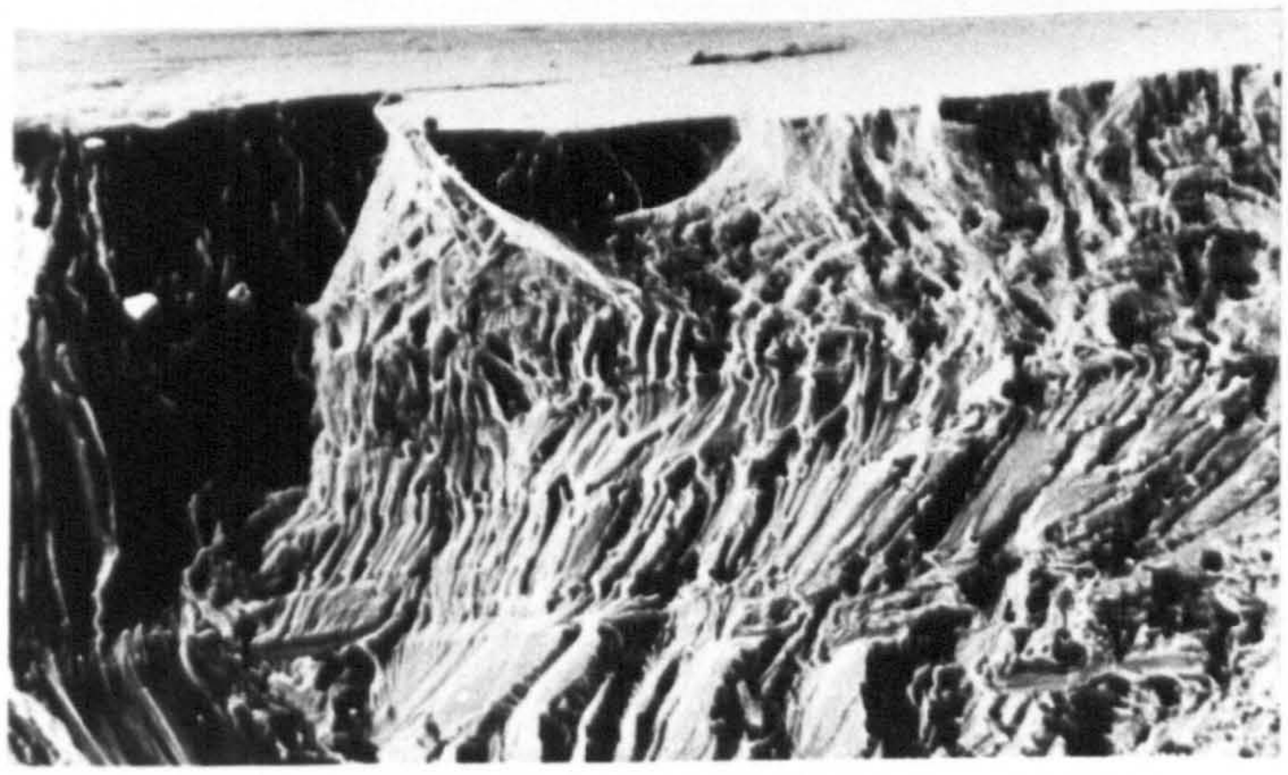

16c) Alloy 7010 (shot-peened).

250μm

PLATE 16. Fracture surfaces in the unpeened and heavily peened 7010 alloy reversed-bending specimens.

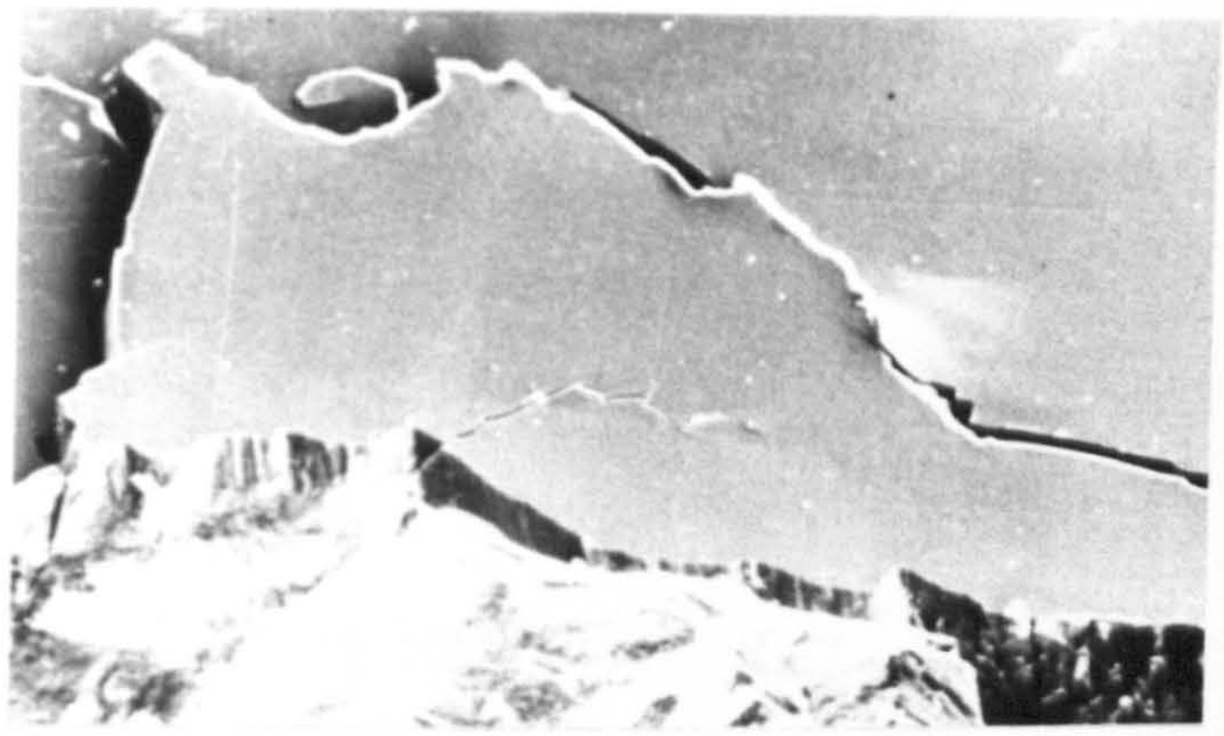

PLATE 17. Fatigue cracks at the base of the notch in a fractured, unpeened reversed-bending specimen (alloy 8090).

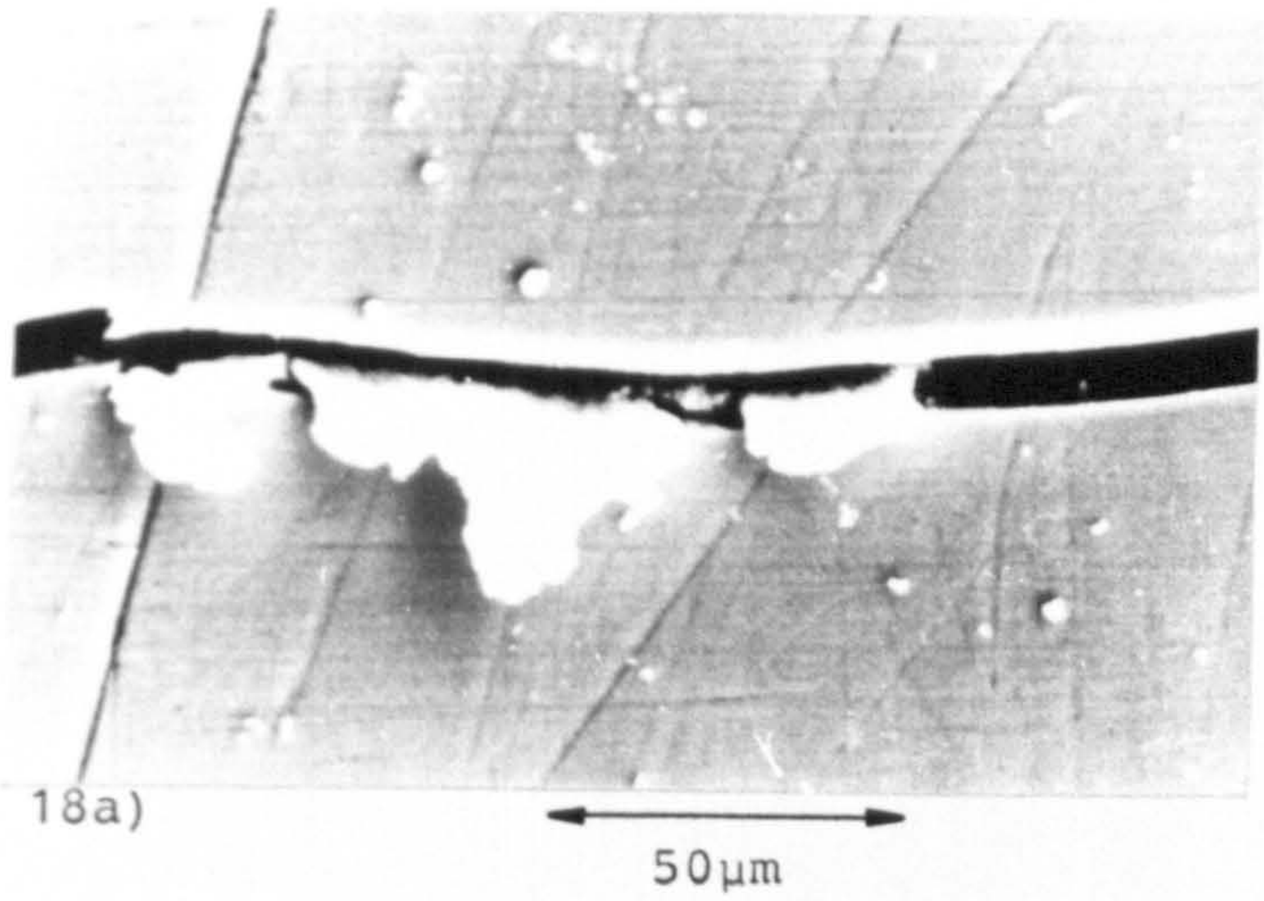

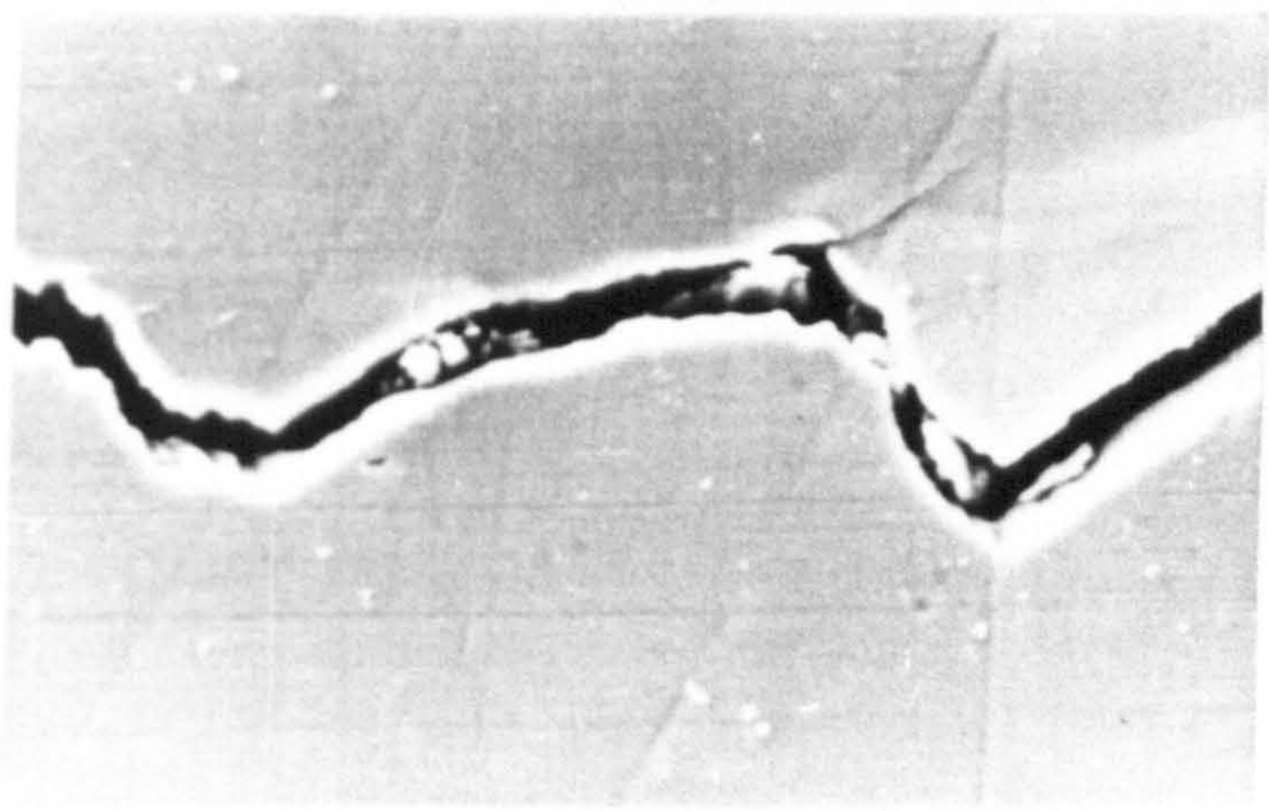

PLATE 18. Oxide exuding from a fatigue crack in the base of the notch in an unpeened, 8090 alloy reversed bending specimen.

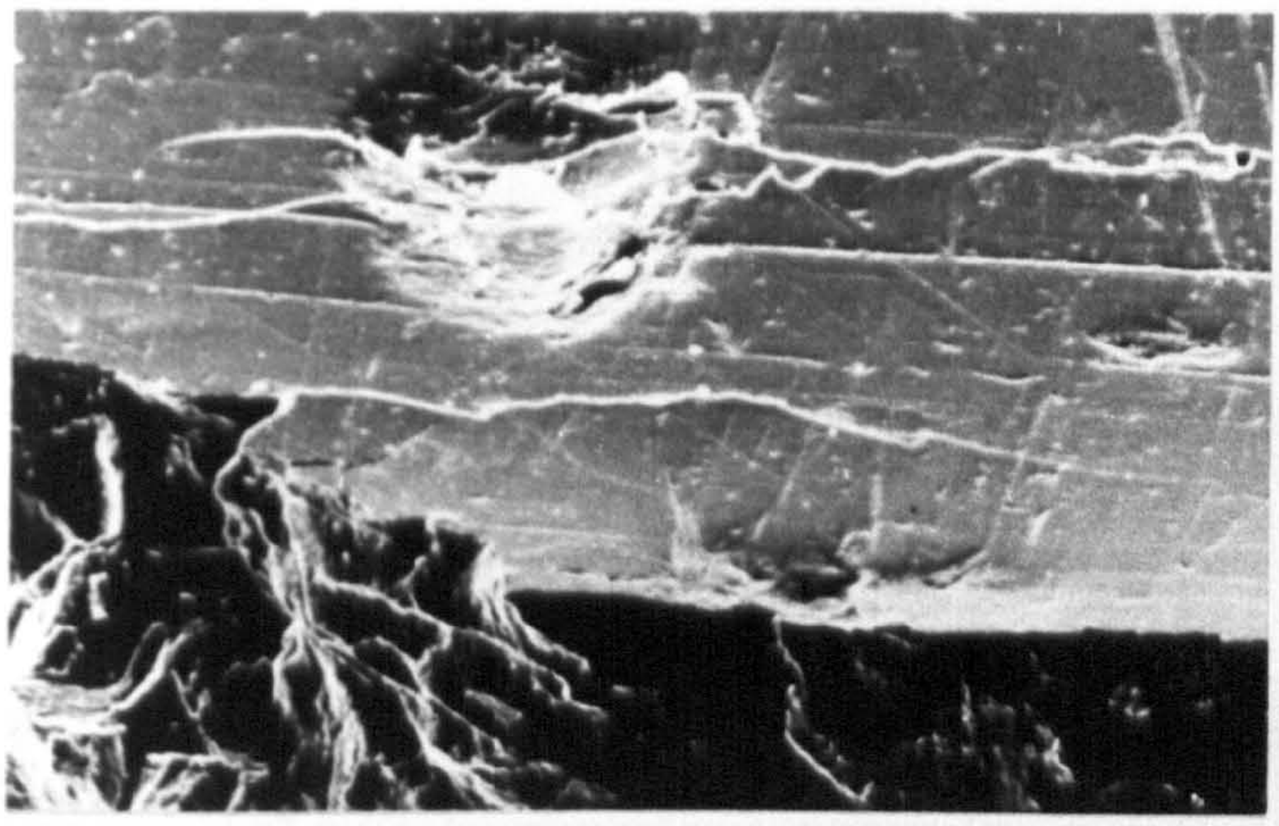

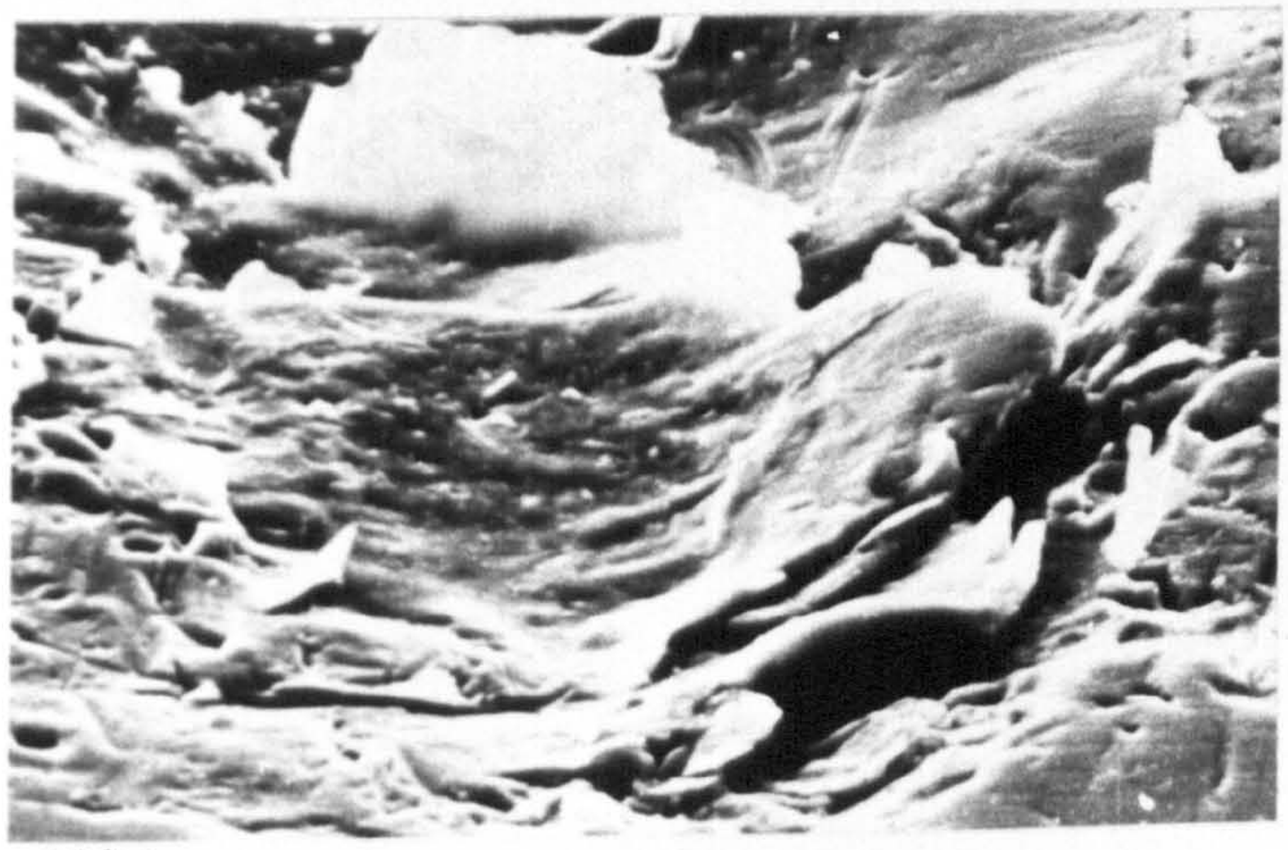

PLATE 19. Fatigue cracking around a heavily deformed dimple in the base of the notch of a heavily peened 8090 alloy reversed-bending specimen.

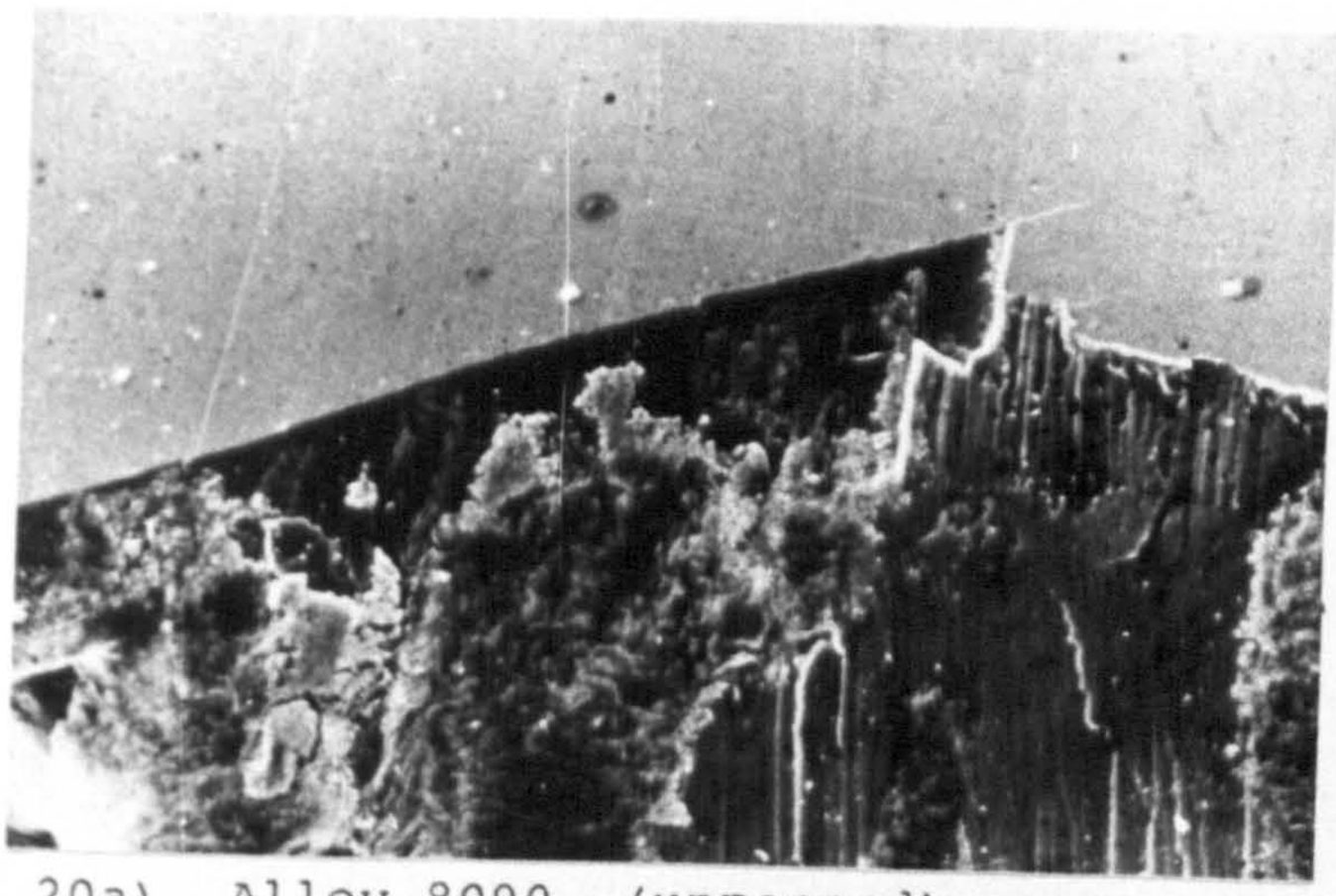

20a) Alloy 8090 (unpeened).

200μm

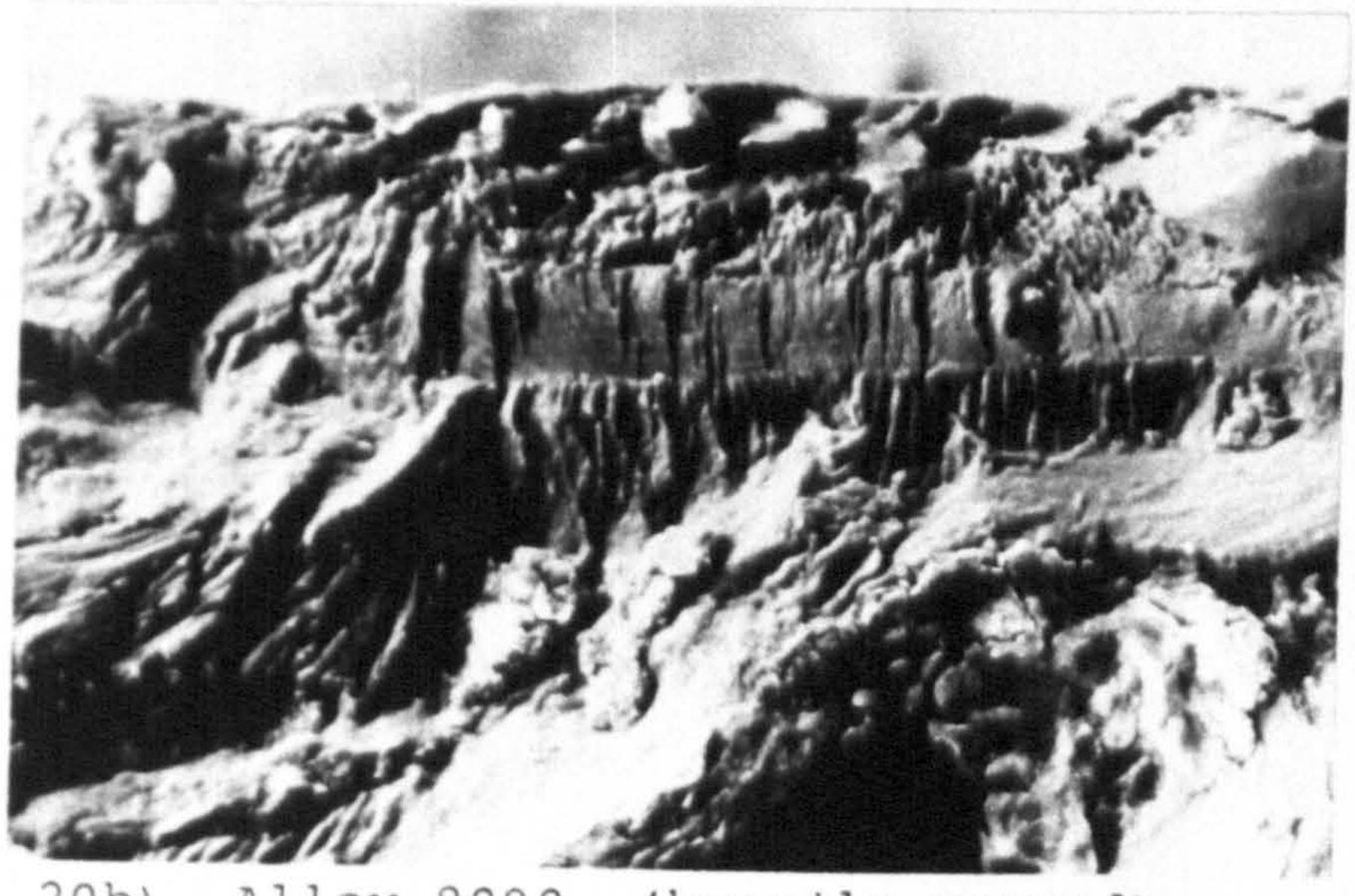

20b) Alloy 8090 (heavily peened).

200μm

PLATE 20. Fracture surfaces in the unpeened and heavily peened 8090 alloy reversed-bending specimens.

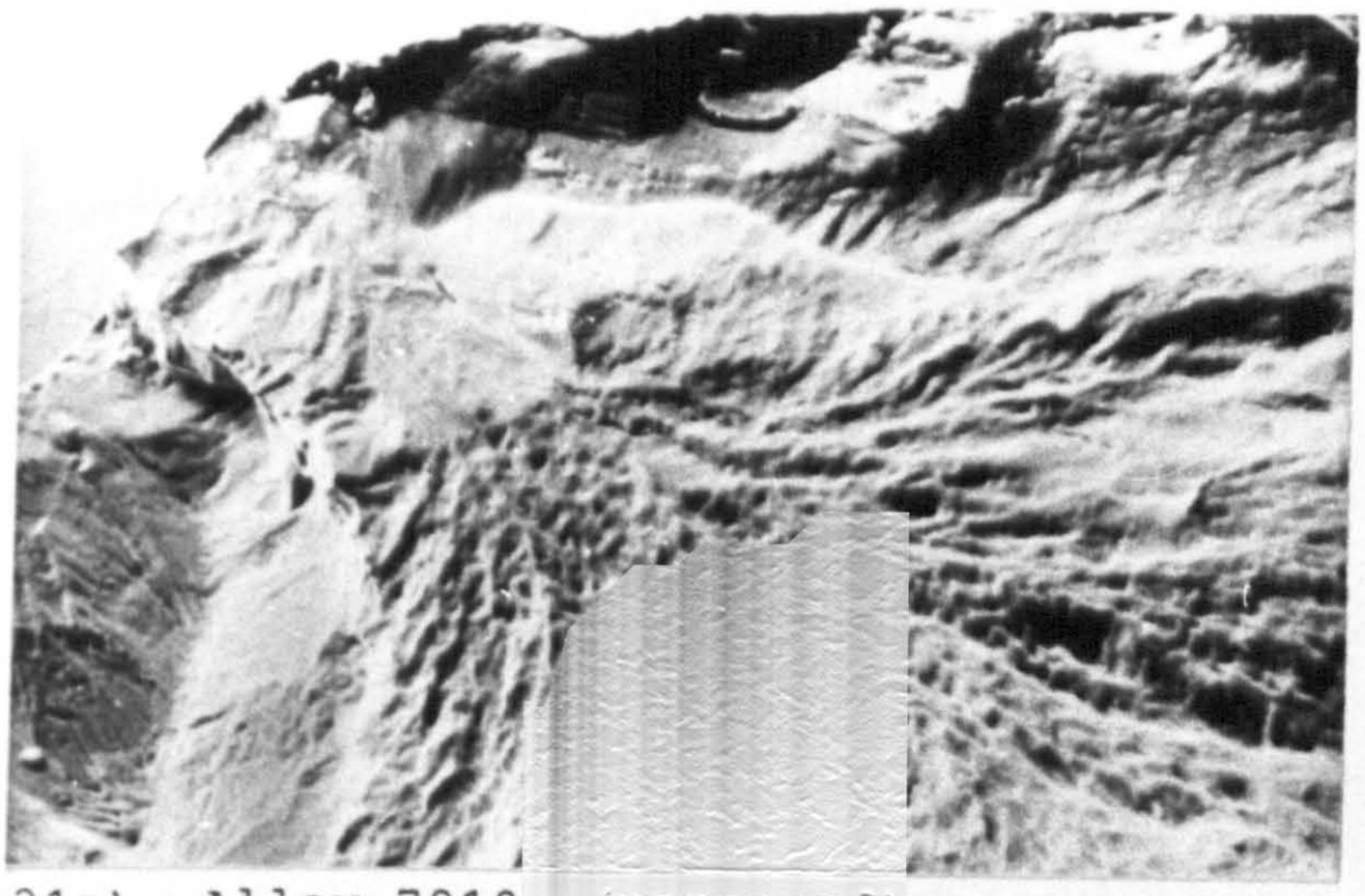

21a) Alloy 7010 (unpeened).

200μm

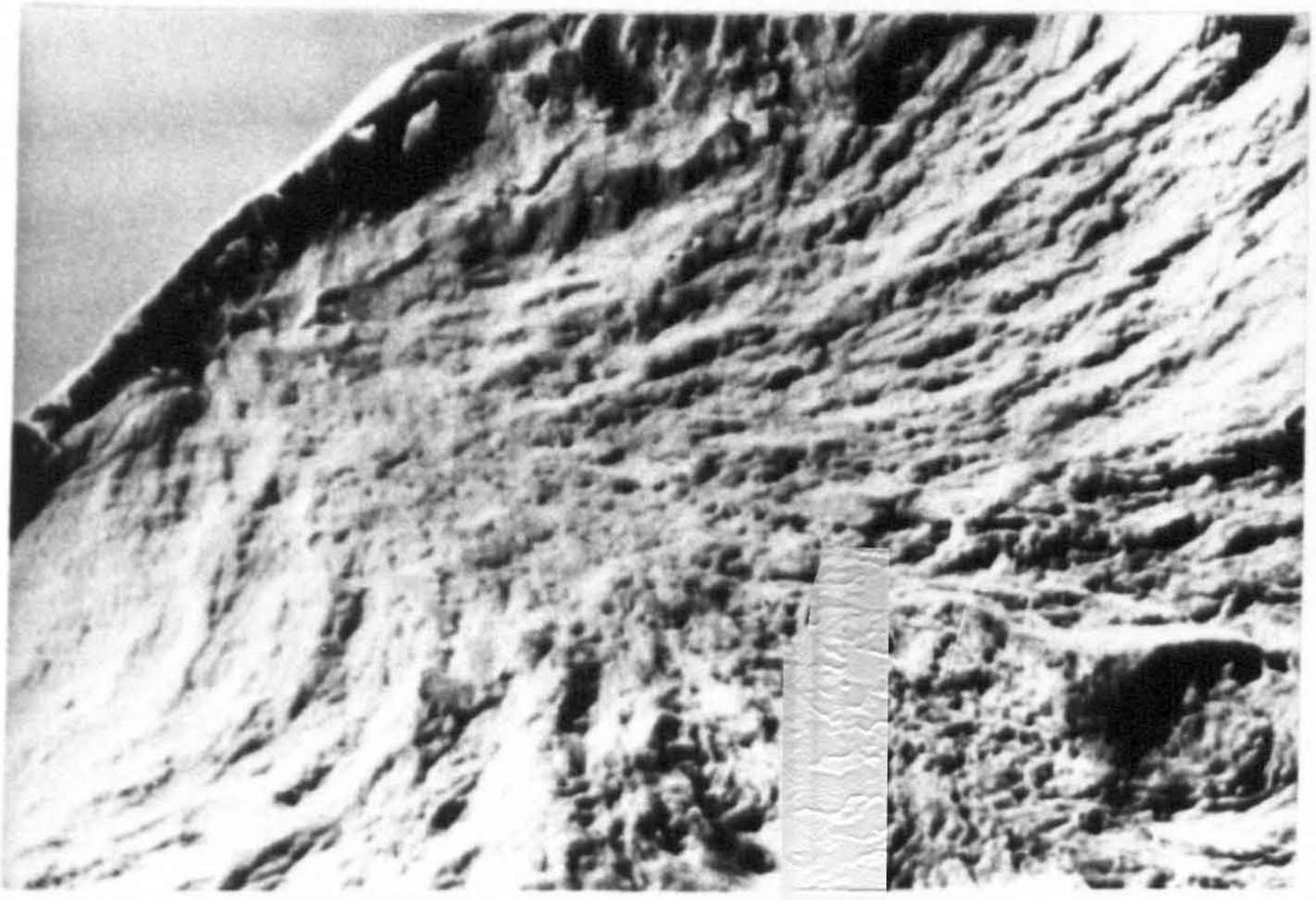

21b) Alloy 7010 (heavily peened).

200μm

PLATE 21. Fracture surfaces in the unpeened and heavily peened 7010 alloy rotating-bending specimens tested in plain fatigue.

22a) Alloy 7010 (unpeened).

200μm

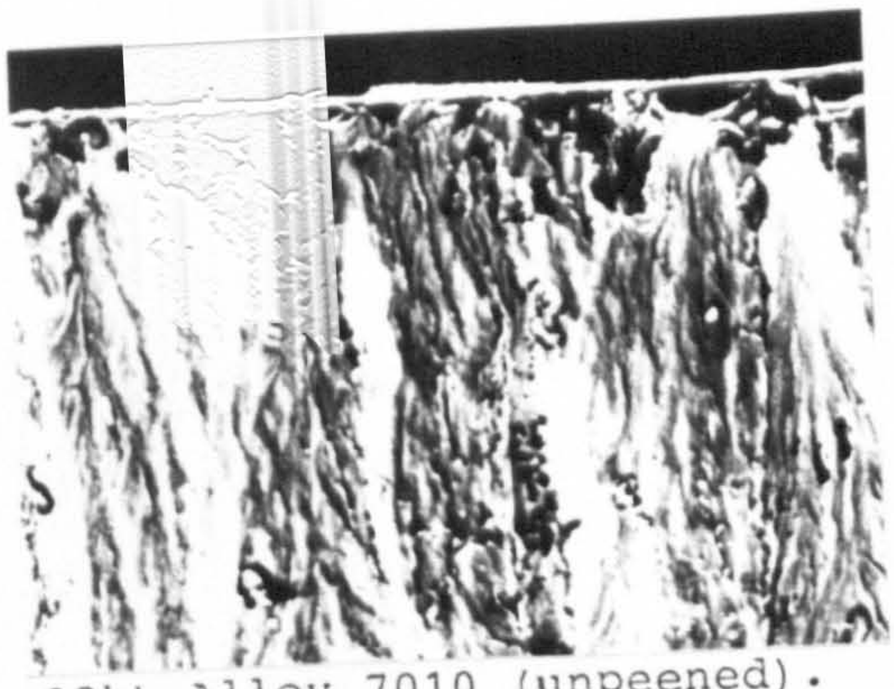

22b) Alloy 7010 (unpeened).

250μm

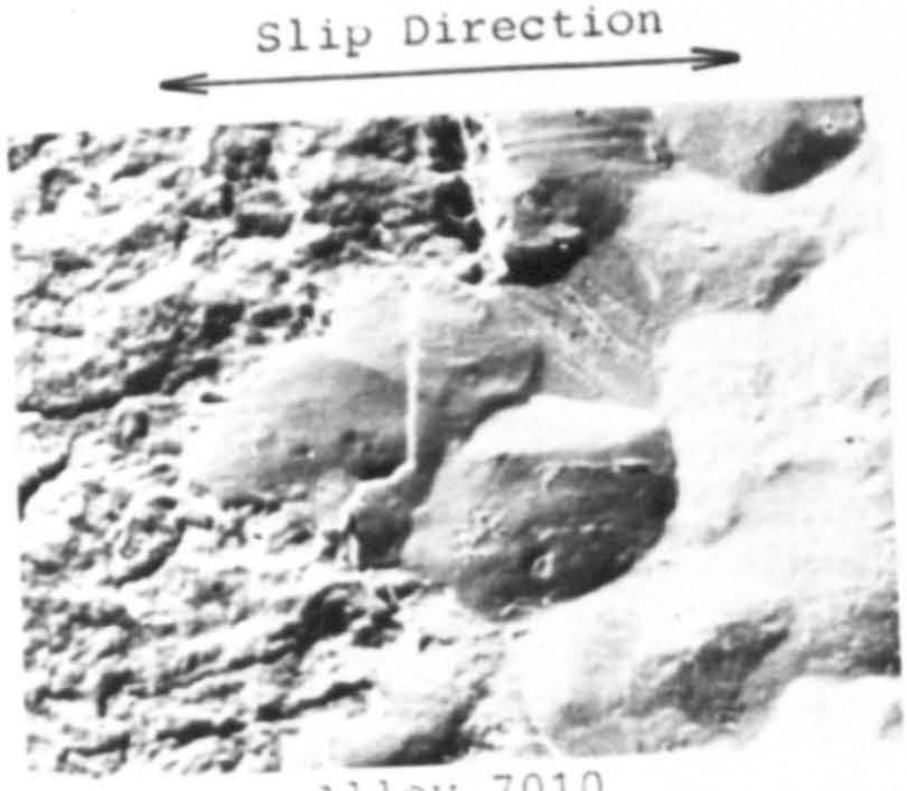

22c) Alloy 7010 (lightly peened)

200μm

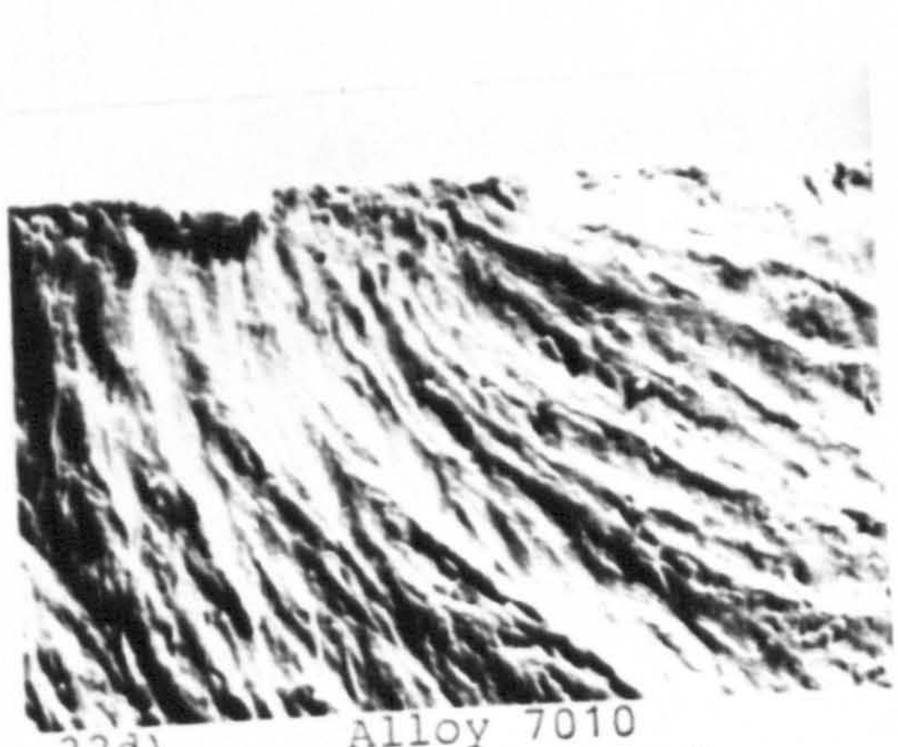

22d) Alloy 7010 (lightly peened)

250μm

PLATE 22. Fatigue cracks and fracture surfaces at the edges of fretting scars in the unpeened and lightly peened 7010 alloy.

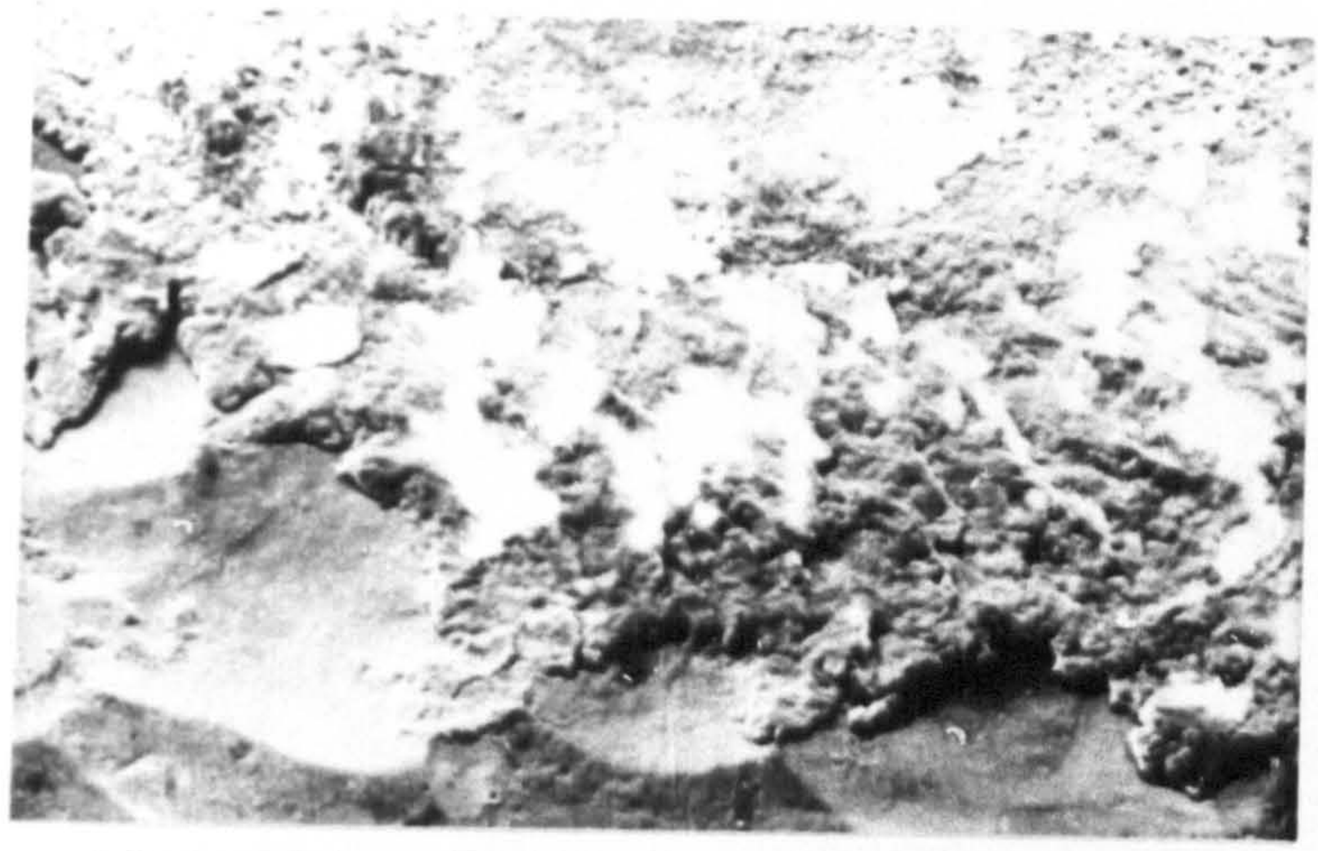

23a) Alloy 7010 (heavily peened)

250µm

Slip Direction

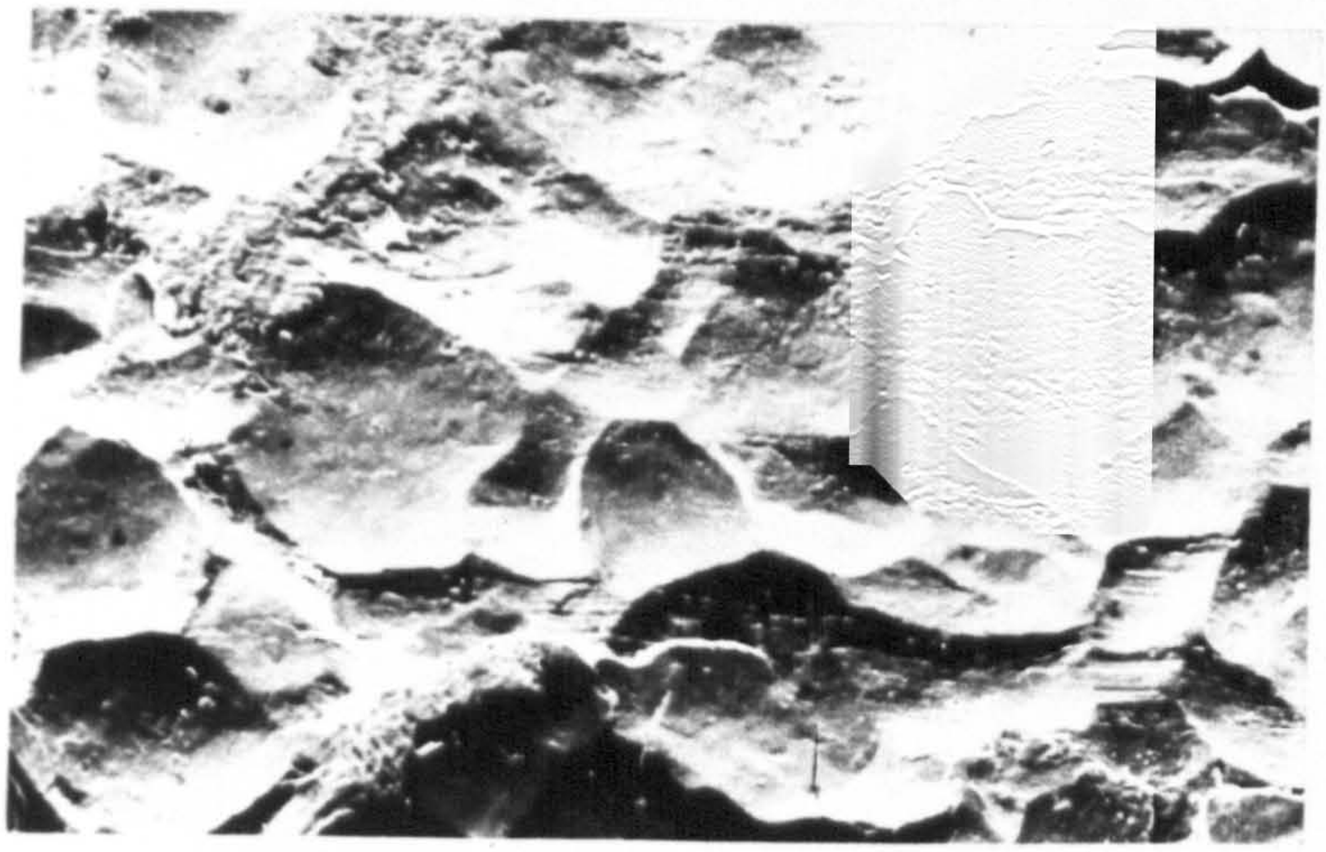

Slip Direction

23b) Alloy 7010 (heavily peened)

500µm

PLATE 23. Fretting scar and plain fatigue cracks in the heavily peened 7010 alloy.

24a) Alloy 7010 (unpeened)

25μm

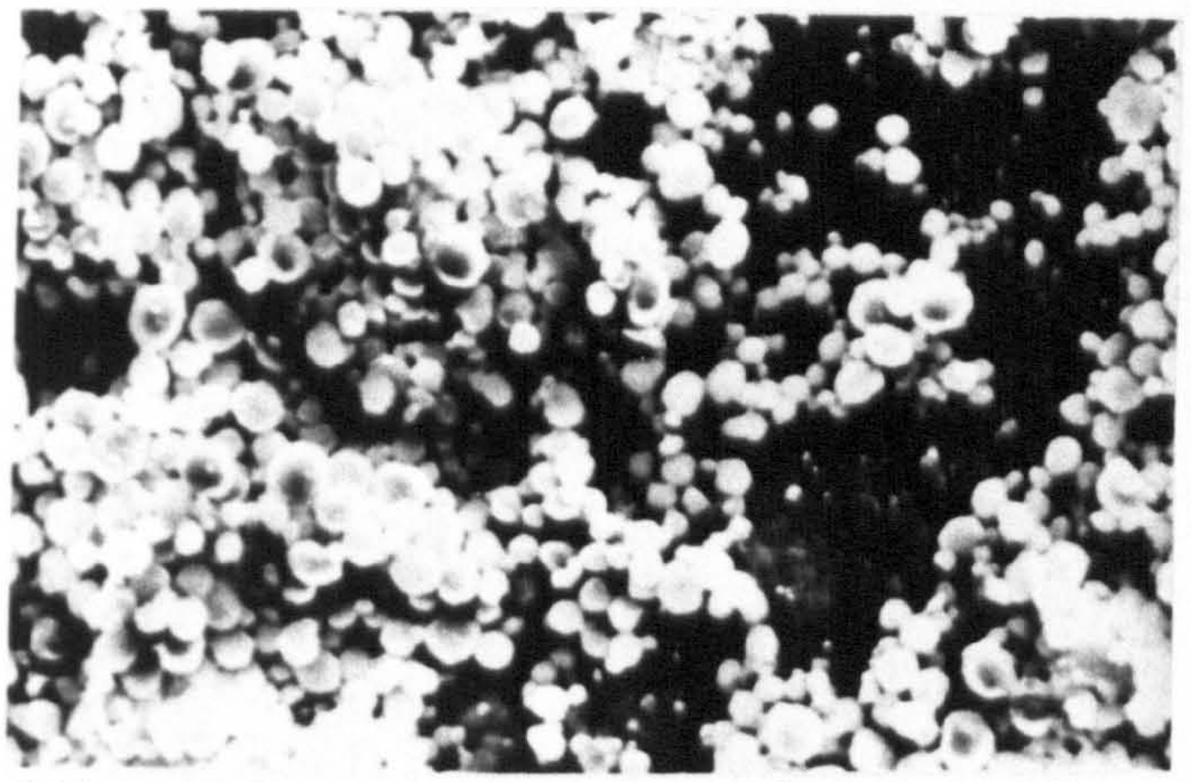

24b) Alloy 7010 (heavily peened)

25μm

24c) Alloy 7010 (heavily peened)

25μm

PLATE 24. Fretting debris on the fretting scars of the unpeened and heavily peened 7010 alloy.

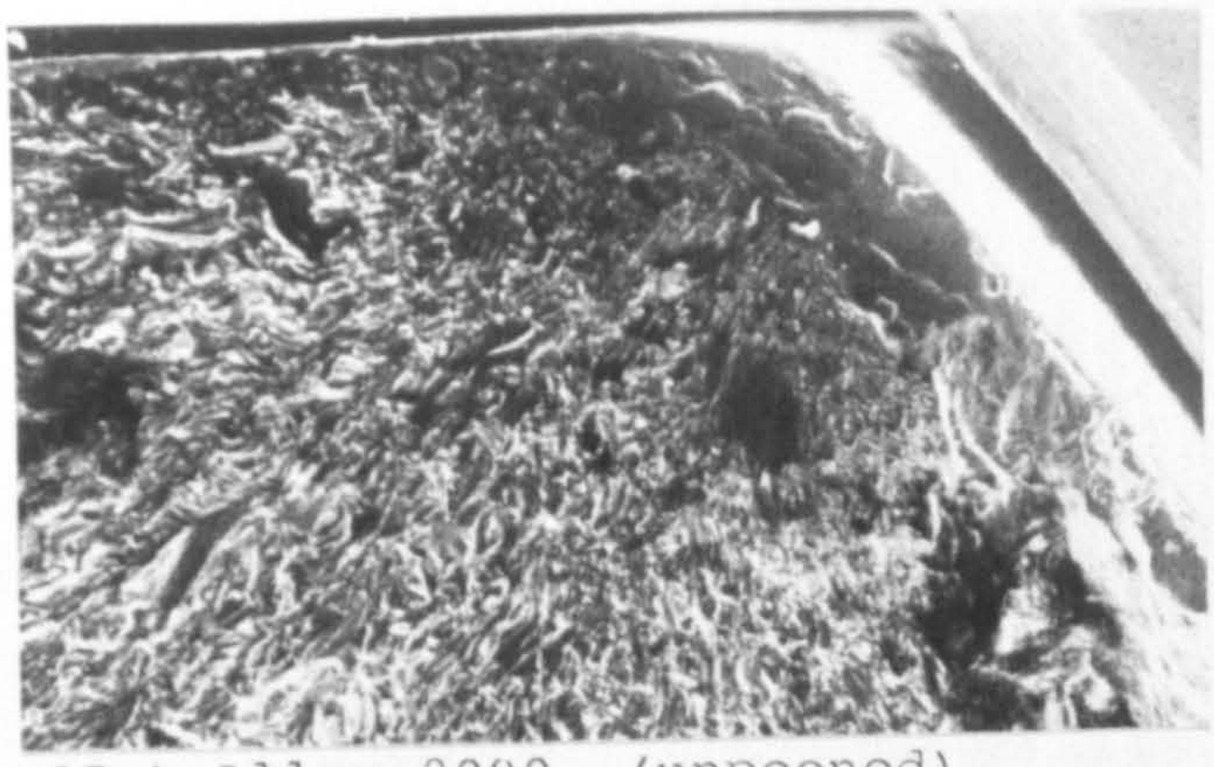

25a) Alloy 8090 (unpeened)

250µm

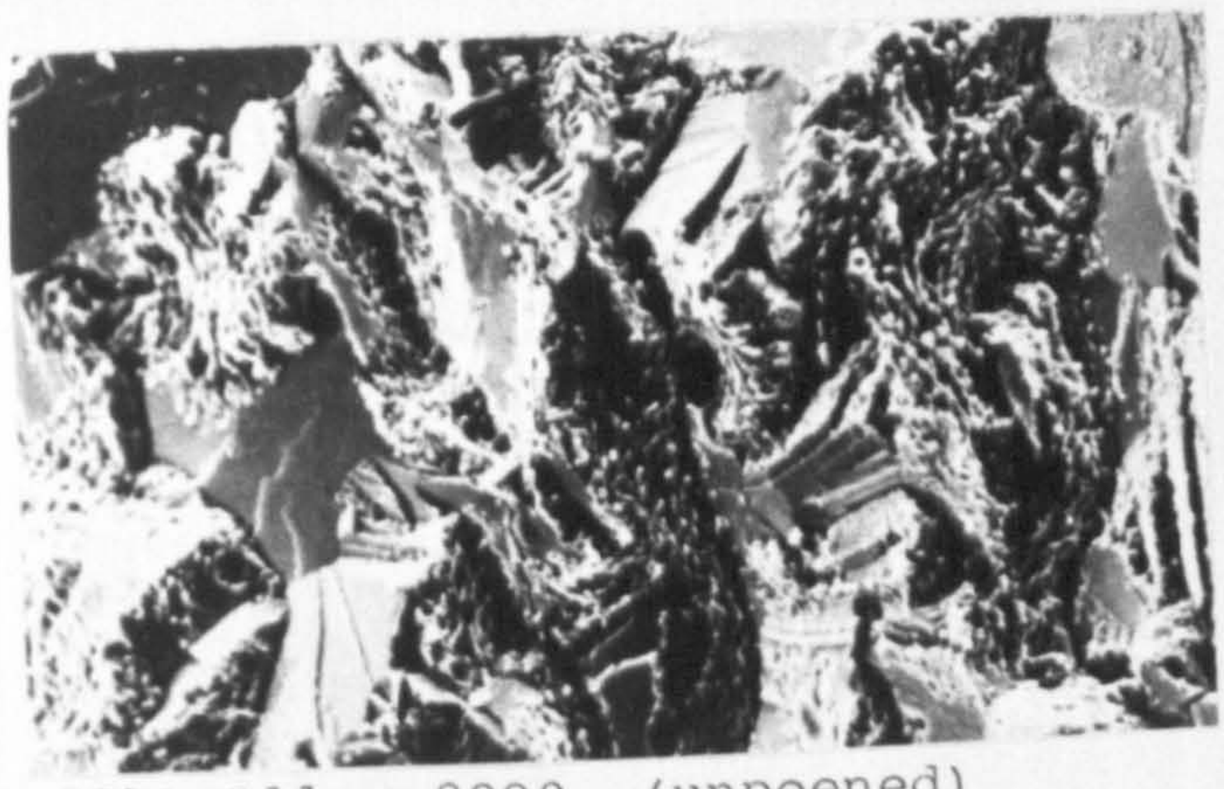

25b) Alloy 8090 (unpeened)

100µm

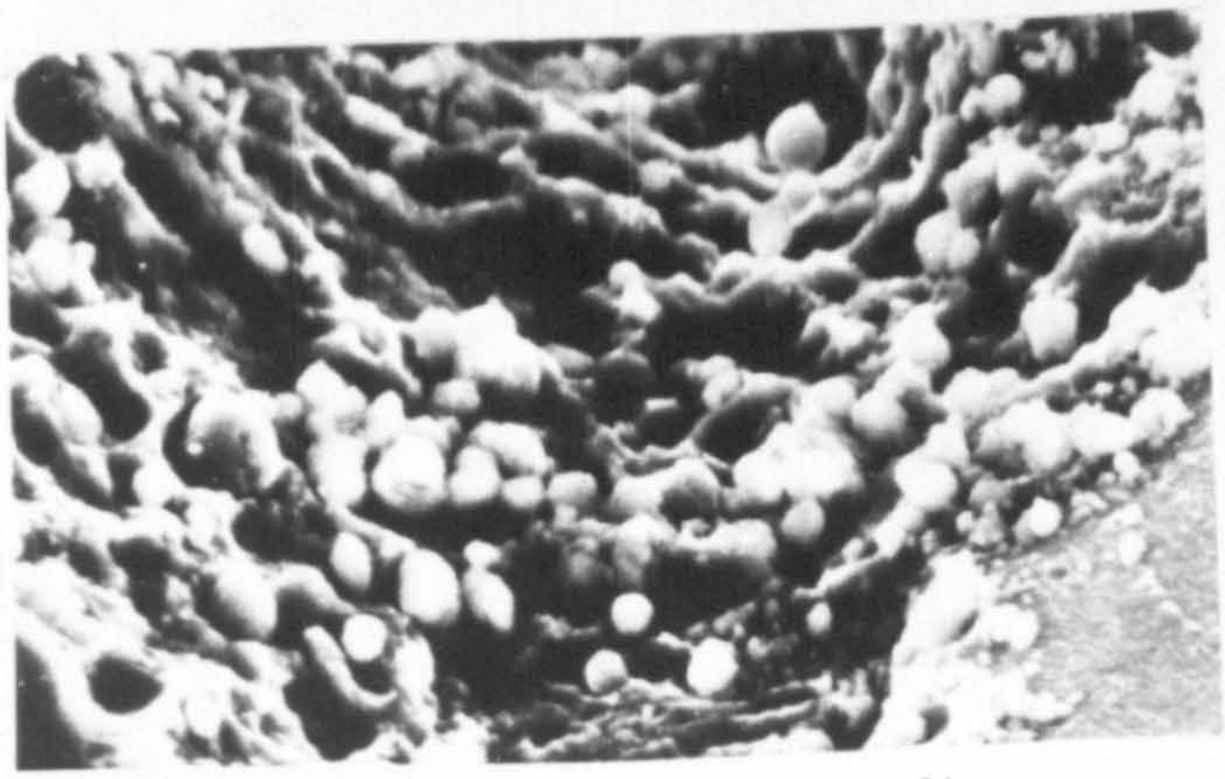

25c) Alloy 8090 (unpeened)

20µm

PLATE 25. Fracture surface and spherical debris on the face of the fracture surface in the unpeened 8090 alloy tested in plain fatigue.

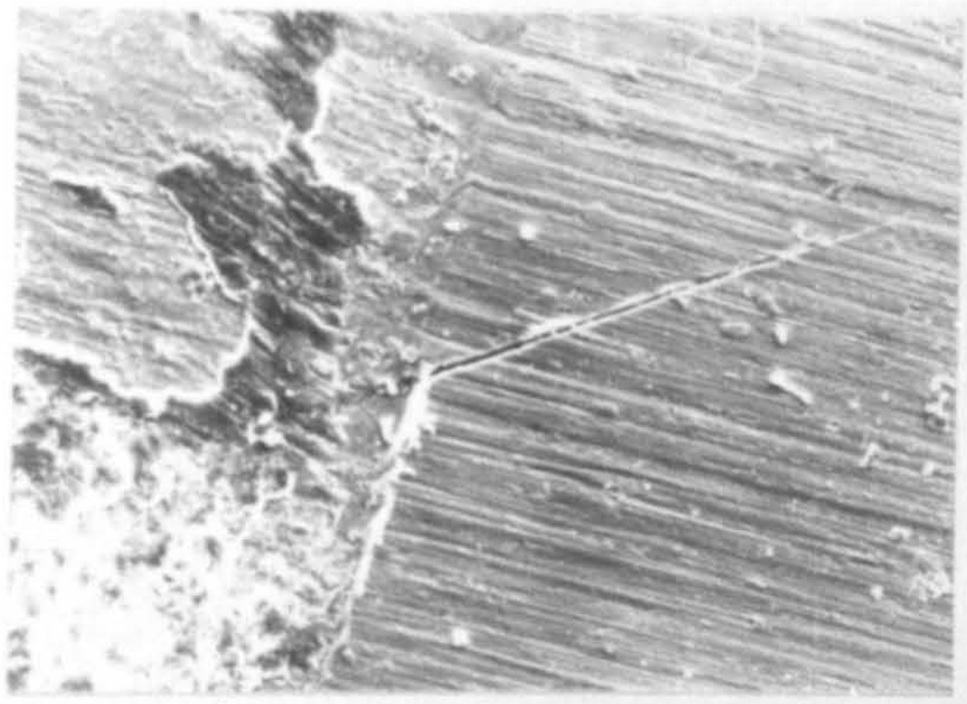

26a) Alloy 8090 (unpeened)

300μm

26b) Alloy 8090 (unpeened)

300μm

Slip Direction

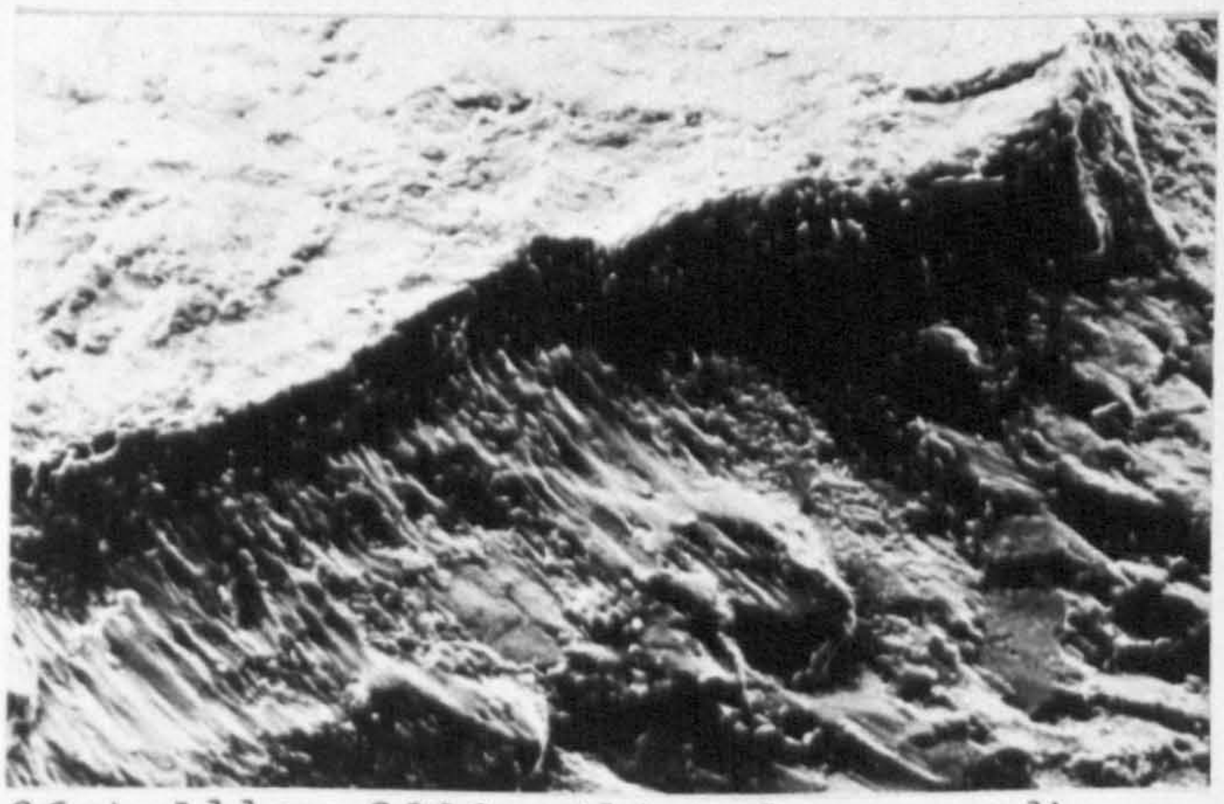

26c) Alloy 8090 (lightly peened)

300μm

PLATE 26. Fatigue cracking at the edges of fretting scars in the unpeened and lightly peened 8090 alloy.

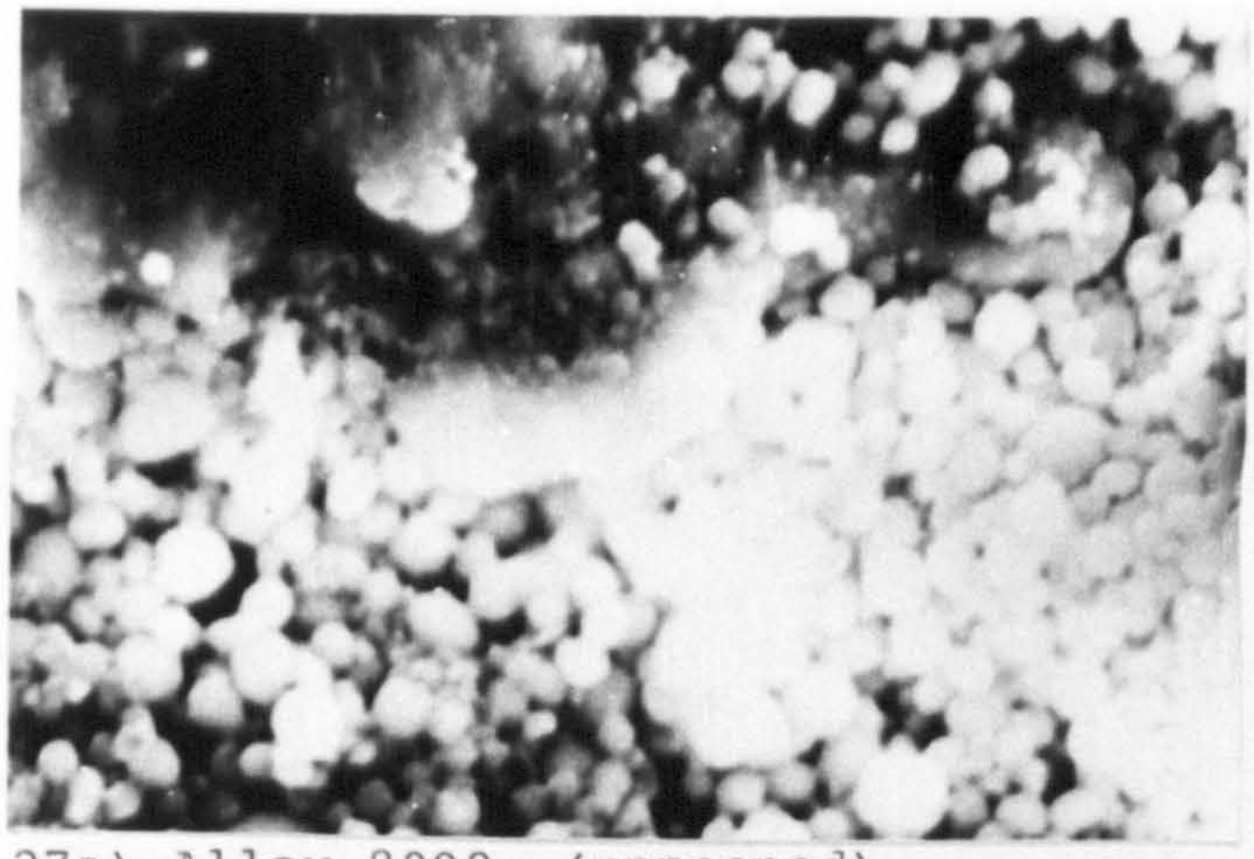

27a) Alloy 8090 (unpeened)

10μm

27b) Alloy 8090 (heavily peened)

50μm

PLATE 27. Debris on the fretting scars of the unpeened and heavily peened 8090 alloy.